

# **Drug screening lysosomal storage diseases with a focus on CLN8 disease**

Rafael Andrés Badell-Grau

**PhD in Biosciences**

**Cardiff University  
School of Biosciences  
2020**

Supervised by

Dr Emyr Lloyd-Evans and Dr Helen Waller-Evans

## **Acknowledgements**

Firstly, I would like to thank Dr Emyr Lloyd-Evans for his unconditional support, guidance, advice, ideas, enthusiasm and friendship throughout the PhD. It has been a pleasure and an honour to have been part of the ELE lab. I would also like to thank Dr Helen Waller-Evans for her constant support in the lab and always being able to help me with anything during this project. Thanks also go to Dr Sean Wyatt for his support and guidance through all of the qPCR experiments during this project.

I would like to thank the Batten Disease Family Association and the Life Science Research Network Wales for the funding that made this project possible. A special thanks again to the Life Science Research Network Wales for additional funding awarded for the translational potential of this projects.

I would next like to thank Dr H. Bernardo Barrios Crispi who not only contributed toward this project but is also a great friend who supported me during this project. I will always be thankful to have met him during my PhD. Likewise, I would like to thank Andrew Brimer and Otis Gazzard for their contribution towards my PhD and my development as a scientist, it was a pleasure to supervisor their lab project.

Thank you to all the present and past members of the ELE lab, who were not only extremely helpful throughout the PhD but also taught me so much. Emily Kirkham, Katie Shipley, Brendan Kelly, Abdullah Alshehri and Sophie Cook have been amazing colleagues and friends that were always there when needed and with whom I shared a lot of great times. I would also like to thank the post-doc in the lab, Dr Luke Haslett who helped at the beginning of the project and Dr Hannah Best who was an amazing addition to the ELE lab towards the end of my PhD. She was an amazing advisor and friend since she joined the ELE lab and I am also thankful for her feedback and advice.

I want to thank my closest and oldest friends and brothers Francisco Görlich and Matt Thorns for the long-lasting friendship and the wellbeing support they provided for me to stay healthy both physically and mentally by motivating each other and sharing techniques for regular exercise and meditation. They were a huge source of encouragement particularly during the most stressful times.

I also need to extend my deepest gratitude to Jordan Cuff, who not only provided moral support throughout the entirety of the PhD but also has been one of my closest

friends since I met him during the MRes. Jordan is not only an amazing friend who gives unconditional support, friendship, wisdom and encouragement but is also one of the nicest people I have ever met. Jordan was not only an incredible friend but was also a very helpful throughout the PhD due to his intellect, his scientific knowledge and his academic advice. Likewise, his fiancé Dr Bhavana Gupta was an incredible friend and provided excellent advice throughout this project on both an academic and personal level as such I am grateful for everything.

I would like to express a special thanks to the amazing Sabrina Lewis (Ba Sing Se!) for her love, support and incredible patience, particularly during the writing/COVID19 lockdown phase.

Finally, none of this would have ever been possible without the love and support of the most important people in my life, my **family** my dad, my mum and my sisters Jessica and Maria, who have always supported me and are the source of my drive in my life. This is particular true for my mum and dad who supported me, pushed me and believe in me throughout my academic life in spite of the challenges associated with my dyslexia and dyspraxia.

## **Abstract**

The neuronal ceroid lipofuscinoses (NCLs) are a group of childhood-onset neurodegenerative lysosomal storage diseases (LSDs) characterised by the accumulation of autofluorescent lipopigment in a variety of cells and tissue, particularly neurons. LSDs are inherited rare diseases that arise from mutations in genes encoding endo-lysosomal proteins, causing the intra-lysosomal accumulation of material such as lipids, proteins and polysaccharides. To develop therapies to mitigate these debilitating diseases, robust cell-based drug screens using cellular phenotypes can be developed. These phenotypes can also provide therapeutic targets.

This project explores cellular phenotypes in CLN8 patient cells by first investigating common LSD phenotypes such as lysosomal storage, autophagy defects, ER stress,  $\text{Ca}^{2+}$  signalling and defects in lysosomal enzyme activities. CLN8 disease had a high degree of unexplained phenotypic variability between and within patient cell lines which was not observed with other LSD patient cells. Of the four CLN8 patient cell lines explored, one displayed some robust non-variable phenotypes, resulting in deeper phenotypic exploration of this cell line which identified defects in  $\text{Ca}^{2+}$  homeostasis such as decreased lysosomal  $\text{Ca}^{2+}$ .

Due to the high phenotypic variability in CLN8 patient cells, another method for compound screening was required. Niemann-Pick C1 (NPC1) disease was used as a model for all LSDs for the screening of potential therapeutic compounds given its extent of characterisation. Despite this, however, approved small molecules or those in clinical testing for NPC disease are often neglected by high-throughput screening (HTS) approaches. This project therefore aimed to uncover the reasons behind these failings by first validating a fast-growing NPC1 cell model with robust phenotypes to facilitate rapid drug screening and 2) exploring a whole range of variables that might explain why approved drugs are being missed. The ultimate aim is to deliver an improved approach for an HTS platform applicable to all LSDs.

This project then explored alternative drug screens using control cell material to identify drugs of benefit to CLN8 and possibly other LSDs. Previous studies have reported defects in galactosylceramidase (GALC) activity in CLN8 disease, mutations in which are known to cause Krabbe disease, another LSD. A high-throughput enzymatic drug screen to identify compounds that modulate GALC activity was

therefore prioritised. This identified ambroxol, ibudilast and mycophenolate mofetil as potential GALC chaperones and thus may be of benefit to LSDs such as Krabbe disease and CLN8 disease.

Finally, currently approved small molecule modulators of other LSDs or nutraceutical compounds that could be repurposed and used to treat CLN8 were tested. Miglustat, which reduces lysosomal storage of glycosphingolipids, was tested in CLN8, CLN2 and CLN7 patient cells. The potential effects of miglustat were explored using cellular phenotypes such as lysosomal volume, autophagic compartment, ganglioside GM1 storage and mis-localisation, mitochondrial  $\text{Ca}^{2+}$  and ER  $\text{Ca}^{2+}$ . Potential benefits to CLN7, CLN8 and particularly CLN2 patient cells was identified which merits further investigation in these diseases.

Curcumin is a nutraceutical that increases cytosolic  $\text{Ca}^{2+}$ . The potential benefit of two common curcumin nanoformulations (BCM95s and  $\text{SLN}_L$ ) on LSDs such as Niemann-Pick A, CLN3, CLN7, CLN8 and CLN10 were explored by investigating their effect on lysosomal volume and cholesterol accumulation. BCM95s may be of benefit to LSDs by overcoming reduced lysosomal  $\text{Ca}^{2+}$  levels in CLN7, CLN8 and possibly CLN10.  $\text{SLN}_L$  was conversely found to be cytotoxic due to a combination of the nanoparticle fatty acid lipid mix in conjunction with curcumin, detrimentally affecting the mitochondria. This highlights the importance of exploring the interaction between active components and their excipient formulations as the excipient itself may be detrimental to some diseases and reduce the benefits conferred by the active compound in isolation. This is, to our knowledge, the first report of a detrimental effect of an excipient on LSDs.

Overall, this study increased the understanding of the cellular pathologies underlying CLN8 disease, validated and characterised a fast-growing cellular model that may be used for high-throughput drug screening, identified compounds that may act as possible GALC chaperones, found that miglustat may be of benefit to certain NCLs and determined that curcumin may be beneficial to LSDs with decreased lysosomal  $\text{Ca}^{2+}$ , but that care should be taken with certain drug formulations. Together, this provides an advance in the identification of therapies for these debilitating diseases, and the screening of these compounds highlighted herein to progress toward the improvement of treatment and patient lives.

# Publications

## Publications directly resulting from this project

**Badell-Grau\***, R. A., Maguire\*, E., Waller-Evans, H. Haslett, L. J., Welton, J. L., Goike, J. Kirkham, E. D., Knifton, H. R., Clark, E. H., Shrestha, R., Alshehri, A. S., Wager, K., Webb, R. and Lloyd-Evans, E. (Submitted) Biological consequences of lipid nanoparticle drug delivery vectors on Alzheimer and lysosomal diseases.

## Publications during this project

**Badell-Grau, R. A.**, Cuff, J. P., Kelly, B. P., Waller, Evans, H. and Lloyd-Evans, E. (2020) The prevalence of reactive online searching in the COVID-19 pandemic. Journal of Medical Internet Research. DOI: 10.2196/19791

Cook\*, S. R., **Badell-Grau\***, R. A., Kirkham\*, E. D., Jones, K. M., Kelly, B. P., Winston, J., Waller-Evans, H., Allen, N. D., and Lloyd-Evans, E. (2020) Detrimental effect of zwitterionic buffers on lysosomal homeostasis in culture cell lines and iPSC-derived neurons. AMRC Open Research 2:21 DOI: <https://doi.org/10.12688/amrcopenres.12903.1>

Cuff, J. P., Hunt, R., Oluwaseun, S. Tercel, M. P. T. G., Morley, P., **Badell-Grau, R. A.**, Vaughan, I. P., Bell, J. R., Orozco-terWengel, P., Symondson, W. O. C. and Müller, C. T., (Under review) MEDI: Macronutrient Extraction and Determination from Invertebrates, a rapid, cheap and streamlined protocol. Methods in Ecology and Evolution

## **Publications in preparation for submission from this project**

**Badell-Grau\***, R. A., Barrios-Crispi\*, H. B., Evans\*, C., Alshehri, A. S., Mackeen M. and Lloyd-Evans, E. (In prep) A comparison of small molecules screening strategies for lysosomal storage disorders.

Best, H., **Badell-Grau, R. A.**, de Haviland, C. and Lloyd-Evans, E. (In prep) CLN7 cellular phenotypes and the effects of miglustat.

**Badell-Grau, R. A.**, and Lloyd-Evans, E. (In prep) Variability in cellular phenotypes between and within different CLN8 mutation.

Powell\*, S., **Badell-Grau\***, R. A., Haslett, L. J., Barrios-Crispi, H. B., Clark, E., Maguire, E., Goffin, E., Killick, N., Goike, J., Finn, K., Eldridge, A., Williams, I. M., Shrestha, R., Valionyte, E., Platt, F. M., Waller-Evans, H. and Lloyd-Evans, E. (In prep) Combination therapy of miglustat and metformin acts synergistically to rescue cellular phenotypes in a novel Niemann-Pick disease Type C 1 mouse astroglial cell line.

Fenn, D. G., **Badell-Grau, R. A.**, White, S., Tonkin, R., Lloyd-Evans, E. and Waller-Evans, H. (In prep) Characterisation of a recombinant lysenin toxin from a European *Eisnia foetida* strain with improved specificity for sphingomyelin.

Waller-Evans, H., Alshehri, A. S., **Badell-Grau, R. A.**, Best, H., Haslett, L. J., Maguire, E., Copner, J., Gruszka, M., Peterneva, K., Nutthakki, I., Churchill, G. C., Platt, F. M., Watson, P. J., Lloyd-Evans, E. (In prep) Lyso-glycosphingolipids induce reduction in lysosomal Ca<sup>2+</sup> and secondary Niemann Pick disease phenotypes across multiple lysosomal diseases

## **Conferences presented at**

1. BDFA Family conference, Stratford-upon-Avon, United Kingdom, 2016  
Drug development for lysosomal storage disease: a focused approach on the childhood epilepsy CLN8. **Badell-Grau, R. A.**, and Lloyd-Evans, E.
2. Life Science Research Network Wales Annual Drug Discovery Congress, Cardiff, United Kingdom, 2016  
Characterising the fundamental cell biology of CLN8 for the identification of potential therapies for the NCLs and lysosomal storage diseases. **Badell-Grau, R. A.**, Pertusati, F. and Lloyd-Evans, E.
3. European Study Group on Lysosomal Disease, Lyon, France, 2016  
Characterising the fundamental cell biology of CLN8 disease for the purpose of drug screening. **Badell-Grau, R. A.**, Alshehri, A. and Lloyd-Evans, E.
4. BDFA Family conference, Stratford-upon-Avon, United Kingdom, 2017  
Characterising the fundamental cell biology of CLN8 disease for the purpose of drug screening. **Badell-Grau, R. A.**, and Lloyd-Evans, E.
5. Life Science Research Network Wales Postgraduate Conference, Cardiff, United Kingdom, 2017  
Characterising the fundamental cell biology of CLN8 disease for the purpose of drug screening. **Badell-Grau, R. A.**, Pertusati, F. and Lloyd-Evans, E.
6. Life Science Research Network Wales Annual Drug Discovery Congress, Cardiff, United Kingdom, 2017  
Identifying potential therapies for the NCLs and lysosomal storage disease. **Badell-Grau, R. A.**, and Lloyd-Evans, E.
7. NCL 2018, London, United Kingdom, 2018  
Changes in expression of *CLN8* partially restores storage in patient cells with specific *CLN8* mutations. **Badell-Grau, R. A.**, Wyatt, S. and Lloyd-Evans, E.
8. European Study Group on Lysosomal Disease, Barcelona, Spain, 2019  
Curcumin as a Ca<sup>2+</sup> modulating therapy for LSDs. **Badell-Grau, R. A.**, Maguire, E., Waller-Evans, H., Eldridge, A. and Lloyd-Evans, E.

# Table of Contents

<b>Acknowledgements</b> .....	<b><i>i</i></b>
<b>Abstract</b> .....	<b><i>iii</i></b>
<b>Publications</b> .....	<b><i>v</i></b>
<b>Publications directly resulting from this project</b> .....	<b><i>v</i></b>
<b>Publications during this project</b> .....	<b><i>v</i></b>
<b>Publications in preparation for submission from this project</b> .....	<b><i>vi</i></b>
<b>Conferences presented at</b> .....	<b><i>vii</i></b>
<b>Table of Figures</b> .....	<b><i>xiii</i></b>
<b>Table of Tables</b> .....	<b><i>xvi</i></b>
<b>Abbreviations</b> .....	<b><i>xvii</i></b>
<b>Chapter 1: Introduction</b> .....	<b><i>1</i></b>
<b>1.1 The lysosome and lysosomal storage diseases (LSDs)</b> .....	<b><i>1</i></b>
1.1.1 Lysosomes .....	<i>1</i>
1.1.2 Lysosomal storage diseases (LSDs) .....	<i>6</i>
1.1.3 The role of the autophagy in LSDs.....	<i>8</i>
1.1.4 The role of the ER and ER stress in LSDs.....	<i>10</i>
1.1.5 Cellular Ca <sup>2+</sup> regulation and LSDs .....	<i>11</i>
1.1.6 Circadian rhythms and changes in gene expression in LSDs .....	<i>16</i>
<b>1.2 Neuronal ceroid lipofuscinosis</b> .....	<b><i>18</i></b>
1.2.1 Neuronal ceroid lipofuscinosis .....	<i>18</i>
1.2.2 NCL disease mechanisms.....	<i>21</i>
1.2.3 CLN8 disease.....	<i>23</i>
1.2.4 The CLN8 protein.....	<i>26</i>
<b>1.3 Current therapies for treating lysosomal storage disease</b> .....	<b><i>29</i></b>
1.3.1 Haematopoietic stem cell transplantation (HSCT) .....	<i>30</i>
1.3.2 Enzyme replacement therapy (ERT) .....	<i>30</i>
1.3.3 Gene therapy.....	<i>31</i>
1.3.4 Substrate reduction therapy (SRT) .....	<i>32</i>
1.3.5 Pharmacological Chaperone therapy .....	<i>33</i>
1.3.6 Neutraceuticals .....	<i>34</i>

1.3.7 Combination therapies.....	35
1.3.8 Novel therapies .....	36
<b>1.4 Aims &amp; Objectives.....</b>	<b>38</b>
<b>Chapter 2: Materials and Methods .....</b>	<b>40</b>
<b>2.1 Cell Culture .....</b>	<b>40</b>
2.1.1 Human fibroblasts (HF).....	40
2.1.2 Astroglial cell lines .....	41
2.1.3 Drug treatments .....	41
<b>2.2 Fixed Immunocytochemistry .....</b>	<b>42</b>
2.2.1 Paraformaldehyde cell fixation .....	42
2.2.2 Blocking buffer .....	43
2.2.3 Cholesterol staining with filipin .....	43
2.2.4 Ganglioside GM1 staining with FITC tagged cholera toxin B subunit .....	43
2.2.5 Antibody staining of HSP70 .....	44
2.2.6 Nucleus counter-staining.....	44
2.2.7 Coverslip mounting .....	44
<b>2.3 Live Cell staining .....</b>	<b>44</b>
2.3.1 Cell seeding .....	44
2.3.2 Lysosomal staining .....	45
2.3.3 Lysosomal 96-well plate assay.....	45
2.3.4 Autophagic compartment visualisation.....	46
2.3.5 Endoplasmic reticulum staining .....	46
2.3.6 Mitochondrial staining .....	46
2.3.7 Complete Hank's balance salt solution (HBSS).....	47
2.3.8 Ca <sup>2+</sup> measurements .....	47
2.3.9 Visualisation of Mitochondrial Ca <sup>2+</sup> levels.....	50
<b>2.4 Fluorescence microscopy .....</b>	<b>50</b>
2.4.1 Microscopy .....	50
2.4.2 Microscopy analysis.....	51
<b>2.5 Reverse transcription quantitative polymerase chain reaction (RT-qPCR) .....</b>	<b>52</b>
2.5.1 Cell seeding .....	52
2.5.2 RNA extraction .....	52
2.5.3 Reverse transcription .....	52
2.5.3 Quantitative polymerase chain reaction (qPCR) .....	52

<b>2.6 Lysosomal enzyme assays .....</b>	<b>54</b>
2.6.1 Cell homogenate preparation .....	54
2.6.2 Determining protein concentration .....	54
2.6.3 Enzyme activity fluorescent assays .....	55
<b>2.7 High-throughput enzyme drug screening .....</b>	<b>59</b>
2.7.1 Sample preparation.....	59
2.7.2 Galactosylceramidase (GALC) assay .....	59
2.7.3 Primary screen of FDA-approved drug library.....	60
2.7.4 Secondary screen of FDA-approved drug library.....	60
<b>2.8 Statistical Analysis .....</b>	<b>61</b>
<b>Chapter 3: CLN8 disease cellular phenotyping for the purposes of drug screening.....</b>	<b>62</b>
<b>3.1 Introduction .....</b>	<b>62</b>
3.1.1 CLN8 disease.....	62
3.1.2 Cellular phenotypes in LSDs .....	64
3.1.3 Primary patient fibroblast (HFs) .....	67
3.1.4 Chapter aims .....	68
<b>3.2 Summary of Methods .....</b>	<b>68</b>
<b>3.3 Results.....</b>	<b>69</b>
3.3.1 Lysosomal area in CLN8.....	69
3.3.2 Cholesterol staining in CLN8 HFs.....	72
3.3.3 Autophagy in CLN8 patient fibroblasts.....	73
3.3.4 Mitochondrial staining in CLN8 patient fibroblasts.....	74
3.3.5 Changes in mRNA expression in CLN8 patient cells .....	75
3.3.6 Lysosomal enzyme activities in CLN8 patient fibroblasts.....	84
3.3.7 Thapsigargin mediated ER Ca <sup>2+</sup> release in CLN8 patient fibroblasts .....	88
3.3.8 Further Ca <sup>2+</sup> in CLN8 534 HF .....	90
<b>3.4 Discussion.....</b>	<b>94</b>
3.4.1 Lysosomal expansion in CLN8.....	95
3.4.2 Cholesterol accumulation in CLN8 .....	97
3.4.3 Autophagic vacuole expansion in CLN8.....	97
3.4.4 Mitochondrial staining in CLN8 .....	98
3.4.5 Variability in CLN8 phenotypes and drug screening.....	98
3.4.6 Temporal changes in CLN8 mRNA .....	101
3.4.7 Changes in <i>TFEB</i> , <i>MTOR</i> , <i>MCOLN1</i> , <i>CLN5</i> and <i>CLN6</i> mRNA in CLN8 disease .....	103
3.4.8 Changes in lysosomal enzyme activity in CLN8 .....	106

3.4.9 Changes in SERCA-mediated Ca <sup>2+</sup> release in CLN8 .....	108
3.4.10 Further phenotypes in CLN8 534 HF .....	110
<b>3.5 Conclusion .....</b>	<b>111</b>
<b>Chapter 4: Developing a drug screening protocol for lysosomal storage diseases .....</b>	<b>113</b>
<b>4.1 Introduction .....</b>	<b>113</b>
4.1.1 NPC1 disease .....	113
4.1.2 Cellular drug screening.....	117
4.1.3 Chapter aims .....	117
<b>4.2 Summary of Methods .....</b>	<b>118</b>
<b>4.3 Results.....</b>	<b>119</b>
4.3.1 Lysosomal expansion in <i>Npc1</i> <sup>-/-</sup> glia.....	119
4.3.2 Ganglioside GM1 accumulation in <i>Npc1</i> <sup>-/-</sup> glia .....	120
4.3.3 Autophagic vesicle accumulation in <i>Npc1</i> <sup>-/-</sup> glia .....	121
4.3.4 ER stress in <i>Npc1</i> <sup>-/-</sup> glia .....	122
4.3.5 Choosing the most appropriate phenotype for a successful drug screen .....	123
4.3.6 Choosing an appropriate standardisation method .....	124
4.3.7 Determining the working concentration of arimoclomol for NPC1 .....	127
4.3.8 Cholesterol levels following arimoclomol treatment in <i>Npc1</i> <sup>-/-</sup> glia .....	129
4.3.9 Cholesterol levels following arimoclomol treatment in NPC patient HF .....	129
4.3.10 HSP70 levels following arimoclomol treatment in <i>Npc1</i> <sup>-/-</sup> glia .....	130
4.3.11 Arimoclomol-like compound drug screen using <i>Npc1</i> <sup>-/-</sup> glia.....	131
<b>4.4 Discussion.....</b>	<b>133</b>
4.4.1 Confirmation of NPC1 disease phenotypes in <i>Npc1</i> <sup>-/-</sup> glia.....	133
4.4.2 Selecting appropriate phenotypes for drug screening.....	134
4.4.3 Arimoclomol in NPC1 disease.....	137
4.4.4 Future work .....	139
<b>4.5 Conclusion .....</b>	<b>140</b>
<b>Chapter 5 Drug repurposing for lysosomal storage diseases .....</b>	<b>141</b>
<b>5.1 Introduction .....</b>	<b>141</b>
5.1.1 Drug repurposing.....	141
5.1.2 Enzyme assay high-throughput drug screening .....	142
5.1.3 Miglustat repurposing .....	142
5.1.4 Curcumin nutraceuticals.....	144
5.1.5 Chapter aims .....	145

<b>5.2 Summary of Methods .....</b>	<b>146</b>
<b>5.3 Results.....</b>	<b>148</b>
5.3.1 Galactosylceramidase (GALC) enzyme assay optimisation.....	148
5.3.2 GALC enzyme based high throughput drug screen .....	149
5.3.2 Secondary GALC enzyme screen to confirm the hits.....	152
5.3.3 Selecting modulators of GALC for cell-based screening.....	154
5.3.4 Repurposing miglustat for CLN2, CLN7 and CLN8 .....	156
5.3.5 Effect of miglustat on autophagy in CLN2, CLN7 and CLN8.....	157
5.3.6 Effect of miglustat on ganglioside GM1 in CLN2, CLN7 and CLN8.....	158
5.3.7 Effect of miglustat on Ca <sup>2+</sup> stores in CLN2, CLN7 and CLN8 .....	160
5.3.8 Lysosomal volume following miglustat in CLN8 .....	163
5.3.9 Curcumin nutraceuticals for NPC1, NPA, CLN3, CLN7, CLN8 and CLN10.....	164
<b>5.4 Discussion.....</b>	<b>178</b>
5.4.1 GALC enzyme drug screen.....	178
5.4.2 Miglustat for NCLs .....	182
5.4.3 Curcumin for LSD with Ca <sup>2+</sup> defects.....	187
<b>5.5 Conclusion .....</b>	<b>190</b>
<b><i>Chapter 6 Overall Discussion &amp; Conclusions .....</i></b>	<b><i>191</i></b>
<b>6.1 Summary of findings .....</b>	<b>191</b>
<b>6.2 Discussion.....</b>	<b>192</b>
6.2.1 CLN8 phenotypic variability.....	192
6.2.2 LSD drug screening model .....	193
6.2.3 LSD drug screening .....	195
<b>6.3 Future direction .....</b>	<b>197</b>
<b>6.4 Conclusions.....</b>	<b>200</b>
<b><i>References.....</i></b>	<b><i>201</i></b>
<b><i>Appendix.....</i></b>	<b><i>233</i></b>
<b>A3.1 Lysosomal enzyme assays in CLN8 patient fibroblasts.....</b>	<b>233</b>

## Table of Figures

Figure number	Figure heading	Page
<b>Figure 1.1</b>	Endo-lysosomal system	2
<b>Figure 1.2</b>	Sphingolipid biosynthesis pathway	4
<b>Figure 1.3</b>	Comparison of healthy (WT) lysosome vs an LSD lysosome	7
<b>Figure 1.4</b>	Outline of CLN8 protein structure	28
<b>Figure 2.1</b>	Drug mediated Ca <sup>2+</sup> release measurement protocol outline	47
<b>Figure 3.1</b>	Lysosomal area is variable between CLN8 patient fibroblasts.	70
<b>Figure 3.2</b>	Lysosomal area in CLN8 patient fibroblasts is highly variable.	71
<b>Figure 3.3</b>	Increased Cholesterol puncta in some CLN8 patient fibroblast.	72
<b>Figure 3.4</b>	Presence of autophagic compartment area is highly variable in CLN8 patient fibroblasts.	73
<b>Figure 3.5</b>	Mitochondrial area in CLN8 patient fibroblast.	75
<b>Figure 3.6</b>	Expression levels of Batten disease mRNAs in mouse liver over 42 hours.	76
<b>Figure 3.7</b>	Changes in the expression levels of CLN8 and TFEB mRNAs across different time courses.	79
<b>Figure 3.8</b>	CLN8 mRNA levels are variable between in CLN8 patient fibroblasts.	80
<b>Figure 3.9</b>	Changes in expression levels of LSDs associate mRNAs are altered CLN8 patient HF.	82
<b>Figure 3.10</b>	Following 100 nM dexamethasone treatment <i>CLN8</i> mRNA expression increases in control 1 HF and lysosomal area in CLN8 534 HF appears to decrease.	84
<b>Figure 3.11</b>	Heat map of changes lysosomal enzyme activity in CLN8 patient fibroblast.	86
<b>Figure 3.12</b>	Total Cathepsin B levels is increased in CLN8 534 HF.	88
<b>Figure 3.13</b>	Thapsigargin mediated Ca <sup>2+</sup> release is variable between CLN8 patient fibroblast.	89
<b>Figure 3.14</b>	CCCP and antimycin/oligomycin mediated Ca <sup>2+</sup> release in CLN8 patient fibroblasts.	91
<b>Figure 3.15</b>	Ionomycin and Ryanodine mediated Ca <sup>2+</sup> release in CLN8 patient fibroblasts.	92
<b>Figure 3.16</b>	GPN-mediated lysosomal Ca <sup>2+</sup> is decreased but not basal cytoplasmic Ca <sup>2+</sup> CLN8 534 HF.	94
<b>Figure 4.1</b>	Lysosomal area is increase in <i>Npc1</i> <sup>-/-</sup> glia.	120
<b>Figure 4.2</b>	Ganglioside GM1 is increased in <i>Npc1</i> <sup>-/-</sup> glia.	121

<b>Figure 4.3</b>	Autophagic compartments are increased in <i>Npc1</i> <sup>-/-</sup> glia.	122
<b>Figure 4.4</b>	Endoplasmic reticulum area is increased in <i>Npc1</i> <sup>-/-</sup> glia.	123
<b>Figure 4.5</b>	Miglustat treatment has no effect on cholesterol storage but does affect lysosomal volume	124
<b>Figure 4.6</b>	Nuclear staining is variable across LSDs	126
<b>Figure 4.7</b>	Lysosomal 96-well plate assay comparing different cell seeding densities in <i>Npc1</i> <sup>+/+</sup> and <i>Npc1</i> <sup>-/-</sup>	127
<b>Figure 4.8</b>	Arimoclomol treatment decreases lysosomal volume at one concentration but not others in <i>Npc1</i> <sup>+/+</sup> and <i>Npc1</i> <sup>-/-</sup> glia cells	128
<b>Figure 4.9</b>	Cholesterol levels <i>Npc1</i> <sup>-/-</sup> glia treated with arimoclomol	129
<b>Figure 4.10</b>	Cholesterol storage levels NPC1 patient cells treated with arimoclomol	130
<b>Figure 4.11</b>	HSP70 levels <i>Npc1</i> <sup>-/-</sup> glia treated with arimoclomol	131
<b>Figure 4.12</b>	Arimoclomol-like compound screen in <i>Npc1</i> <sup>-/-</sup> glia	132
<b>Figure 5.1</b>	Sphingolipid biosynthesis pathway and miglustat mechanism of action	144
<b>Figure 5.2</b>	GALC enzyme assay optimisation	149
<b>Figure 5.3</b>	Heatmaps of GALC primary drug screen.	150
<b>Figure 5.4</b>	Statistical quality control of the GALC primary drug screen	151
<b>Figure 5.5</b>	Determination of thresholding for the selection of activating and inhibiting compounds of GALC	152
<b>Figure 5.6</b>	Heatmaps of GALC secondary drug screen	153
<b>Figure 5.7</b>	Secondary screen on destabilised GALC	154
<b>Figure 5.8</b>	Structure of compounds taken further for cell-based screening	155
<b>Figure 5.9</b>	Effect of miglustat on lysosomal area in CLN2, CLN7 and CLN8 patient cells	157
<b>Figure 5.10</b>	Autophagic compartment area in CLN2, CLN7 and CLN8 patient cells following miglustat treatment	158
<b>Figure 5.11</b>	Effect of miglustat on ganglioside GM1 punctate distribution in CLN2, CLN7 and CLN8 patient fibroblasts	160
<b>Figure 5.12</b>	CCCP mediated mitochondrial Ca <sup>2+</sup> release in CLN2, CLN7 and CLN8 patient fibroblast following miglustat treatment	161
<b>Figure 5.13</b>	Ryanodine mediated Ca <sup>2+</sup> release in CLN2, CLN7 and CLN8 patient fibroblast following miglustat treatment	162
<b>Figure 5.14</b>	Lysotracker plate assay in CLN8 patient cells following miglustat treatment	163
<b>Figure 5.15</b>	GPN-mediated lysosomal Ca <sup>2+</sup> is decreased in NPC1, CLN7 474, CLN8 and CLN10 but increased in NPA and CLN3	165
<b>Figure 5.16</b>	Thapsigargin mediated Ca <sup>2+</sup> is increased in CLN7, CLN8 and CLN10 but decreased in NPC	167

<b>Figure 5.17</b>	Ionomycin mediated $\text{Ca}^{2+}$ is significantly increased in CLN10 but not altered in NPC1, NPA, CLN3, CLN7 and CLN8	169
<b>Figure 5.18</b>	Basal $\text{Ca}^{2+}$ is unchanged in NPC1, NPA, CLN7 CLN8 and CLN10	170
<b>Figure 5.19</b>	Lysosomal area in NPA, CLN3, CLN7, CLN8 and CLN10 following patient cells following curcumin BCM95s	172
<b>Figure 5.20</b>	Elevated cholesterol area in NPA, CLN3, CLN7 and CLN8 and CLN10 is not affected by BCM95s treatment	174
<b>Figure 5.21</b>	Treatment with curcumin nanoformulations decreases Antimycin / Oligomycin mediated mitochondria $\text{Ca}^{2+}$ release in control HFJs	176
<b>Figure 5.22</b>	Mitochondrial $\text{Ca}^{2+}$ staining in <i>Npc1<sup>-/-</sup></i> and control glia following 24-hour treatment with 30 $\mu\text{M}$ curcumin nanoformulations	177

## Table of Tables

Table number	Table heading	Page
<b>Table 1.1</b>	Overview of NCLs	18
<b>Table 1.2</b>	Function of NCL proteins	20
<b>Table 1.3</b>	CLN8 disease clinical phenotypes	24
<b>Table 2.1</b>	Primer & probe set for qPCR experiments	53
<b>Table 2.2</b>	Lysosomal enzyme assay conditions	56
<b>Table 3.1</b>	Outline of patient cell lines used in Chapter 3	63
<b>Table 3.2</b>	Summary of phenotypic variability in CLN8 HF <sub>s</sub> compared to Control HF <sub>s</sub>	95
<b>Table 4.1</b>	Examples of common cellular phenotypes in LSD <sub>s</sub>	115
<b>Table 4.2</b>	Outline of patient cell lines used in Chapter 4	117
<b>Table 5.1</b>	Outline of patient cell lines used in Chapter 5	146
<b>Table 5.2</b>	Physical and chemical properties of compounds that activated destabilised GALC and were chosen for subsequent cell-based screening	155
<b>Table 5.3</b>	Properties of the curcumin nanoformulations screened	171
<b>Table 6.1</b>	Experiments impacted due to lab closure	198

## Abbreviations

**4MU:** 4-Methylumbelliferone  
**AAV:** Adeno-associated virus  
**AMC:** 7-Amindo-4-methylcoumarine  
**ASM:** Acid sphingomyelinase  
**B2M:** Beta-Microglobulin  
**BBB:** Blood brain barrier  
**BCA:** Bicinchoninic acid  
**BHQ1:** Black hole quencher-1  
**BiP:** Binding immunoglobulin protein  
**BSA:** Bovine serum albumin  
**CCCP:** Carbonyl cyanide m-chlorophenyl-hydrazone  
**cdNA:** Complimentary deoxyribonucleic acid  
**CHO:** Chinese hamster ovary  
**CHOP:** CCAAT-enhancer-binding protein  
**CLEAR:** Coordinate lysosomal expression and regulation network  
**CLN:** Ceroid lipofuscinosis, neuronal  
**CNS:** Central nervous system  
**CtxB-FITC:** Cholera toxin B subunit with FITC tag  
**D-PBS:** Dulbecco's phosphate-buffered saline  
**DMEM:** Dulbecco's Modified Eagle's Medium  
**DMSO:** Dimethyl sulfoxide  
**DNA:** Deoxyribonucleic acid  
**EDTA:** Ethylenediaminetetraacetic acid  
**EGRESS:** ER-to-Golgi relaying of enzymes of the lysosomal system  
**EMA:** European Medicines Agency  
**EPMR:** Progressive epilepsy with mental retardation  
**ER:** Endoplasmic reticulum  
**ERGIC:** ER-Golgi intermediate compartment  
**ERT:** Enzyme replacement therapy  
**FAM:** Fluorescein amidite  
**FBS:** Foetal bovine serum  
**FDA:** U.S. Food & Drug Administration

**FITC:** Fluorescein isothiocyanate  
**GALC:** Galactosylceramidase  
**GalCer:** Galactosylceramide  
**GAPDH:** Glyceraldehyde 3-phosphate dehydrogenase  
**GPN:** Glycyl-L-phenylalanine- $\beta$ -naphthylamide  
**GWAS:** Genome wide association study  
**HBSS:** Hank's balanced salt solution  
**HDAC:** Histone deacetylases  
**HF:** Human fibroblast  
**HMU:** 6-Hexadecanoylamino-4-methylumbelliferyl-phosphorylcholine  
**HSCT:** Haematopoietic stem cell transplantation  
**HSP70:** Heat shock protein 70  
**HTS:** High-throughput screening  
**IP<sub>3</sub>:** Inositol 1,4,5-trisphosphate  
**LAMP1:** Lysosomal-associated membrane protein 1  
**LAMP2:** Lysosomal-associated membrane protein 2  
**LBPA:** Lyso-(bis)-phosphatidic acid  
**LC3:** Light chain 3  
**LDL:** Low density lipoprotein  
**LSD:** Lysosomal storage disease  
**MCA:** Methyl coumaric acid  
**MPS:** Mucopolysaccharidosis  
**mRNA:** Messenger ribonucleic acid  
**MTOR:** Mammalian target rapamycin  
**NAADP:** Nicotinic acid adenine dinucleotide phosphate  
**NAGA:**  $\alpha$ -N-acetylgalactosaminidase  
**NCL:** Neuronal ceroid lipofuscinosis  
**NPA:** Niemann Pick Type A  
**NPC1:** Niemann-Pick type C1  
**ORP1L:** Oxysterol-binding-related protein 1L  
**PBS:** Phosphate buffered saline  
**PFA:** Paraformaldehyde  
**PKC:** Protein kinase C  
**PPT1:** Palmitoyl-protein thioesterase  
**qPCR:** Quantitative polymerase chain reaction

**RNA:** Ribonucleic acid  
**RNase:** Ribonuclease  
**RT-qPCR:** Reverse transcription quantitative polymerase chain reaction  
**RyR:** Ryanodine receptor  
**SCMAS:** Subunit C of the mitochondrial F<sub>0</sub>/F<sub>1</sub> synthase  
**SCN:** Suprachiasmatic nucleus  
**SERCA:** Sarco-endoplasmic reticulum Ca<sup>2+</sup> ATPase  
**SNP:** Single nucleotide polymorphism  
**SRT:** Substrate reduction therapy  
**TBP:** Tata binding protein  
**TCNa:** Sodium taurocholate  
**TFEB:** Transcription factor ER  
**TPCs:** Two-pore channels  
**TPP1:** Tripeptidyl peptidase 1  
**TRPML:** Transient receptor potential cation channel, mucolipin subfamily

# **Chapter 1: Introduction**

## **1.1 The lysosome and lysosomal storage diseases (LSDs)**

### **1.1.1 Lysosomes**

The lysosome is often referred to as the recycling centre of the cell as its main role is to enzymatically degrade cellular material. Lysosomes, first described by Christian de Duve (1955), are acidic organelles with a pH of around 4.5 that are found in all mammalian cells, and make up 5% of the total volume of the cell (Luzio et al. 2007). Lysosomes are generally described as spherical membrane-bound compartments no more than 1  $\mu\text{m}$  in diameter; however, the shape, size, number, localisation and enzymes present in the lysosome in cells can vary drastically depending on the material it has to degrade (Ballabio 2016; Perera and Zoncu 2016).

Macromolecules are delivered to lysosomes by endocytosis, phagocytosis and autophagy (Figure 1.1). Encased by a 7-10 nm single phospholipid bilayer membrane, within the lysosome there are a myriad of catabolic enzymes to break down and recycle the macromolecules delivered to the lysosome (Ballabio 2016; Saftig et al. 2010). The phospholipid bilayer is extremely important to protect the rest of the cell from degradation from the catabolic enzymes. Due to the acidity and high content of hydrolytic enzymes found in the lysosome, there is a layer of highly glycosylated protein such as lysosomal-associated membrane protein 1 and 2 (LAMP1 and LAMP2, ~40% of the total lysosomal protein content). This layer of highly glycosylated protein is called the glycocalyx, and creates a protective barrier that prevents lytic enzymes in the lysosomes from breaking down the lysosomal membrane and thus prevents cellular self-digestion (Cox and Cachón-González 2012; Platt et al. 2012; Perera and Zoncu 2016).

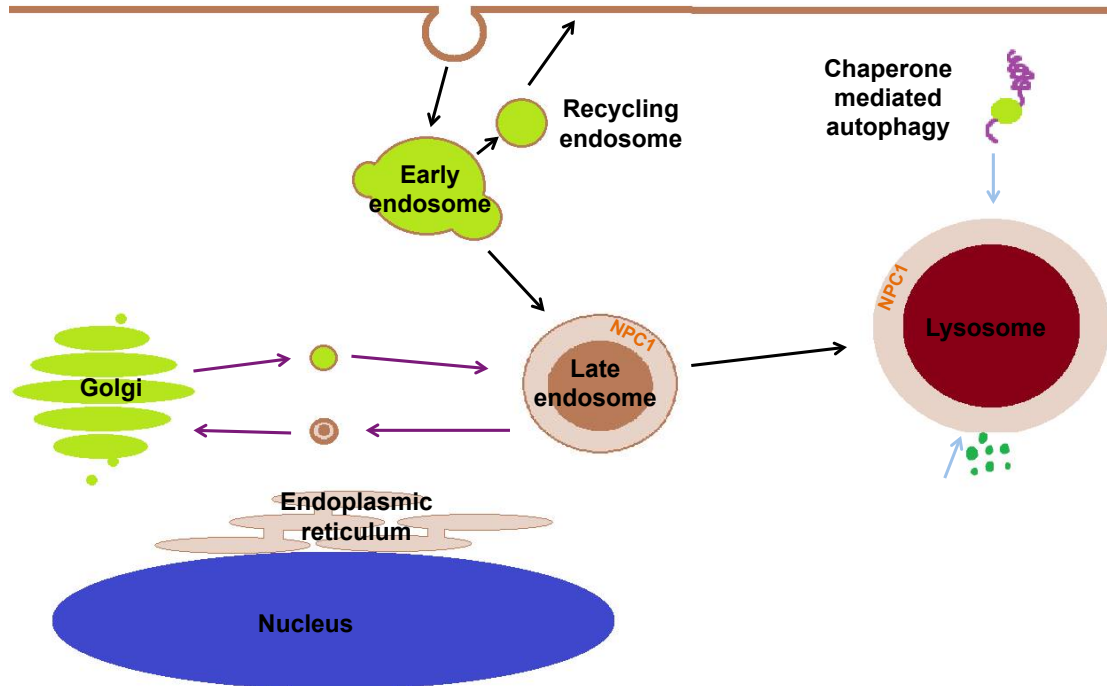


**Figure 1.1: Endo-lysosomal system.** The endo-lysosomal system is involved in the degradation and recycling of macromolecules including protein and lipids. Trafficking within this system is affected in lysosomal storage diseases such as Niemann Pick Type C (NPC) disease. NPC1 localisation in late endosome and lysosomes is shown in orange. Arrows denote the movement through the endo-lysosomal system to lysosomes, where black and light blue arrows denote the endocytic and autophagic systems, respectively. Arrow indicates the flow of macromolecules to the lysosome. The blue arrow indicates autophagy processes, black arrows denote endocytic processes. Figure adapted from (Lloyd-Evans and Haslett 2016).

#### 1.1.1.1 Lysosomal biogenesis regulation network

The mechanisms behind the regulation of lysosomal function are not fully understood. Lysosomal biogenesis and autophagy, the process by which dysfunctional cellular components are broken down, are thought to be transcriptionally regulated by a network of genes called the coordinate lysosomal expression and regulation network (CLEAR). These genes are controlled by the transcription factor EB (TFEB) (Sardiello et al. 2009; Ballabio 2016). Settembre *et al.* (2013) demonstrated that TFEB overexpression leads to a rescue of lysosomal storage disease (LSD) phenotypes by inducing lysosomal biogenesis. Furthermore, TFEB overexpression has been shown to induce lysosomal exocytosis (Medina et al. 2011). Other studies have shown that other transcription factors similar to TFEB such as TFE3 can also promote lysosomal clearance (Martina et al. 2014). Nonetheless, it is widely accepted that TFEB is the master regulator of lysosomal biogenesis (Ballabio 2016).

### 1.1.1.2 Lysosomal functions

The lysosome performs its primary function of degrading and recycling with around 60 different hydrolytic enzymes and transporter proteins (Ballabio 2016). These enzymes have an acidic pH optima which facilitates the degradation of various cellular materials such as lipids, proteins, carbohydrates, deoxyribonucleic acid (DNA) and ribonucleic acid (RNA) (Schöder et al. 2010). Lysosomes are not, however, merely the recycling centre of the cell, as they also perform an important role in several other cellular processes, such as lipid metabolism, plasma membrane repair and cellular signalling (Schulze and Sandhoff 2011; Ballabio 2016).

The lysosome can fuse with the plasma membrane, via lysosomal exocytosis, to repair wounds in a process mediated by increased cytosolic  $\text{Ca}^{2+}$  (Rodríguez et al. 1997). Additionally, studies have found that lysosomes contain  $\sim 500 \mu\text{M}$   $\text{Ca}^{2+}$  making them the second largest  $\text{Ca}^{2+}$  store in the cell after the endoplasmic reticulum (ER), and have an important role in intracellular signalling (Christensen et al. 2002; Lloyd-Evans et al. 2008). This demonstrates that the lysosome possesses many crucial cellular roles beyond just degrading and recycling cellular material.

### 1.1.1.3 Lysosomes and lipid

The lipid composition of vesicle membranes is an extremely important regulator of endo-lysosomal function, since lipids are bioactive molecules involved not only in anchoring and transporting proteins, but also in regulating their function. Current understanding of lipid biosynthesis, transport and breakdown is therefore crucial to fully understanding the function of lysosomes, the primary sites of lipid catabolism, in these processes and how they are impaired in disease. This means that dysfunction in the endo-lysosomal system leads to lipid accumulation, and *vice-versa* (Gault et al. 2010).

Sphingolipids are exclusively degraded within the lysosomal system and are considered the most potent signalling lipids (Gault et al. 2010). Therefore, sphingolipids are one of the most well-studied lipid classes (Kolter and Sandhoff 2005; Schulze and Sandhoff 2011). Sphingolipids are a family of lipids made up of a ceramide backbone (Figure 1.2) with glycosphingolipids having a carbohydrate group attached at the C-1 position of the backbone (Magnusson 1994). The ceramide

backbone of these lipids comprises of a long carbon chain sphingoid base, fatty acid, and an amine head group. Sphingolipids have one polar group and two non-polar tails. The main sphingoid base, which acts as a highly active signalling molecule is sphingosine (Fyrst and Saba 2010).

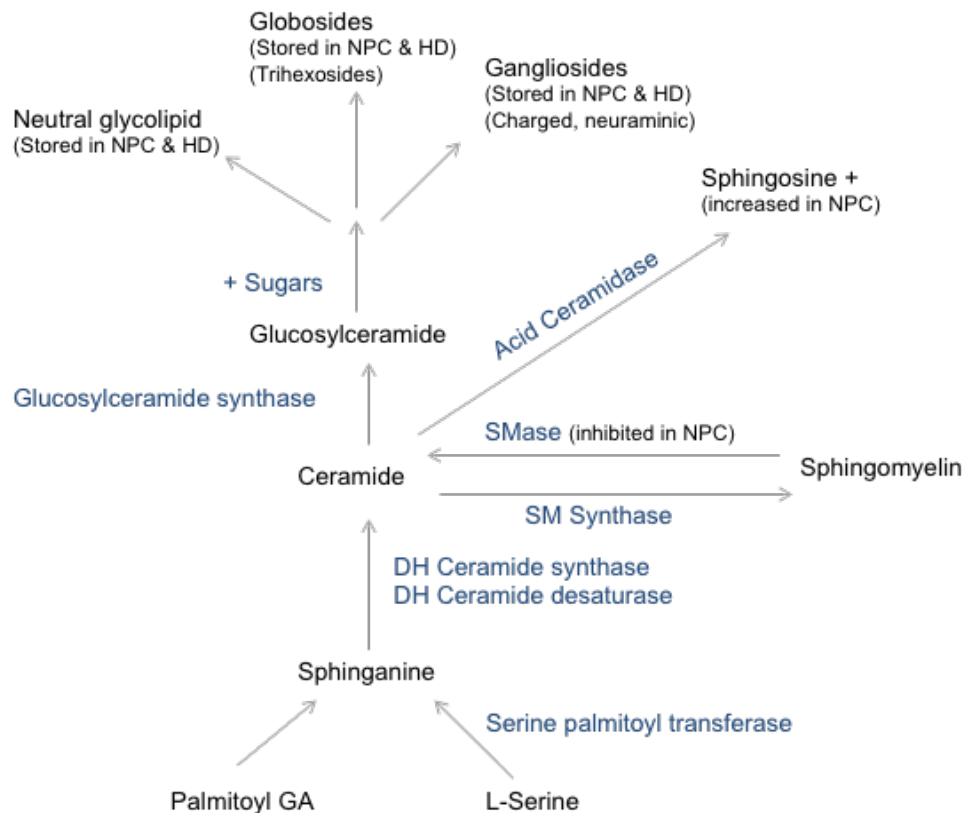


**Figure 1.2: Sphingolipid biosynthesis pathway.** Sphingolipids synthesis begins in the endoplasmic reticulum by the enzyme serine palmitoyl transferases which condense L-serine and palmitoyl CoA to give rise to sphinganine (Gault et al. 2010). Dihydroceramide synthase and Dihydroceramide desaturase enzymes then give rise to ceramide which is a membrane anchor for sphingolipids with a sphingosine backbone (Gault et al. 2010) and a pro-apoptotic lipid. This may then be further metabolised to form either sphingomyelin or glycosphingolipids. In order to synthesis glycosphingolipids, ceramide must be transported to the Golgi where a glucose moiety is added by glucosylceramide synthase (Gault et al. 2010). Glucosylceramide can then be modified into lactosylceramide by the addition of galactose. This can then be further modified into other glycosphingolipids such as gangliosides (important central nervous system lipids) through the addition of a sialic acid group. Sphingomyelin may be synthesised at the Golgi or the plasma membrane through the addition of phosphocholine to ceramide by sphingomyelin synthase (Gault et al. 2010).

Lipids such as the sphingolipids are transported via the endo-lysosomal system to the plasma membrane which is important to help maintain membrane structure as they partition into signalling micro-domains (formerly known as lipid rafts) and act as recognition molecules for immune receptors or as internalisation partners for growth factors such as brain-derived neurotrophic factor binding p75 neurotrophin receptor (MacPhee and Barker 1997; Simpson et al. 2004; Gault et al. 2010).

Sphingolipids are broken down in lysosomes following delivery from the plasma membrane via the endo-lysosomal system (Figure 1.1) through early endosomes which are transported through late endosomes to eventually form lysosomes (Schulze and Sandhoff 2011). As previously mentioned, the lysosome degrades materials such as lipids so that the components may be recycled back to the cell via lysosomal membrane transporters or vesicular transport to other organelles. Sphingosine, the end product of sphingolipid degradation within lysosomes, is either transported to the ER and converted to ceramide, or converted to sphingosine 1-phosphate, an important signalling molecule that is crucial for correct brain and vascular development (Kolter and Sandhoff 2005; Schulze and Sandhoff 2011). This illustrates further that lysosomal function is critical and highlights the impact that impairments to lysosomal function may have on other cellular pathways (Kunkel et al. 2013).

Previous studies have estimated that in an hour, around half of the plasma membrane is endocytosed: most is recycled back to the plasma membrane, with the remainder being degraded in the lysosome. This highlights the lysosome's importance in cell membrane homeostasis (Schulze and Sandhoff 2011). Another important lipid crucial for endocytic function regulation is cholesterol, whose levels inside the cell are largely controlled by its uptake and recycling through the lysosome via the endo-lysosomal system (Chang et al. 2006).

Cholesterol is internalised by clathrin-dependant endocytosis of low density lipoprotein (LDL) bound to the LDL receptor (Chang et al. 2006). Once endocytosed, cholesterol dissociates from the LDL which separates from its receptor, which is recycled to the plasma membrane via late endosomes. Cholesterol is liberated from LDL within lysosomes via the action of lysosomal acid lipase (Du and Yang 2013). The levels of cholesterol in the plasma membrane are key in regulating membrane fluidity, further indicating the importance of not only cholesterol localisation in membranes, but of the endo-lysosomal system in plasma membrane homeostasis (Kolter and Sandhoff

2005; Schulze and Sandhoff 2011). Defects in the metabolism or recycling of cholesterol in or out of lysosomes, as has been reported in lysosomal storage diseases, can have significant detrimental effects on not only endo-lysosomal function but plasma membrane maintenance (Millard et al. 2000; Wassif et al. 2002).

### **1.1.2 Lysosomal storage diseases (LSDs)**

Lysosomal storage diseases (LSDs) are a group of approximately 70 genetically inherited disorders caused by lysosomal dysfunction, leading to accumulation of material in lysosomes (Figure 1.3). This accumulation disrupts lysosomal function, which affects cellular processes in all cell types. Most LSDs are neurodegenerative diseases that comprise the most common cause of neurodegeneration in children. Together, LSDs have an estimated prevalence of approximately 1 in 7,000 live births (Meikle et al. 1999; Meikle and Hopwood 2003). This number, however, may in fact be an underestimation, as there are likely to be undiagnosed cases (Wassif et al. 2016). An example of this is the LSDs Nieman Pick Type C1 (NPC1) which has an estimated prevalence of around 1 in 104,000; however, bioinformatics tools estimated the incidence of NPC1 disease may be around 1 in 92,000 (Wassif et al. 2016).

Recently, evaluations of NPC1 variants and late onset forms of the disease, implies the incidence of the disease may be around 1 in 39,000 (Wassif et al. 2016). This suggests that the incidence of LSDs as a whole may in fact be higher than is currently believed. The majority of LSD patients are born with no apparent health problems. Nonetheless, with time, these diseases affect patients' blood vessels, kidneys, heart and nervous systems simultaneously (Platt et al. 2012). The clinical symptoms typically begin during childhood but there are, however, adult-onset forms of some LSDs. Clinically, most LSDs are characterised by progressive neurodegeneration.

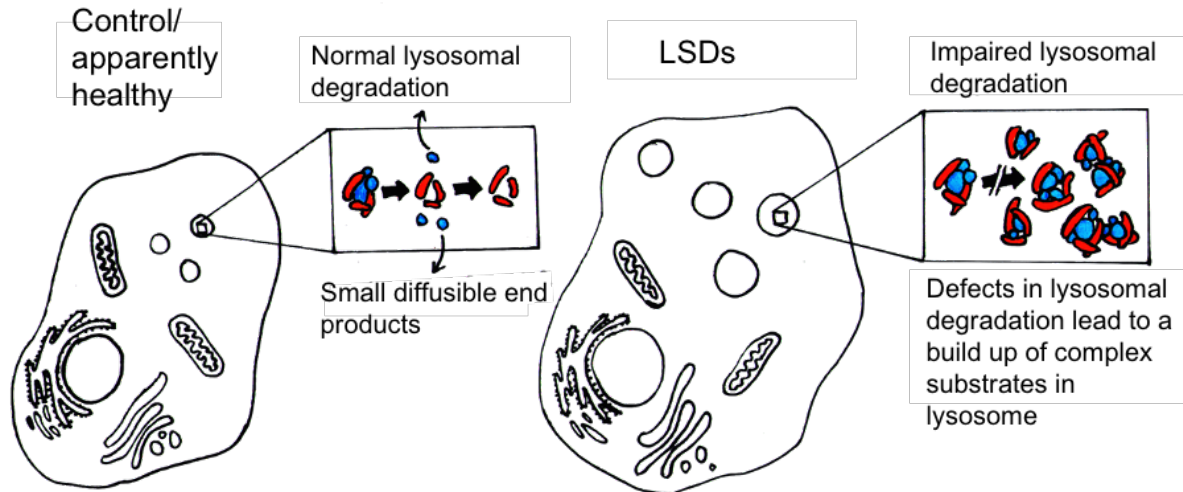


**Figure 1.3: Comparison of healthy (WT) lysosome vs an LSD lysosome.** LSDs are caused by the inability of the lysosome to clear material, leading to the expansion and accumulation of lysosomes within the cell which causes cellular dysfunction.

Mutations in genes involved in lysosomal function are responsible for LSDs; for example, Gaucher disease is caused by mutations in *GBA1*, which encodes for the glucocerebrosidase enzyme that degrades the glycosphingolipid glucosylceramide, leading to accumulation of glucosylceramide in lysosomes (Broadhead and Butterworth 1977). LSDs can also arise from mutations in non-enzymatic lysosomal proteins, such as the LSD NPC1 disease which arises from loss-of-function mutations in the *NPC1* gene encoding the lysosomal transmembrane protein NPC1 leading to the storage of multiple lipids (Lloyd-Evans and Platt 2010). In this disease, loss of the NPC1 protein leads to retardation of transport between the early and late endosomes, and an almost complete cessation of fusion between late endosomes and lysosomes and the recycling of lipids from lysosomes.

As LSDs are caused by different mutations in different lysosomal associated proteins, storage material can be different between different LSDs. For example, in the NPC1 disease the primary storage material is sphingosine (Lloyd-Evans et al. 2008). In many of the neuronal ceroid lipofuscinosis (NCLs), discussed below (Section 1.2), subunit C of the mitochondrial  $F_0/F_1$  ATP synthase (SCMAS; Table 1.1) has been reported to be the main storage material in lysosomes (Elleder et al. 1997; Anderson et al. 2013; Mukherjee et al. 2019). In some NCLs, however, the main storage material has been reported to be the sphingolipid activator proteins, saposins A & D. The saposins are lysosomal glycosphingolipid binding proteins that deliver hydrophobic

lipids to their corresponding enzymes (Schulze and Sandhoff 2011; Schulze and Sandhoff 2014).

The accumulation of lipids in lysosomes in LSDs leads to an increase in lysosome volume and number (Lloyd-Evans and Haslett 2016; Lloyd-Evans and Waller-Evans 2019). Given the lysosome's aforementioned involvement in many cellular processes, lysosomal dysfunction is detrimental to other cellular processes such as  $\text{Ca}^{2+}$  signalling and autophagy. Although LSDs are caused by mutations in a range of proteins that lead to different materials accumulating in lysosomes, they have many overlapping cellular and clinical features such as the Neuronal ceroid lipofuscinosis disease outlined below in Section 1.2 (Platt et al. 2012).

Lysosomal dysfunction has been linked to numerous other neurodegenerative diseases such as Alzheimer, Parkinson, and Huntington diseases (Badell-Grau 2016; Malik et al. 2019; Nixon 2020). Lee *et al.* (2010a) found that mutations in *PSEN1*, which encodes the Alzheimer disease-associated protein Presenilin 1, leads to lysosomal dysfunction and contributed to disease pathogenesis observed in familial Alzheimer patients (Lee et al. 2015). Other studies have found that people heterozygous for the mutation in *GBA1* that causes Gaucher disease have a 6-11 fold increased rate of developing Parkinson disease (Rosenbloom et al. 2011). Moreover, the foremost risk factor for Parkinson disease is mutation in the *GBA1* gene (Sidransky et al. 2009). Likewise, many cellular pathways that have been reported to be altered in other neurodegenerative diseases, like Alzheimer disease, Parkinson disease and Huntington disease, have also been reported to have a role in LSDs.

### **1.1.3 The role of the autophagy in LSDs**

Autophagy is a cellular process that removes dysfunctional or unnecessary cellular material such as protein, cellular debris, damaged organelles and lipids via the lysosome. There are multiple genes that encode the machinery required for autophagy to begin. There are two ubiquitination-like systems for the development of autophagosomes. One is a complex containing the proteins Atg5-Atg12-Atg6 and the other is phosphatidylethanolamine-conjugated microtubule-associated protein 1 light chain 3 (LC3-II) (Mizushima et al. 1998; Klionsky 2014).

The process begins with a phagophore, which is a lipid bilayer thought to be donated by the endoplasmic reticulum (ER), endosome and/or Golgi; however, its precise origin is unclear (Wei et al. 2018). The phagophore collects cargo and material for degradation, expanded into a double membrane vesicle called the autophagosome. The autophagosome is then delivered to the lysosome and fuses with it to form the autolysosome, enabling the lysosome's hydrolytic enzymes to break down or recycle the material. Autophagosomes can also mature by fusing with late endosomes to create amphisomes, which eventually fuse with the lysosome to degrade and recycle the cargo (Glick et al. 2010).

TFEB, the transcription factor that regulates lysosomal biogenesis as mentioned previously, also regulates the expression of genes related to autophagy (Settembre et al. 2011; Settembre and Medina 2015). Medina *et al.* (2015) reported that lysosomal  $\text{Ca}^{2+}$  signalling through the transient receptor potential cation channel mucolipin 1 (TRMPL1) lysosomal  $\text{Ca}^{2+}$  channel incites TFEB to localise to the nucleus. Both of these further highlight the link between lysosomal function and autophagy.

Therefore, proper lysosomal function is crucial for autophagy and, as such, lysosomal dysfunction can lead to defects in autophagy which have been linked to neurodegenerative diseases (Lee et al. 2010a; Thelen et al. 2012; Nixon 2013; Vidal-Donet et al. 2013; Boland et al. 2018; Shipley 2019). Defects in autophagic pathways include accumulation of autophagic vacuoles, increased autophagosome-associated LC3-II protein, and reduced co-localisation of LC3-II with LAMP1 (Glick et al. 2010).

Autophagy is known to be upregulated under stress conditions such as lipid accumulation in order to remove toxic material and promote cell survival (Glick et al. 2010; Nixon 2013). Martinez-Vicente *et al.* (2010) reported that elevation in reactive oxygen species and cell stress due to auto-lysosomal defects lead to brain cell death in Huntington disease. It is not surprising that neurodegeneration is particularly sensitive to lysosomal and autophagy defects as post-mitotic neurons are unable to proliferate after differentiation, making the nervous system especially sensitive to lysosomal and autophagy defects as they rely on autophagy to clear cellular waste (Son et al. 2012). The role of autophagy in neurodegeneration and LSDs not only highlights the importance of autophagy but also the importance of proper lysosomal function.

#### 1.1.4 The role of the ER and ER stress in LSDs

The ER is the major hub for protein folding, quality control and N-glycosylation, and is the biggest source of  $\text{Ca}^{2+}$  store for intracellular  $\text{Ca}^{2+}$  signalling. The protein and lipid content of the ER is highly controlled in order to maintain its essential quality-control functions (Platt et al. 2012). As lipid content is tightly regulated in the ER, proper lysosomal function is important for correct ER function. The lysosome and ER interact with one another via membrane contact sites, which are domains formed when the organelles are in close proximity.

An example of a membrane contact site mechanism that is well characterised is the interaction between the ER and the endo-lysosomal vesicles in response to cholesterol (Johansson et al. 2007; Rocha et al. 2009). Endosomes with high levels of cholesterol tend to gather close to the periphery of the cell; whereas, endosomes with low levels of cholesterol congregate close to the centre of the cell. In low levels of cholesterol the oxysterol-binding-related protein 1L (ORP1L) binds ER-bound Vamp-associated proteins creating a membrane contact site between the endosome and the ER (Johansson et al. 2007; Rocha et al. 2009).

Membrane contact sites between the ER and the endo-lysosome system have also been reported to play a role in  $\text{Ca}^{2+}$  modulation. These contact sites between the ER and lysosomes were found to be rich in inositol 1,4,5-trisphosphate ( $\text{IP}_3$ ) receptors (outlined below in Section 1.1.5.1) which selectively deliver  $\text{Ca}^{2+}$  from the ER to the lysosome (Atakpa et al. 2018). This interaction between the ER and the lysosome is dependent on lysosomal pH; increasing lysosomal pH using bafilomycin A1 inhibited  $\text{Ca}^{2+}$  uptake by the lysosome and disturbed the membrane contact site interaction between the ER and lysosomes (Atakpa et al. 2018).

Some LSDs such as GM1 gangliosidosis and Ceroid lipofuscinosis, neuronal 8 (CLN8) disease have reported ER stress, including an increase in the unfolded protein response (Tessitore et al. 2004; Sano et al. 2009; Galizzi et al. 2011). Tessitore *et al.* (2004) found that GM1 accumulation in neurons leads to ER  $\text{Ca}^{2+}$  depletion and initiation of the unfolded protein response which leads to apoptosis. Additionally, GM1 accumulation has been reported to disrupt contact sites between ER and other organelles such as mitochondria, leading to defects in mitochondrial function (Sano et al. 2009; Annunziata et al. 2018). The major impact of lipid storage and lysosomal

dysfunction disorders on the ER function is on ER  $\text{Ca}^{2+}$  regulation, discussed below (Pelled et al. 2003; Brini and Carafoli 2009; Lloyd-Evans and Waller-Evans 2019).

### **1.1.5 Cellular $\text{Ca}^{2+}$ regulation and LSDs**

Free ionic calcium ( $\text{Ca}^{2+}$ ) is the most important intracellular messenger in biological organisms (Carafoli and Krebs 2016).  $\text{Ca}^{2+}$  is essential for the regulation of a myriad of cellular events such as fertilisation, metabolism, division, growth, motility and others (Berridge et al. 2000; Braakman and Hebert 2013). Levels of  $\text{Ca}^{2+}$  in the cytosol are tightly regulated at around 100 nM through various proteins such as  $\text{Ca}^{2+}$  pumps like the plasma membrane  $\text{Ca}^{2+}$  ATPase and  $\text{Na}^+/\text{Ca}^{2+}$  exchangers localised in different organelle membranes including the ER, the lysosome and the mitochondria, which remove excess cytosolic  $\text{Ca}^{2+}$  (Williams 2006; Clapham 2007; Lloyd-Evans and Platt 2011; Lloyd-Evans and Waller-Evans 2019).

Alterations in  $\text{Ca}^{2+}$  homeostasis lead to cellular dysfunction and contribute to pathogenesis in many LSDs (Lloyd-Evans et al. 2008; Lloyd-Evans and Waller-Evans 2019). This highlights the importance of regulating and maintaining  $\text{Ca}^{2+}$  content. Intracellular organelles help maintain cytosolic  $\text{Ca}^{2+}$  levels by functioning to buffer and induce changes in cytosolic  $\text{Ca}^{2+}$  levels.

#### **1.1.5.1 ER $\text{Ca}^{2+}$**

The ER is the largest  $\text{Ca}^{2+}$  store with a concentration of around 1 mM, which it maintains via the action of several transmembrane proteins such as  $\text{IP}_3$  receptors,  $\text{Ca}^{2+}$  leak channels, the ryanodine receptor (RyR) and a major  $\text{Ca}^{2+}$  up-take pump called the sarco-endoplasmic reticulum  $\text{Ca}^{2+}$  ATPase (SERCA) (Bultynck et al. 2014; Takeshima et al. 2015). The high concentration of  $\text{Ca}^{2+}$  in the ER is extremely important for ER function, such as protein folding and processing, as well as being a  $\text{Ca}^{2+}$  reservoir for signalling events (Braakman and Hebert 2013). The second messengers  $\text{IP}_3$  and cyclic ADP-ribose, which arise from extracellular signals, are the main mediators of  $\text{Ca}^{2+}$  release from the ER. The release of  $\text{Ca}^{2+}$  from the ER can be augmented by processes such as  $\text{Ca}^{2+}$ -induced  $\text{Ca}^{2+}$  release (Galione and Churchill 2002).

There are three isoforms of the IP<sub>3</sub> receptors which comprise a family of ER Ca<sup>2+</sup> channels that are ubiquitously expressed. IP<sub>3</sub> receptors may be homo or heterotetramers comprised of four 300 kDa subunits. They contain a ligand binding pocket located near the N-terminus, a 6 transmembrane domain near the C-terminus and a regulator domain in the cytosol. The transmembrane region forms the Ca<sup>2+</sup> channel region (Fan et al. 2015). IP<sub>3</sub> receptors are important in signalling pathways that help maintain cellular Ca<sup>2+</sup> homeostasis. As briefly mentioned above, extracellular signals lead to IP<sub>3</sub> being generated by phospholipase C cleaving phosphatidylinositol 4,5-bisphosphate. Soluble IP<sub>3</sub> binds to IP<sub>3</sub> receptors, which induces Ca<sup>2+</sup> release from the ER (Atakpa et al. 2018).

RyR are ubiquitously expressed ER Ca<sup>2+</sup> channels that are in the same family as IP<sub>3</sub> receptors. RyR are large homotetramers comprising of four 565 kDa monomers. As with IP<sub>3</sub> receptor, there are three isoforms of RyR that are expressed in different human tissues. When cytosolic Ca<sup>2+</sup> is low, RyR tend to be closed (Fill and Copello 2002). When cytosolic Ca<sup>2+</sup> is at micromolar concentration, Ca<sup>2+</sup> binds to specific binding sites on RyR that cause the channel to open with maximal RyR activity at around 10 μM cytosolic Ca<sup>2+</sup> (Fill and Copello 2002).

SERCA, which as mentioned is the major ER Ca<sup>2+</sup> uptake channel, is a 110 kDa ER transmembrane P-type ATPase pump protein that transports two Ca<sup>2+</sup> ions from the cytosol into the lumen of the ER using the energy from the hydrolysis of one molecule of ATP (Guerrero-Hernandez et al. 2010). The active transport of Ca<sup>2+</sup> into the ER helps create and maintain a concentration gradient between the ER and the cytosol, which allows Ca<sup>2+</sup> to be used as a second messenger for several cellular pathways as mentioned above. There are 3 SERCA protein isoforms (SERCA1, 2 and 3) with more than 10 alternative splice variants. The expression of these different SERCA proteins is cell type dependant. For example, SERCA1 is expressed in fast-twitch muscle, whereas SERCA2 is expressed in cardiac and slow-twitch muscle (MacLennan et al. 1985; Brandl et al. 1986).

Alterations in the level of ER Ca<sup>2+</sup> have been reported in LSDs such as Sandhoff disease and neurodegenerative diseases including Parkinson disease (Pelled et al. 2003; Lim et al. 2008; Brini and Carafoli 2009; Lloyd-Evans and Waller-Evans 2019; Shipley 2019). Defects in ER Ca<sup>2+</sup> in LSDs have been reported to lead to an elevated Ca<sup>2+</sup> concentration in the cytosol which is buffered by mitochondria (Sano et al. 2009).

The dysfunction in ER  $\text{Ca}^{2+}$  and prolonged elevation in mitochondrial  $\text{Ca}^{2+}$  has been found to lead to neuronal dysfunction and cell death (Duchen 2000; Tessitore et al. 2004).

Studies have linked defects in the specific ER  $\text{Ca}^{2+}$  channels IP<sub>3</sub> receptor, SERCA and RyR to neurodegenerative disease such as Parkinson disease, Alzheimer disease and LSDs (Stutzmann et al. 2004; Ginzburg and Futerman 2005; Green et al. 2008; Brini and Carafoli 2009). Ginzburg and Futerman (2005) reported that there was a loss of IP<sub>3</sub> receptors in the mouse model of the LSD Niemann-Pick Type C1 disease.

Defective ER  $\text{Ca}^{2+}$  in the LSD Gaucher disease was linked to the interaction between glucosylceramide storage in the disease and RyR. The storage of glucosylceramide enhances the amount of  $\text{Ca}^{2+}$  released via the RyR in response to other signals (Korkotian et al. 1999; Lloyd-Evans et al. 2003). In the *Hexb*<sup>-/-</sup> mouse model, which is a  $\beta$ -hexosaminidase knockout model of the LSD Sandhoff disease,  $\text{Ca}^{2+}$  uptake via SERCA was slower. The defect was associated with storage of ganglioside GM2 inhibiting the activity of SERCA (Pelled et al. 2003). This defect was corrected following treatment with miglustat, which is a glucosylceramide synthase inhibitor that decreases glycolipid synthesis (Pelled et al. 2003). Both the RyR and SERCA defects, in Gaucher and Sandhoff diseases respectively, emphasise the detrimental effect that the lipid accumulation seen in LSDs has on ER  $\text{Ca}^{2+}$  homeostasis.

#### 1.1.5.2 Lysosomal $\text{Ca}^{2+}$

The lysosome is the second largest intracellular  $\text{Ca}^{2+}$  store after the ER with  $\sim 500$   $\mu\text{M}$   $\text{Ca}^{2+}$ , and has emerged as an important intracellular  $\text{Ca}^{2+}$  store (Christensen et al. 2002; Patel and Cai 2014). As the lysosome makes up around 3% of the total cell volume in mammalian cells, their overall contribution of  $\text{Ca}^{2+}$  to total cellular  $\text{Ca}^{2+}$  signalling is relatively low when compared to the ER, even with the high concentration of  $\text{Ca}^{2+}$  inside the lysosome (Lloyd-Evans and Haslett 2016; Lloyd-Evans and Waller-Evans 2019). Nonetheless, studies have shown that lysosomal  $\text{Ca}^{2+}$  can initiate cellular  $\text{Ca}^{2+}$  signalling changes (Medina et al. 2015; Atakpa et al. 2018; Rosato et al. 2019).

The high concentration of  $\text{Ca}^{2+}$  within the lysosome is likely to be maintained by mechanisms that transport  $\text{Ca}^{2+}$  into the lysosome from the cytosol or from the ER as recently suggested (Garrity et al. 2016). The channels that transport  $\text{Ca}^{2+}$  into the lysosome in mammals remain unclear; however, a myriad of mechanisms have been suggested (Lloyd-Evans and Waller-Evans 2019).

Studies in lower order organisms have suggested potential  $\text{Ca}^{2+}/\text{H}^+$  exchangers and active ATPase  $\text{Ca}^{2+}$  transporters may be involved in  $\text{Ca}^{2+}$  uptake in vacuoles (Pittman 2011; Melchionda et al. 2016). Studies have so far identified  $\text{Ca}^{2+}/\text{H}^+$  exchangers in almost all species except placental mammals (Melchionda et al. 2016). This suggests that there are mechanisms for active  $\text{Ca}^{2+}$  transport into lysosomes in mammalian cells that remain unclear. Additionally, a recent study suggested mechanisms for lysosomal  $\text{Ca}^{2+}$  filling involving ER contact points mentioned above in Section 1.1.4 (Garrity et al. 2016; Atakpa et al. 2018).

The  $\text{Ca}^{2+}$  concentration inside the lysosome is tightly regulated by transmembrane proteins such as the transient receptor potential cation channel mucolipins (TRMPLs) and the two-pore channels (TPCs). Lysosomal  $\text{Ca}^{2+}$  signalling has been associated with cellular processes such as autophagy, endo-lysosomal trafficking, membrane repair and exocytosis (Patel and Cai 2014).

The TRMPLs are a family comprised of three endosomal  $\text{Ca}^{2+}$  channels, TRPML1, TRPML2 and TRPML3. TRPML1, the best characterised of the TRPML channels, is a 6 transmembrane domain channel critical for lysosomal function, and is associated with autophagy and ER stress regulation by lysosomal  $\text{Ca}^{2+}$  release, plasma membrane repair by lysosomal exocytosis, and reactive oxygen species sensing (Di Paola et al. 2018). Studies have reported that the signalling lipids phosphatidylinositols activate and inhibit the TRPML1 channel. The endo-lysosomal specific phosphatidyl-(3,5)-bisphosphate ( $\text{PI}(3,5)\text{P}_2$ ) activates TRPML1; whereas,  $\text{PI}(4,5)\text{P}_2$ ,  $\text{PI}(3,4)\text{P}_2$  and  $\text{PI}(3,4,5)\text{P}_3$  inhibit TRMPL1 (Dong et al. 2010).

The importance of proper TRMPL1 function is highlighted by the fact that mutation in *MCOLN1*, the gene that encodes for TRPML1, causes the LSD Mucopolidosis type IV (Dong et al. 2008). Dysfunction of TRMPL1 in MLIV patients has been shown to lead to a decrease in the recruitment of PI3P-binding proteins to the phagophore, part of the initial steps in autophagy outlined above, indicating a role for autophagy in MLIV

pathogenesis and for TRPML1 in the regulation of autophagy biogenesis (Rosato et al. 2019). TRPML1 has also been reported to be able to pump other ions from the lysosomal lumen to the cytosol such as  $H^+$ ,  $K^+$ ,  $Fe^{2+}$ ,  $Zn^{2+}$ ,  $Na^+$  and  $Mn^{2+}$  (Dong et al. 2009; Waller-Evans and Lloyd-Evans 2015; Minckley et al. 2019). These experiments have only been shown in reconstituted bilayers and lysosomes swollen using vacuolin, and thus have not been replicated in physiological conditions.

Another family of channels that regulate  $Ca^{2+}$  levels inside the endo-lysosomal system is the TPCs which are non-selective cation channels found on the membrane of endo-lysosomal vesicles (Galione 2011; Wang et al. 2012b). The best characterised of the TPCs is TPC2, which is a  $Ca^{2+}$  efflux channel that is activated by nicotinic acid adenine dinucleotide phosphate (NAADP). The activation of TPC2 by NAADP was demonstrated using HEK cells overexpressing TPC2, which increased NAADP binding and led to lysosomal  $Ca^{2+}$  release, with the specificity of this effect being confirmed in TPC2 knockdown cells (Calcraft et al. 2009; Ruas et al. 2010; Galione 2011). TPC2 has also been reported to act as a sensor of luminal pH and  $Ca^{2+}$ . Low luminal pH was shown to lead to  $Ca^{2+}$  release following NAADP binding, whereas neutral pH leads to inactivation of the TPC2 channel (Pitt et al. 2010).

Defects in lysosomal  $Ca^{2+}$  levels and signalling have been shown to contribute to the pathogenesis of diseases such as the LSD NPC1 (Lloyd-Evans et al. 2008; Lloyd-Evans and Waller-Evans 2019). Lloyd-Evans *et al.* (2008) found a reduction in lysosomal  $Ca^{2+}$ , as well as defects in NAADP mediated  $Ca^{2+}$  signalling, in *NPC1* null mice, *NPC1* null Chinese hamster ovary (CHO) cells, and *NPC1* patient cells. Disturbed lysosomal  $Ca^{2+}$  homeostasis has also been reported in other LSDs such as CLN3 (Lloyd-Evans and Platt 2010; Chandrachud et al. 2015; Lloyd-Evans and Haslett 2016; Lloyd-Evans and Waller-Evans 2019).

#### 1.1.5.3 Mitochondria $Ca^{2+}$

The concentration of  $Ca^{2+}$  within mitochondria has been reported to be similar to that of the cytosol (Bagur and Hajnóczky 2017; Lloyd-Evans and Waller-Evans 2019). During cell stress, however, the concentration of mitochondrial  $Ca^{2+}$  can change (Celsi et al.) as it acts as a  $Ca^{2+}$  buffer in order to prevent high levels of cytosolic  $Ca^{2+}$ , which are toxic to cells (Lloyd-Evans and Waller-Evans 2019). As with the lysosome and the

ER, there are specific transmembrane proteins that regulate mitochondrial  $\text{Ca}^{2+}$  such as the mitochondrial  $\text{Ca}^{2+}$  uniporter, the  $\text{Na}^+/\text{Ca}^{2+}$  exchanger and the  $\text{H}^+/\text{Ca}^{2+}$  exchanger (Gunter and Pfeiffer 1990).

In order for  $\text{Ca}^{2+}$  to enter the mitochondria, it has to cross two lipid bilayers. On the outer bilayer there is an abundance of channels that are permeable to ions called the mitochondrial porin or voltage-dependent anion channels (Celsi et al. 2009). The inner bilayer seems to be more impermeable to ions and  $\text{Ca}^{2+}$  enters the mitochondrial matrix via the mitochondrial  $\text{Ca}^{2+}$  uniporter (Kirichok et al. 2004). The mitochondrial  $\text{Ca}^{2+}$  uniporter maintains the electrochemical gradient within the mitochondria (Celsi et al. 2009).

During cell stress or increases in cytosolic  $\text{Ca}^{2+}$ , as has been reported in some LSDs (Pelled et al. 2003), mitochondria act as a  $\text{Ca}^{2+}$  buffer (Duchen 2000; Celsi et al. 2009; Sano et al. 2009). Mitochondrial  $\text{Ca}^{2+}$  alterations have been found to lead to mitochondrial dysfunction, and have been reported in LSDs such as the CLN8 disease (outlined below), where mitochondrial  $\text{Ca}^{2+}$  has been suggested to play a role in disease pathogenesis in the  $\text{CLN8}^{\text{mnd}}$  mouse (Carafoli 1974; Kolikova et al. 2011).

### **1.1.6 Circadian rhythms and changes in gene expression in LSDs**

The defects in  $\text{Ca}^{2+}$  homeostasis in LSDs could potentially impact many cellular processes, such as circadian rhythms, that rely on  $\text{Ca}^{2+}$  stores for signalling pathways that regulate them (Shim et al. 2007; Richardson et al. 2016). Circadian rhythm is the cellular process that has developed through natural selection that allows organisms to regulate diurnal variations in gene expression over a near-24-hour period (Mazzoccoli 2011; Huang et al. 2020).

Mammalian circadian rhythms are regulated by a central master oscillator in the suprachiasmatic nucleus (SCN) of the brain (Schibler and Sassone-Corse 2002). The SCN is synchronised in response to environmental light/dark cycles (Hasting et al. 2003). The photic inputs are received by the SCN from the retina directly via the retinohypothalamic tract, and these timing signals are conveyed to the rest of the organism through direct and indirect signalling pathways (Schibler and Sassone-Corse 2002; Hasting et al. 2003).

Defects in circadian rhythm regulation are not well studied in the LSDs; however, there have been reports of alterations in circadian rhythm gene expression in LSDs such as Hunter syndrome (Mazzoccoli et al. 2013). In some LSDs, including glycogen storage disease, Mucopolysaccharidosis type I, aspartylglucosaminuria, and CLN3, disruption in sleep patterns have been reported, suggesting a possible role for circadian rhythm deregulation (Gadoth and Oksenberg 2014).

Some studies have reported sleep and circadian rhythm disruption in neurodegenerative disease such as Alzheimer disease, Huntington disease and the LSD Sandhoff disease (Wulff et al. 2010; Goodman et al. 2011; Musiek et al. 2015; Richardson et al. 2016). Richardson *et al.* (2016) found that Sandhoff disease model *Hex*<sup>-/-</sup> mice exhibited changes in the expression of the circadian rhythm associated gene *Per1*; whereas, no disruption to circadian rhythms were observed in the NPC1 mouse model *Npc*<sup>nih</sup> even though substantial cholesterol storage was observed in the SCN. This report suggested that the accumulation of specific metabolites in LSDs contributes to circadian deregulation (Richardson et al. 2016).

Protein kinase C (PKC), an important signalling protein involved in many pathways, including circadian rhythm regulation (Shim et al. 2007; Bosnall and Lall 2013), has been found to be disrupted in many LSDs (Hannun and Bell 1989; Onyenwoke and Brenman 2015). The PKC defects in LSDs reported are not only due to the defects in Ca<sup>2+</sup> stores outlined above, but due to disturbances in sphingolipid metabolism and storage of lysosphingolipids, which inhibit PKC (Hannun and Bell 1989).

Furthermore, there have been reports of alterations in gene expression profiles in LSDs such as mucopolysaccharidosis and Fabry disease (Vallim et al. 2019; Brokowska et al. 2020). Ultimately, the link between circadian rhythm and lysosomal storage, and the effects of lysosomal storage on circadian rhythms and *vice versa* have not been explored and are poorly understood.

## **1.2 Neuronal ceroid lipofuscinosis**

### **1.2.1 Neuronal ceroid lipofuscinosis**

The neuronal ceroid lipofuscinosis (NCLs) are a group of 13 autosomal recessive neurodegenerative LSDs (Table 1.1). Overall, the NCLs have an incidence of around 1 in 12,000 live births, making them the most common group of LSDs in the UK (Mukherjee et al. 2019). The NCLs are commonly referred to as Batten diseases after Sir Fredrick Batten due to his early reports characterising the disease (Batten 1903,1914). The term “NCL” was later coined when the group of diseases was differentiated from Tay-Sachs disease, another LSD, by Zeman and Dyken (1969).

**Table 1.1: Overview of the NCLs.** This overview of the 14 NCLs identified to date displays the disease-causing gene, gene loci, protein localisation, protein function and main storage material in each of the NCLs (Mukherjee et al. 2019).

<b>NCL</b>	<b>Gene (protein)</b>	<b>Gene Loci</b>	<b>Protein localisation</b>	<b>Main storage material</b>
CLN1	<i>CLN1/ PPT1</i> (palmitoyl-protein thioesterase 1)	1p34.2	Lysosome	Saposins A & D
CLN2	<i>CLN2/ TPP1</i> (tripeptidyl peptidase 1)	11p15.4	Lysosome	SCMAS
CLN3	<i>CLN3</i> (CLN3/Batenin)	16p12.1	Lysosome	SCMAS
CLN4	<i>CLN4/ DNAJC5</i> (Cysteine-string protein alpha)	15q23 20q13.33	Neuronal synaptic vesicles	SCMAS
CLN5	<i>CLN5</i> (CLN5)	13q22.3	Lysosome	SCMAS
CLN6	<i>CLN6</i> (CLN5)	15q23	ER	SCMAS
CLN7	<i>CLN7</i> (MSFD8)	4q28.2	Lysosome	SCMAS
CLN8	<i>CLN8</i> (CLN8)	8p23.3	ER	SCMAS
CLN10	<i>CLN10/ CTSD</i> (Cathepsin D)	11p15.5	Lysosome	Saposins A & D
CLN11	<i>CLN11/ GRN</i> (Progranulin and granulins)	17q21.31	ER/ Golgi	Still unknown
CLN12	<i>CLN12</i> (ATP13A2)	1p36.13	Lysosome	SCMAS
CLN13	<i>CLN13/CTSF</i> (Cathepsin F)	11q13.2	Lysosome	Still unknown
CLN14	<i>CLN14/KCTD7</i> (Potassium channel tetramerization domain-containing protein 7)	7q11.21	Cytosolic	SCMAS

The NCLs are characterised by progressive motor and cognitive decline, visual deterioration, epileptic seizures, neuronal loss, intracellular accumulation of autofluorescent material and premature death (Shacka 2012). It has been found that the hydrophobic membrane SCMAS of the mitochondria is the main storage component across most the NCLs, including CLN3, CLN5, CLN7 and CLN8 (Palmer et al. 2013). The accumulation of SCMAS is not only seen in neurons, but also throughout numerous cell types including cells in the central nervous system, liver, pancreas and kidney. While clinical symptoms across the NCLs are mostly similar, the age of onset and disease progression rate varies depending on the genetic defect. Currently, mutations in 13 different genes (table 1.1) have been found to cause Batten disease (Palmer et al. 2013).

**Table 1.2: Function of NCL proteins.** A summary of the NCL CLN genes products and function (Camp and Hofman 1993; Kousi et al. 2012; Anderson et al. 2013; Beel et al. 2017; di Ronza et al. 2018; Mukherjee et al. 2019; Bajaj et al. 2020).

<b>NCL</b>	<b>Gene</b>	<b>Protein Function</b>
CLN1	<i>CLN1/PPT1</i>	Glycoprotein that removes thioester-linked fatty acyl group from modified cysteine for protein degradation.
CLN2	<i>CLN2/TPP1</i>	Pro-enzyme that, when activated, acts as a serine protease involved in the cleavage of N-terminal tripeptides from substrates.
CLN3	<i>CLN3</i>	Transmembrane protein of unknown function thought to be involved in ion transport to help maintain acidic lysosomal pH, endocytosis, transporting proteins, apoptosis, cell division and osmoregulation.
CLN4	<i>CLN4/DNAJC5</i>	Is part of a complex of proteins, found on the membrane of synaptic vesicles that plays a role in nerve impulse transmission as it recycles the proteins involved by re-folding misfolded proteins for use in further transmissions.
CLN5	<i>CLN5</i>	Although the function of CLN5 is still unknown it is produced as an inactive preprotein that, when activated, is transported to the lysosome.
CLN6	<i>CLN6</i>	Transmembrane protein of unknown function found in the endoplasmic reticulum but is involved in processing and transporting proteins and lipids between endoplasmic reticulum and lysosomes. Recently shown to form a CLN6-CLN8 complex that recruits lysosomal enzymes at the ER and transfers them to the Golgi playing a key role in lysosome biogenesis.
CLN7	<i>CLN7/MSFD8</i>	Lysosomal transmembrane protein of unknown function that belongs to the major facilitator superfamily.
CLN8	<i>CLN8</i>	Endoplasmic reticulum transmembrane protein recently reported to be part of a CLN6-CLN8 complexes that plays a key role in lysosomal biogenesis by transporting lysosomal enzymes from the ER to the Golgi.
CLN10	<i>CLN10/CTSD</i>	Lysosomal enzyme called cathepsin D which is part of the cathepsin protein family that act as protease enzymes which hydrolyses proteins.
CLN11	<i>CLN11/GRN</i>	Protein called granulin which is found through the body but is most active in cells that divide rapidly such as skin where it helps regulates growth, division and cell survival. It also has a role in early embryonic development, wound healing and immune response regulation. Granulin has been suggested to act as chaperone for Cathepsin D.
CLN12	<i>CLN12/ATP13A2</i>	ATPases member of the P5 subfamily which transports inorganic cations. Certain mutation has been associated with childhood onset Parkinson's disease (Kufor-Rakeb syndrome).
CLN13	<i>CTSF</i>	Lysosomal enzyme called cathepsin F is expressed ubiquitously throughout the body and is another member of the cathepsin family and is therefore involved protein degradation.
CLN14	<i>KCTD7</i>	K <sup>+</sup> channel tetramerization domain-containing protein of unknown function.

### 1.2.2 NCL disease mechanisms

Currently, the NCLs remains a group of diseases that are not fully understood; the mechanisms behind their pathogenesis and similarities remain unclear. One cellular pathology that has been explored as a link between the NCLs is the accumulation of SCMAS. Nonetheless, not all the NCLs appear to have SCMAS as the main storage component, as some accumulate saposins A and D instead.

Storage of SCMAS in lysosomes leads to aggregates of SCMAS and lipids forming protein-lipid complexes known as lipofuscin, which are relatively insoluble and protease-resistant (Elleder et al. 1995). Studies have found that Tripeptidyl Peptidase 1 (TPP1), the enzyme deficient in CLN2, is essential for SCMAS degradation; however, TPP1 activity is not affected across all of the NCLs, including those that store SCMAS (Ezaki et al. 1999; Junaid and Pullarket 1999). Additionally, it has also been suggested that cathepsin D, the enzyme deficient in CLN10, is linked to the degradation of SCMAS, indicating that the catabolism of SCMAS may be multi-step process (Ezaki et al. 1999). Thus, it may be the case that NCLs are linked via defects in the pathway of SCMAS degradation leading to the common phenotypic characteristics (Cao et al. 2011).

There have been other studies that have attributed NCL pathogenesis to defects in autophagy and not specifically to SCMAS. As outlined above, autophagy is the cellular process by which organelles and macromolecules are degraded in the endo-lysosomal system. This link has arisen from studies reporting autophagy defects in the NCLs such as in the CLN6 mouse model, where there is an increase in LC3-II with neuronal p62 positive aggregates, suggesting a defect in autophagosome-lysosome fusion (Thelen et al. 2012). These p62 positive toxic aggregates, and the defect in autophagy, have been suggested to lead to the neuronal degeneration seen in CLN6 (Thelen et al. 2012).

Similarly, studies have reported autophagy defects in CLN3 cells, and have used these to identify compounds that are able to correct the autophagy-lysosomal phenotypes to identify new potential therapeutic candidates (Chandrachud et al. 2015; Petcherski et al. 2019). The levels of LC3-II were also reported to be increased in CLN3<sup>Δex7/8</sup> mice; whereas, LC3-II colocalisation with endo-lysosomal markers was reduced. Cao *et al.* (2006) found that autophagic vacuoles isolated from CLN3<sup>Δex7/8</sup>

mice were less mature than control autophagic vacuoles when comparing ultrastructural morphology. This suggests that there may be a defect in autophagic vacuole maturation in CLN3 disease.

Further studies have shown that the accumulation of SCMAS occurs within acidic organelles and not in the mitochondria, supporting the hypothesis that there is a defect in the degradation process via the autophagosome-lysosomal pathway (Cao et al. 2011). Therefore, NCL proteins may be essential in the cellular mechanisms that link the autophagosome-lysosomal pathway and mitochondrial turnover of SCMAS.

Previous studies have also explored the role of ER stress in NCL pathogenesis, as the ER is involved in many crucial cellular processes including protein synthesis and modification,  $Ca^{2+}$  homeostasis and lipid metabolism. Defects in ER homeostasis have been shown to lead to misfolded proteins being accumulated, and activation of the unfolded protein response. Several NCLs, including CLN1, CLN3, CLN6 and CLN8 have been reported to be linked to ER stress and the UPR (Galizzi et al. 2011; Marotta et al. 2017).

Certain mutations in the *TPP1* gene that lead to CLN1 disease (Table 1.1 & 1.2) result in misfolded TPP1 protein not being transported to the lysosome and thus accumulating in the ER (Das et al. 2001). Furthermore, studies have reported ER stress-mediated caspase activation leading to elevated levels of apoptosis in CLN1 patient brain biopsies (Riikonen et al. 2000; Kim et al. 2006b). Similarly, ER morphological abnormalities along with the activation of the UPR has been reported in CLN1 mouse models (Zhang et al. 2006).

Research into CLN3 disease has also uncovered ER stress with CLN3 overexpression mutations leading to a decrease in the expression of the ER chaperone protein Binding immunoglobulin protein (BiP) and increased expression of C/EBP homologous protein, which is a protein known to be induced by ER stress. Further research also reported this in siRNA knockdown CLN3 models (Wu et al. 2014). These alteration in the BiP and the CCAAT-enhancer-binding protein (CHOP) expression suggest that deficiency in CLN3 function leads to defects in the cell's ability to manage ER stress. Likewise, CLN6 has been reported to be linked with ER stress due to the dyshomeostasis of metals such as  $Zn^{2+}$ ,  $Mn^{2+}$  and  $Cu^{2+}$  that has been observed in CLN6 sheep models. This metal dyshomeostasis is believed to lead to

defects in the protein folding process in the ER, causing ER stress (Kenninen et al. 2013; Grubman et al. 2014).

CLN8 disease, outlined below, has also been linked to ER stress. The levels of ER stress marker BIP, CHOP and caspase 12 have been reported to be elevated in the central nervous system of the CLN8<sup>mind</sup> mouse. In fact, ER stress has been suggested to play a role in CLN8 disease pathogenesis (Ranta et al. 1999; Galizzi et al. 2011). Nonetheless, the exact mechanism by which mutation in NCL proteins lead to ER stress remain unclear and requires further investigation. It may be due to mutations that cause misfolded protein accumulation in the ER, alterations in ER protein expression, alterations in levels of metals in cells, or simply due to the disruption these mutations cause to the endo-lysosomal system leading to ER stress.

Some studies have reported Ca<sup>2+</sup> defects in some NCLs such as CLN3 and CLN8 disease (Kolikova et al. 2011; Chandrachud et al. 2015; Bosch and Kielian 2019). Recent studies reported increased lysosomal Ca<sup>2+</sup> levels in *Cln3* mutant mouse cerebellar cells (Chandrachud et al. 2015). As mentioned above in Section 1.1.6, Kolikova *et al.* (2011) proposed that CLN8 pathogenesis is linked to a reduction in the mitochondria's ability to buffer Ca<sup>2+</sup>.

The common pathological mechanisms that link the NCLs are still unclear and poorly understood; however, most studies focus on specific aspects of the disease rather than investigating causative up-stream events. Nonetheless, most research agrees that the NCL genes perform a role in the development of the central nervous system and are likely components in the same metabolic pathways (Weimer et al. 2002). To fully understand these diseases, and ultimately identify therapeutic intervention points of benefit to all the NCLs and potentially all LSDs, it is crucial to identify the common pathological pathways affected in the NCLs.

### **1.2.3 CLN8 disease**

CLN8 disease, also known as progressive epilepsy with mental retardation (EPMR) or Northern Epilepsy, is an autosomal recessive disorder caused by mutations in the *CLN8* gene on chromosome 8 which encodes a 33 kDa transmembrane ER protein (Table 1.1 & Table 1.2). The CLN8 protein has recently been shown to act as a chaperone, required, in a complex with CLN6, for the transport of approximately two

thirds of lysosomal enzymes from the ER to the Golgi before being delivered to lysosomes (di Ronza et al. 2018; Bajaj et al. 2020). The disease is classified into two distinct clinical phenotypes: EPMR and a more severe form that is clinically and pathological, described in Table 1.3, similar to the late-infantile NCL variants such as CLN5, CLN2 and CLN7 (Striano et al. 2007; Jalanko and Braulke 2009; Passantino et al. 2013).

**Table 1.3: CLN8 disease clinical phenotypes.** Outline of differences between two variants of CLN8 disease (Striano et al. 2007).

CLN8 variant	Phenotypes differences
<b>EPMR</b>	Onset ~5-10 years Behavioural abnormalities are sometimes seen Progressive mental retardation Cognitive decline (increased during puberty) Epileptic seizures (increased during puberty and decreased after)
<b>Late-infantile variant</b>	Onset ~2-7 years Visual impairment Medication-resistant epileptic seizures Behavioural abnormalities are common Rapid progression Severe neurological deterioration ~8-10 years

CLN8 disease is characterised by epileptic seizures with an onset at five to ten years of age, which subsequently advance to progressive mental retardation and cognitive decline (Lonka et al. 2000). Seizure frequency and cognitive deterioration is accelerated during puberty. Patients may also exhibit behavioural disturbances such as restlessness and irritability (Striano et al. 2007). The number of seizures decreases spontaneously after puberty and become sporadic by the third decade. Nonetheless, cognitive decline continues alongside motor function loss (Mole et al. 2011). The late-infantile variant CLN8 disease is characterised by onset at around two to seven years of age with myoclonic seizures, irregular gait and eventually clonic seizures. In these more severe cases, cognitive decline is accelerated, and visual impairment and behavioural abnormalities are frequently observed (Mole et al. 2011; Beesley et al. 2017). By the age of eight to ten years, patients show severe deterioration of neurological and cognitive skills, spasticity, dystonic posturing, tremors and epilepsy resistant to medication (Striano et al. 2007; Mole et al. 2011).

To date, around 30 different mutations, outlined further in Section 1.2.4, such as missense mutations and genomic deletions, have been linked to CLN8 disease, most of which lead to the late-infantile variant of CLN8 disease (Beesley et al. 2017). As CLN8 disease has not been extensively studied, little is known about the full effect of the different types of mutation; however, the predicted outcome of the different types of mutations, and the outcome of specific mutations that have been reported, are outlined in Chapter 3 section 3.1.1.

There is a naturally occurring mouse model, the CLN8<sup>mnd</sup> mouse, which exhibits phenotypes similar to the late-infantile variant, that has been used to study the disease (Ranta et al. 1999; Jalanko and Braulke 2009; Passantino et al. 2013). Studies using the CLN8<sup>mnd</sup> mouse have identified altered lipid metabolism, mitochondrial dysfunction, oxidative stress, ER stress (as outlined above in Section 1.2.2) and defects in Ca<sup>2+</sup> homeostasis (Vance et al. 1997; Bertamini et al. 2002; Guarneri et al. 2004; Hermansson et al. 2005; Galizzi et al. 2011; Kolikova et al. 2011; Kuronen et al. 2012).

There have been reports of alterations in lipid metabolism in CLN8 disease (Hermansson et al. 2005; Kuronen et al. 2012). Sphingolipid profiling in the CLN8<sup>mnd</sup> mouse demonstrated a reduction in myelin-enriched galactolipids. Additionally, the activity and messenger ribonucleic acid (mRNA) expression of UDP-galactose:ceramide galactosyltransferase, a crucial enzyme in galactolipid synthesis, was reduced in the brain of the CLN8<sup>mnd</sup> mouse. These results suggest defects in galactolipid processing. Furthermore, these galactolipid deficiencies were reported to cause delayed myelin maturation in early CLN8 disease pathogenesis, which leads to defects in oligodendrocyte maturation (Kuronen et al. 2012).

Another study found that there were significant changes in the levels of ceramide, galctosyl and lactosylceramide, and sulfatide, as well as altered composition of phosphatidylserines, phosphatidylethanolamines and phosphatidylinositol in two CLN8 patient post-mortem brain samples measured by liquid chromatography/mass spectrometry. Remarkably, the changes in the levels and compositions of these lipids were not the same in the CLN8 patient brain samples and, in fact, in most cases these were oppositely affected between the two CLN8 patient brains samples (Hermansson et al. 2005). This variation in brain sphingo and phospholipid profiles may lead to

defects in membrane stability, vesicular trafficking and even neurotransmission, and thus may contribute to CLN8 pathogenesis (Hermansson et al. 2005).

Mitochondrial function has been suggested to be affected in CLN8 disease through alterations in mitochondrial import of lipids and proteins due to defective linkages between ER-like membranes and mitochondria. Furthermore, studies have found that the mitochondrial proteins NADH:cytochrome b5 reductase and SCMAS were partially mis-localised to microsomes in the CLN8<sup>mnd</sup> mouse liver (Vance et al. 1997).

Likewise, other studies have reported significant alterations in mitochondrial enzyme activities in the CLN8<sup>mnd</sup> mouse cortical regions. This study reported that mitochondrial complexes I and IV, and citrate synthase, were decreased, as was the rate of oxygen consumption in the CLN8<sup>mnd</sup> mouse (Bertamini et al. 2002). Bertamini *et al.* (2002) suggested that mitochondrial defects, as reported in the CLN8<sup>mnd</sup> mouse, are linked to oxidative stress, and that this plays an important role in the pathogenesis of this motor neuron disease.

As explained in Section 1.1.3, levels of Ca<sup>2+</sup> are tightly regulated and thus changes in Ca<sup>2+</sup> levels lead to cellular dysfunction. Mitochondrial Ca<sup>2+</sup> buffering has been reported to be affected in the CLN8<sup>mnd</sup> mouse. The ability of hippocampal neurons to clear large Ca<sup>2+</sup> loads was impaired in CLN8<sup>mnd</sup> mice due to defects in mitochondrial Ca<sup>2+</sup> uptake (Kolikova et al. 2011). Ca<sup>2+</sup> uptake by SERCA and Ca<sup>2+</sup> efflux via the plasma membrane were not affected. In fact, Kolikova *et al.* (2011) suggested that the neurodegeneration seen in CLN8 disease is primarily caused by the reduction in the capacity in mitochondrial Ca<sup>2+</sup> buffering.

#### **1.2.4 The CLN8 protein**

CLN8 is mainly found in the ER membrane, but has also been localised to the ER-Golgi intermediate compartment (ERGIC) (Lonka et al. 2000; Passantino et al. 2013). Nonetheless, in polarized CaCo2 cells, CLN8 is found in specialized sub-compartments (Lonka et al. 2000), in mouse fibroblasts it is found in the Golgi, endosomes and lipid rafts (Persaud-Sawin et al. 2007), and in hippocampal neurons it is found in proximity of the plasma membrane (Lonka et al. 2000; Vantaggiato et al. 2009).

The CLN8 protein interacts with other NCL proteins such as CLN2, CLN3, CLN5 and CLN6 in different sub-compartments (Persaud-Sawin et al. 2007; Lyly et al. 2009). Additionally, previous work has found that proteins associated with biological processes such as lipid transport, vesicular transport, autophagy and apoptosis including VAPA which is an ER-lysosomal contact point protein, c14orf/hERG28, STX8, GATE16, BNIP3 and BNIP3L proteins, potentially interact with the CLN8 protein (Passantino et al. 2013).

The CLN8 protein (Figure 1.4) contains five-hydrophobic transmembrane regions, a 200 amino acid-long TLC (TRAM-LAG1-CLN8) domain (amino acid 62-262) and a C-terminal ER-retrieval KKRP signal for recycling from the ERGIC. The TLC domain is linked to a family of TLC-domain homologues that have been hypothesised to have a role in lipid synthesis, transport or sensing (Winter and Ponting 2002; Rusyn et al. 2008; Kuronen et al. 2012). Other members of the family have been demonstrated to enable the transport of newly synthesized membrane proteins into the ER, as well as export glycosphosphatidylinositol-anchored protein out of the ER. Other reports have suggested a role for TLC proteins in acyl-CoA-dependent ceramide synthesis (Hermansson et al. 2005).

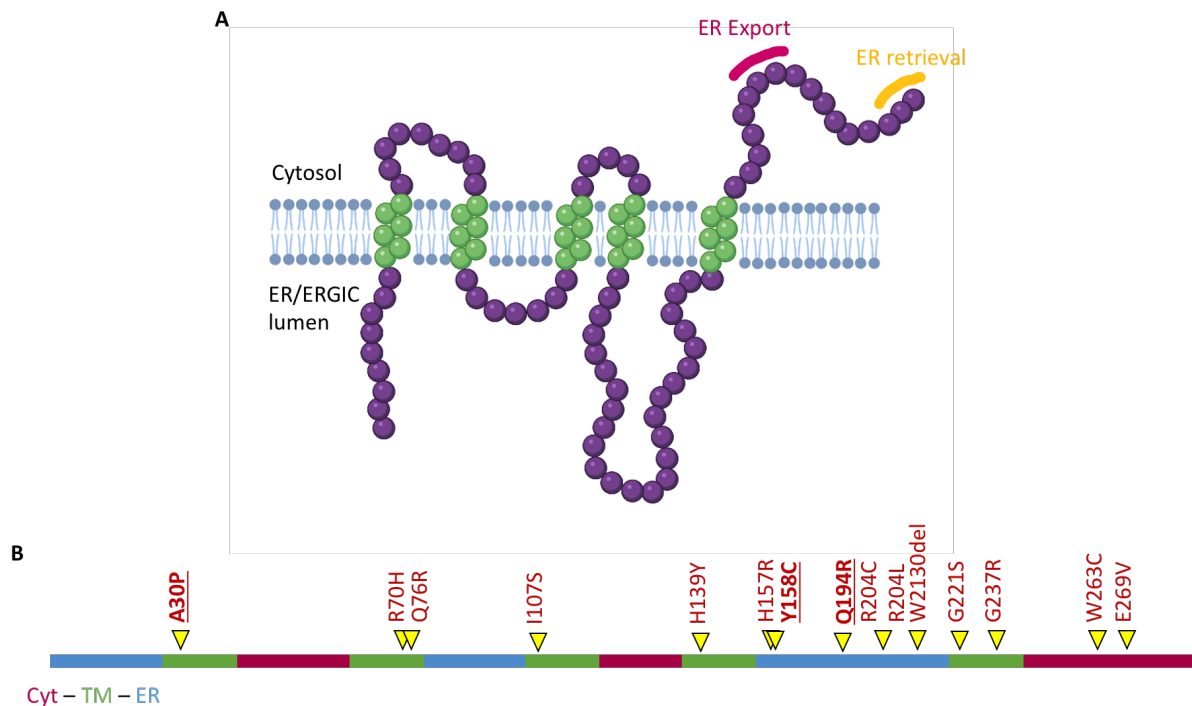


**Figure 1.4: Outline of CLN8 protein structure:** **A:** Representation of the CLN8 with transmembrane domains in green and cytosolic and ER/ERGIC lumen domains in purple. **B:** The line represents the CLN8 protein sequence with the ER lumen sections in blue, the transmembrane sections in green and the cytosolic sections in red. Some of the known patient mutations are outline in along the protein sequence with some of the ones used in Chapter 3 of this thesis in bold and underlined. Figure adapted from (di Ronza et al. 2018).

The CLN8 protein, as is the case for many of the NCL proteins, has not been extensively studied and, as such, there is a dearth of knowledge about the protein and the disease. Recently, however, CLN8 was demonstrated to have a key role in lysosomal enzyme maturation, as approximately 2/3<sup>rd</sup>s of lysosomal enzymes required CLN8 to facilitate their transport from the ER to the Golgi via the ERGIC (di Ronza et al. 2018). In this study, di Ronza *et al.* (2018) determined that the absence of CLN8 causes lysosomal enzyme trafficking to be disrupted.

Following this work, a recent study found that CLN8 forms a complex with CLN6, referred to as EGRESS (ER-to-Golgi relaying of enzymes of the lysosomal system), which recruits lysosomal enzyme in the ER and promotes their transfer to the Golgi. Therefore, the CLN8-CLN6 complex or EGRESS was found to be a key player in lysosomal biogenesis (Bajaj et al. 2020). This emerging role for CLN8 in the transport of lysosomal enzymes from the ER to the Golgi might explain why previous studies localised the CLN8 protein in the ER, ERGIC, and Golgi (Lonka et al. 2000; Persaud-

Sawin et al. 2007; Passantino et al. 2013; Beesley et al. 2017). Nonetheless, the full role of CLN8 in lysosomal homeostasis, and the specific effects of patient mutations on lysosomal and cellular function remain unclear and understudied.

Previously, mutations in the TLC domain were thought to result in the more severe late-infantile variant CLN8 (Beesley et al. 2017). An example of this is a patient with the missense mutation Q194R who suffers from the more severe infantile variant CLN8 disease (Cannelli et al. 2006). Missense mutations outside of this domain, such as R24G and W263C, were reported to result in the less severe form, EPMR (Zelnik et al. 2007; Kousi et al. 2012; Beesley et al. 2017). Nevertheless, it is now widely accepted that mutations in different specific protein domains do not lead to differences in clinical severity (Kousi et al. 2012). In fact, some patients with the more severe infantile-variant of the disease have more than one mutation in the *CLN8* gene, such as a Turkish patient with five mutations and an Italian patient with four (Ranta et al. 2001; Cannelli et al. 2006).

Recently, mutations in CLN8, particularly P260L, have been found to be a possible 'biomarker gene' of Parkinson disease. In fact, the P260L mutation was reported to be deleterious to Parkinson disease (Odaumpatta and Mohanapriya 2020). Furthermore, SNPs that lead to changes in CLN8 protein expression have been linked to the severity of the LSD Gaucher disease (Zhang et al. 2012). Zhang *et al.* (2012) reported that mild Gaucher disease patients exhibit higher levels of CLN8 protein expression.

### **1.3 Current therapies for treating lysosomal storage disease**

The mechanistic understanding of LSDs has substantially increased over the past decade. It has become apparent, as mentioned above, that lysosomal dysfunction leads to a number of secondary cellular responses that eventually lead to cell death. The first therapeutic strategies developed for LSDs were introduced in the 1990s. One such strategy involves replacement or restoration of the defective enzyme, and most approaches that have been developed for treating LSDs so far are aimed at increasing levels of defective enzyme in those diseases. The missing or defective enzyme can be remedied using haematopoietic stem cell transplantation (HSCT), chaperone therapy, enzyme replacement therapy (ERT) and gene therapy. In most cases, even

minor increases in enzymatic activity of up to 10% can be enough to see clinical benefit and partial phenotypic correction in LSDs patients (Parenti et al. 2012). Alternatively, the material being accumulated in lysosomes can be reduced by decreasing the synthesis of the substrates stored in lysosomes, termed substrate reduction therapy (SRT).

### **1.3.1 Haematopoietic stem cell transplantation (HSCT)**

HSCT was the first available therapy for LSDs. This therapy relies on the transplantation of hematopoietic stem cells from a healthy donor into the patients (Parenti et al. 2012). This therapy works by repopulating specific tissues with the donor cells, which secrete functional lysosomal enzymes that are then taken up by the patient cells. One significant advantage of HSCT is that donor cells are able to cross the blood brain barrier. This therapeutic approach is, however, slow and limited to a few lysosomal disorders.

### **1.3.2 Enzyme replacement therapy (ERT)**

In recent years, one of the greatest breakthroughs in treating LSDs has been ERT, which is a therapy based on re-introducing defective enzymes into patients via weekly or fortnightly infusions of recombinant enzymes (Parenti et al. 2012; Beck 2017). Examples of ERT being used effectively can be found in the reduction of glycosaminoglycan storage in Mucopolysaccharidosis (MPS) and globotriaosylceramide in Fabry disease. In some cases, it even improves patient organ function, such as heart function in Fabry disease (Marshall et al. 2010; van der Veen et al. 2020). Recently, Brineura was approved by the U. S. Food & Drug Administration (FDA) and the European Medicines Agency (EMA) as an ERT therapy for CLN2 in which recombinant TPP1 is administered intrathecally (Kohlschütter and Schulz 2016; European Medicine Agency 2017; US Food & Drug Administration 2017).

Nonetheless, ERT has variable efficacy between patients, as patients severely affected with some LSDs may exhibit irreversible organ damage that does not respond to ERT (Marshall et al. 2010). Furthermore, ERT therapeutic efficiency can decrease in patients over time if they develop antibodies against the recombinant enzyme, which

has been observed in a severe infantile form of Pompe disease (Banugaria et al. 2011).

Nevertheless, there are some limitations to ERT such as the high cost of therapy and the limited bioavailability, as ERT does not cross the blood brain barrier. The high cost associated with ERT results from the cost of producing large amounts of recombinant enzyme that can be administered to human patients. Unfortunately, ERT may cost as much as several hundred thousand dollars per patient per year such as Brineura for CLN2 disease which cost more than £500,000 per patient per year (Smith 2019).

### **1.3.3 Gene therapy**

Gene therapy is another strategy for treating LSDs by injecting a vectored healthy copy of the affected gene directly into affected tissues. As with most of the strategies for treating LSDs, gene therapy is aimed at increasing the levels of the defective enzyme in patients. As LSDs are monogenic disorders, gene therapy is a viable therapeutic approach. Additionally, as lysosomal enzymes can be secreted and taken up by other cells via the mannose-6-phosphate receptor, they are attractive targets for gene therapy as the gene does not need to be transferred to all cells. Many different viral vectors have been and are being tested, such as Herpesviruses, lentiviruses, adeno-associated viruses, and adenoviruses (Cardone 2007).

An example of *in vivo* gene therapy is the current clinical trial in CLN2 patients, where a healthy copy of the TPP1 gene is being delivered intracerebrally using an adeno-associated virus (AAV) vector in patients, that has displayed promising outcomes in patients (Kohlschütter and Schulz 2016). Intracerebral injection of AAV with a healthy gene is also under investigation for other LSDs and neurodegenerative diseases such as MPS IIIB, metachromatic leukodystrophy and Parkinson disease (Hocquemiller et al. 2016).

There are, however, still many concerns around gene therapy including issues with viral vector safety and carcinogenesis following gene transfer mediated by retrovirus or adenovirus. This may be overcome using AAV vectors which generally do not integrate into the host genome (Parenti et al. 2012). Nonetheless, there are other limitations to gene therapy such as patients developing immune responses, and the

inability of this treatment to cross the blood-brain barrier (Parenti et al. 2012; Beck 2017).

#### **1.3.4 Substrate reduction therapy (SRT)**

Another approach to treating LSDs is to reduce the material being stored by inhibiting specific steps of the biosynthetic pathway; this decreases production of the material and helps restore equilibrium between material synthesis and catabolism (Platt and Jeyakumar 2008; Schiffmann 2010).

*N*-butyldeoxynojirimycin, or miglustat, is an example of an SRT that is approved and is being used to treat LSDs including Gaucher disease type 1 and NPC1 disease. Miglustat is an imino sugar analogue of D-glucose that acts by inhibiting glucosylceramide synthase, leading to partial inhibition of the biosynthesis of glycosphingolipids that ultimately results in reduced lysosomal lipid storage (Platt et al. 1994; Lachmann et al. 2004).

Miglustat treatment reduces lysosomal storage, ameliorates endo-lysosomal trafficking defects, rescues Purkinje neuron function and survival in NPC disease (Lachmann et al. 2004; Patterson et al. 2007; Stein et al. 2012). Furthermore, miglustat slows progression of NPC1 disease in adults; whereas, in children, neurological symptoms are stabilised, motor decline is decreased and eye movement velocity and swallowing are improved (Lachmann et al. 2004; Patterson et al. 2007; Stein et al. 2012).

A new drug called eliglustat is a novel ceramide glucosyltransferase inhibitor which has recently been approved in the United States and Europe for treating Gaucher disease (Beck 2017). SRT is also currently being explored for treatment in other LSDs including Fabry disease (Marshall et al. 2010), Pompe disease (Douillard-Guilloux et al. 2010) and Sandhoff (Ashe et al. 2011). The use of small-molecule SRT has advantages compared to ERT and gene therapy, particularly bioavailability across different tissues, the lack of immune response, and the opportunity for oral administration (Parenti et al. 2012; Beck 2017). Nonetheless, this treatment option is not available for many LSDs yet, as further understanding of the biochemical pathways affected in LSDs is needed.

### 1.3.5 Pharmacological Chaperone therapy

Many of the LSDs are caused by mutations that lead to improper protein folding; this prevents them from reaching the lysosome and carrying out their function, as misfolded proteins are tagged for degradation in the ER by protein quality control systems (Parenti et al. 2012). In some of these LSDs, the enzyme may recover partial or full function if it is able to fold properly (Beck 2017). Pharmacological molecules called chaperones can be used to treat diseases resulting from protein misfolding as they may help proteins fold appropriately by interacting with the mutant protein and enhancing its stability, thus avoiding degradation and partially rescuing the mutant protein (Parenti 2009).

The first example of a chaperone therapy for an LSD is the imino sugar 1-deoxygalactonojirimycin or migalastat which is used to treat Fabry disease as it is a competitive inhibitor of the enzyme affected in this disease,  $\alpha$ -galactosidase (Giugliani et al. 2013). Migalastat (Galafold), at sub-inhibitory concentrations, acts as a chemical chaperone that competitively binds to the enzyme, allowing certain mutant  $\alpha$ -galactosidase to fold to the correct conformation, facilitating lysosomal trafficking and thus increasing catalytic activity (Giugliani et al. 2013). This drug has been through all of the required safety trials and has recently been approved by the FDA and EMA for Fabry patients with certain mutations (Parenti et al. 2012; European Medicines Agency 2016; US Food & Drug Administration 2018).

A more recent example of a chaperone therapy that has been reported to have potential benefit for the LSD Gaucher disease is ambroxol (Maegawa et al. 2009; Magalhaes et al. 2018). Ambroxol is an expectorant that has been previously used to treat respiratory disease associated with mucus hypersecretion (Magalhaes et al. 2018). Maegawa *et al.* (2009) reported that ambroxol acts as a chaperone of certain glucocerebrosidase mutants, the enzyme deficient in Gaucher disease, stabilising the enzyme and improving translocation to the lysosome, where it dissociates at the acidic pH. Further work also reported that ambroxol increases the levels of the glucocerebrosidase activator saposin C and the activity of cathepsin D, another lysosomal enzyme (Ambrosi et al. 2015).

However, there are some disadvantages to chaperone therapies, including their effectiveness for only certain mutations, with others unresponsive to treatment. For a

chaperone therapy to work, the mutation must be located in specific domains of the protein (Flanagan et al. 2009). Additionally, there is a risk that chaperone molecules may inhibit activity instead of enhancing it if they reach high enough concentrations (Parenti et al. 2012; Beck 2017). This may be overcome, however, by finding new molecules that interact with allosteric sites and not the active site; for example, recent computational screens have identified allosteric chaperones for  $\alpha$ -glucosidase which may be used in the future to treat Pompe disease (Porto et al. 2012).

### 1.3.6 Nutraceuticals

Nutraceuticals or 'bioceuticals' are compounds or substances that may have physiological benefit in chronic disease but are not regulated by the FDA or EMA as they fall under the same category as dietary supplements (Nasri et al. 2014). Nutraceuticals have been reported to have many health benefits, with many recently receiving considerable interest due to their potential therapeutic effects on a myriad of diseases such as Alzheimer, cardiovascular disease, cancer, diabetes, Parkinson disease and LSDs (Lloyd-Evans et al. 2008; Nasri et al. 2014; Makkar et al. 2020).

An example of a nutraceutical that has been reported to have potential benefit to an LSD is curcumin (Lloyd-Evans et al. 2008). Curcumin, found in turmeric, is a widely used spice, flavouring and herbal nutraceutical that is an anti-oxidant and modulator of  $\text{Ca}^{2+}$  homeostasis, that has been shown to have beneficial effects in *Npc1<sup>-/-</sup>* mice (Lloyd-Evans et al. 2008). This nutraceutical has also been reported, in thousands of publications, to have anti-inflammatory, anti-cancer, anti-microbial and other beneficial effects, including improvement in patients with different diseases such as cancer and Alzheimer disease (Monroy et al. 2013; Shanmugam et al. 2015). Furthermore, curcumin is able to cross the blood-brain barrier, which is important to treat diseases such as LSDs, where the brain is primarily affected (Tsai et al. 2011).

Curcumin is known to be able to inhibit all 3 isoforms of the  $\text{Ca}^{2+}$  channel SERCA by inducing a conformational change that blocks ATP binding (Bilmen et al. 2001). As mentioned above, SERCA is an important protein in that it regulates ER and cytosolic  $\text{Ca}^{2+}$  by pumping  $\text{Ca}^{2+}$  from the cytosol to the ER. Therefore, inhibiting SERCA leads to cytosolic  $\text{Ca}^{2+}$  increases via the action of ER  $\text{Ca}^{2+}$  leak channels which, in turn, stimulate further  $\text{Ca}^{2+}$  release from the ER. Lloyd-Evans *et al.* (2008) reported that it

is possible that the increase in cytosolic  $\text{Ca}^{2+}$  benefits NPC1 disease by compensating for the decrease in lysosomal  $\text{Ca}^{2+}$  release, resulting in a correction of defective  $\text{Ca}^{2+}$ -dependent endo-lysosomal fusion events and an improvement in lipid storage.

There are, however, concerns around the use of nutraceuticals for LSDs, considering the lack of regulation around the formulation of nutraceuticals that may generate compounds that ultimately cause more harm than good (Cohen 2014). The lack of regulation may also lead to batch inconsistencies and inaccurate labelling, which has caused issues in the past (Cohen 2014). An example of the dangers of unregulated nutraceuticals is the more than 200 cases of selenium poisoning caused by a multivitamin supplement in 2008 (Cohen 2014). Therefore, care must be taken when selecting nutraceuticals that may be of benefit to LSDs in order to find formulations that provide benefit without toxicity.

### **1.3.7 Combination therapies**

Ultimately, all LSDs present a variety of cellular dysfunction and clinical symptoms and, as such, targeting multiple pathogenic events at the same time using different therapeutic approaches will lead to the most effective treatments for the disease (Specchio et al. 2020). An approach that may be used in order to target multiple pathogenic events as well as increase the likelihood of treatment efficacy is using combination therapies, which is the use of multiple approaches to treat a disease.

There have already been studies of combination therapies in *Npc1*<sup>-/-</sup> mice; miglustat to decrease sphingolipid synthesis and storage, curcumin to increase cytosolic  $\text{Ca}^{2+}$  to compensate for reduced lysosomal  $\text{Ca}^{2+}$ , and ibuprofen to decrease neuroinflammation. The study concluded maximum clinical benefit was achieved by using the combination approach that targets different steps of the pathogenic cascade (Williams et al. 2014).

Chaperone therapy can also be used in combination therapies. One example of chaperone therapy being used in combination with another therapy is in Pompe disease where patients were treated with both chaperone therapy and ERT. Pompe disease is an LSD caused by a deficiency in the enzyme  $\alpha$ -glucosidase. Some patients have been allowed to receive 1-deoxynojirimycin or duvelgotat HCL (AT2220) orally in combination with ERT of the recombinant  $\alpha$ -glucosidase through orphan drug

designation. The combination of these therapies leads to an approximate two-fold increase in  $\alpha$ -glucosidase activity compared to ERT alone (Kishnani et al. 2017).

Even the approval of therapies for some LSDs such as miglustat for NPC1 or Brineura for CLN2 bring about a new era of novel disease progression patterns in treated patients (Specchio et al. 2020). The novel phenotypes that are uncovered as each patient's disease progress into stages not seen before will ultimately require other therapies to treat them, highlighting further the importance of combination therapies.

### **1.3.8 Novel therapies**

Many LSDs are caused by premature stop-codon mutations, which lead to the formation of truncated non-functional proteins (Brooks et al. 2016). Certain drugs, such as gentamicin, can be used to induce read-through of premature stop-codons, resulting in production of full-length proteins with some or even normal enzymatic activity. Therefore, pharmacological compounds that are able to do this may be used to treat diseases caused by premature stop-codons. Keeling *et al.* (2001) found that treating patient MPS disease I fibroblast cells containing various premature stop-codon mutations with gentamicin increased the levels of the deficient enzyme iduronidase (Keeling et al. 2001; Keeling 2016).

The positive effects of this type of treatment were further demonstrated in animal models of MPS I carrying a homologous mutation to one of the early stop-codon mutations in patients, which were treated with the drug aminoglycoside NB84 (Wang et al. 2012a). Following a 28-week treatment of this drug, the animal models showed significantly increased iduronidase activity in several organs, improved heart function, reduced glycosaminoglycan accumulation and improved activity (Gunn et al. 2014). There are, however, no currently approved therapies using drugs that induce read-through of premature stop-codons.

Other pharmacological compounds that may be of benefit to LSDs by aiding lysosomal clearance are being developed and applied to clinical trial. These compounds include the heat shock protein modulator arimoclomol, discussed further in Chapter 4, to treat NPC, Huntington disease and amyotrophic lateral sclerosis (Kirkegaard et al. 2010; Kirkegaard et al. 2016), the anti-inflammatory drug pentosane

polysulfate to treat MPS I (Hennermann et al. 2016) and the sphingosine 1-phosphate receptor modulator fingolimod to treat NPC, the NCLs and Huntington disease (Brunkhorst et al. 2014; Groh et al. 2017).

Recently, a regulatory application for arimoclomol to treat NPC1 disease was made to the FDA (Orphazyme 2020). There are even some pharmacological compounds in clinical trial where the exact mechanisms of action are not well understood, such as cyclodextrin, a cyclic oligosaccharide, being tested in NPC patients as it improves neurological function and stabilises disease progression in animal models and NPC patients (Megias-Vericat et al. 2017). Nonetheless, it was reported to cause hearing loss and not have as much of an effect in patients as it did in the animal models which lead to the trials in Europe being stopped (Crumling et al. 2017).

Mycophenolate mofetil is another example of a compound that has been reported to be potentially beneficial for LSDs (Seehafer et al. 2011; Augustine et al. 2019). This compound is an FDA approved immunosuppressant that has been used as an off-label treatment for autoimmune neurological conditions (Augustine et al. 2019). Studies have reported that mycophenolate mofetil treatment in *Cln3<sup>Δex1-6</sup>* mice, which is a CLN3 mouse model, reduced levels of autoantibodies, decreased neuroinflammation and improved motor function (Seehafer et al. 2011). Nonetheless, a short-term study in CLN3 disease patients showed no clinical benefit and suggested that long-term trials are needed (Kohlschütter and Schulz 2016).

Currently, there are very few FDA and/or EMA approved therapies for LSDs. In fact, most LSDs currently have no therapy, making them an urgent unmet medical need. All current therapies have limitations and do not apply to all LSDs. Remarkably, other than for CLN2, there are no therapies for the NCLs, despite them being the largest group of LSDs (Mukherjee et al. 2019) and sharing many common pathological mechanisms.

Small molecule therapies that target common cellular pathologies across the LSDs can be used in combination with other therapies across different LSDs. As such, more research to increase the understanding of the mechanisms behind LSD pathology, as well as drug screening and development for LSDs is needed. By understanding the pathological mechanisms that affect the NCLs, small molecule therapies can be

identified that can help reduce lysosomal storage in the NCLs and across the LSDs by targeting common cellular mechanisms affected.

Finding and developing drugs for rare diseases, and indeed for all diseases, is extremely difficult and expensive. This will ultimately lead to unsustainable costs for services like the NHS, as companies seek to recoup research and development costs. Drug repurposing, outlined further in Chapter 5 Section 5.1.1, offers an increased likelihood of reaching patients and lower development costs, as these drugs have already been tested for other diseases and, as such, have safety data available (Pushpakom et al. 2019). Therefore, drug repurposing should be prioritised as a method of drug discovery for rare disease, to develop much needed therapies in this area of unmet medical need.

#### **1.4 Aims & Objectives**

There is a dearth of knowledge surrounding the pathogenic mechanisms in CLN8 disease and thus further research is needed to identify the cellular processes that are altered in the disease, which will enable the identification of therapeutic targets and phenotypes that can be used for drug screening. Furthermore, LSDs in general are poorly understood and currently have few to no available therapies, making them an urgent unmet medical need. The aim of this project is to explore cellular phenotypes in CLN8 patient cell lines that can increase our understanding of the disease and be used for drug screening, as well as developing and carrying out drug screens that may identify compounds that may be of benefit to other or multiple LSDs.

**Chapter 2** describes the materials and methods that were used throughout this study.

**Chapter 3** investigates cellular phenotypes in four CLN8 patient cell lines to identify possible therapeutic intervention targets and categorise cellular phenotypes for future drug screening in the disease.

**Chapter 4** characterises and validates a cellular model for NPC1 disease using *Npc1*<sup>-/-</sup> glial cells for high-throughput drug screening and confirmation studies.

**Chapter 5** explores 3 drug repurposing projects: 1. A high-throughput screen of an FDA approved drug library for molecules that can increase activity of the galactosylceramidase enzyme, whose function is lost in the LSD Krabbe disease. 2. Cellular based screen of the potential benefit of miglustat in some NCL patient cells. 3. Exploration of the potential mechanisms by which curcumin may be of benefit to several LSDs.

**Chapter 6** summarises the conclusions of this thesis with a general discussion, including the future implications of the findings in this report, and proposes future works that should be undertaken.

## **Chapter 2: Materials and Methods**

All materials and chemicals were purchased from Sigma Aldrich, Poole, United Kingdom unless specified otherwise.

### **2.1 Cell Culture**

#### **2.1.1 Human fibroblasts (HF)**

Human fibroblast cells (HFs) are well-characterised skin derived cell lines that were taken from patients (Table 3.1, 4.2 & 5.1) and have been used in publications previously (Pal et al. 2006; de Mezer et al. 2011). HFs are a good model for LSDs studies as they contain the relevant patient mutation and can be passaged multiple times (up to 20 and always closely matched in all experiments). HFs are non-excitabile cells meaning that fundamental changes in organelle function can be explored in the absence of enhanced cellular responses to extracellular factors and have been previously used to characterise disease phenotypes (Auburger et al. 2012). HFs were cultured as a monolayer in Dulbecco's Modified Eagle's Medium (DMEM) with 10% heat-inactivated foetal bovine serum (FBS; PAN Biotech® Aidenbach, Bavaria, Germany) and 2 mM L-glutamine in a humidified incubator at 37 °C and 5% CO<sub>2</sub>. The passage number between different cell lines were kept within a range of +/- 2 in every experiment to ensure the different cell lines were passage matched.

Briefly, human fibroblasts (HFs) in this project acquired from Coriell Cell Repository (Camden, NJ, United States) were apparently healthy control 1-year-old GM05399 (control 1 HF), 6-year-old GM05400 (control 2 HF), CLN2 HF (GM16486), NPC1 HF (GM03123) and NPA HF (GM00112). CLN7 474 HF, CLN8 462 HF, CLN8 533 HF, CLN8 534 HF, CLN8 535 HF and CLN10 HF were kindly provided by Professor Sara Mole, University College London.

### 2.1.2 Astroglial cell lines

*Npc1* knockout (*Npc1*<sup>-/-</sup>) glia and control (*Npc1*<sup>+/+</sup>) glia were established previously in Lloyd-Evans *et al.* (2008). The cells were isolated from the cortex of newborn post-natal day 1 mice, allowed to adhere and then subcultured by trypsinization (Lloyd-Evans *et al.* 2008). The resulting astroglial cell lines were genotyped to select *Npc1*<sup>+/+</sup> and *Npc1*<sup>-/-</sup> cultures and then maintained as a monolayer in DMEM with 10% heat-inactivated fetal bovine serum and 2 mM L-glutamine in a humidified incubator at 33 °C and 5% CO<sub>2</sub>. The passage number between different cell lines were kept within a range of +/- 2 in every experiment to ensure the different cell lines were passage matched.

### 2.1.3 Drug treatments

Drug treatment longer than 2 days were refreshed every 48 hours and the cells were maintained at no more than 80% confluency. The precise concentration and treatment lengths for each experiment are outlined in each figure legend.

#### 2.1.3.1 Miglustat treatments

Cells in culture, as outlined above, were treated with 50 µM miglustat (outlined in detail in Chapter 5 Section 5.1.3; Toronto Research Chemicals, Toronto, Ontario, Canada) in DMEM as this has been shown to be an appropriate *in vitro* concentration of the drug (Guerrera and Ladisch 2003). The cells were then incubated in humidified incubators for 24 hours or 7 days (Lachmann *et al.* 2004; te Vruchte *et al.* 2004).

#### 2.1.3.2 Arimoclomol treatments

Arimoclomol is a small molecule hydroxylamine derivative that induces HSP70 expression leading to upregulation of the genome and has been identified as a potential therapy for LSDs such as NPC1 (Hesselink 2017; Fog *et al.* 2018; Orphazyme 2020). Arimoclomol treatments were carried out at a concentration of 50 µM, 100 µM, 200 µM, 400 µM and 800 µM in DMEM from a Dimethyl sulfoxide (DMSO) stock solution and incubated in humidified incubator for 3 days (Hesselink 2017; Fog

et al. 2018). Arimoclomol-like compound, provided by SOM Biotech, treatments were done at 5  $\mu$ M, 50  $\mu$ M, 100  $\mu$ M and 200  $\mu$ M for three days.

#### 2.1.3.3 Curcumin treatments

Curcumin nanoformulations (Life Extension, Fort Lauderdale, FL, United States; Nutrivine, Middle Rivers, MD, United States), outlined in Chapter 5 Section 5.1.4 & Table 5.3, were used to treat cells at 30  $\mu$ M from a DMSO stock 10mM solution in DMEM ensuring that the DMSO content in treat cells was always at 0.3% v/v. Treated cells were then incubated in humidified incubator for 4 hours or 24 hours. For each nanoformulation the stock solution was made by calculating the ratio carrier/bulking agents as stated by the manufacturer (Table 5.3) as well as thin layer chromatography separation and confirmation of curcuminoid content (Badell-Grau *et al.* in prep).

#### 2.1.3.4 Dexamethasone treatments

Dexamethasone treatments were carried out at a concentration of 100 nM in DMEM from a DMSO stock solution and then incubated in humidified incubator 30 minutes before being refreshed with DMEM without drug and left overnight before being used for an experiment as this concentration has been previously suggested to possibly reset circadian rhythms in cells (Balsalobre et al. 2000; Nagoshi et al. 2004).

## **2.2 Fixed Immunocytochemistry**

### **2.2.1 Paraformaldehyde cell fixation**

To prepare cells for immunohistochemistry, 10,000 cells were plated on acid-washed glass coverslips in a 24-well plate (Greiner, Kremsmünster, Austria) or 15,000 cells were plated directly in a sterile 96-well Ibidi  $\mu$ -plate (Thistle Scientific, Glasgow, United Kingdom) and left to grow overnight; the growth media was removed on the following morning and the cells were washed in non-sterile Dulbecco's phosphate-buffered saline (D-PBS). Following the D-PBS wash, the coverslips were treated with 4% paraformaldehyde (PFA) in D-PBS at pH 7 for 10 minutes at room temperature.

The cells were then washed once in DMEM followed by three washes in D-PBS. Once fixed, cells were stored in 1 ml of D-PBS at 4 °C until required for staining and were maintained in this manner for no more than a maximum of 4 weeks.

### **2.2.2 Blocking buffer**

Fixed cells were blocked in D-PBS supplemented with 1% bovine serum albumin (BSA) and 0.01% saponin for 30 minutes in order to prevent non-specific antibody binding and aid permeabilization of cells, respectively. Aliquots of blocking buffer were stored until required at -20 °C.

### **2.2.3 Cholesterol staining with filipin**

The blue auto-fluorescent antibiotic filipin, with an excitation and emission at 380 nm and 450 nm, respectively, was used to visualise unesterified cholesterol levels in the cells fixed as described above. Filipin has been used previously in publications to bind unesterified cholesterol (te Vruchte et al. 2004; Maxfield and Wüstner 2012; Vanier and Latour 2015) and is specific as cells lacking cholesterol but containing all other sterol species are not labelled (Wassif et al. 2002). Fixed cells were incubated for 30 minutes in a 175 µg/ml filipin solution in DMEM with 10% FBS. Following filipin incubation, cells were washed for five minutes in D-PBS three time before being fixed in PFA (Section 2.2.1), mounted (Section 2.2.5) and then imaged (Section 2.4).

### **2.2.4 Ganglioside GM1 staining with FITC tagged cholera toxin B subunit**

Ganglioside GM1 cellular localisation and levels were visualised using cholera toxin B subunit with a FITC tag (CtxB-FITC) which has an excitation and emission at 490 nm and 525 nm, respectively (Blank et al. 2007). CtxB specifically binds to ganglioside GM1 making it an appropriate probe to visualise ganglioside GM1 levels and localisation (Blank et al. 2007). Fixed cells were incubated in 1 µg/ml CtxB-FITC solution in DMEM and incubated overnight at 4 °C. Following the incubation, cells were washed three times for five minutes in D-PBS before being fixed in PFA (Section 2.2.1), mounted (Section 2.2.5) and then imaged (Section 2.4).

### **2.2.5 Antibody staining of HSP70**

HSP70 staining was carried out using a polyclonal antibody against human HSP70 (CAT25405-1-AP; ThermoFisher Scientific, Massachusetts, United States). The anti-HSP70 antibody was used at a dilution of 1:100 in blocking buffer (Section 2.2.2) overnight at 4 °C before washing the cells 3 times for 5 minutes in blocking buffer. The cells were then incubated at room temperature with the secondary antibody Dylight 488 anti-rabbit IgG (Vector Scientific, Golden, CO, United States) with excitation and emission at 493 nm and 518 nm respectively. Finally, the cells were then washed 3 more times for 5 minutes in D-PBS before being fixed in PFA (Section 2.2.1), mounted (Section 2.2.5) and then imaged (Section 2.4).

### **2.2.6 Nucleus counter-staining**

Nuclei in fixed and live cell-staining (section 2.3) were visualised by incubating with a 4 µg/ml Hoechst33342 solution (ThermoFisher Scientific) in D-PBS, with an excitation and emission at 350 nm and 461 nm, respectively, for 10 minutes before being washed three times for five minutes in D-PBS.

### **2.2.7 Coverslip mounting**

Following staining procedures outlined above, cells grown on coverslips were mounted on twin frosted-glass slides (ThermoFisher Scientific) using Fluoroshield™ mounting medium. Mounted coverslips were imaged, as described in section 2.4, after being left to dry in the dark for at least 12 hours at room temperature. Whereas, cells seeded in the sterile 96-well Ibidi µ-plate were visualised in the plate in D-PBS and thus did not require mounting.

## **2.3 Live Cell staining**

All cells were counterstained with Hoechst33342 as outlined above in Sections 2.2.2.

### **2.3.1 Cell seeding**

To prepare cells for live staining 8,000 cells per well were seeded the day before

imaging into sterile 8-well Ibidi  $\mu$ -slide or 5,000 cells per well into a sterile 96-well Ibidi  $\mu$ -plate (Ibidi). The seeded cells were then incubated in a humidified incubator at the correct temperature as outlined in Section 2.1.

### **2.3.2 Lysosomal staining**

LysoTracker green DND-26 (ThermoFisher Scientific), with an excitation and emission at 504 nm and 511 nm, respectively, was used to investigate the relative number and size of lysosomes in patient HFs compared to control HFs, as it preferentially loads into acidic organelles (pH <5.5). Cells in Ibidi  $\mu$ -slide or Ibidi  $\mu$ -plate (Section 2.3.1) were washed once in D-PBS and then incubated in a 200 nM LysoTracker solution in D-PBS for 15 minutes at 37 °C. Cells were washed three times in D-PBS, counter-stained, and then imaged live in D-PBS.

### **2.3.3 Lysosomal 96-well plate assay**

LysoTracker green DND-26 was also used to measure total fluorescence levels using a fluorescence plate assay format (Xu et al. 2014) by seeding cells in a collagen I coated 96 well plate (ThermoFisher Scientific). Cell densities were cell type dependant, for human fibroblast 50,000 cells per well were seeded; whereas, for glia cells 60,000 cells were used, mainly as the glia cells are slightly smaller. These final cell seeding densities were determined after testing the fluorescence output over a range of cell densities; 20,000, 30,000, 40,000, 50,000, 60,000, 70,000, 80,000 and 90,000 cells per well. Cells were plated and incubated overnight in a humidified incubator before being incubated with 200 nM LysoTracker solution in D-PBS for 15 minutes at 37 °C. Cells were washed three times in D-PBS before being left in DPBS and the fluorescence measured in live cells using a monochromator based SpectraMAX Gemini EM (Molecular Devices) plate reader with SoftMax Pro software. Plates were measured with the excitation set to 485 nm and the emission at 520 nm, background autofluorescence was determined and then subtracted using cells not loaded with lysotracker green.

### **2.3.4 Autophagic compartment visualisation**

CytoID autophagy green detection kit 2.0 (Enzo Life Sciences, New York, United States), with an excitation and emission at 460 nm and 527 nm, respectively, was used to investigate the relative number and size of autophagic compartments in patient HFs compared to control HFs. CytoID is a probe that stains autophagic vacuoles, as it is a cationic amphiphilic tracer dye that is internalised by cells in manner similar to phospholipids; however the exact mechanism by which it preferentially accumulates in autophagic vacuole is unknown (Shang et al. 2017; Miyayama et al. 2018). Cells previously plated in Ibidi  $\mu$ -slides were washed once in D-PBS and incubated in 100  $\mu$ l of DMEM containing 2  $\mu$ l CytoID stock solution for 30 minutes at 37 °C. Cells were then washed three times in D-PBS, counter-stained, and then imaged live in D-PBS.

### **2.3.5 Endoplasmic reticulum staining**

ER-Tracker green (BODIPY<sup>TM</sup> FL Glibenclamide; ThermoFisher Scientific), with an excitation and emission at 504 nm and 511 nm, respectively, was used to investigate the relative size and distribution of the ER in patient HFs compared to control HFs. This probe labels the ER as glibenclamide binds to the sulphonylurea receptors of ATP-sensitive K<sup>+</sup> channels which are present on the ER. Cells in Ibidi  $\mu$ -slide or Ibidi  $\mu$ -plate (Section 2.3.1) were washed once in D-PBS and then incubated in a 200 nM ER-Tracker solution in D-PBS for 15 minutes at 37 °C. Cells were washed three times in D-PBS, counter-stained, and then imaged live.

### **2.3.6 Mitochondrial staining**

MitoTracker red FM (ThermoFisher Scientific) is a cell-permeant probe that localises to the mitochondria independent of membrane potential. This probe was used to investigate the relative distribution of the mitochondria in patient HFs compared to control HFs and has excitation and emission at 581 nm and 644 nm, respectively. Cells in Ibidi  $\mu$ -slide or Ibidi  $\mu$ -plate (section 2.3.1) were washed once in D-PBS and then incubated in a 200 nM MitoTracker solution in D-PBS for 15 minutes at 37 °C. Cells were washed three times in D-PBS, counter-stained, and then imaged live.

### **2.3.7 Complete Hank's balance salt solution (HBSS)**

Imaging buffer for  $\text{Ca}^{2+}$  experiments (Section 2.3.8) comprised of ultra-low  $\text{Ca}^{2+}$  containing Hank's balanced salt solution (HBSS; ThermoFisher Scientific) with 1 mM 4-(2-hydroxyethyl)-1-piperazineethanesulfonic acid (HEPES; Lonza, Basel, Switzerland), 1 mM  $\text{MgCl}_2$  and approximately 0.025 mM  $\text{CaCl}_2$  in MilliQ water (Barnstead purifier, ThermoFisher Scientific). The concentration of  $\text{Ca}^{2+}$  was kept low in order to avoid extracellular  $\text{Ca}^{2+}$  interference when measuring intracellular  $\text{Ca}^{2+}$  (Section 2.3.8) but was never reduced to zero as this is also detrimental to plasma membrane integrity (De Luisi and Hofer 2003).

### **2.3.8 $\text{Ca}^{2+}$ measurements**

Organelle  $\text{Ca}^{2+}$  levels were measured using the cell permeable  $\text{Ca}^{2+}$  probe Fura-2,AM (ThermoFisher Scientific) with an excitation at 360 nm and 380 nm, and emission at 525 nm (Grynkiewicz et al. 1985) as explained in Figure 2.1. The  $\text{Ca}^{2+}$  release was calculated ratiometrically between the two excitation wavelengths of 360 nm and 380 nm (Figure 2.1). Cells plated in Ibidi  $\mu$ -plate (Section 2.3.1) were washed in pre-cooled DMEM with 1% BSA before being incubated with 5  $\mu\text{M}$  Fura-2,AM in DMEM with 0.005% Pluronic F127 and 1% BSA for an hour  $<16^\circ\text{C}$  to prevent internalisation of the dye into intracellular organelles. After this, the cells were washed for 10 minutes in low  $\text{Ca}^{2+}$  containing HBSS to ensure complete hydrolysis of the membrane permeant acetoxymethyl (AM) ester and full release of the loaded Fura 2,AM (Sections 2.3.7). Cells were then washed once more in the same HBSS before being imaged in 100  $\mu\text{l}$  of HBSS (Sections 2.4).

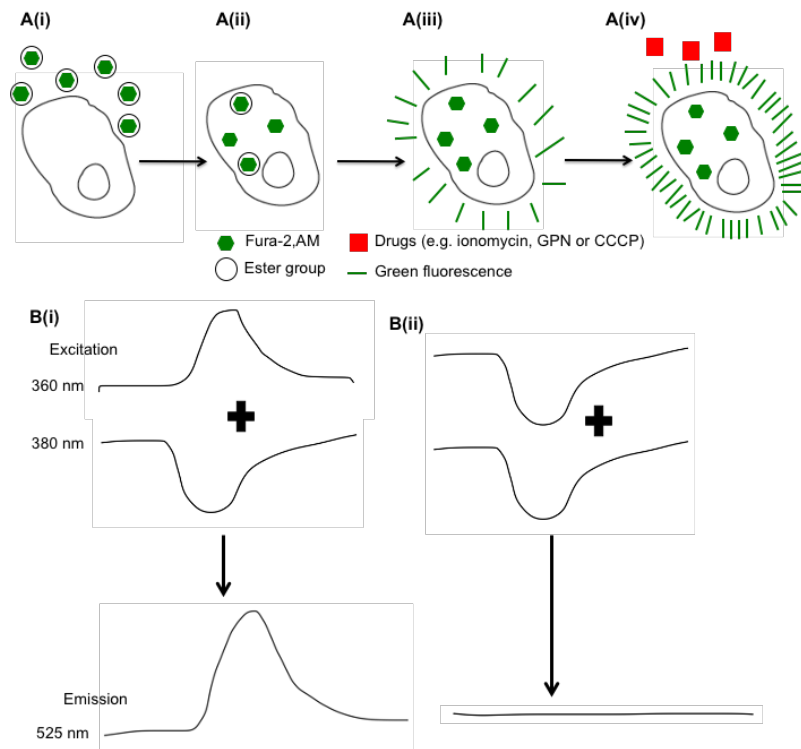


**Figure 2.1: Drug mediated  $\text{Ca}^{2+}$  release measurement protocol outline.** **A(i):** Cells were incubated with the cell permeant probe Fura-2,AM (denoted by green hexagon) for an hour at  $<16^\circ\text{C}$  allowing to probe to enter the cytosol. The incubation was done cold in order to prevent the probe from being endocytosed and entering the endo-lysosomal system. **A(ii):** After the incubation cells were washed in low  $\text{Ca}^{2+}$  containing HBSS and incubated for 10 minutes at room temperature which allows the esterases in the cell to cleave the ester group (indicated by the black circle). **A(iii):** Once the ester group is cleaved the Fura-2,AM probe becomes proportionally fluorescent to the  $\text{Ca}^{2+}$  concentration in the cytosol. **A(iv):** The corresponding drug is added (indicated by red squares) to induce  $\text{Ca}^{2+}$  release from the target organelle which leads to an increase in fluorescence measured using a fluorescence microscope (Sections 2.4). **B:** Outline of how the  $\text{Ca}^{2+}$  release peaks (emission at 520nm) are calculated ratiometrically between the excitation wavelengths of 360 nm and 380 nm. As the probe is ratiometric, noise is cancelled out which ensures that the signal tested and measure is almost always due to changes in  $\text{Ca}^{2+}$ .

### 2.3.8.1 Ionomycin mediated $\text{Ca}^{2+}$ release

During imaging, drugs were added to stimulate  $\text{Ca}^{2+}$  release from the target organelle and the release was recorded (Figure 2.1B). Ionomycin (Merck Millipore, Massachusetts, United States) was added at a concentration of  $2\ \mu\text{M}$  to induce  $\text{Ca}^{2+}$  release for all  $\text{Ca}^{2+}$  stores except for the lysosome through permeation of non-lysosomal membranes (Liu and Hermann 1978) which predominantly detects ER  $\text{Ca}^{2+}$  as the biggest intracellular  $\text{Ca}^{2+}$  store.

#### 2.3.8.2 Glycyl-L-phenylalanine- $\beta$ -naphthylamide (GPN) mediated $\text{Ca}^{2+}$ release

Lysosomal  $\text{Ca}^{2+}$  was measured after emptying all  $\text{Ca}^{2+}$  stores with ionomycin by adding 300  $\mu\text{M}$  glycyl-L-phenylalanine- $\beta$ -naphthylamide (GPN; Alfa Aesar, Ward Hill, United States) which is a cathepsin C substrate that when cleaved within lysosomes generates a product that causes osmotic lysis of the lysosome membrane and releases of  $\text{Ca}^{2+}$  into the cytoplasm (Berg et al. 1994).

#### 2.3.8.3 Thapsigargin mediated $\text{Ca}^{2+}$ release

Thapsigargin at a concentration of 1  $\mu\text{M}$  was used to measure ER  $\text{Ca}^{2+}$  content and release as it is a competitive inhibitor of SERCA. The inhibition of the ER  $\text{Ca}^{2+}$  importer SERCA using thapsigargin leads to an increase in cytosolic  $\text{Ca}^{2+}$  concentration due to ER  $\text{Ca}^{2+}$  release via the ER  $\text{Ca}^{2+}$  leak channels that then trigger  $\text{Ca}^{2+}$  induced  $\text{Ca}^{2+}$  release from the ryanodine (RyR) and IP3 receptors; this ultimately acts as a surrogate assay that, assuming no alteration to the function of the leak channels or associate proteins (Morimoto et al. 2018) enables the measurement of total ER  $\text{Ca}^{2+}$  (Berman 2000), which should tally with the ionomycin method.

#### 2.3.8.4 Ryanodine mediated $\text{Ca}^{2+}$ release

The addition of 10  $\mu\text{M}$  ryanodine was used as another method to measure ER  $\text{Ca}^{2+}$  homeostasis by determining  $\text{Ca}^{2+}$  release from the ER RyR upon which ryanodine is an agonist at this concentration (Fill and Copello 2002).

#### 2.3.8.5 Antimycin / oligomycin mediated $\text{Ca}^{2+}$ release

Levels of mitochondrial  $\text{Ca}^{2+}$  were determined using 5  $\mu\text{M}$  antimycin in combination with 5  $\mu\text{M}$  oligomycin as antimycin is a strong electron transport chain inhibitor while oligomycin is a strong uncoupling agent that blocks the  $\text{F}_0$  subunit of ATP synthase that when combined prevent mitochondrial  $\text{Ca}^{2+}$  uptake leading to mitochondrial  $\text{Ca}^{2+}$  leak.

#### 2.3.8.6 Carbonyl cyanide m-chlorophenyl-hydrazine (CCCP) mediated Ca<sup>2+</sup> release

CCCP at a concentration of 50 µM is also known to induce mitochondrial Ca<sup>2+</sup> release as carbonyl cyanide m-chlorophenyl-hydrazine (CCCP) leads to mitochondrial depolarisation which in turn causes mitochondrial Ca<sup>2+</sup> leak (Montero et al. 2001). This may, however, also impact upon Golgi function but the Ca<sup>2+</sup> content of this organelle currently remains unknown.

### 2.3.9 Visualisation of Mitochondrial Ca<sup>2+</sup> levels

Mitochondrial Ca<sup>2+</sup> was visualised using the mitochondrial Ca<sup>2+</sup> Rhod-2,AM (ThermoFisher Scientific) in DMSO which was mixed with equal part F-127 pluronic vortexed and then added to DMEM to make a final concentration of 2 µM. The Rhod-2,AM DMEM solution was then added to cells and incubated at 37 °C for 30 minutes. Following this, fresh DMEM was added to the cells and these were left in the incubator overnight 37 °C before being imaged the next day as outlined in 2.4.

## 2.4 Fluorescence microscopy

### 2.4.1 Microscopy

Fixed immunocytochemistry and live-cell staining were imaged on an inverted Colibri widefield fluorescence microscope (Zeiss, Cambridge, United Kingdom) with a high speed Zeiss MRm monochrome charge-coupled device (CCD) digital camera, a Colibri LED light source (Zeiss), a 40x magnification oil immersion lens (Zeiss) and Axiovision 4.7.1 software (Zeiss 2008). The Colibri widefield fluorescence microscope contains 4 excitation LEDs at 360 nm, 380 nm, 485 nm and 565-585 nm. For all experimental repeats, images were taken with identical LED power and exposure, and if edited brightness/contrast were manipulated identically to allow for direct comparison between different genotypes with the exception of localisation experiments.

Ca<sup>2+</sup> measurements (Section 2.3.8) were carried out live using either the Colibri setup above with the Physiology package or a Zeiss Axiovert 35 microscope fitted with

a dimmable X-cite HXP lamp, Optospin excitation and emission filter wheels (Carin Research, Faversham, United Kingdom), A Hamamatsu Orca Flash 4.0LT sCMOS camera, Zeiss objectives optimised for Fura-2,AM and Metafluor software (Molecular devices, Wokingham, United Kingdom). In all cases, regions of interest were over the whole cell, images were captured at 1 second intervals during and post additions and 2-5 second intervals during baseline re-establishment, a background region was used for subtraction and the ratios were calculated as 340/380 nm within the software.

#### **2.4.2 Microscopy analysis**

Image adjustments and pseudo-colouring, where applicable, was carried out using Photoshop version CS6 (Adobe 2012). Analysis of images were carried out using ImageJ Version 1.53a (Schneider et al. 2012). Comparison of fluorescence intensity of Magic Red staining in puncta and Rhod-2,AM staining in mitochondria were carried out by drawing a line through the cell in ImageJ and then using the plot profile function.

Staining area analysis was done as delineated in Cook *et al.* (2020). Briefly, images were opened in ImageJ and changed to 8-bit monochrome, after which the threshold was set to cover only the area in the images that displayed visible fluorescence staining. The particles were then analysed with the size (inch<sup>2</sup>) range set from 0.0005-infinity to eliminate background noise (speckles). An outline was drawn around each cell and the total area of fluorescence per cell was recorded and copied to Microsoft Excel. The averaged area per cell per data set or N was transferred to Prism 8 for statistical analysis as outlined in Sections 2.8. Note that particle analysis (e.g. lysosomal number) was not possible as often the lysosomes would clump or overlap, various means were attempted to correct for this but none matched with the total fluorescence readings from microplate assays, as such, these data are not included as they are mis-leading.

## **2.5 Reverse transcription quantitative polymerase chain reaction (RT-qPCR)**

### **2.5.1 Cell seeding**

To prepare cells to examine CLN8 expression, 20,000 cells per well were seeded into a sterile 24-well plate (Greiner). The seeded cells were then incubated in a humidified incubator at the correct temperature depending on cell type (section 2.1).

### **2.5.2 RNA extraction**

Adherent cells (section 2.6.1) were lysed by adding 350  $\mu$ l of the RLT buffer (Qiagen, Hilden, Germany), which contains a high concentration of guanidine isothiocyanate, which supports the binding of RNA to the silica membrane, with 1%  $\beta$ -mercaptoethanol and were harvested at different intervals over a different length period as defined in each relevant figure. Lysates were stored in ribonuclease (RNAse) free plastics at 4 °C in-between collecting samples and all the samples were stored for no more than 48 hours before RNA was extracted. RNA was extracted from lysates by using the RNeasy Micro Kit exactly as outlined in the protocol (Qiagen). Extracted genetic material was transferred to a 96-well plate and stored at -80 °C.

### **2.5.3 Reverse transcription**

From each sample, 6  $\mu$ l were taken for reverse transcription for 1 hour at 45 °C following the AffinityScript kit (Agilent, Santa Clara, United States) protocol provided. The reverse transcription was primed by adding random hexamers (ThermoFisher Scientific). The resulting complementary DNA (cDNA) samples were stored at -80 °C.

### **2.5.3 Quantitative polymerase chain reaction (qPCR)**

From each sample of cDNA 2  $\mu$ l was added to 18  $\mu$ l of solution of the Brilliant III ultrafast qPCR master (Agilent) containing the appropriate primers and the appropriate Fluorescein amidite (FAM) / Black hole quencher-1 (BHQ1) dual-labelled probes (Eurofins Scientific, Luxembourg; Table 2.1), at 225 nM and at 500 nM, respectively. The qPCR was carried out using the Mx3000P platform (Agilent) and consisted of 45

cycles at 95 °C for 12 seconds and 60 °C for 35 seconds. Standard curves were made for each qPCR run using a five-fold serial dilution of adult mouse brain RNA extract (Zyagen, San Diego, United States). The data was then exported to Microsoft Excel and the relative expression in relation to the reference mRNAs was calculated.

**Table 2.1: Primer & probe set for qPCR experiments.** Specific primers and FAM/BHQ1 for each gene of interest are outlined in this table.

Gene	Primer	Sequence (5' to 3')
CLN8	Forward	CCT CAT TTG ACA CTG TTC
	Reverse	GAG TCT TCT TAT GGG TCC
	Probe	FAM-ACT GGC TCT GCT TAC GCT AAT CA-BHQ1
TFEB	Forward	GGA GAA TCC CAC ATC CTA
	Reverse	CAG CAA ACT TGT TCC CAT A
	Probe	FAM-CAG CAG TCG CAG CAT CAG AAG-BHQ1
TRPML1	Forward	ACG CTC AAA TTC CAC AAG
	Reverse	AGG ACG CTG AAG GTA TAG
	Probe	FAM-TCA ATG TCA CCA TCC ACT TCC G-BHQ1
Mammalian target of rapamycin (MTOR)	Forward	GCA TGA TAG ACC AGT CCC
	Reverse	GTG TGA TGA TGA GAG AGT G
	Probe	FAM-CTG TCA GCC TGT CAG AAT CCA AGT-BHQ1
CLN5	Forward	GGA CAT TAGT TCA AGT AGC
	Reverse	GTC TCAT AAT AAA TTC CTG TTTC
	Probe	FAM-CCT GTT TCA CCC ACT TTG CCA-BHQ1
CLN6	Forward	CTG CTC TTC AGT GGC TAC
	Reverse	TGA CCC AGG TAC TCA TCA
	Probe	FAM-CCT GTC TGT CCG TGA GAA CCC-BHQ1
Tata binding protein (TBP)	Forward	CTC ACA GAC TCT CAC AAC
	Reverse	AGG TCA AGT TTA CAA CCA A
	Probe	FAM-CGG GCA CCA CTC CAC TGT ATC C-BHQ1
Glyceraldehyde 3-phosphate dehydrogenase (GAPDH)	Forward	TGG TCT CCT CTG ACT TCA
	Reverse	GCT GTA GCC AAA TTC GTT G
	Probe	FAM-AGC GAC ACC CAC TCC TCC AC-BHQ1
Beta-2-Microglobulin (B2M)	Forward	CCT GAA TTG CTA TGT GTC
	Reverse	CAG TGT AGT ACA AGA GAT AGA
	Probe	FAM-CAT CCA TCC GAC ATT GAA GTT GAC-BHQ1

## **2.6 Lysosomal enzyme assays**

### **2.6.1 Cell homogenate preparation**

Human fibroblast cells were harvested at around 90% confluency by removing DMEM, washed twice with D-PBS and incubated for 5 minutes in 0.25% trypsin/Ethylenediaminetetraacetic acid (EDTA). Detached cells were suspended in DMEM to inactivate the trypsin before being pelleted by centrifugation at 102 g for 5 minutes. Following centrifugation, media was removed, and the cells were resuspended in D-PBS. This step was repeated two more times to wash the pellets before they were stored as a dry pellet at -80 °C. In order to minimise the effects of multiple freeze-thawing on enzyme activity, once the protein concentration was determined, single use concentrated aliquots were made and stored at -80 °C.

### **2.6.2 Determining protein concentration**

In order to estimate the protein concentration of the harvested pellets a bicinchoninic acid (BCA) assay was used (Smith et al. 1985). The BCA assay was carried out according to the manufacturer's instructions. Briefly, the pellets were resuspended in MilliQ water and homogenised by first three freeze-thaw cycles to break open the membranes and then being passed through a 26-gauge needle 20 times. After this, 50 µM of homogenate solution was then taken and centrifuged at 13,000 g for 30 minutes at 4 °C to pellet the membrane associated clumped protein and retain the soluble protein fraction. By comparing against a 0-75 µg/ml BSA standard curve the homogenate supernatant was diluted at 1:5, 1:10 and 1:20 and the protein concentration of the samples determined by microplate assay. The sample and the standard curve were plated onto a clear 96 well microplate (Greiner) and incubated with the BCA reagent (10 ml of BCA solution to which is added and mixed 200 µl of 0.02% Cu<sub>2</sub>SO<sub>4</sub>) at 37 °C for 30 minutes. The absorbance was then measured at 570 nm using a Tecan Infinite F50 microplate reader (Tecan Group, Switzerland).

### 2.6.3 Enzyme activity fluorescent assays

The enzyme activity of different lysosomal enzymes was carried out by using the enzyme assay conditions outlined in Table 2.2. Briefly, 10  $\mu$ l of homogenate was added to 10  $\mu$ l of the fluorescent substrate at the corresponding concentration and pH (Table 2.2), plated in a 96 well microplate and incubated at 37 °C for the indicated time (Table 2.2). Standards specific to each fluorophore (Table 2.2) were prepared at a concentration ranging between 0 – 200  $\mu$ M. The reaction was ended by the addition of 180  $\mu$ l of the indicated stopping buffer (Table 2.2). The fluorophore released during the assay was then measured using a monochromator based SpectraMAX Gemini EM fluorescence plate reader with SoftMax Pro software. The excitation/emission was set to 360/406 nm for 4-methylumbelliferone (4MU, ThermoFisher Scientific), 404/460 for 6-hexadecanoylamino-4-methylumbelliferyl-phosphorylcholine (HMU; Moscerdam, Compton, United Kingdom), 320/420 nm for methyl coumaric acid (MCA) and 360/460 nm 7-amido-4-methylcoumarine (AMC; CarboSynth, Newbury, United Kingdom). For the p-nitroanilide standard, absorbance was read at 405 nm using a Tecan Infinite F50 microplate reader.

**Table 2.2: Lysosomal enzyme assay conditions.** Specific fluorometric assays conditions for determination of lysosomal enzyme activities are outlined in this table.

Enzyme	Standard	Substrate (concentration)	Protein quantity added	Inhibitor (concentration)	Reaction buffer (pH)	Incubation condition	Stop buffer (pH)	References
<b><math>\alpha</math>-Galactosidase</b>	4MU	4MU- $\alpha$ -D-galactopyranoside (2 nM)	2 $\mu$ g	N-butyldeoxygalactonojirimycin (1 nM)	Phosphate citrate (pH 4.5)	1 hr @ 37 °C	Glycine/NaOH (pH 10.6)	(Mayes et al. 1981; Olivova et al. 2009; Caudron et al. 2015)
<b><math>\alpha</math>-Glucosidase</b>	4MU	4MU- $\alpha$ -glucopyranoside (4 mM)	2 $\mu$ g	n/a	Phosphate citrate, (pH 4) + 0.1% triton acarbose	4 hr @ 37 °C	Glycine/NaOH (pH 10.6)	(Broadhead and Butterworth 1978; Jack et al. 2006)
<b><math>\alpha</math>-Mannosidase</b>	4MU	4MU- $\alpha$ -D-mannopyranoside (2 nM)	2 $\mu$ g		Sodium acetate (pH 4.5) + 0.1% triton	1 hr @ 37 °C	Glycine/NaOH (pH 10.6)	(Prencz and Natowicz 1992; Gotoda et al. 1998)
<b>Acid lipase</b>	4MU	4MU-oleate (0.1 mg/ml; CarboSynth)	2 $\mu$ g	Orlistat (1 $\mu$ M)	Sodium acetate (pH 4) + 1% triton	1 hr @ 37 °C	Glycine/NaOH (pH 10.9)	(Moheimani et al. 2012)
<b>Acid phosphatase</b>	4MU	4MU-phosphate (150 $\mu$ M)	2 $\mu$ g		Acetate (pH 5) + 0.2% triton	1 hr @ 37 °C	Glycine/NaOH (pH 10.6)	(Leake et al. 1982)
<b>Aspartylglucosaminidase</b>	AMC	L-aspartic acid- $\beta$ -7-amido-4-methyl coumarin (1 mM; CarboSynth)	4 $\mu$ g	L-asparagine (1 nM)	Phosphate citrate (pH 4.5)	17 hr @ 37 °C	Phosphate citrate (pH 4.5)	(YaV et al. 1993)
<b>Acid sphingomyelinase</b>	HMU	HMU-sphingomyelin (0.5 mM; Moscerdam)	2 $\mu$ g	Zoledronic acid (1 mM)	Sodium acetate (pH 4.5) + 0.2% NaTc + 0.02% NaAz	1 hr @ 37 °C	Na <sub>2</sub> CO <sub>3</sub> (pH 10.9) + 2.5% triton	(van Diggelen et al. 2005)
<b><math>\beta</math>-Galactosidase</b>	4MU	4MU- $\beta$ -galactoside (2 nM)	2 $\mu$ g	Zoledronic acid (1 mM)	Sodium acetate (pH 4.5) + 0.1% 5 mM NaCl + NaTc	1 hr @ 37 °C	Glycine/NaOH, (pH 10.6)	(Nowakowski et al. 1988; Nowroozi et al. 2001)

Enzyme	Standard	Substrate (concentration)	Protein quantity added	Inhibitor (concentration)	Reaction buffer (pH)	Incubation condition	Stop buffer (pH)	References
<b>β-Glucosidase</b>	4MU	4-methylumbelliferyl-β-D-glucopyranoside (2 nM)	2 µg	CBE (500 µM)	Sodium acetate (pH 5.6) + 0.1% triton + 0.2% NaTc	1 hr @ 37 °C	Glycine/NaOH (pH 10.6)	(Broadhead and Butterworth 1977; Jack et al. 2006)
<b>β-Glucuronidase</b>	4MU	4-β-D-glucuronide (2 nM)	2 µg	Suramin (100 µM)	Sodium acetate (pH 4) + 0.1% triton	1 hr @ 37 °C	Na <sub>2</sub> CO <sub>3</sub> (pH 10.9)	(Bramwell et al. 2014)
<b>Cathepsin L</b>	AMC	Z-phe-arg-7-amido-4-methylcoumarin (50 µM; Bachem Holding, Bubendorf, Switzerland)	4 µg	Z-Phe-Ala-7-amido-4-methylcoumarin (50 µM)	Phosphate citrate (pH 5.5) + 0.005% BRIJ + mM EDTA + 8 mM DTT	30 minutes @ 37 °C	n/a	(Creasy et al. 2007; Viswanathan et al. 2012; Ismael et al. 2016)
<b>Cathepsin B</b>	AMC	Z-arg-arg-7-amido-4-methylcoumarin (50 µM; Merck)	4 µg	Z-Phe-Ala-diazomethylketone (10 µM)	Sodium acetate (pH 5.5) + 0.8 mM EDTA + 8 mM DTT	30 minutes @ 37 °C	n/a	(Headlam et al. 2006; Creasy et al. 2007; Viswanathan et al. 2012)
<b>Cathepsin D &amp; E</b>	MCA	Z-methoxycoumarin-4-acetyl-gly-lys-pro-leu-leu-phe-phe-arg-leu-lys-dinitrophenyl-D-arg-amide (50 µM; Enzo Life Sciences)	4 µg		Phosphate citrate (pH 4.5) + 2 mM EDTA + 50 mM NaCl	1 hour @ 37 °C	n/a	(Ismael et al. 2016)
<b>Dipeptidyl peptidase-4</b>	p-nitroanilide	Gly-pro-p-nitroanilide (2.5 mM; Santa Cruz Biotechnology, Dalla, United States)	2 µg	n/a	Tris HCL (pH 7.4)	2 hr @ 37 °C	Sodium acetate (pH 4.4)	(Beckenkamp et al. 2015)

Enzyme	Standard	Substrate (concentration)	Protein quantity added	Inhibitor (concentration)	Reaction buffer (pH)	Incubation condition	Stop buffer (pH)	References
<b>Fucosidase</b>	4MU	4MU- $\alpha$ -L-fucopyranoside (1 mM)	2 $\mu$ g	Deoxyfuconojirimycin hydrochloride (20 nM; Snta Cruz)	Citrate buffer (pH 5)	1 hr @ 37 °C	Na <sub>2</sub> CO <sub>3</sub> (pH 10.9)	(Winchester et al. 1990)
<b>Hexosaminidase A</b>	4MU	4MU-N-acetyl- $\beta$ -D-glucosamine-6-sulphate (2 mM)	2 $\mu$ g	n/a	Citrate buffer (pH 4.6) + 0.01% triton	1 hr @ 37 °C	Na <sub>2</sub> CO <sub>3</sub> (pH 10.9)	(Bayleran et al. 1987)
<b>Hexosaminidase B</b>	Total Hexosaminidase assay, using heated cells (50 °C for 2 hours) to inactivate Hexosaminidase A as it is heat sensitive							
<b>Total Hexosaminidase</b>	4MU	4MU-N-acetyl- $\beta$ -D-glucosamine (2 mM)	2 $\mu$ g	n/a	Citrate buffer (pH 4.6) + 0.01% triton	1 hr @ 37 °C	Na <sub>2</sub> CO <sub>3</sub> (pH 10.9)	Tropak <i>et al.</i> 2004)
<b>Iduronidase</b>	4MU	4MU- $\alpha$ -L-iduronate (1 mM; CarboSynth)	2 $\mu$ g	n/a	Sodium formiate (pH 3.2)	1 hr @ 37 °C	Na <sub>2</sub> CO <sub>3</sub> (pH 10.9)	(Hopwood et al. 1979; Kingma et al. 2013)
<b><math>\alpha</math>-N-Acetylgalactosaminidase</b>	4MU	4MU- $\alpha$ -N-acetylglucosaminide (1 mM)	2 $\mu$ g	n/a	Sodium acetate (pH 4.5)	4 hr @ 37 °C	Glycine/NaOH (pH 10.6)	(Mauri et al. 2013)
<b>Palmitoyl-protein thioesterase</b>	4MU	4MU-6-thiopalmityl $\beta$ -D-glucoside (0.5 mM; CarboSynth)	2 $\mu$ g	ABC44 (200 nM)	Phosphate citrate (pH 4) + 15 mM DTT + 0.375% triton + 0.1 $\beta$ -glucosidase	4 hr @ 37 °C	Na <sub>2</sub> CO <sub>3</sub> (pH 10.9) + 0.025% triton	(van Diggelen et al. 1999)
<b>Sialidase</b>	4MU	4MU-N-acetyl neuraminic acid (0.2 mM; Toronto Research Chemicals)	4 $\mu$ g	n/a	Sodium acetate (pH 4.5)	4 hr @ 37 °C	Glycine/NaOH (pH 10.6)	Winter <i>et al.</i> 1980; Yamada <i>et al.</i> 1983; Hayre <i>et al.</i> 2012)
<b>Tripeptidyl peptidase 1</b>	AMC	Ala-ala-phe-7-amindo-4-methylcourmarin (0.5 mM; Bachem)	2 $\mu$ g	n/a	Sodium acetate (pH 4.5) + 0.05% triton + 10% EDTA + 0.08% E64 + 0.012% PepstatinA	1 hr @ 37 °C	Phosphate citrate (pH 4.5)	Di Giacopo <i>et al.</i> 2015)

## **2.7 High-throughput enzyme drug screening**

### **2.7.1 Sample preparation**

Cultured cells as outlined in Section 2.1.1 were harvested and homogenised as outlined in Section 2.6.1 and the protein concentration was determined as explained in Section 2.6.2.

### **2.7.2 Galactosylceramidase (GALC) assay**

The high-throughput enzyme drug screen was conducted against GALC enzyme activity to identify compounds that modulate the activity of control cell homogenate GALC, prepared as outlined Sections 2.6.1. The GALC enzyme assay was carried out using the synthetic fluorogenic substrate 4MU- $\beta$ -galactoside (ThermoFisher Scientific). The substrate is also known to react with  $\beta$ -galactosidase, as such  $\beta$ -galactosidase activity was inhibited by the addition of 11 mM AgNO<sub>3</sub> (Martino et al. 2009). Sodium taurocholate (0.5 mg/ml) has also been reported to enhance GALC activity, but not  $\beta$ -galactosidase (Ribbens et al. 2013). The addition of sodium taurocholate also potentially decreases the amount of starting protein needed for the assay ensuring it is more efficient (Ribbens et al. 2013; Elliott et al. 2016).

The 4MU- $\beta$ -galactoside substrate was added at a concentration of 3 mM in the reaction buffer consisting of sodium phosphate (0.7 M) and citric acid (0.1 M) at pH 4.0. As mentioned above (Section 2.7.1) the reaction buffer was supplemented with AgNO<sub>3</sub> (11 mM) and sodium taurocholate (0.5 mg/ml). A pooled Control 1 cell homogenate (10  $\mu$ l) containing 15  $\mu$ g of protein was added in triplicate in a 96-well plate with 10  $\mu$ l of the reaction buffer containing the 4MU- $\beta$ -galactoside fluorescent substrate. Two negative controls were added to each plate by 1) heat-inactivating the cell homogenate at 95 °C for 15 minutes to denature the enzyme but the substrate is still added and 2) separately in another well including the non-denatured homogenate but not the substrate. The plate was incubated for 30 minutes at 37 °C after being gently shaken for 1 minute at 37 °C. The reaction time length was also tested at 60 minutes, 120 minutes, 180 minutes and 240 minutes to determine potential saturation.

The reaction was stopped via addition of 180  $\mu$ l of a stopping buffer comprising of glycine (0.2 M; ThermoFisher Scientific) and NaOH (0.2) at pH 10.6. The increase in pH following the addition of the stopping buffer both stops the reaction as the pH is too high for GALC enzyme to breakdown substrate (Martino et al. 2009) and also enhances the fluorescence of the 4MU product. Fluorescence was measured using a SpectraMAX Gemini EM fluorescence plate reader with SoftMax Pro software with the excitation and emission at 360 nm and 446 nm, respectively.

### **2.7.3 Primary screen of FDA-approved drug library**

An FDA-approved drug library comprising 635 small molecule compounds from the National Institute of Health Clinical Collections was kindly provided by Dr Sridhar Vasudevan (Department of Pharmacology, University of Oxford) in a sealed 384-well plate in DMSO at a concentration of 10  $\mu$ M which was stored at 80 °C. The compounds in the 384-well plate were all FDA approved compounds for at least one disease and as such already have approved safety and pharmacokinetic profiles.

The small molecule compounds were initially tested at a concentration of 1  $\mu$ M added manually to the GALC reaction buffer outlined in Section 2.7.1 prior to addition of the homogenate. Drug autofluorescence was estimated by measuring the fluorescence of the plate prior to addition of the homogenate. Each drug was assayed in triplicate in the 96-well plate. The data was then normalised as a percentage activity relative to the vehicle-only DMSO control in order to reduce plate-to-plate variation and thus enabling comparison across plates (Malo et al. 2006).

### **2.7.4 Secondary screen of FDA-approved drug library**

The compounds selected from the primary screen were then re-screened at both 1  $\mu$ M and 0.1  $\mu$ M and in cell homogenate that had undergone multiple freeze/thaw cycles which destabilises the GALC enzyme (Bhatnagar et al. 2007). The assay was then carried out as outlined in Section 2.7.1. Compounds that were able to increase activity from this secondary screen were then selected based on their ability to act as chaperones of this destabilised GALC.

## **2.8 Statistical Analysis**

All statistical analyses were carried out in Prism 8 (GraphPad 2018). The number of Ns is indicated in each figure. All assumptions for statistical tests were tested prior to analysis, with non-parametric tests selected where appropriate and indicated in the figure legends. To test for normality, a Shapiro-Wilk normality test was carried out in favour of alternatives given that it is more appropriate for the smaller data sets, representative of cell biology, resulting in its adoption as the most widely recommended normality test for such applications (Mishra et al. 2019). Following normality testing the specific statistical test used is outlined in each figure legend.

# **Chapter 3: CLN8 disease cellular phenotyping for the purposes of drug screening**

## **3.1 Introduction**

### **3.1.1 CLN8 disease**

As outlined in Chapter 1 Section 1.2.3, CLN8 disease is a childhood neurodegenerative disease caused by mutations in the *CLN8* gene. CLN8 is characterised by epileptic seizures with progressive mental retardation and cognitive decline (Lonka et al. 2000). Although CLN8 is an ER-transmembrane protein, a recent study has revealed the mechanisms by which dysfunction of this protein causes an LSD, a link which was previously unclear (Vantaggiato et al. 2009; di Ronza et al. 2018).

Di Ronza *et al.* (2018) found that the CLN8 protein is needed for lysosomal enzyme maturation by transportation of lysosomal proteins from the ER to the Golgi, via the ER-Golgi intermediate compartment. Absence of CLN8 leads to lysosomal enzyme trafficking being disrupted and these not reaching the lysosome (di Ronza et al. 2018). Furthermore, Bajaj *et al.* (2020) recently reported that CLN8 forms a complex with CLN6 which is required for lysosome enzyme transport to the Golgi.

#### **3.1.1.1 CLN8 patient mutations**

Specific patient mutations have not been extensively studied and as such little is known about their specific effect on protein structure and functions. Previously, studies have found that missense mutation, including A30P (CLN8 534 HF), Y158C (CLN8 535 HF) and Q194R (CLN8 533 HF) have been reported to not affect correct protein targeting and thus may disrupt functional properties instead (Lonka et al. 2000; Vantaggiato et al. 2009; Kousi et al. 2012). The Q194R and Y158C mutations present in CLN8 533 HF and CLN8 535 HF, respectively (Table 3.1), have been reported to lead to a decreased association with the lysosomal enzymes N-acetylgalactosamine-

6-sultase, cathepsin D, palmitoyl-protein thioesterase 1 (PPT1; CLN1), tripeptidyl peptidase 1 (TPP1; CLN2) and neuraminidase by around 50% (di Ronza et al. 2018).

On the other hand, genomic deletions have been predicted to lead to instable mRNA as Reinhardt et al. (2010) detected no transcript. Nonetheless, it has been previously reported that genomic deletion, like c66delG, when present in compound heterozygosity with non-truncated protein, as in CLN8 533 HF and CLN8 535 HF, lead to slightly milder clinical phenotypes (Reinhardt et al. 2010; Kousi et al. 2012).

**Table 3.1: Outline of the patient cell lines used in Chapter 3.**

Cell line	Description	Mutation
Control 1 HF	<i>Apparently healthy control 1 (GM05399) cell line</i>	N/A
Control 2 HF	<i>Apparently healthy control 2 (GM05400) cell line</i>	N/A
CLN8 462 HF	<i>CLN8 patient cell line</i>	c.543 + 1G>A homozygous
CLN8 533 HF	<i>CLN8 patient cell line</i>	Q194R/c.66delG
CLN8 534 HF	<i>CLN8 patient cell line</i>	A30P homozygous
CLN8 535 HF	<i>CLN8 patient cell line</i>	Y158C/c.66delG

### 3.1.1.2 CLN8 disease therapies

Currently, there are no therapies for CLN8 disease and only palliative treatments are available. Therefore, research is needed to advance current knowledge of the disease to both increase our understanding of the role of the CLN8 protein, and lead to the identification of therapeutic targets for drug screening assays for this disease. Phenotypic drug screens have previously identified drugs that may be of benefit to other LSDs (Geng et al. 2011; Chandrachud et al. 2015; Szabo et al. 2017). In order to establish such screens for CLN8 disease, it is crucial to find robust phenotypes that can be used for primary drug screens, as well as, further confirmation screening of the possible beneficial effects that the therapy may have on cellular dysfunction (Chandrachud et al. 2015; Jang et al. 2016; Szabo et al. 2017).

### 3.1.2 Cellular phenotypes in LSDs

As outlined in Chapter 1 (Section 1.1.2 – Section 1.1.6 & Section 1.2.2), even though different LSDs arise from mutation in different proteins associated with lysosomal function, LSDs share many cellular pathologies (Platt et al. 2012). An example of this is lysosomal accumulation which is a hallmark of most LSDs, as dysfunction of lysosomal proteins lead to the accumulation of lipids, proteins and other materials in the lysosomes, resulting in the expansion of these organelles. In fact, LysoTracker, which is a fluorescent probe that loads into acidic organelles only, has been used as a clinical monitoring tool in other LSDs (Sztolsztener et al. 2012; Xu et al. 2014). This indicates that lysosomal expansion and the use of LysoTracker are robust phenotypes that can even be used to monitor patients.

Lipids are important for cellular homeostasis as they maintain plasma membrane integrity and fluidity. They also act as signalling intermediates and provide substrates that are used as energy in a variety of cellular processes (Simons and Ikonen 1997; Wassall et al. 2004; Schulze and Sandhoff 2011; Ademowo et al. 2017). Understanding how lipids are affected in LSDs can help understand the disease pathogenesis and help find potential therapies that may be beneficial to the disease. An example of this is the use of Miglustat, outlined further in Chapter 5, that reduces sphingolipid synthesis and is used to treat diseases that store sphingolipids like NPC1 and Gaucher disease (Lachmann et al. 2004; Patterson et al. 2007; Stein et al. 2012).

One lipid that has been reported to be stored in LSDs, as mentioned in Chapter 1, and is crucial for plasma membrane regulation is cholesterol. Cholesterol has been seen to accumulate in the lysosomes of many LSDs such as NPC1 disease (Karten et al. 2002; Vanier and Latour 2015). There are several lysosomal proteins and enzymes that are involved in different aspects of the processing of cholesterol such as acid lipase, NPC1 and NPC2 (Kwon et al. 2009; Dudland and Francis 2015). Furthermore, storage of other lipids in LSDs such as glycosphingolipids is known to trap cholesterol leading to cholesterol accumulation in lysosomes (Puri et al. 2003). A previous study found that cholesterol levels, and levels of other lipids outlined in Chapter 1, in post-mortem brain samples from CLN8 patients both elevated and reduced when compared to the control (Hermansson et al. 2005).

Defects in autophagy have been seen and measured in LSDs including the NCLs as well as other neurodegenerative diseases, such as Huntington disease (Cao et al. 2006; Jing and Lim 2012; Thelen et al. 2012; Cortes and La Spada 2014; Chandrachud et al. 2015). As mentioned in Chapter 1 autophagy is a process responsible for the clearance of damaged organelles and proteins. Defective autophagy can in turn cause cellular dysfunction, leading to cytotoxicity. The accumulation of lysosomes, and lipids within these organelles, may affect autophagy as material accumulation in lysosomal and autophagosomes (Glick et al. 2010; Jing and Lim 2012).

Mitochondrial dysfunction has been also reported in many LSDs and neurodegenerative diseases as a downstream event in the pathogenic cascade (Carafoli 1974; Bertamini et al. 2002; Kolikova et al. 2011). Furthermore, mitochondrial dysfunction can lead to cell damage due to aberrant production of reactive oxygen species (Bertamini et al. 2002) and changes in energy generation which is particularly important for neurons which have a lot of mitochondria. Moreover, studies in the CLN8 mouse, CLN8<sup>mnd</sup> mouse, have indicated that the mitochondria ability to buffer Ca<sup>2+</sup> was affected (Kolikova et al. 2011).

Disruption to circadian rhythms and the cell cycle have been linked to neurodegenerative diseases such as Alzheimer and Parkinson disease (Heintz 1993; Hood and Amir 2017; Pantazopoulos et al. 2018; Zisapel 2018). Studies have identified a role for the circadian rhythms in many major neurological disorders such as depression, bipolar disorder, schizophrenia, anxiety, stress and neurovegetative diseases (Pantazopoulos et al. 2018; Zisapel 2018). This, however, remains largely understudied in neurological diseases and even less so in LSDs.

Alteration in gene expression have been reported in LSDs such as NPC1, mucopolysaccharidoses, Sandhoff disease (Dhami et al. 2006; Richardson et al. 2016; Brokowska et al. 2020). Like with circadian rhythms, alteration in gene expression in LSDs remains understudied and poorly understood. Therefore, exploring alteration in lysosomal related genes may uncover defects or alteration in the lysosomal pathways.

TFEB is the transcription factor that is known to regulate lysosomal biogenesis as well as the expression of some autophagy related genes (Settembre et al. 2011; Settembre and Medina 2015). Similarly, MTOR is known as the 'master switch' of

cellular catabolism and anabolism given its regulation of the autophagic system (Castedo et al. 2002). Therefore, the expression of these genes is integral to the regulation of the lysosome and autophagy.

Other genes such as *MCOLN1*, *CLN5* and *CLN6* are genes that are involved in lysosomal processes and as such their expression is likely linked to general lysosomal biogenesis. Both *MCOLN1* and *CLN5* encoded for lysosomal protein, the former is the transmembrane  $\text{Ca}^{2+}$  channel (TRPML1; outlined in Chapter 1 Section 1.1.5.2) and the latter is a soluble lysosomal enzyme of unknown function which has been related with an NCL disease called CLN5 disease (Dong et al. 2008; Lyly et al. 2009).

*CLN6*, as mentioned in Chapter 1, is involved in forming a complex with *CLN8* that recruits lysosomal enzymes and transports them from the ER to the Golgi (Bajaj et al. 2020). Furthermore, the *CLN5* protein has been reported to interact with many other NCL proteins including *CLN3*, *CLN2* and *CLN8* (Lyly et al. 2009; Haddad et al. 2012). Therefore, exploring the expression of genes such as *MCOLN1*, *CLN5* and *CLN6* may be used to further understand lysosomal dysfunction.

Deficiencies in proteins associated with lysosomal storage also lead to alterations in other lysosomal enzymes. Alteration in lysosomal enzyme activity such as hydrolases and activator enzymes leads to the accumulation of material in lysosomes, propagating cellular pathogenesis (Lloyd-Evans and Platt 2010). Moreover, *CLN8* is required for the maturation of two-thirds of lysosomal enzymes by transferring them from the ER to the Golgi (di Ronza et al. 2018). Therefore, alteration in *CLN8* protein may lead to defects in other lysosomal enzymes.

The levels of intracellular and organelle  $\text{Ca}^{2+}$  content, as outlined in Chapter 1, are tightly regulated and are important for a range of signalling events (Berridge et al. 2000; Braakman and Hebert 2013). Alteration in the  $\text{Ca}^{2+}$  content of organelles such as the ER and the lysosomal can cause impairment in these signalling pathways. As mentioned in Chapter 1 Section 1.1.5 alteration in levels of ER and lysosomal  $\text{Ca}^{2+}$  have not only been reported in LSD such as *NPC1*, Gaucher disease and Sandhoff disease but these have been reported to contribute to the pathogenesis of these diseases (Korkotian et al. 1999; Lloyd-Evans et al. 2003; Pelled et al. 2003; Lloyd-Evans et al. 2008).

Therefore, characterising cellular phenotypes in CLN8 patient cells such as lysosomal storage, cholesterol intracellular storage, autophagy vesicle storage, mitochondrial staining and mitochondrial  $\text{Ca}^{2+}$ , CLN8 circadian expression, changes in the expression of lysosomal related genes, lysosomal enzyme activities and  $\text{Ca}^{2+}$  dyshomeostasis may help further the understanding of CLN8 disease pathogenesis and contribute to the identification of therapeutic intervention points as well as phenotypes that may be used for drug screening.

Furthermore, uncovering cellular pathogenesis of disease can improve the understanding of the pathogenic mechanisms of the disease. An example of this is how research into the pathology of NPC1 disease has led to the pathogenic cascade of events in NPC1 disease to be uncovered (Lloyd-Evans and Platt 2010). This, therefore, increases the understanding of the pathogenesis in the disease and gives rise to the possibility of optimal therapeutic intervention points being identified.

### **3.1.3 Primary patient fibroblast (HFs)**

The use of patient fibroblast cells has been extremely valuable in the study of the fundamental cellular pathology of LSDs including  $\text{Ca}^{2+}$  levels, organelle function defects, autofluorescence and a myriad of fluorescent indicators with advances in imaging techniques. Fibroblast have been used to increase our understanding of many diseases including LSDs which ultimately leads to potential treatments for these diseases (Connolly 1998; Auburger et al. 2012).

In fact, patient fibroblast have even been used for the diagnosis of LSDs by looking at the accumulation of macromolecules as was the case with the filipin test to visualise cholesterol accumulation to diagnose NPC1 disease (Vanier and Millat 2003). Furthermore, as HFs are non-excitabile cells it makes them very useful to understand fundamental mechanisms in cellular dysfunction such as  $\text{Ca}^{2+}$  homeostasis by providing an opportunity to study basal  $\text{Ca}^{2+}$  and resting  $\text{Ca}^{2+}$  levels of the stores (Lloyd-Evans et al. 2008; Lloyd-Evans and Waller-Evans 2019).

There is, however, a naturally occurring mouse model of CLN8 disease called the CLN8<sup>mn</sup> mouse which has been useful to increase our understanding of CLN8 disease such as the mitochondrial buffering defect reported by Kolikova *et al* (2011). Nonetheless, the lifespan of mice reduces their suitability for high throughput drug

screening when compared to cell models such as fibroblasts. Even though, mice models have been used to further the understanding of different diseases they do not allow for the visualisation of cellular mechanisms and cellular dysfunction as can be done with cell models. Therefore, fibroblasts are among the most powerful models for LSD characterisation providing a model that can be used to further the understanding of the cellular pathologies and disease cascades involved in LSDs (Lloyd-Evans and Platt 2010).

### **3.1.4 Chapter aims**

This chapter aimed to characterise cellular phenotypes in CLN8 disease that then may guide drug screening and further confirmation studies using patient cells (Table 3.1). This was done by exploring cellular phenotypes commonly observed across other LSDs, such as those outlined in Section 3.1.2 above. This chapter also explores more CLN8 specific phenotypes by exploring enzymes affected and mRNA expression changes in CLN8 disease.

### **3.2 Summary of Methods**

In this chapter the cells outlined in Table 3.1 were cultured as outlined in Section 2.1. In order to explore cellular phenotypes in the CLN8 patient cells, lysosomal area were determined using LysoTracker (Section 2.3.2 & Section 2.3.3), cholesterol area was determined using the auto-fluorescent antibiotic filipin (Section 2.1.3), autophagic vacuoles were examined using CytolD green (Sections 2.3.4) and mitochondrial network was visualised using MitoTracker green (Section 2.3.6). These were imaged using the inverted Colibri widefield fluorescence microscope (Section 2.4.1) and analysed using Image J (Section 2.4.2).

The levels of mRNA expression in CLN8 and control patient cells were quantified by reverse transcription qPCR (Section 2.5) with the indicated cells treated previously with 100 nM dexamethasone as outlined in Section 2.1.5.

The activity of the lysosomal enzymes assayed in this Chapter were carried out as outlined in Chapter 2 Section 2.6. The data that makes up the heat maps seen in

Section 3.2.7 below, was taken for each enzyme assay found in separate graphs in the Appendix (Figure A3.1 – A3.22). The total levels of cathepsin B using the cathepsin B fluorescent probe Magic Red (Section 2.6.4).

To examine the levels of  $\text{Ca}^{2+}$  in the ER three different approaches were used, 1  $\mu\text{M}$  thapsigargin which inhibits SERCA, 2  $\mu\text{M}$  ionomycin to stimulate  $\text{Ca}^{2+}$  from all stores but lysosomes and 10  $\mu\text{M}$  ryanodine to activate the ryanodine receptor (Section 2.3.8). Mitochondrial levels were measured by inducing  $\text{Ca}^{2+}$  release from these organelles using 10  $\mu\text{M}$  CCCP and 5  $\mu\text{M}$  Antimycin / 5  $\mu\text{M}$  oligomycin (Section 2.3.8). To induce  $\text{Ca}^{2+}$  release from the lysosome,  $\text{Ca}^{2+}$  release from other stores was first induced using 2  $\mu\text{M}$  ionomycin and then 500  $\mu\text{M}$  GPN was added to burst lysosomes (Section 2.3.8). All  $\text{Ca}^{2+}$  measurements mentioned above were visualised and measured using a Zeiss Axiovert 35 microscope as outlined in Section 2.4.1.

### **3.3 Results**

#### **3.3.1 Lysosomal area in CLN8**

The characterisation of CLN8 patient cell lines for drug screening began with lysosomal live staining via microscopy and plate assay. Lysosomal staining showed an approximate 2-fold statistically significant increase in CLN8 534 HF lysosome area, when compared to both controls (Figure 3.1) suggesting lysosomal accumulation and reduced lysosomal clearance. Similarly, CLN8 462 HF displayed a less-than 2-fold increase in lysosomal staining compared to the control cell lines (Figure 3.1 A & B) but this was not significant and as such may require more repeats. Additionally, CLN8 535 HF has a trend of lower lysosomal area but not statistically significant and perhaps requires further repeats (Figure 3.1 A & B). These findings were reproduced when examining lysosomal volume using LysoTracker in a plate assay, with a 2-fold increase in CLN8 534 HF and no clear change in the other cell lines (Figure 3.1 C).

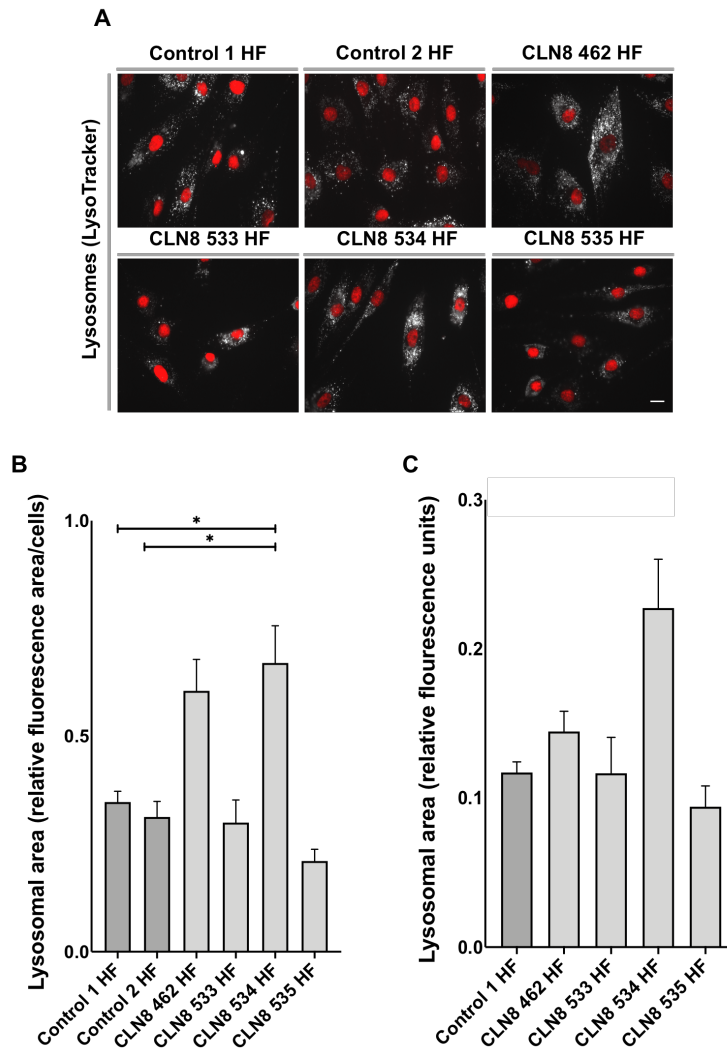


**Figure 3.1: Lysosomal area is variable between CLN8 patient fibroblasts.** **A:** Representative images of lysosomal staining (LysoTracker; greyscale) quantified in **B** with a Hoescht33342 nuclear counter stain pseudo coloured red. Scale bar = 10  $\mu$ m. **B:** Quantitative analysis of lysosomal area in apparently healthy (control 1 HF and control 2 HF) and CLN8 patient fibroblasts (CLN8 462, 533, 534 & 535 HF). N = 3 for Control 2 HF, CLN8 533 HF and CLN8 535 HF. N = 7 for Control 1 HF, CLN8 462 HF and CLN8 534 HF. **C:** Quantitative plate reader data of control 1 HF and CLN8 HF cells stained with LysoTracker. N = 2 and the error bars indicate SEM. In **C** each N comprised of 5 well of cells per cell line. \* $p \leq 0.05$ , One-way ANOVA with post-hoc Tukey.

The observed lysosomal area per cell in the CLN8 cell lines (Figure 3.1 A), particularly CLN8 462 HF and 534 HF, seems to be more variable than in the control cells. This variability was better observed in Figure 3.2 A where the lysosome area of each cell was individually plotted. This demonstrates the wide range of variability in lysosomal area in CLN8 462 HF and CLN8 534 HF. This led to the variability in CLN8 patient fibroblasts being explored further, by quantifying lysosomal area every 4 hours

over a period of 20 hours (Figure 3.2). The percentage difference between CLN8 HF lysosomal area and control 1 HF is different depending on when the lysosomal staining was imaged (Figure 3.2 B & C). When the lysosomal area was analysed as a percentage of control 1 HF it was clear that lysosomal area in the CLN8 462 and CLN8 534 was extremely variable as it was seen to be both higher and lower than the control 1 HF cells line (Figure 3.2 A & B). Specifically, CLN8 534 HF lysosomal area was around 208% of that measured in control 1 HF at 0 hours, yet at 16 hours CLN8 534 HF lysosomal area was 86% of that observed in control 1 HF (Figure 3.2 A).

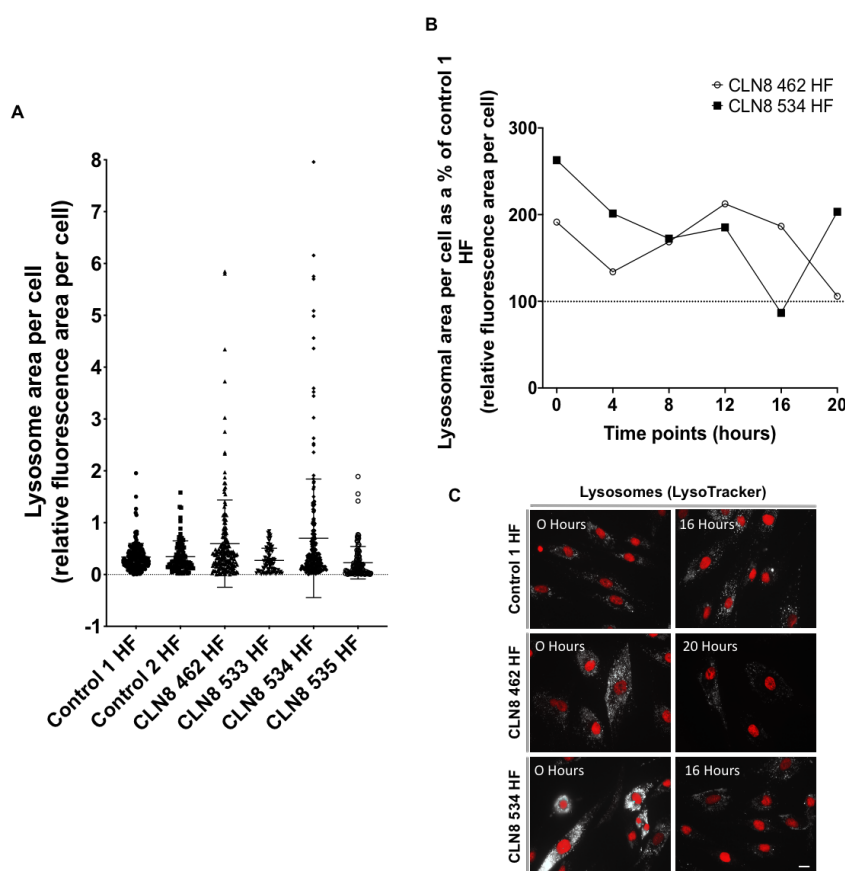


**Figure 3.2: Lysosomal area in CLN8 patient fibroblasts is highly variable.** **A:** Quantitative analysis of the lysosomal area of individual cells from all experiments in apparently healthy (control) and CLN8 patient fibroblasts **B:** Quantitative analysis of lysosomal area in CLN8 patient fibroblast as a percentage of control 1 HF where control 1 HF is 100%. N= 1 at each time point. **C:** Examples of the variability between individual cells in CLN8 patient fibroblast lysosomal staining (LysoTracker; greyscale) with a Hoescht33342 nuclear counter stain pseudo coloured red. The white text indicates the time point from which the representative image is from. Scale bar = 10  $\mu$ m. **A** and **B** represent data from N= 3-7.

### 3.3.2 Cholesterol staining in CLN8 HF

With the observation of possible lysosomal storage, suggested by increased LysoTracker, in two of the CLN8 patient cell lines, the next step was to check for storage of cholesterol. Cholesterol containing vesicles in CLN8 patient and control HF were visualised using the cholesterol-binding autofluorescent antibiotic filipin (Maxfield and Wüstner 2012; Vanier and Latour 2015) .

Cholesterol staining indicated a significant increase of around 1.7-fold in endo-lysosomal cholesterol in CLN8 534 HF compared to both control 1 HF and control 2 HF (Figure 3.3 B). Similarly, there was a significant increase of around 1.3-fold in endo-lysosomal cholesterol distribution in CLN8 462 HF compared to control 2 HF (Figure 3.3 B). Both CLN8 533 HF and CLN8 535 HF had no change in cholesterol levels (Figure 3.3).

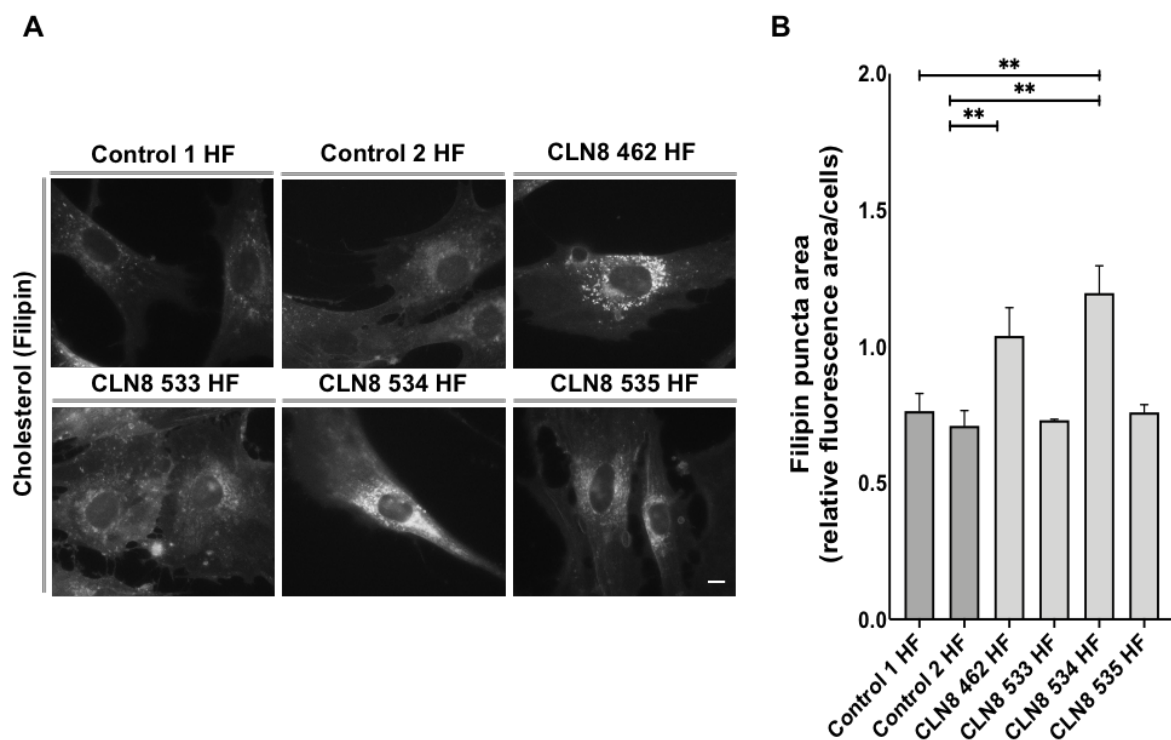


**Figure 3.3: Increased Cholesterol puncta in some CLN8 patient fibroblast.** **A:** Representative images of cholesterol staining (Filipin; greyscale) quantified in **B**. Scale bar = 10  $\mu$ m. **B:** Quantitative analysis of cholesterol puncta area in control and CLN8 patient fibroblasts. N=4 and the error bars indicate SEM. \*p  $\leq$  0.05, \*\*p < 0.01, One-way ANOVA with post-hoc Tukey.

### 3.3.3 Autophagy in CLN8 patient fibroblasts

Having observed the presence of lysosomal expansion and lipid storage in some of the CLN8 HF cells, alteration in autophagy, a process that requires normal lysosomal function, were explored (Figure 3.4). LSDs commonly feature autophagy defects (Liu and Lieberman 2019) and thus, this was the next cellular compartment explored in CLN8 patient cells (Figure 3.4). Autophagic vesicle staining, using CytoID Green, (Figure 3.4) in CLN8 patient cells showed no significant difference when compared to either control HF cell lines. This may be due to the effect size as both CLN8 462 HF and CLN8 534 HF average displays around 2-fold increase in autophagic vesicle area compared to the control HFs (Figure 3.4 B), however, the variability seen in the autophagic vesicle staining appeared to be greater than that observed with lysosomal storage (Figure 3.1 & 3.2) and as such more repeats are clearly needed.

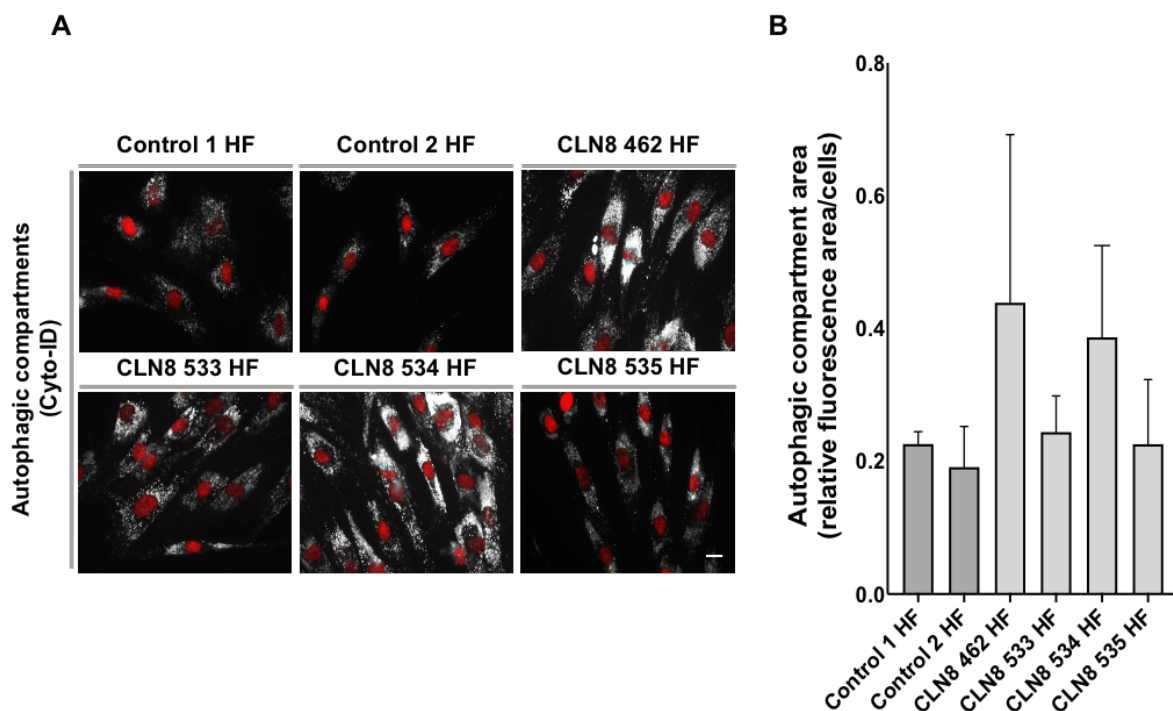


**Figure 3.4: Presence of autophagic compartment area is highly variable in CLN8 patient fibroblasts.** **A:** Representative images of autophagic compartment staining (Cyto-ID Green; greyscale) quantified in **B** with a Hoescht33342 nuclear counter stain pseudo coloured red. Scale bar = 10  $\mu$ m. **B:** Quantitative analysis of autophagic compartment area in control and CLN8 patient fibroblasts. N = 4 and the error bars indicate SEM. There was no significant difference seen using One-way ANOVA with post-hoc Tukey.

### **3.3.4 Mitochondrial staining in CLN8 patient fibroblasts**

After detecting the presence of potential defects in autophagy in some of the CLN8 HF, defects in mitochondria were explored as mitochondrial defects, like lysosomal dysfunction, contributes to defects in autophagy (Thelen et al. 2012). Mitochondrial stress was explored by using MitoTracker green which stains mitochondria (Figure 3.3). Similar to the observations of the lysosomal and autophagic compartment volumes, the CLN8 533 HF and CLN8 535 HF showed little change in mitochondrial staining (Figure 3.3); whereas, CLN8 462 HF and CLN8 534 HF displayed a trend to increase in mitochondrial staining that was not significant probably due to the variability in these cell lines (Figure 3.3). As such, more repeats are needed to confirm whether CLN8 462 HF and CLN8 534 HF have an increase in mitochondrial staining.

The staining pattern of MitoTracker was also examined as it has been reported to show whether the mitochondrial network is fully formed as it has been reported to be fragmented in other NCLs (Shiple 2019). As can be seen in Figure 3.5 there appears to be no difference in mitochondrial staining pattern suggesting that the mitochondrial network is fully formed in all CLN8 patient cells.

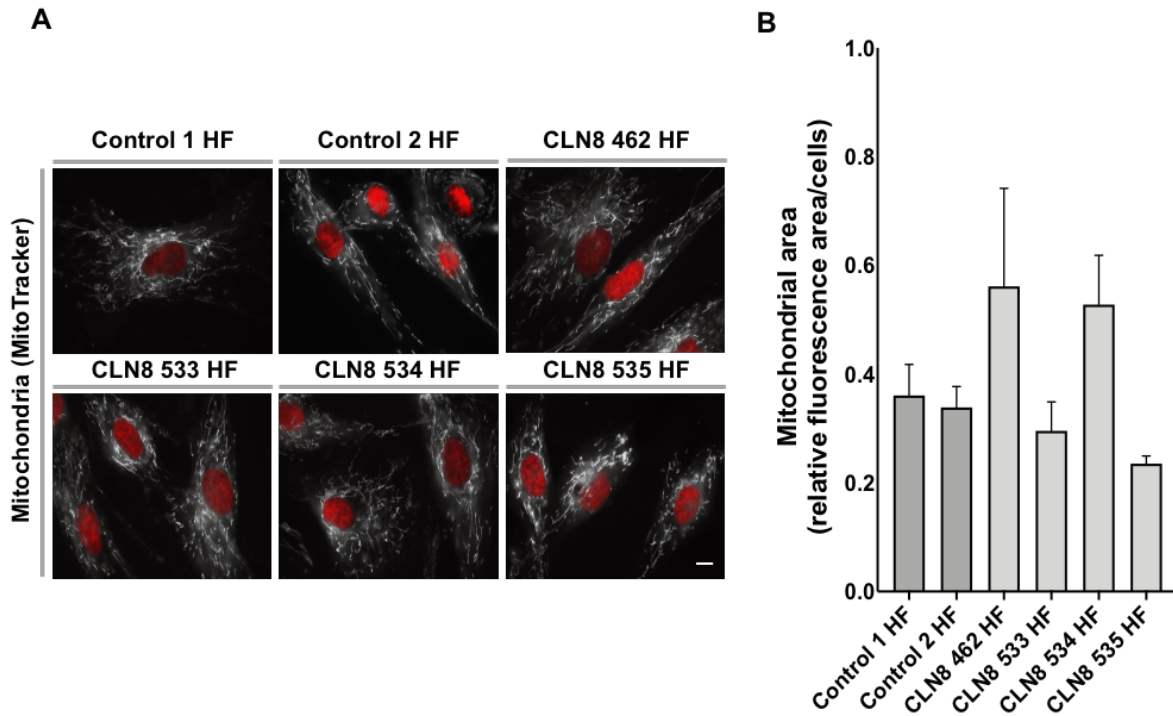


**Figure 3.5: Mitochondrial area in CLN8 patient fibroblast.** **A:** Representative images of mitochondrial staining (MitoTracker; greyscale) quantified in **B** with a Hoescht33342 nuclear counter stain pseudo coloured red. Scale bar = 10  $\mu$ m. **B:** Quantitative analysis of mitochondrial area in control and CLN8 patient fibroblasts. N = 4 and the error bars indicate SEM. There was no significant difference seen using One-way ANOVA with post-hoc Tukey.

### 3.3.5 Changes in mRNA expression in CLN8 patient cells

In order to understand the possible explanation behind the lack of consistency in CLN8 cellular phenotypes the levels of CLN8 mRNA, and other NCL protein mRNA, expression in mouse tissues over time were explored using data from the CIRCA DB online database. The changes in expression levels were calculated by looking at the fold change in mRNA levels from the lowest to the highest expression during a 24-hour period which is suggestive of circadian expression of these proteins. A change in mRNA expression of more than 1.5 fold is thought to be likely to lead to changes in protein levels (Hughes et al. 2010).

It was found that CLN8 mRNA shows an approximate 2-fold temporal change in expression over a 24-hour period (Hughes et al. 2010), this is the most variable change in expression when compared to the expression of other NCL proteins (Figure

3.6). Other Batten disease proteins show a lower than 2-fold change in mRNA expression during the 24-hour period (Figure 3.6).

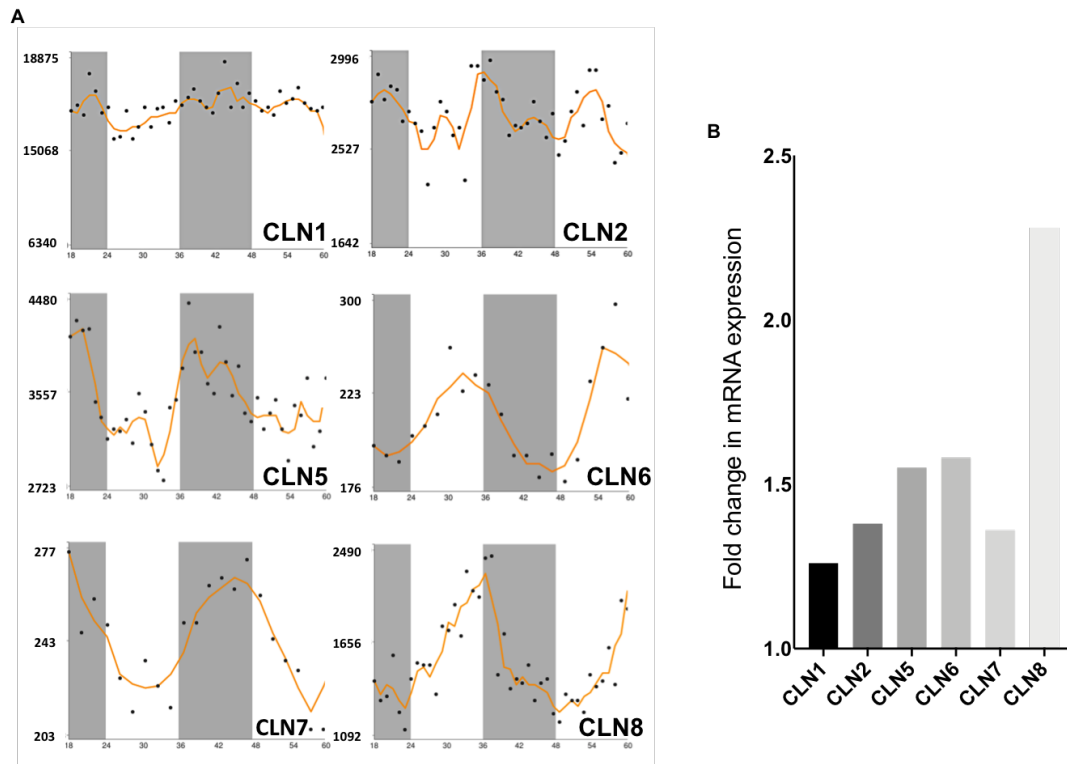


**Figure 3.6: Expression levels of Batten disease mRNAs in mouse liver over 42 hours. A:** Circadian cycles of the Batten disease proteins in mouse liver (**B**) with approximate fold change in expression in a 24-hour period, adapted from CircaDB, the Circadian Expression Profiles Data Base (Hughes et al. 2010). The axes in **A** are not equal as such these were used to calculate the approximate fold change and displayed more clearly in (**B**).

In order to determine whether there are changes in the levels of mutant CLN8 protein expression in the patient fibroblasts, which may explain the variability in cellular phenotypes seen above, the levels of *CLN8* mRNA were examined in the absence of a CLN8 antibody. Initially, four different CLN8 antibodies were tested to detect levels of CLN8 protein expression; however, none of the antibodies tested were able to detect CLN8. Therefore, mRNA levels were explored instead using RT-qPCR analysis to quantify relative levels of CLN8 mRNA in cells at different time points throughout a 12-hour time course (Figure 3.7).

Initial investigation over a 12-hour period showed all 3 CLN8 patient HF appeared to have higher levels of *CLN8* mRNA, with CLN8 534 HF increasing in expression around 2.8 times by the second time point (4 hours; Figure 3.7 A). Following this, levels of *CLN8* mRNA, as well as the regulator of lysosomal biosynthesis *TFEB*, were explored over a 30-hour time course with 6-hour intervals, and for a further 39-hour time course with 3-hour intervals (Figure 3.7 B-E) in order to explore whether the time course or the time between intervals meant changes in mRNA were being missed.

Although changes in the expression of both *CLN8* and *TFEB* mRNA were seen throughout the time course experiments, it was not possible to identify, and subsequently reproduce, any pattern that resembled a circadian-like cycling in the expression of *CLN8* mRNA or *TFEB* mRNA. Nonetheless, an increase of approximately 1.6-fold was observed in the *CLN8* mRNA expression between 12-hour time point and 24-hour time point in CLN8 534 HF (Figure 3.7 B) but no significant change in expression of *CLN8* mRNA was seen in control 1 HF cells during the same time period. During the same time course experiment, a 2.7-fold increase of *TFEB* mRNA was seen between the 24-hour time point and 30-hour time point in CLN8 534 HF (Figure 3.7 C). Similarly, between the 18-hour time point and the 30-hour time point an increase of around 1.4 times was seen in *TFEB* mRNA levels (Figure 3.7 C) indicating increase in lysosomal biogenesis.

Changes in the expression of *CLN8* mRNA and *TFEB* mRNA were seen in control 1 HF during a longer time course with short intervals (Figure 3.7 C & D). There was approximately 3.4 times less *CLN8* mRNA expression between the 6-hour and the 33-hour time points (Figure 3.7 C). There was around 4 times lower expression of *TFEB* mRNA seen between the 6-hour and 33-hour time course (Figure 3.7 D). Overall, changes in both *CLN8* mRNA and *TFEB* mRNA were observed during different time courses in both CLN8 patient cells and control cells, but as previously mentioned no clear pattern was found (Figure 3.7).

It is important to note that the data in each graph is N = 1 with 3-4 technical replicates. These data were to examine the presence of circadian rhythm in the cells but all that was seen was a large amount of inconsistency in the expression levels of *CLN8* mRNA compared to control, as was seen in the LysoTracker data. Furthermore, there was no real synergy with the master regulator *TFEB*. Therefore, as it was not

possible to replicate any pattern in expression and these experiments are both time consuming and costly, this avenue was not pursued further.

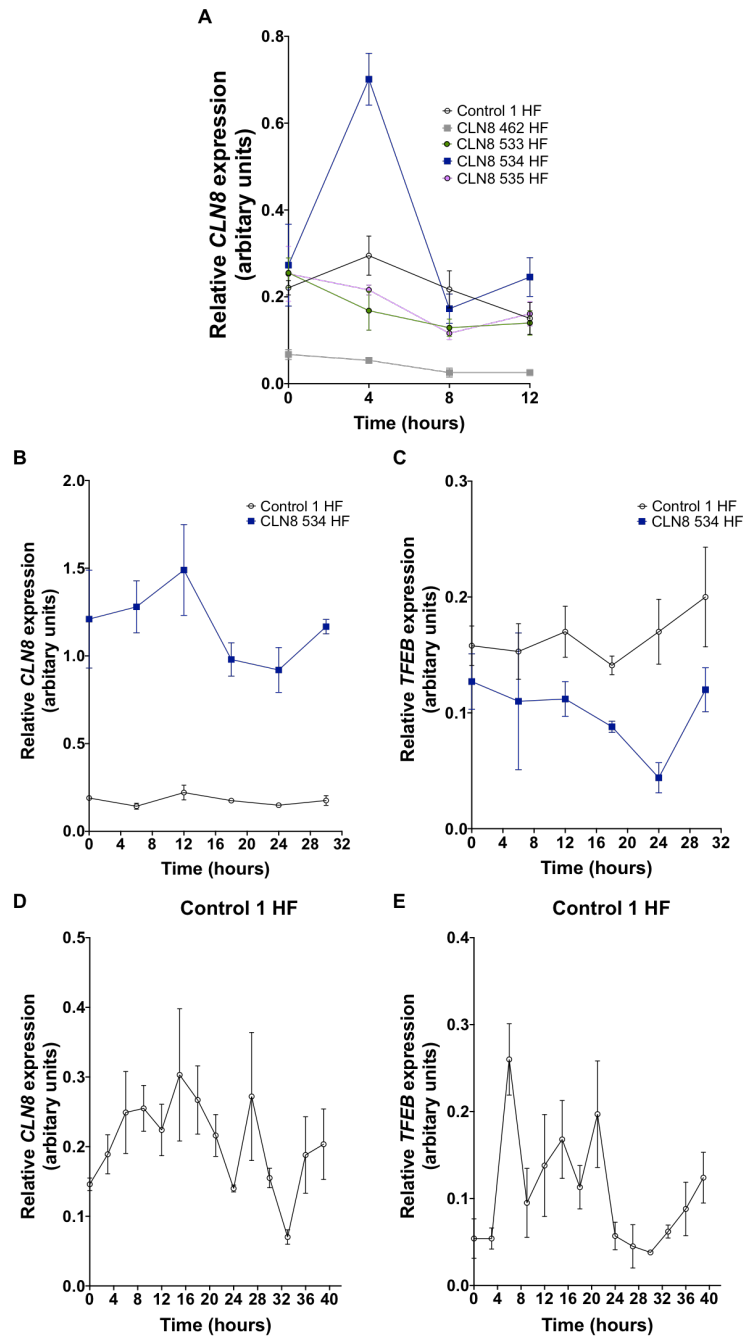


**Figure 3.7: Changes in the expression levels of CLN8 and TFEB mRNAs across different time courses.** **A:** Expression levels of CLN8 mRNA in CLN8 patient and control 1 HF measured every 4 hours across a 12-hour time course. **B:** Expression levels of CLN8 mRNA in CLN8 534 patient and control 1 HF measured every 4 hours across a 32-hour time course. **C:** Expression levels of TFEB mRNA in CLN8 534 patient and control 1 HF measured every 4 hours across a 32-hour time course. **D:** Expression levels of CLN8 mRNA in control 1 HF measured every 3 hours across a 39-hour time course. **E:** Expression levels of TFEB mRNA in control 1 HF measured every 3 hours across a 39-hour time course. All (A-E) expression data is relative to the expression of the geometric mean of the reference mRNAs (GAPDH, TBP & B2M) from N = 1 with 3 wells per data point. Expression data is relative to the expression of the geometric mean of the reference mRNAs. All (A-C, E) error bars indicate SEM.

Given the possible changes in *CLN8* mRNA observed temporally above (Figure 3.7) the levels of total *CLN8* mRNA, across the experiments, were explored in *CLN8* patient HF and control HF (Figure 3.8). Both *CLN8* 534 HF and *CLN8* 535 HF, showed a significant increase in *CLN8* mRNA levels with approximately 3 times and 2 times more *CLN8* mRNA respectively (Figure 3.8). *CLN8* 462 HF, however, seems to have significantly lower levels of *CLN8* mRNA exhibiting around 6 times lower expression of *CLN8* mRNA (Figure 3.8). This indicates that levels of *CLN8* mRNA is variable both within (Figure 3.7) and between (Figure 3.8) patients although no clear time course expression patterns were detected.

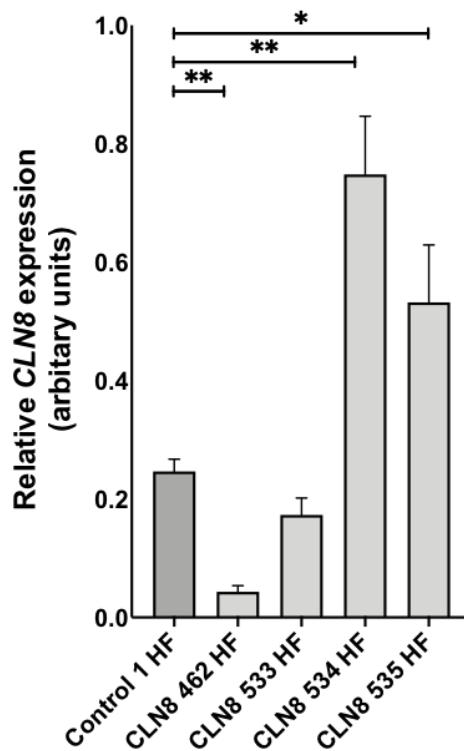


**Figure 3.8: *CLN8* mRNA levels are variable between in *CLN8* patient fibroblasts.** Quantified qPCR data of *CLN8* mRNA in *CLN8* patient and control 1 HFs. Expression data is relative to the expression of the geometric mean of the reference mRNAs (GAPDH, TBP & B2M). N = 4-16. Error bars indicate SEM. \* $p \leq 0.05$ , \*\* $p < 0.01$ , One-way ANOVA with post-hoc Tukey.

Having seen the variability in phenotypes and in the expression of *CLN8* mRNA, the expression of *TFEB*, *MTOR*, *MCOLN1*, *CLN5* and *CLN6* were next explored in *CLN8* patient cells (Figure 3.7 & 3.8). These were selected as *TFEB* is the master regulator of lysosomal biogenesis, *MTOR* is involved in the regulation of autophagy,

TRPML1 (*MCOLN1*) is a lysosomal membrane protein, CLN5 is a soluble lysosomal enzyme and CLN6 is another ER transmembrane protein associated with NCL disease. The expression of *TFEB*, *MTOR*, *MCOLN1*, *CLN5* and *CLN6* was explored in CLN8 534 HF and CLN8 535 HF as CLN8 534 HF is the CLN8 HF cell line in which more phenotypes have been observed and CLN8 535 HF is the cell line with the least variability.

In both CLN8 534 HF and CLN8 535 HF, significantly lower levels of *TFEB* expression were seen with *TFEB* mRNA levels being around 1.5 times and around 7 times lower in CLN8 534 HF and CLN8 535 HF, respectively (Figure 3.9 A). On the other hand, no significant difference in *MTOR* expression was seen in CLN8 534 and CLN8 535 HF (Figure 3.9 B). The lysosomal ion channel *MCOLN1* was seen to have significantly higher mRNA expression by roughly 2 times and 1.8 times more *MCOLN1* mRNA levels in CLN8 534 and CLN8 535, respectively (Figure 3.9 C).

CLN5 was seen to have both significantly increased and significantly decreased expression in CLN8 patient fibroblasts, depending on the cell line studied (Figure 3.9 D). There were approximately 1.2 times higher levels of *CLN5* mRNA (Figure 3.9 D) in CLN8 534 HF; whereas, there were approximately 2.3 times less *CLN5* mRNA in CLN8 535 HF (Figure 3.9 D). *CLN6* was found to have significantly less mRNA expression, at about 2 times less in CLN8 534 compared to control 1 HF (Figure 3.9 E). Conversely, there was no difference in the level of *CLN6* mRNA seen in CLN8 535 HF (Figure 3.9 E).

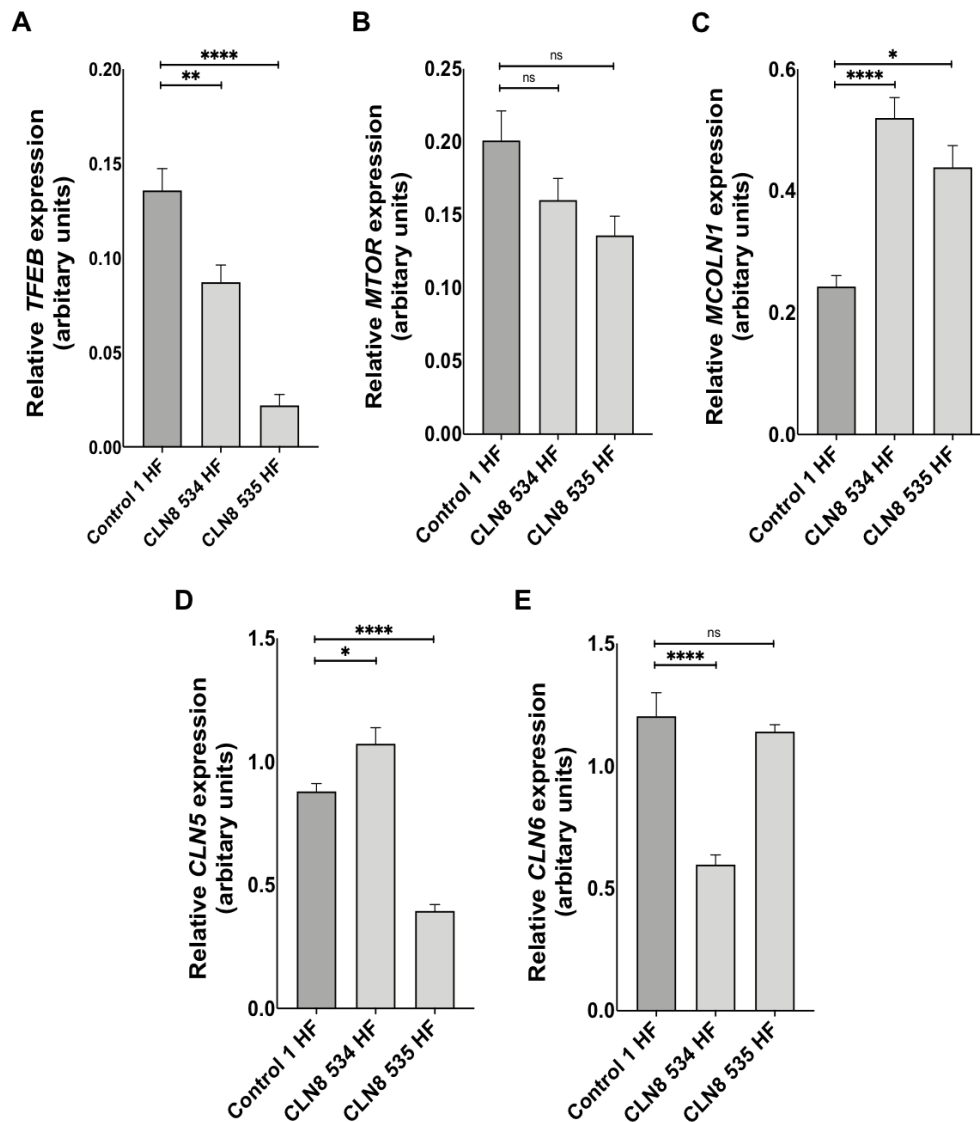


**Figure 3.9: Changes in expression levels of LSD associate mRNAs are altered CLN8 patient HFs.** Expression levels of *TFEB* mRNA (A), *MTOR* mRNA (B), *MCOLN1* mRNA (C), *CLN5* mRNA (C) and *CLN6* mRNA (C) in CLN8 534 HF, CLN535 HF patient and control 1 HF. All (A-E) expression data is relative to the expression of the geometric mean of the reference mRNAs (*GAPDH*, *TBP* & *B2M*). N = 12, except for CLN8 535 HF which was N = 6. All (A-E) error bars indicate SEM. \* $p \leq 0.05$ , \*\* $p < 0.01$ , a One-way ANOVA was used for all except for *MCOLN1* (C) which was not normally distributed, so a Kruskal-Wallis test was used.

In another attempt to explore whether circadian rhythms and the changing levels of CLN8 expression played a role on the variability in cellular phenotypes observed above, cells were treated with 100 nM dexamethasone for 30 minutes as dexamethasone at this concentration and treatment length has been reported to be a synchronizer of circadian rhythm (Balsalobre et al. 2000; Nagoshi et al. 2004).

Following treatment with 100 nM dexamethasone, however, significantly increased CLN8 mRNA levels in control 1 HF cells by 1.5 times (Figure 3.10). Additionally, lysosomal levels, as measured by the area of lysosomal staining with LysoTracker, appeared to be decreased in CLN8 patient cells following dexamethasone treatment; however, this was not significant (Figure 3.10 D & E). It is important to note the data in Figure 3.10 D & E are only preliminary experiments as N = 2 and thus further repeats are required to confirm these findings.

The levels of *TFEB* and *MTOR* mRNA were also examined following dexamethasone treatment. Nonetheless, treatment with dexamethasone did not seem to have any significant effect on the levels of *TFEB* and *MTOR* mRNA (Figure 3.10 B and C).

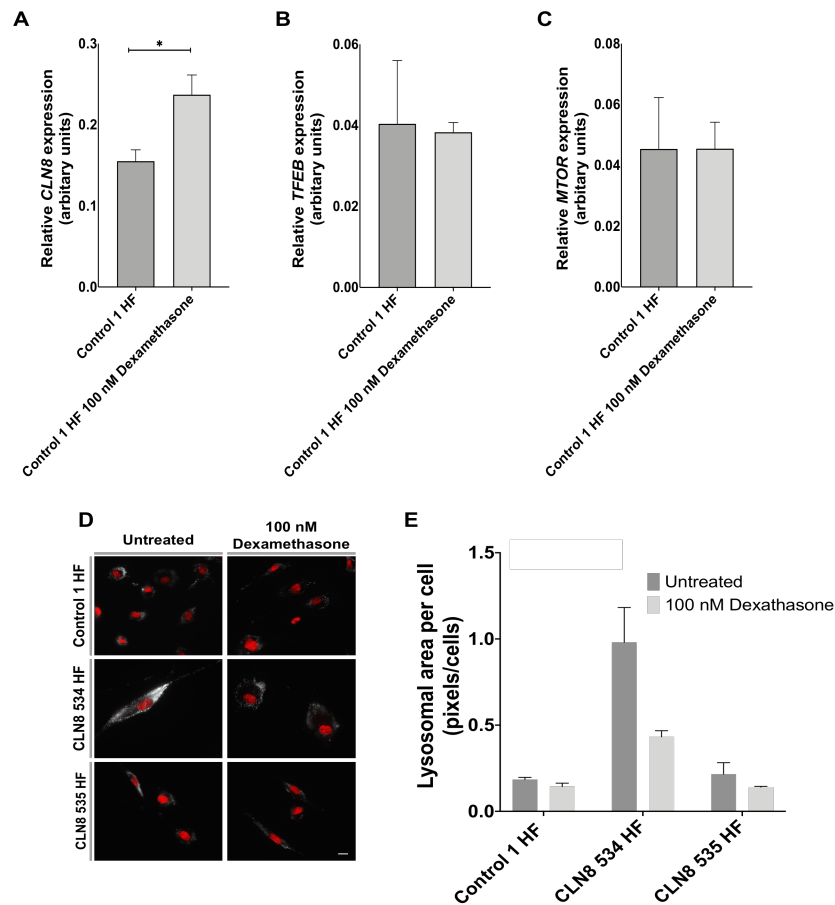


**Figure 3.10: Following 100 nM dexamethasone treatment *CLN8* mRNA expression increases in control 1 HF and lysosomal area in CLN8 534 HF appears to decrease.** Expression levels of *CLN8* mRNA (A), *TFEB* mRNA (B) and *MTOR* mRNA (C) in control 1 HF untreated and treated with 100 nM treatment for 30 minutes 24 hours prior to mRNA levels being measured. All (A-C) expression data is relative to the expression of the geometric mean of the reference mRNAs (*GAPDH*, *TBP* & *B2M*). N = 1 with 3 well per data point. As the data (A-C) was normally distributed statistical analysis was done by a two tailed t-test. D: Representative images of lysosomal staining (LysoTracker, greyscale) in CLN8 534 HF, CLN8 535 HF and control 1 HF untreated and treated with 100 nM treatment for 30 minutes 24 hours before being imaged. A Hoescht33342 nuclear counter stain pseudo coloured red was used. E. Scale bar = 10  $\mu$ m. E: Quantitative analysis of lysosomal area from (D). N = 2 and error bars represent SEM. All (A-C, E) error bars indicate SEM. \* $p \leq 0.05$ , two-way ANOVA.

### 3.3.6 Lysosomal enzyme activities in CLN8 patient fibroblasts

As CLN8 disease is a lysosomal storage disease and the CLN8 protein has been found to play an important role in lysosomal enzyme maturation (di Ronza et al. 2018),

the activity of 22 lysosomal enzymes in CLN8 patient cells were examined (Figure 3.11 & A7.1-A7.22). This was carried out using lysosomal enzyme assays optimised and outlined during this project and by Alshehri (2019). In line with the other results of this chapter so far, the recorded alterations in enzyme activity were highly variable between the different CLN8 patient cell lines (Figure 3.11 & A7.1-A7.23).

Broadly, most if not all, enzymes showed either increased or decreased activity in the CLN8 HF patient cells lines. As an example,  $\alpha$ -galactosidase,  $\alpha$ -mannosidase,  $\beta$ -galactosidase,  $\beta$ -glucosidase, hexosaminidase B, fucosidase, total hexosaminidase,  $\alpha$ -N-acetylgalactosaminidase (NAGA) and palmitoyl-protein thioesterase (PPT1) were seen to have increased activity in only CLN8 534 HF and not the others, with some having decreased activity in the other CLN8 HF lines (Figure 3.11, A7.1, A7.2, A7.8, A7.19 & A7.20). Acid sphingomyelinase was the only enzyme assayed that seemed to have a consistent change, seen as decreased activity, in all the CLN8 HF patient cells (Figure 3.11 & A7.7).

Of the enzyme assays carried out,  $\alpha$ -galactosidase,  $\alpha$ -glucosidase, acid phosphatase, aspartylglucosaminidase,  $\beta$ -galactosidase,  $\beta$ -hexosaminidase, acid sphingomyelinase (ASM), cathepsin L, cathepsin B, fucosidase, hexosaminidase, iduronidase, NAGA and PPT1 had a significant change in enzyme activity in CLN8 patient cells lines when compared to control 1 HF (Figure 3.11, A7.1 – A7.23).

The main conclusions from these enzyme assays are that a variety of lysosomal enzymes have altered activity in CLN8 patient cell; however, the alterations in enzyme activity are variable between different CLN8 patient HF except for ASM which had significantly decrease activity across all CLN8 patient cells (Figure 3.11).

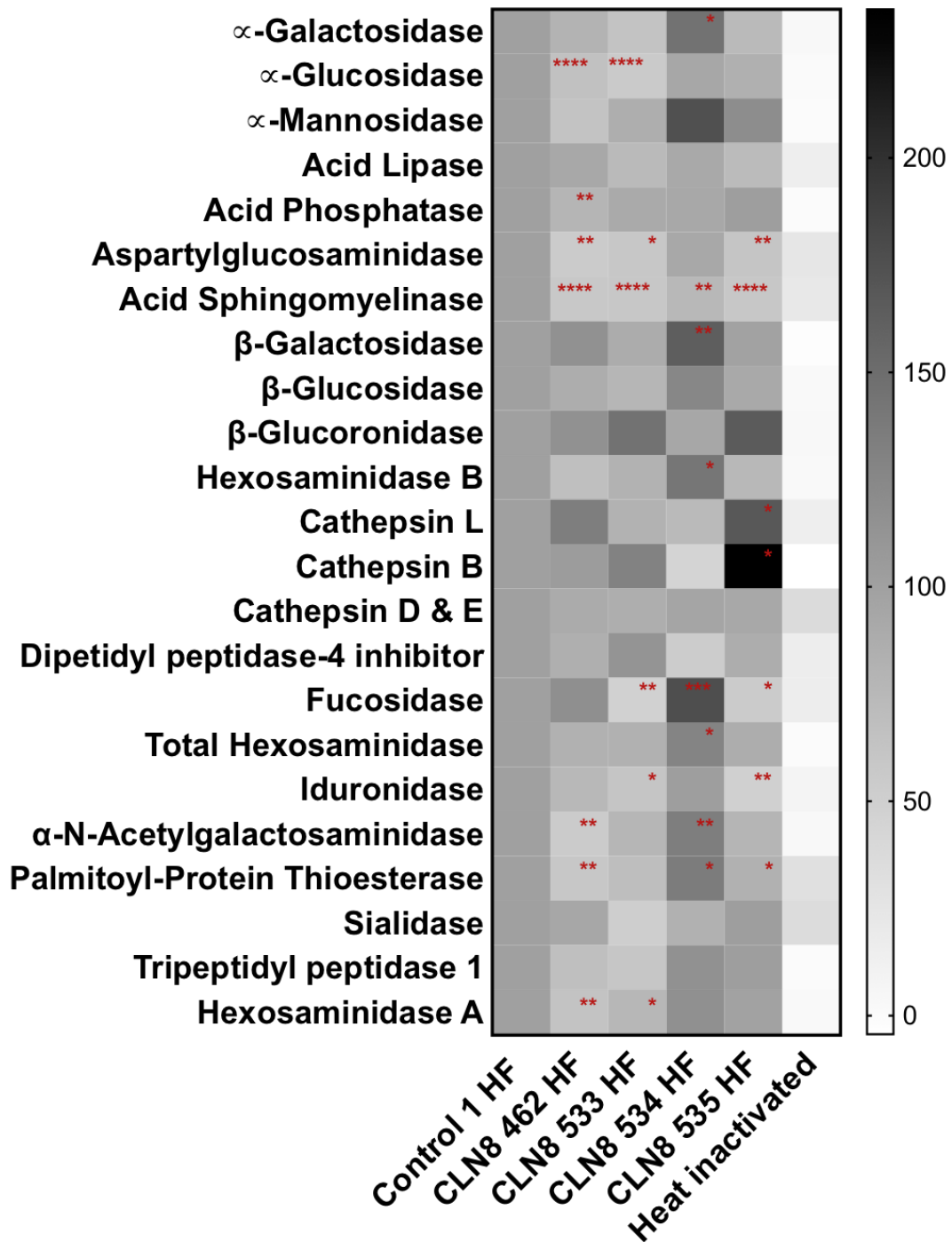


**Figure 3.11: Heat map of changes in lysosomal enzyme activity in CLN8 patient fibroblast.** The heatmaps depict the lysosomal enzyme activity in CLN8 patient HFs and control HFs. The heatmaps were generated from the means of enzyme activity compared to control 1 HF as 100% activity (Figure A1-A20). Each row represents a different lysosomal enzyme assayed and the columns represent the different cell lines as indicated. The scale illustrates the percentage change in enzyme activity compared to the control 1 HF. Darker grey denotes increased enzyme activity; whereas, lighter grey indicates higher enzyme activity. N = 3-4 \*p  $\leq$  0.05, \*\*p < 0.01, \*\*\*p < 0.001, \*\*\*\*p < 0.001, One-way ANOVA.

As an example of an enzyme that seems to have variable activity across the CLN8 patient fibroblasts, cathepsin B was further explored in CLN8 534 HF (Figure 3.11 & 3.12). This stain was readily available in the lab, and thus was used to explore the lower activity seen in CLN8 534 HF, with a potentially higher expression in the other CLN8 HF lines. Cathepsin B staining revealed that approximately double the amount of cathepsin B was present in CLN8 534 HF compared to control 1 HF (Figure 3.12). On the other hand, fluorescence intensity which correlates to the amount of fluorescent probe being released by active cathepsin B appear to be high in the control 1 HF (Figure 3.12 C).

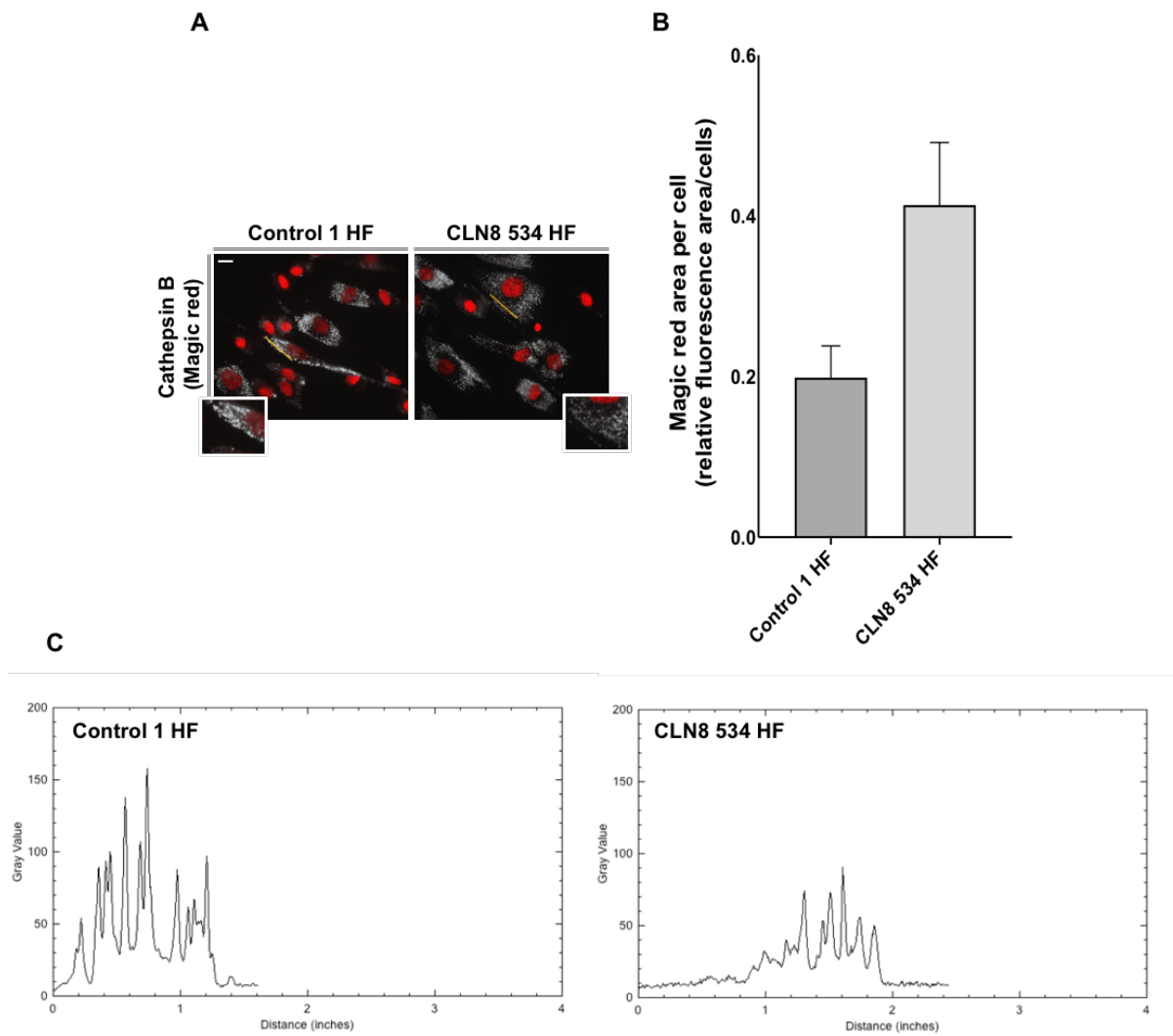


**Figure 3.12: Total Cathepsin B levels is increased in CLN8 534 HF.** **A:** Representative images of cathepsin b staining (Magic red; greyscale) quantified in **B** with a Hoescht33342 nuclear counter stain pseudo coloured red. Scale bar = 10  $\mu\text{m}$ . **B:** Quantitative analysis of cathepsin B levels in apparently healthy (control) and CLN8 patient fibroblast. **C:** Representative profile plot fluorescence intensity of each Magic red containing lysosomal puncta with the indicated region shown in A. N = 3 and the error bars indicate SEM.

### 3.3.7 Thapsigargin mediated ER $\text{Ca}^{2+}$ release in CLN8 patient fibroblasts

Several LSDs have defects in  $\text{Ca}^{2+}$  homeostasis (Pelled et al. 2003; Ginzburg and Futerman 2005; Lloyd-Evans et al. 2008). Additionally, previous reports have found accumulation galactosylceramide and accumulation of glycosphingolipids that may lead to changes in ER  $\text{Ca}^{2+}$ . For these reasons' ER  $\text{Ca}^{2+}$  levels were examined in CLN8 patient fibroblasts by inhibiting the SERCA  $\text{Ca}^{2+}$  ATPase with thapsigargin (Figure 3.13), which leads to  $\text{Ca}^{2+}$  leak from the ER as explained in Chapter 2, allowing

the  $\text{Ca}^{2+}$  content of the ER to be measured. This would provide insight into the disease and assess its suitability for drug screening as it has been done before for NPC disease (Tiscione et al. 2019).

Firstly, it is important to note that for thapsigargin mediated  $\text{Ca}^{2+}$  N = 2 for all except control 1 HF and CLN8 534 HF where N =6-7 and as such this data for CLN8 462 HF, CLN8 533 HF and CLN8 535 is preliminary and requires more repeats. The preliminary data in Figure 3.17 showed CLN8 462 HF and CLN8 535 HF appeared to have 1.7- and 2-times lower ER  $\text{Ca}^{2+}$ , respectively, compared to the control HF cells. Conversely, CLN8 534 HF demonstrated approximately 1.5 times significantly higher thapsigargin ER  $\text{Ca}^{2+}$  (Figure 3.17).

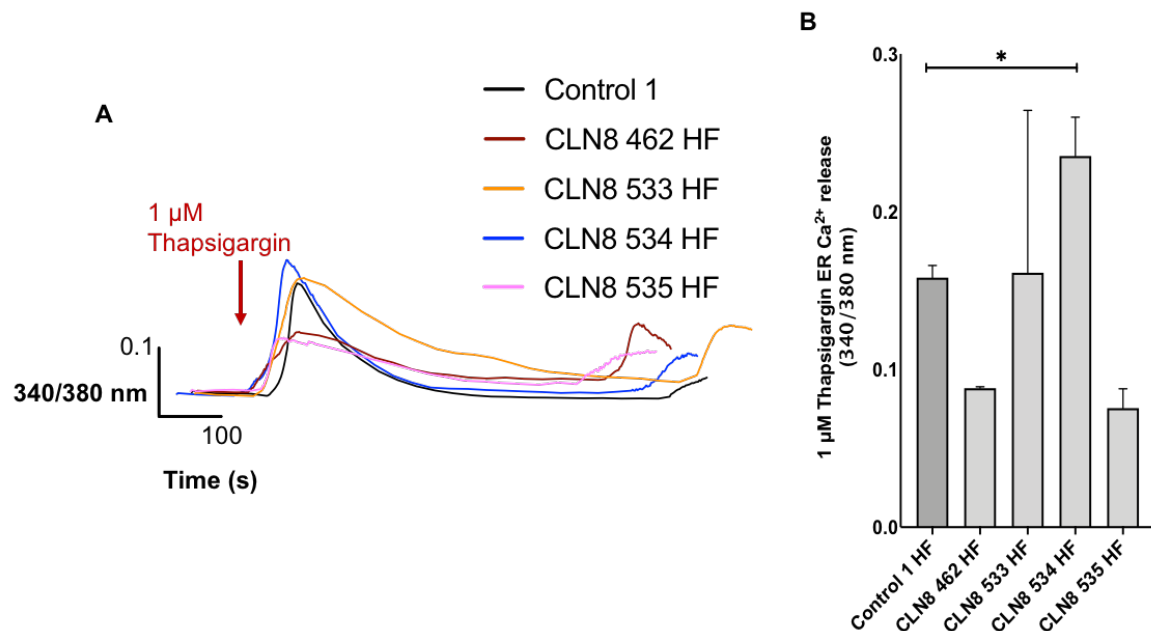


**Figure 3.13: Thapsigargin mediated  $\text{Ca}^{2+}$  release is variable between CLN8 patient fibroblast. A:** Representative traces of the average data for thapsigargin (indicated by red arrow) mediated ER  $\text{Ca}^{2+}$  release quantified in **(B)**. **B:** Quantified change in intracellular  $\text{Ca}^{2+}$  release following thapsigargin **(A)** in CLN8 HF and control HF. N = 2-7. Error bars indicate SEM. As only CLN8 534 HF had enough Ns for stats a two tailed t-test was used, \*p ≤ 0.05.

### 3.3.8 Further Ca<sup>2+</sup> in CLN8 534 HF

As CLN8 534 HF had the clearest and most robust phenotypes of the CLN8 patient cell lines explored, with increased lysosomal storage, defects in autophagy, defects in lysosomal enzyme activities as well as increase thapsigargin mediated Ca<sup>2+</sup> release, further Ca<sup>2+</sup> stores were explored in CLN8 534 HF. Having observed ER Ca<sup>2+</sup> in CLN8 534 HF, mitochondrial Ca<sup>2+</sup> release was examined by inducing Ca<sup>2+</sup> with CCCP as well as separately with antimycin/oligomycin.

CLN8 534 HF appeared to have 3 times lower CCCP-mediated mitochondrial Ca<sup>2+</sup> compared to control 1 HF (Figure 3.14 A & B). CCCP mediated Ca<sup>2+</sup> release is indicative of mitochondrial and Golgi Ca<sup>2+</sup> as outlined in (Chapter 2) suggesting possible lower mitochondrial Ca<sup>2+</sup> of Golgi Ca<sup>2+</sup> in CLN8 534 HF. On the other hand, combined treatment with antimycin/oligomycin, which only induces mitochondrial Ca<sup>2+</sup> leak as described in Chapter 2 (Section 2.3.8), resulted in a trend to 1.5 times higher Ca<sup>2+</sup> leak in CLN8 534 HF compared to control HF that was not significant, so further repeats are needed to confirm this (Figure 3.14 C & D).

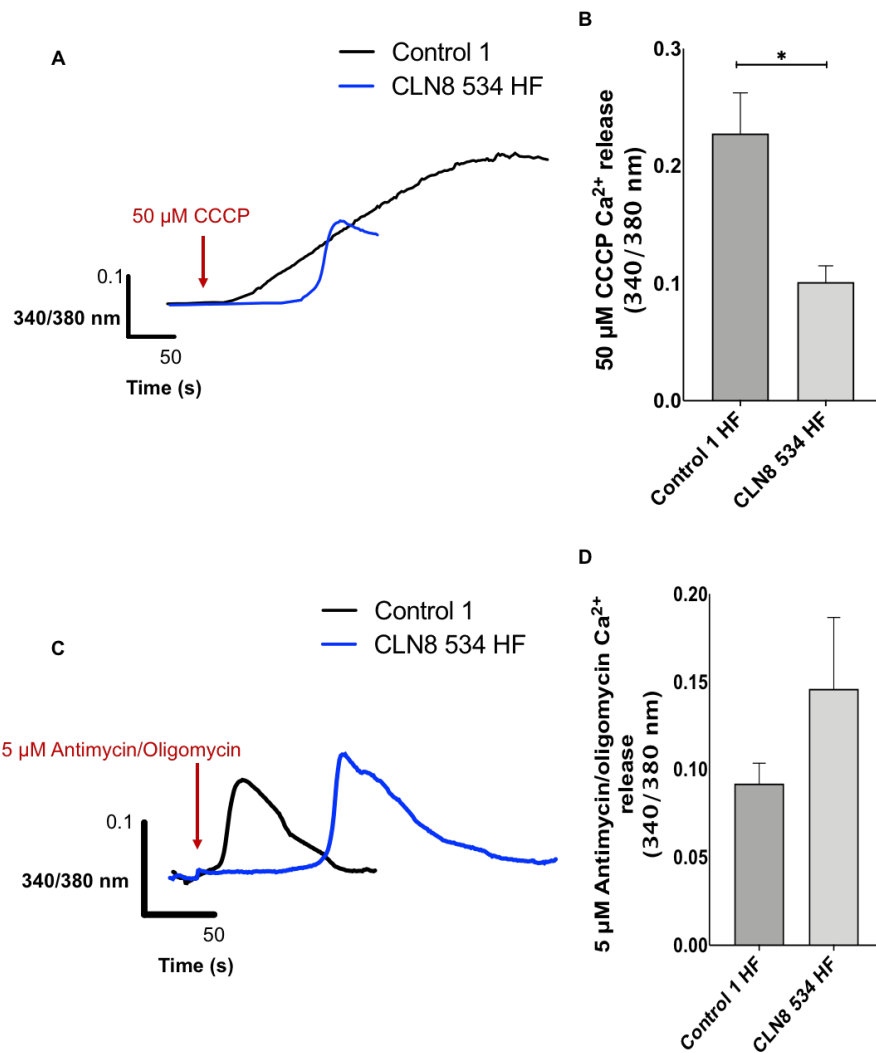


**Figure 3.14: CCCP and antimycin/oligomycin mediated mitochondrial Ca<sup>2+</sup> release in CLN8 patient fibroblasts.** **A:** Representative traces of the average data for CCCP (indicated by the red arrow) mediated mitochondrial Ca<sup>2+</sup> and Golgi Ca<sup>2+</sup> release quantified in **(B)**. **B:** Quantified change in intracellular Ca<sup>2+</sup> release following CCCP **(A)** in CLN8 534 HF and control 1 HF N = 3-5. Error bars indicate SEM. There was no significant difference between CLN8 534 HF and control 1 HF. **C:** Representative traces of the average data for antimycin/oligomycin (indicated by the red arrow) mediated mitochondrial Ca<sup>2+</sup> release quantified in **(D)**. **D:** Quantified change in intracellular Ca<sup>2+</sup> release following antimycin/oligomycin **(C)** in CLN8 534 HF and control 1 HF. N = 2-5. Error bars indicate SEM. \*p ≤ 0.05, two tailed t-test.

Following the defect in ER Ca<sup>2+</sup> seen in Figure 3.13 as well as the possible defect in Golgi Ca<sup>2+</sup> in CLN8 534 HF ER Ca<sup>2+</sup> was further explored using ionomycin and ryanodine (Figure 3.15). As explained in Chapter 2 ionomycin induces Ca<sup>2+</sup> release from all stores except the lysosomes and ryanodine acts as both an inhibitor (high concentrations >20 μM) and activator (low concentrations <20 μM) of the ryanodine

receptor so at the concentration of 10  $\mu\text{M}$  used, it acts as an activator leading to  $\text{Ca}^{2+}$  release from the ER to the cytosol via the ryanodine receptor. Unlike thapsigargin, however, a difference was not seen in either ionomycin or ryanodine mediated ER  $\text{Ca}^{2+}$  release (Figure 3.15) suggesting no change in total ER  $\text{Ca}^{2+}$ .

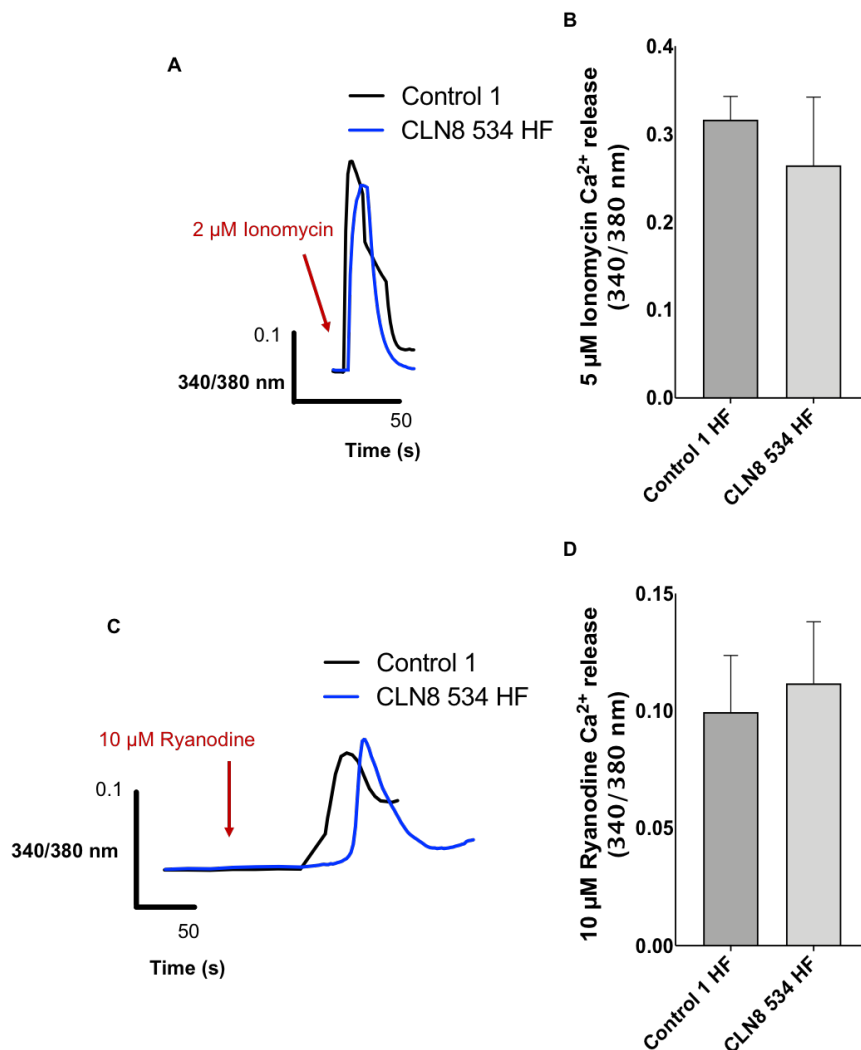


**Figure 3.15: Ionomycin and Ryanodine mediated  $\text{Ca}^{2+}$  release in CLN8 patient fibroblasts. A:** Representative traces of the average data for ionomycin (indicated by red arrow) mediated  $\text{Ca}^{2+}$  release quantified in **(B)**. **B:** Quantified change in intracellular  $\text{Ca}^{2+}$  release following ionomycin **(A)** in CLN8 534 HF and control 1 HF.  $N = 4-7$ . Error bars indicate SEM. There was no significant difference between CLN8 534 HF and control 1 HF. **C:** Representative traces of the average data for ryanodine (indicated by red arrow) mediated ER  $\text{Ca}^{2+}$  release quantified in **(D)**. **D:** Quantified change in intracellular  $\text{Ca}^{2+}$  release following ryanodine **(C)** in CLN8 534 HF and control 1  $N = 4-5$ . Error bars indicate SEM. There was no significant difference between CLN8 534 HF and control 1 HF using a two tailed t-test.

As CLN8 is a lysosomal storage disease and as lysosomal  $\text{Ca}^{2+}$  defects have been observed in many lysosomal storage diseases (Lloyd-Evans and Platt 2011), the next step was to explore lysosomal  $\text{Ca}^{2+}$  levels in CLN8 patient fibroblasts (Figure 3.16). Almost half the amount of lysosomal  $\text{Ca}^{2+}$  was seen in CLN8 534 HF cells compared to control 1 HF when measuring lysosomal  $\text{Ca}^{2+}$  with GPN (Figure 3.16 A & B) as GPN leads to lysosomal  $\text{Ca}^{2+}$  release as explained in Chapter 2.

$\text{Ca}^{2+}$  is tightly regulated as previously mentioned, as such, having observed defects in thapsigargin, CCCP and GPN mediated  $\text{Ca}^{2+}$  from the ER, Golgi and the lysosome respectively the basal levels of intracellular  $\text{Ca}^{2+}$  as outlined in Chapter 2 Section 2.3.8. Basal cytoplasmic  $\text{Ca}^{2+}$  was explored but no difference was seen between CLN8 534 HF and control 1 HF (Figure 3.16 C). Therefore, the defects in  $\text{Ca}^{2+}$  in the ER, Golgi and lysosome do not appear to affect cytosolic  $\text{Ca}^{2+}$  levels.

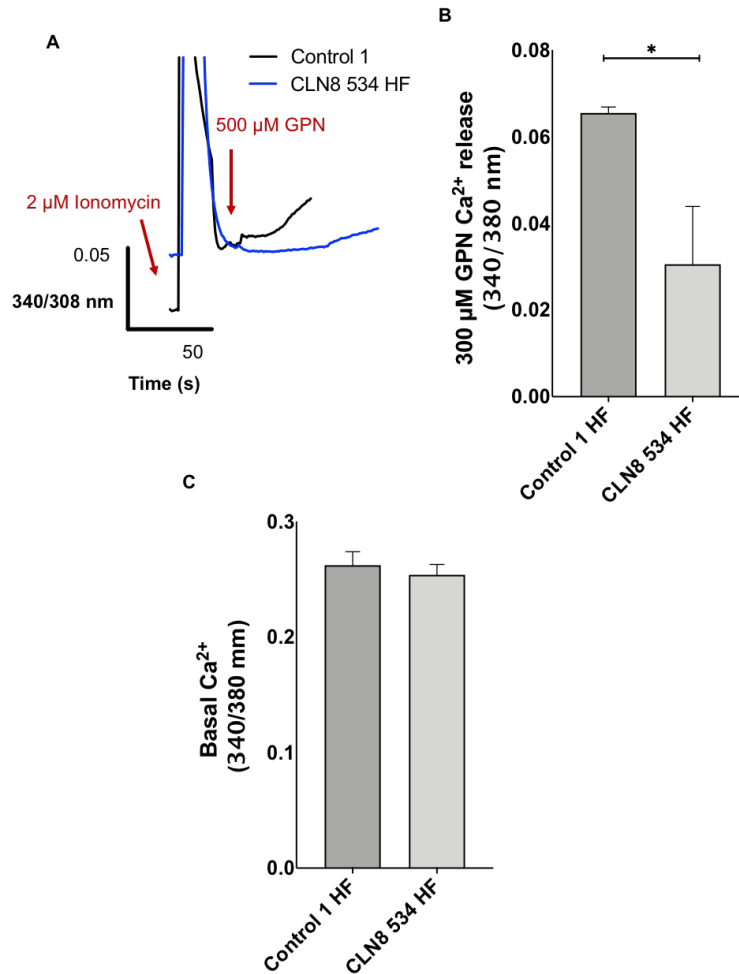


**Figure 3.16: GPN-mediated lysosomal  $\text{Ca}^{2+}$  release and basal cytoplasmic  $\text{Ca}^{2+}$  CLN8 534 HF. A:** Representative traces of the average data for GPN (indicated by red arrow) mediated lysosomal  $\text{Ca}^{2+}$  release quantified in (B). **B:** Quantified change in intracellular  $\text{Ca}^{2+}$  release following GPN (A) in CLN8 534 HF and control 1 HF N = 2-4. Error bars indicate SEM. There was no significant difference between CLN8 534 HF and control 1 HF. **C:** Quantified intracellular  $\text{Ca}^{2+}$  in CLN8 534 HF and control 1 HF. N = 11-21. Error bars indicate SEM. There was no significant difference between CLN8 534 HF and control 1 HF. \* $p \leq 0.05$ , \*\* $p < 0.01$ , two tailed t-test.

### 3.4 Discussion

This chapter aimed to characterise disease phenotypes in CLN8 patient fibroblasts to utilise in therapeutic drug screening. Investigation of the cellular pathology underpinning CLN8 patient HF has uncovered changes in several cellular compartments across some of the CLN8 patient cells lines examined. These include increases in lysosomal area reflective of an expansion in lysosomal number, defects

in autophagic vacuole clearance, altered endo-lysosomal distribution of cholesterol and possible increases in thapsigargin mediated  $\text{Ca}^{2+}$  release (Figures 3.1, 3.3, 3.4, 3.5 & 3.6). Further alteration to ER and lysosomal  $\text{Ca}^{2+}$  levels was observed in one of the CLN8 HF lines and alteration in the expression of different lysosomal enzymes was also seen across two of the CLN8 patient cell lines. Defects in a range of lysosomal enzyme activities were also observed across the patient cell lines with only acid sphingomyelinase being significantly affected across all the CLN8 patient cell lines. Intriguingly, there was large variability across the phenotypes measured (Table 3.2), not only between the different CLN8 patient cell lines, but more remarkably within individual cells in the patient cell lines.

**Table 3.2: Summary of phenotypic variability in CLN8 HFs compared to Control HFs.** An increase is denoted by  $\uparrow$ , a decrease is denoted by  $\downarrow$ , a high degree of variability is indicated by  $\approx$ , an increase with high variability is denoted by  $\uparrow\approx$  and no change is indicated  $/$ . Only phenotypes that were found to be significant in this Chapter are outlined in the table below.

Cellular Phenotype	CLN8 462 HF	CLN8 533 HF	CLN8 534 HF	CLN8 535 HF
Lysosomal area	$\approx$	$/$	$\uparrow\approx$	$/$
Cholesterol puncta	$\uparrow$	$/$	$\uparrow$	$/$
Autophagic compartments	$\approx$	$/$	$\approx$	$\approx$
Mitochondria area	$\approx$	$/$	$\approx$	$/$
Relative <i>CLN8</i> expression	$\downarrow$	$/$	$\uparrow\approx$	$\approx$
Relative <i>TFEB</i> expression	n/a	n/a	$\downarrow$	$\downarrow$
Relative <i>MTOR</i> expression	n/a	n/a	$/$	$/$
Relative <i>MCOLN1</i> expression	n/a	n/a	$\uparrow$	$\uparrow$
Relative <i>CLN5</i> expression	n/a	n/a	$\uparrow$	$\downarrow$
Relative <i>MTOR</i> expression	n/a	n/a	$\downarrow$	$/$
ER $\text{Ca}^{2+}$	$\downarrow$	$\approx$	$\uparrow$	$\downarrow$

### 3.4.1 Lysosomal expansion in CLN8

Lysosomal staining revealed an increase in lysosomal area only in the A30P homozygous CLN8 534 HF and not the other CLN8 cell lines (Figure 3.1). This increase in lysosomal staining was also seen using the LysoTracker plate assay

(Figure 3.1C) confirming that CLN8 534 HF was the only patient cell line that has significant increases in lysosomal volume. This indicates that only one of the 4 patient cell lines examined in this chapter exhibits lysosomal storage; whereas, the other CLN8 patient cells either do not, or fluctuate as seen in Figure 3.2.

These findings may mirror reports of LSDs, such as CLN10, which do not exhibit an increase in LysoTracker staining but do have an expanded lysosomal network or even substantial lysosomal storage (Lim et al. 2016). In the case of CLN10 it has been suggested that LysoTracker staining is not increased because CLN10 has a lysosomal pH defect (Holpainen et al. 2001). Therefore, the fact that no increase in LysoTracker is seen in some of the CLN8 cells might suggest that there is no lysosomal accumulation of macromolecules but cannot guarantee this is the case. It may therefore be of interest to explore lysosomal pH in these CLN8 cell lines in order to confirm whether lysosomal pH in CLN8 may lead to the lack of LysoTracker increase seen in some of the CLN8 patient cells.

It may also be the case that some CLN8 patient mutations lead to lysosomal storage and others do not. A recent study, di Ronza *et al.* (2018), mentioned in Section 3.1, found that different CLN8 mutations affected the ability of CLN8 to chaperone lysosomal enzymes out of the ER, which may be what leads to the difference in lysosomal volume seen between the different CLN8 patient cells lines.

The increase in lysosomal volume measured in CLN8 534 HF was not a consistent phenotype (Figure 3.2). Lysosomal imaging of the CLN8 cell lines required a high N number in order to ensure confidence in the results. Whilst this is ideal for confirmation of cellular dysfunction, such a large number of repeats is not feasible for drug screening of large-scale drug libraries. This variation is particular to CLN8 as such broad changes in lysosomal measurement were not seen in other LSDs tested in this project (Figure 4.1 & 5.9) as well as other projects, and in the literature (Sugimoto et al. 2001; Platt et al. 2012; Xu et al. 2014; Vanier and Latour 2015). This suggests that the variability seen between and within CLN8 patient cell lines is specific to the CLN8 protein and its functions; however, what leads to the variation is unclear.

### **3.4.2 Cholesterol accumulation in CLN8**

In this study, cholesterol punctate staining, indicative of cholesterol accumulation in lysosomes, was increased in the CLN8 462 HF and CLN8 534 HF patient cell lines (Figure 3.3). This, however, was not the case for the other two CLN8 cell lines, which indicates that different mutations in CLN8 differentially affect lysosomal cholesterol accumulation in lysosomes (Figure 3.5). This could be due to the different mutation affecting lysosomal maturation differently, in which some CLN8 mutations lead to proteins that are important for the transport of cholesterol such as NPC2 and NPC1 to be affected in those patient cell lines, or enzymes involved in lysosomal processing of cholesterol esters such as acid lipase. Recently, NPC1 has been shown to be involved in the ER-lysosomal contact point for lipid transport. Additionally, CLN8 has been found to interact with VAPA, as mentioned in Section 1.2.4, which is part of the ER-lysosomal lipid transport complex (Passantino et al. 2013). Therefore, it may be that the ER-lysosomal lipid transport mechanisms are affected in CLN8; however, the data in this report indicates defects in CLN8 mechanisms may be mutation specific.

Taken together, the lysosomal expansion and increase in cholesterol seen in CLN8 534 HF suggests that the CLN8 patient cells (CLN8 534 HF) that exhibit increases in lysosomal volume have accumulation of lysosomal cholesterol. Similarly, other studies with the CLN8<sup>mnd</sup> knockout mouse model found that levels of cholesterol in the brain were elevated which would further imply defects in lysosomal cholesterol regulation in CLN8 disease (Hermansson et al. 2005).

### **3.4.3 Autophagic vacuole expansion in CLN8**

Using Cyto-ID to measure autophagic vacuole levels in CLN8 patient fibroblasts, an increased level was seen in CLN8 426 HF and CLN8 534 HF, but not in CLN8 533 HF and CLN8 535 HF (Figure 3.4). Imaging of autophagic vacuoles in CLN8 was again found to be very variable, both between and within the different patient cell lines. The variability seen in the autophagic staining in the CLN8 lines (Table 3.2) was even greater than what was observed with the lysosomal staining (Figure 3.1 & 3.4), perhaps associated to the fact that CLN8 is an ER protein and the autophagic vacuole membrane emerges from that organelle (Wei et al. 2018). Furthermore, in previous studies, CLN8 protein was found to interact with GATE16 and other proteins which are

essential for autophagy (Weidberg et al. 2010; Passantino et al. 2013). In this study CLN8 462 HF and CLN8 534 displayed a trend towards increase in CytoID staining but the degree of variability in CytoID staining in CLN8 patient cell lines was too high to observe any significant difference.

Increased Cyto-ID staining area in cells indicates accumulation of autophagosomes and autophagic cargo within autophagic compartments as well as increase autophagosome volume, biogenesis or clearance failure. Nonetheless, it does not distinguish between increased autophagy production or decreased clearance. An experiment that can be carried out in future, to determine if autophagy is increased or if there is a defect in clearance, could be done by using GFP-LC3 and monitoring the flux through the autophagosome system. These experiments, however, may be best performed in CLN8 null cells, where we anticipate less variability in phenotypes.

#### **3.4.4 Mitochondrial staining in CLN8**

Mitochondrial staining in CLN8 HF resembled that seen in lysosomal and autophagic vesicle staining (Figure 3.5). CLN8 462 HF and CLN8 534 HF appeared to have increased mitochondrial staining. Increased mitochondrial staining may indicate that mitochondria are not being cleared, by autophagy, and are accumulating possibly due to autophagosome-lysosomal fusion defects. CLN8 533 HF seemed to have no change in mitochondrial staining; however, CLN8 535 potentially has lower mitochondrial staining. Overall, there was a high degree of variability seen in mitochondrial staining in each of the CLN8 patient fibroblast. Another way to further examine mitochondrial function, which may be used in future experiments for CLN8, could be the use of the Seahorse bioanalyzer that tests for mitochondrial stress.

#### **3.4.5 Variability in CLN8 phenotypes and drug screening**

It is interesting that patients with the same disease showed such variability in cellular phenotypes. This inter-patient variability, however, has been reported previously to the extent that, as mentioned in Chapter 1, CLN8 disease is sub-categorised into two different clinical diagnoses (Kousi et al. 2012). A previous study found both increased and decreased levels of certain lipids in post-mortem brains of CLN8 disease patients (Hermansson et al. 2005). Specifically, the study found that

sphingomyelin,  $\alpha$ -galactosylceramide, sulfatide, ceramide and lactosylceramide were decreased in a subset of post-mortem brains of CLN8 patients compared to healthy controls, whereas, these same lipids were elevated in a different set of CLN8 post-mortem brain samples when compared to controls (Hermansson et al. 2005).

Overall, CLN8 462 HF and CLN8 534 HF displayed the greatest variability of phenotypes tested in this study. The phenotypic variability seen within CLN8 cell lines between different Ns has not been reported before. This may be due to the dearth of research into CLN8 disease. Moreover, there have been minimal reports on the cellular pathology of CLN8 disease. To date, most of the phenotypic studies of CLN8 disease are either clinical reports, very few *in vitro* experiments using knockout cell lines, or *in vivo* studies using the naturally- occurring CLN8<sup>mnd</sup> mouse, a mouse model for neurodegenerative disease with mutations in CLN8 (Ranta et al. 1999; Lonka et al. 2000; Striano et al. 2007; Galizzi et al. 2011; Kolkova et al. 2011; di Ronza et al. 2018; Bajaj et al. 2020). The scarcity of research into the cellular pathogenesis of CLN8 means that the variation within CLN8 patient fibroblasts has not been reported before, making this study the first to do so and a potentially useful resource once published to assist with research in this area.

It was particularly noteworthy that the lysosomal expansion seen in the CLN8 534 HF line varied temporally to the extent that sometimes there was no lysosomal expansion, and other times the lysosomal system was expanded 2-fold (Figure 3.3 A & B). This pronounced temporal variation in cellular disease phenotypes is believed to be unique amongst the LSDs.

SNPs that affect CLN8 expression levels have been linked to Gaucher disease severity (Zhang et al. 2012). Patients with mild Gaucher disease exhibit higher levels of CLN8 expression (Zhang et al. 2012). As mentioned above, CLN8 has been identified as being involved in lysosomal enzyme maturation. Even though glucocerebrosidase, the enzyme affected in Gaucher disease (Bennett and Mohan 2013), is not one of the enzymes reported to require CLN8 for maturation (di Ronza et al. 2018), increased expression of CLN8 led to higher levels of other enzymes in lysosomes. This increased levels of enzymes in lysosomes may alleviate storage in Gaucher disease patients, in turn alleviating disease severity (Zhang et al. 2012). Therefore, therapies that increase CLN8 expression may be of benefit to Gaucher

disease and potentially other LSDs by increasing the transport of lysosomal enzyme to the lysosome alleviating lysosomal storage.

The unforeseen degree of variability within and between CLN8 patient fibroblasts limits the findings of this study. The great difference between patient mutations means that there is a need for each CLN8 patient fibroblast to be studied independently for further characterisation. Since the main aim of this Chapter was to characterise phenotypes that could be used for drug screening, each CLN8 cell line was not individually explored in depth, but it is something that merits further exploration.

To circumvent the issues relating to the variability between and within cells, knockout cell lines could be useful, although these do not necessarily fully represent the disease. The main issue, however, is the immense cost associated with creating knockout cell lines (Wilkinson et al. 2010). During this project, several attempts were made to obtain knockout or even haploid CLN8 cell lines, but this was not possible within the budget.

Furthermore, gene silencing approaches were considered, but as no good antibody was available with which to detect knockdown, it was not possible to say for sure if the approach has been successful. Furthermore, as the half-life of the CLN8 protein is not known the use of qPCR to monitor mRNA levels may not reflect residual CLN8 protein levels. As incomplete knockdown may cause phenotypic variability and the presence or absence of CLN8 cannot be confirmed, it was decided not to progress with this avenue. Clearly, a good CLN8 antibody is a necessity for future advancement of this field. In this study the mutation of the CLN8 patient cell lines obtained were not independently verified. Future CLN8 studies should always confirm the mutations in the CLN8 patient cell lines used particularly due to the variability observed.

Previous research linked CLN8 expression to the severity of another LSD, as well as the fact that changes over time in CLN8 expression were seen in the CircaDB prompted the investigation that changes in CLN8 expression may be caused by circadian rhythms or other cyclical regulation as a potential factor behind the phenotypic variability seen between and within different CLN8 patient cell lines. Future research should explore the role of CLN8 mRNA expression in circadian rhythms or more likely cell cycle by carrying out qPCR experiments such as those in Figure 3.7. These experiments, however, should ensure that cells are synchronised in cell

cycle/circadian rhythms and should look at the expression of genes known to oscillate within a 24-hour period as well as CLN8 mRNA.

### **3.4.6 Temporal changes in CLN8 mRNA**

The possible relationship between expression of CLN8 and the temporal changes in phenotypic severity led us to investigate the possible circadian rhythm or cell cycle effect on CLN8 protein expression and how this may subsequently affect disease severity. While comparing the expression profiles of several NCLs proteins across a 42-hour time course in mouse liver using the Circadian expression profile data base (Hughes et al. 2010), it became apparent that CLN8 had the highest level of changes in mRNA expression of several NCL genes. CLN8 cells exhibited a more than 2-fold increase in expression over 24-hours (Figure 3.7). Conversely, the highest change in expression for other NCLs was just under 1.5-fold. This large change in mRNA expression may lead to an increase in the CLN8 protein that, even in patients with a mutant CLN8 gene, could increase the expression of a partially functional CLN8 protein enough to rescue some function, thus decreasing phenotypic severity. This, however, has not been reported in any other LSD.

This study then explored the changes in expression of CLN8 over several time-course experiments to uncover time-dependent changes in CLN8 expression (Figure 3.8). Although some changes in CLN8 mRNA were seen over the time courses measured, there was no obvious pattern in CLN8 mRNA expression levels between technical repeats. The experiment was repeated with different cell confluency as well as different time periods between repeats to determine if the proximity of cells within the culture flasks, or the cell cycle effect or length of time between measurements had any effect on the CLN8 mRNA expression.

It was not possible to determine during this study if the changes in CLN8 mRNA expression are due to circadian rhythms, cell cycle effects or otherwise. The major limitation underlying this is that circadian rhythms are tightly regulated by the suprachiasmatic nucleus in the hypothalamus, meaning that fibroblasts in culture like those used in this study will not exhibit the same circadian cycle synchronisation, rendering it extremely difficult to measure circadian effects on protein expression in fibroblast cultures (Pantazopoulos et al. 2018; Zisapel 2018).

#### 3.4.6.1 Increase in *CLN8* mRNA may explain phenotypic variability

Initially, short treatments of dexamethasone were used to synchronize circadian rhythms (Balsalobre et al. 2000; Nagoshi et al. 2004) to determine if there was a link between the cell circadian rhythm and the expression of *CLN8* mRNA. Following dexamethasone treatment, however, expression of some proteins including CLN8 were found to be increased, making it impossible to determine the circadian or cell cycle pattern underlying the changes in CLN8 expression. Not only did dexamethasone increase *CLN8* mRNA, but it seemed to decrease lysosomal expansion in CLN8 534 HF (Figure 3.11).

It is noteworthy that dexamethasone did not increase TFEB, the master regulator of lysosomal biogenesis (de Duve 2005; Settembre et al. 2013; Settembre and Medina 2015; Ballabio 2016; di Ronza et al. 2018), but did increase the expression of CLN8 mRNA. The lack of increase in *MCOLN1*, which encodes the lysosomal ion channel TRPML1 and which is considered as a lysosomal marker (Gómez et al. 2018), following dexamethasone treatment, indicated that the possible reduction in lysosomal expansion seen in CLN8 534 HF was due to the increase in CLN8, and not an increase in the expression of the general lysosomal network of CLEAR genes (Palmieri et al. 2011).

Nonetheless, the decrease observed in lysosomal volume following treatment with dexamethasone could be due to the variability that has been seen in CLN8 patient fibroblasts throughout this Chapter. This does, however, provide at the very least preliminary data that suggest that increases in CLN8 expression leads to decrease in phenotypic severity. It is important to note that dexamethasone is a steroid drug that is not suitable for long term therapy (Black et al. 1960); however, this data suggests that drugs that increase CLN8 expression may be potential therapies for CLN8 disease.

#### 3.4.6.2 *CLN8* mRNA expression

*CLN8* mRNA was also not consistently altered across the different patient fibroblasts compared to controls (Figure 3.9). Only the CLN8 533 HF line showed no significant differences in *CLN8* mRNA levels compared to the control. CLN8 534 HF

was the patient cell line with the least variability and had some evidence of cellular phenotypes during this project.

CLN8 462 HF had significantly lower *CLN8* mRNA expression compared to the control. One of the alleles in CLN8 462 HF is a genomic addition (c.543 +1G; Table 3.1). As previously mentioned, Section 3.1, genomic deletions have been suggested to lead to mRNA instability (Reinhardt et al. 2010). It may be the case that genomic additions also lead to mRNA instability which might be what leads to significantly lower *CLN8* mRNA being detected in this study (Figure 3.9). Previous studies in Tay-Sachs, another LSD, have reported that a 4-bp insertion leads to mRNA instability (Boles and Proia 1995). This, however, has not been previously reported and thus requires further confirmation but may explain the big decrease in *CLN8* mRNA seen in CLN8 462 HF.

Conversely, CLN8 535 HF and particularly CLN8 534 HF demonstrated significantly higher levels of *CLN8* mRNA. Protein expression is commonly increased in diseases to mitigate decreased function. Nonetheless, as with all of the results in this chapter, it is important to highlight that there was a high degree of variability seen between experimental repeats; thus, this may possibly be an artefact of the time these were measured, despite the high number of Ns. Furthermore, these results only reflect mRNA which does not always translate to protein expression (Koussounadis et al. 2015) and as such, if a good antibody were to be developed in future, then further experiments to explore changes in protein expression such as western blotting should be carried out to confirm the changes seen.

#### **3.4.7 Changes in *TFEB*, *MTOR*, *MCOLN1*, *CLN5* and *CLN6* mRNA in CLN8 disease**

Using the CLN8 534 HF line, which exhibited the clearest cellular phenotypes of the CLN8 lines studied in this Chapter, and CLN8 535 HF the cell line with minimal cellular variability, a range of mRNA expression levels were measured by RT-qPCR (Figure 3.10). Gene expression changes have been previously reported in LSDs and neurodegenerative diseases and have the potential to highlight mechanisms of disease or even therapeutic targets (Dhami et al. 2006; Neueder and Bates 2014).

#### 3.4.7.1 TFEB mRNA expression

TFEB, the transcription factor that regulates the expression of all lysosomal genes, exhibited significantly lower levels of mRNA, which may mean lower levels of TFEB. This finding was surprising as one might expect an LSD or a lysosome-affected disease to have an increased level of TFEB to increase lysosomal production. For example, a study found *TFEB* to be significantly upregulated in Huntington's disease (Neueder and Bates 2014), a neurodegenerative disease with known lysosomal dysfunction (Cortes and La Spada 2014; Erie et al. 2015; Badell-Grau 2016). The CLN8 535 HF line exhibited the greatest reduction in *TFEB* expression, which may be possibly due to the lack of lysosomal network expansion; however, this is contradicted by the CLN8 534 line also having lower *TFEB* expression, which was previously found to have an increase lysosomal network.

#### 3.4.7.2 MTOR mRNA expression

Although *MTOR* displayed a trend to decrease mRNA expression in both CLN8 534 HF and CLN8 535 HF, this was not statistically significant (Figure 3.10). *MTOR* has been reported to regulate the subcellular distribution and activation of TFEB (Martina et al. 2012). Like with *TFEB*, *MTOR* expression is elevated in other neurodegenerative diseases (Koga et al. 2011; Neueder and Bates 2014). Nonetheless, as overall autophagy was not significantly increased in CLN8 (Figure 3.4), it would make sense that *MTOR* was not elevated in CLN8 disease.

#### 3.4.7.3 *MCOLN1* mRNA expression

Conversely, both CLN8 534 HF and CLN8 535 HF had significantly increased expression of *MCOLN1* (Figure 3.10). TRPML1, encoded by *MCOLN1*, is a lysosomal ion channel functioning on lysosomes and late endosomes (Gómez et al. 2018) outlined in Chapter 1. It would therefore be logical to assume that *MCOLN1* is elevated in an LSD which presents with lysosomal storage and expansion, particularly in CLN8 534 HF, which in this study was found to have an expanded lysosomal network (Figure 3.1).

Nevertheless, the observation of an increase in *MCOLN1* in CLN8 535 HF is noteworthy as the lysosomal area in the CLN8 535 HF line was not increased (Figure 3.1), suggesting the potential here for lysosomal  $\text{Ca}^{2+}$  signalling defects (Di Paola et al. 2018). Furthermore, both CLN8 534 HF and CLN8 535 HF had significantly lower *TFEB* expression, which has been shown to regulate the expression of *MCOLN1* (Di Paola et al. 2018; Gómez et al. 2018), making this contradiction in expression patterns something that merits further investigation, particularly with respect to the  $\text{Ca}^{2+}$  signalling properties of these cells which may independently mediate changes in *MCOLN1* expression.

#### 3.4.7.4 CLN5 & CLN6 mRNA expression

As outlined in the Chapter 1, CLN5 protein has been reported to interact with many other NCL proteins including CLN3, CLN2 and CLN8 (Lyly et al. 2009; Haddad et al. 2012). *CLN5* mRNA expression was differentially affected in CLN8 534 HF and CLN8 535 HF. There was a significant increase in *CLN5* mRNA expression in CLN8 534 HF (Figure 3.10); whereas, *CLN5* mRNA was significantly decreased in CLN8 535 HF (Figure 3.10).

*CLN6*, also a gene encoding a transmembrane protein associated with an NCL disease which has been recently reported to form a complex with CLN8 required for the maturation of many lysosomal enzymes (Bajaj et al. 2020), had significantly lower expression in CLN8 534 HF but significantly higher expression in CLN8 535 HF. This variability in *CLN6* and *CLN5* mRNA expression further highlights the difficulty in establishing consistent cellular phenotypes in CLN8. The disparity in these results may correlate with the variation seen in other phenotypes such as LysoTracker as CLN8 535 HF, which has higher *CLN6* mRNA, had no increase in LysoTracker; whereas, CLN8 534 HF which had lower *CLN6* mRNA expression, had increased LysoTracker.

Given issues with acquisition of CLN8 antibodies, it was not possible to investigate changes in CLN8 protein as such changes in mRNA expression were examined instead. Future work should examine if the changes in mRNA expression relate to changes in protein expression particularly with respect to the effect of dexamethasone treatment on CLN8 patient cell lysosomal expansion and other cellular phenotypes. CLN8 Western blotting could facilitate examination of whether increases in *CLN8*

mRNA following dexamethasone treatment translates to protein expression and leads to actual increases in potentially semi-functional mutant protein at the ER.

Induction of lysosomal production using trehalose to stimulate the transcription factor TFEB (Rusimini et al. 2019), the master regulator of lysosomal biogenesis, could also help determine if increasing lysosomal genes may also reduce cellular phenotype severity. TFEB domains have been investigated across the NCLs and none have been found in the *CLN8* gene, thus inducing TFEB may determine if it is solely the increase in *CLN8* that decreases severity.

### **3.4.8 Changes in lysosomal enzyme activity in CLN8**

#### 3.4.8.1 Variable changes in enzyme activity

In this project, 22 lysosomal enzymes (Figure 3.12 & Figures A7.1 – A 7.22) were assayed to identify enzymes affected across the *CLN8* patient cell lines. This work was initiated prior to the publication of di Ronza *et al.* (2018) but was extended following that report as it showed that *CLN8* acts as a chaperone for lysosomal enzyme maturation. In this project, defects in the activity of several lysosomal enzymes in *CLN8* patient fibroblasts were identified (Figure 3.12). The differences in enzyme activity, as with the other phenotypes explored in this project, were inconsistent between the different *CLN8* patient cell lines. For example, the activity of fucosidase, NAGA and PPT1 were significantly increased in *CLN8* 534 HF, whereas activity of these same enzymes was significantly decreased in *CLN8* 535 HF.

Moreover, fucosidase showed significantly decreased activity in *CLN8* 533 HF, and NAGA and PPT1 and fucosidase reduced activity in *CLN8* 462 HF. di Ronza *et al.* (2018), found that fucosidase, NAGA and PPT1 required *CLN8* for maturation, the results in this study on enzyme activity support their findings, but the effect of different *CLN8* mutations on enzyme activity suggests a much more complex picture regarding the outcomes in individual patients. Furthermore, some enzymes that require *CLN8* for maturation were only significantly affected in some *CLN8* patient cell lines. For example, cathepsin B has significantly increased activity only in *CLN8* 535 HF, but is decreased in the other *CLN8* HFs, despite needing *CLN8* for its transport from the ER

to the Golgi (di Ronza et al. 2018). These differences in enzyme activity between the patient cell lines further highlights the variability in CLN8 pathogenesis.

It may be the case that, since CLN8 transfers enzymes destined to the lysosome from the ER to the Golgi, different mutations will differentially affect this transport, thus producing different effects on enzymatic activity. The study that found the link between CLN8 and lysosomal enzyme maturation primarily investigated this link using CLN8 knockout cell lines; however, they explored the association of five different mutations in CLN8 with five lysosomal enzymes and confirmed that different mutations were differentially associated with these lysosomal enzymes. One of the mutations di Ronza *et al.* (2018) explored had no effect on the transport of these five lysosomal enzymes, highlighting the variable effects of different mutations on the transfer of lysosomal enzymes.

Nonetheless, Q194R and Y158C significantly affected the transport of several enzymes, including cathepsin D, PPT1 and TPP1. Two of these, cathepsin D and TPP1 were not significantly affected in the patient cell line with the Q194R (CLN8 533 HF) or the Y158C mutation (CLN8 535 HF). This may be because both of these are compound heterozygous cell lines and the other mutation does not affect transport of these enzymes, thus their activity was not significantly altered in the patient line. Additionally, di Ronza *et al.* (2018) showed using CLN8 constructs that the Q194R and Y158C, which are the mutations in CLN8 533 HF and CLN8 535 HF respectively, decreased association with cathepsin D, PPT1 and TPP1 by around 50%. It may be possible that changes in CLN8 protein expression that lead to higher levels of protein present, compensates for the decrease in association caused by these mutations. Thus, cycles or changes in CLN8 expression may decrease disease phenotypes which could lead to the effect of the mutation on the transport of these enzymes being variable in relation to CLN8 expression (Figure A7.1 – A.7.20). Unfortunately, the mutations in our other cell lines were not explored by di Ronza *et al.* (2018).

#### 3.4.8.2 Acid sphingomyelinase (ASM) enzyme activity

Remarkably, of the 22 lysosomal enzymes assayed, ASM was the only enzyme that was significantly decreased across all of the CLN8 patient cell lines. ASM was not one of the lysosomal enzymes identified to require CLN8 for maturation (di Ronza et al.

2018). A decrease in ASM activity has been associated with other LSDs such as Niemann-Pick disease type A (NPA) (Sutrina and Chen 1984). The reduction in ASM activity is seen across all CLN8 patient lines, and as such may present a valid strategy for future screening as well as a therapeutic target that may be of benefit to the treatment of CLN8 disease patients by treating with compounds that have been suggested to increase ASM activity such as arimocloamol (Kirkegaard et al. 2010) or cannabidiol (Burstein et al. 1984).

#### 3.4.8.3 Cathepsin B

Cathepsin B activity was significantly increased in CLN8 535 HF, whereas its activity was found to be decreased in CLN8 534 HF. Using the magic red assay, it was determined that this reduction in activity was not due to decreased presence of cathepsin B. The assay showed that there was an increase in the magic red staining area, indicating higher levels of cathepsin B. The increase in area does not, however, distinguish between pro- and active cathepsin B enzymes (Kirkham 2020). The decrease in cathepsin B activity and the increase in magic red staining suggests that there is an increase in the overall levels of cathepsin B but a decrease in its activity that may be due to pro-cathepsin not being activated.

#### 3.4.9 Changes in SERCA-mediated Ca<sup>2+</sup> release in CLN8

As outlined in Chapter 1 Ca<sup>2+</sup> defects have been reported in many LSDs including the CLN8<sup>mnd</sup> mouse (Kolikova et al. 2011) model making it an obvious phenotype to explore in CLN8 patient cells (Lloyd-Evans et al. 2008; Kolikova et al. 2011; Lloyd-Evans and Waller-Evans 2019). This study found that the CLN8 462 HF and CLN8 535 HF lines appeared to have a trend to lower ER Ca<sup>2+</sup> levels (Figure 3.6) but due to the low number of repeats there was no statistical significance. Further experiments are clearly necessary.

CLN8 534 HF displayed significantly higher ER Ca<sup>2+</sup> (Figure 3.6) which could equally be caused by or lead to problems with protein folding and cellular dysfunction given the importance of Ca<sup>2+</sup> regulation due to its role in cellular processes and signalling. The presence of mutant proteins that give rise to other LSDs such as NPC1 have been reported to cause to ER Ca<sup>2+</sup> defect (Korkotian et al. 1999; Pelled et al.

2003). Other studies have also reported ER-stress in CLN8 and have suggested they may be involved in the progression of CLN8 disease in central nervous system structures in the CLN8<sup>mn</sup> mouse model (Galizzi et al. 2011).

An example of the importance of ER Ca<sup>2+</sup> regulation is the calnexin/calreticulin folding cycle (Braakman and Hebert 2013), which has an important function in the folding of newly synthesised proteins and is also a Ca<sup>2+</sup>-dependent process. Therefore, changes in the levels of Ca<sup>2+</sup> in the ER will consequently have a detrimental effect on protein production. Misfolding of proteins can cause improper function or their retention in the ER, thus leading to loss or decreased function of those proteins (Braakman and Hebert 2013). Furthermore, ER Ca<sup>2+</sup> deregulation has been previously linked to storage materials in LSDs leading to the unfolded protein response (Tessitore et al. 2004; Sano et al. 2009).

There was no difference seen in further experiments of ER Ca<sup>2+</sup> using ionomycin or ryanodine. Ionomycin does not specifically release ER Ca<sup>2+</sup> alone, as it also results in mitochondrial, Golgi and early endosomal membranes to become permeable to Ca<sup>2+</sup> but not lysosomes due to their protective glycocalyx, and as such does not negate the differences seen previously with SERCA. Therefore, ionomycin may provide an idea of ER Ca<sup>2+</sup> but is not specific enough to draw conclusion and could indicate differences in other intracellular organelles such as mitochondria. The lack of difference seen when activating the ryanodine receptor (Figure 3.15) suggests that the previous difference seen in ER Ca<sup>2+</sup> may not be due to defects in the ryanodine receptor but could be caused instead by differences in IP<sub>3</sub> mediated ER Ca<sup>2+</sup> (Atakpa et al. 2018) release which was not explored as there was not enough time to test but should be explored in future.

Studies in Sandhoff disease, another LSD, have reported defects in SERCA Ca<sup>2+</sup> uptake due to ganglioside GM2 storage (Pelled et al. 2003). Therefore, accumulation of lipids affects the activity of SERCA which might be what leads to the increase in ER Ca<sup>2+</sup> levels seen in CLN8. Therefore, the lipid profiles being stored in CLN8 should be further explored; however, this is difficult to do in a disease that seems to display such high levels of variability. Further experiments should confirm if the defect in ER Ca<sup>2+</sup> levels seen is due to higher ER Ca<sup>2+</sup> content. These experiments can be carried out by using Fluo-5N (Kabbara and Allen 2001). Nonetheless, it is important to note that there may also be defects in other Ca<sup>2+</sup> stores which may be caused by the increase

in ER Ca<sup>2+</sup> levels, such as decreased lysosomal Ca<sup>2+</sup> discussed below in Sections 3.3.10.2 (Garrity et al. 2016).

### **3.4.10 Further phenotypes in CLN8 534 HF**

CLN8 534 HF was the only patient line that showed some consistent cellular phenotypes that could be potentially used in primary drug screening. As a result, some further cellular phenotypes were characterised in the CLN8 534 HF line in order to identify more cellular phenotypes that could be later used for drug screening and confirmation studies.

#### **3.4.10.1 Mitochondrial Ca<sup>2+</sup>**

The results showed that CCCP mediated mitochondrial Ca<sup>2+</sup> leak was significantly reduced in CLN8 534 HF, while antimycin/oligomycin mediated Ca<sup>2+</sup> leak was slightly elevated but not significantly. It is noteworthy that while CCCP induces mitochondrial Ca<sup>2+</sup> leak it has also been reported to facilitate Ca<sup>2+</sup> release from the Golgi by inhibiting Ca<sup>2+</sup> uptake into the Golgi mediated by the Ca<sup>2+</sup> pump PMR1 (Virk et al. 1985).

Conversely, as outlined in Chapter 2, addition of antimycin/oligomycin leads to a more specific mitochondrial Ca<sup>2+</sup> release. Therefore, the data in Figure 3.14 suggests that there is no change in CLN8 534 HF mitochondrial Ca<sup>2+</sup> levels but there may be a decrease in Ca<sup>2+</sup> in the Golgi. Nevertheless, this is one of the phenotypes seen in the CLN8 534 HF line that was identified as being more stable in comparison to the other phenotypes, and as such could potentially be used for drug screening efforts (Figure 5.12).

Figure 3.14 appear to show a potential delay in the mitochondrial Ca<sup>2+</sup> release in response to both CCCP and antimycin/oligomycin in CLN8 534 HF which may be worth exploring further as a potential phenotype of CLN8 cellular dysfunction.

#### **3.4.10.2 Lysosomal Ca<sup>2+</sup>**

CLN8 534 HF had a significant reduction in lysosomal Ca<sup>2+</sup> when compared to the control. A similar reduction in lysosomal Ca<sup>2+</sup> was seen in other LSDs (Figure 5.16)

and has been reported in the literature as a key pathogenic event in diseases such as NPC1 (Lloyd-Evans et al. 2008) and Alzheimer disease due to the loss of presenilin 1 function (Lee et al. 2015). Therefore, this finding provides some insight into the pathogenesis of CLN8 but also provides possible therapeutic targets for disease states similar to that of the CLN8 534 HF line.

The reduction in lysosomal  $\text{Ca}^{2+}$  along with the increase in ER  $\text{Ca}^{2+}$ , discussed above in Section 3.4.9, may indicate that there are defects in ER-lysosomal contact points as these contact points have been reported to be important in maintaining lysosomal  $\text{Ca}^{2+}$  levels by transporting  $\text{Ca}^{2+}$  for the ER into the lysosome (Atakpa et al. 2018). Therefore, the defects in lysosomal  $\text{Ca}^{2+}$  and ER  $\text{Ca}^{2+}$  may be due to a defect in the ability of the ER to transport  $\text{Ca}^{2+}$  into the lysosome via these contact points. Furthermore, CLN8 has been suggested to interact with VAPA, a protein that is involved in the ER-lysosomal contact point (Passantino et al. 2013) further suggesting that CLN8 dysfunction might affect the transfer of  $\text{Ca}^{2+}$  between the ER and the lysosome. As the transfer of  $\text{Ca}^{2+}$  from the ER to the lysosome has been reported to be via the  $\text{IP}_3$  receptor, future experiments should therefore explore defects in  $\text{IP}_3$  mediated  $\text{Ca}^{2+}$  signalling as suggested in Section 3.4.9.

### **3.5 Conclusion**

There was a high degree of variability in cellular phenotypes across the phenotyping experiments. This unfortunately means that although there were significant phenotypes identified, some are too variable for drug screening. This would render efforts at high throughput screening more expensive (due to the necessity of high repeat numbers, while drug screens are often  $N = 1$ ) and less robust since a greater number of phenotypes used for drug confirmation in secondary screens equates to a higher likelihood of efficacy and success in later clinical stages (Szabo et al. 2017).

Nevertheless, some phenotypes were identified in CLN8 534 HF that could be utilised for drug screening and confirmation to potentially identify drug therapies. This is further explored in Chapter 5. This patient cell line could therefore be used for primary identification of drugs as it has some cellular phenotypes that can be measured to identify potential CLN8 therapies. Although, it should be pointed out that

the considerable variation in phenotypes across patient cells would suggest that a therapy that works for one may not work for all.

Clearly, a different strategy may be required for treating CLN8 disease, perhaps one of drug repurposing. Focus areas could include enzyme chaperones to replace the loss of function of CLN8 protein, or inhibitors of proteostasis (Mu et al. 2009) to prevent clearance of mutant CLN8 protein, or activators of transcription to increase mutant CLN8 protein expression such as Histone deacetylases (HDAC) inhibitors (Maceyka et al. 2014).

In this study, we provide further evidence that mutations in CLN8 affect the activity of several lysosomal enzymes. Moreover, this report provides evidence that different mutations in CLN8 affect lysosomal enzyme activity differently. This project, however, is the first to suggest that changes in CLN8 expression in patient cell lines leads to differences in the severity of CLN8 cellular phenotypes, including the effect of the mutations on the transport of lysosomal enzyme. These data suggest that increasing CLN8 expression, as was done in this Chapter experimentally with dexamethasone may be an appropriate therapeutic strategy for this disease.

Additionally, enzymes that could be used for drug screening in CLN8 disease were identified. The activity of the enzyme ASM is reduced in all CLN8 patient fibroblasts, confirming this as a potential therapeutic target of benefit to all CLN8 patients, despite the variability between them. Changes in CLN8 expression may explain the variation seen in CLN8 cellular phenotypes. The regulation of these changes, the pattern behind them and their effect on cellular phenotypes still remain unclear. This is, however, the first report of potential cycles in cellular phenotypic severity.

# **Chapter 4: Developing a drug screening protocol for lysosomal storage diseases**

## **4.1 Introduction**

The high degree of variability seen in CLN8 patient fibroblasts complicates their implementation in drug screening. Nonetheless, as this is an orphan life limiting disease there is an ethical and moral imperative to develop methods for drug screening compounds that may be of benefit to CLN8 disease, other LSDs and possibly further diseases with similar pathogenesis. Overall, although, there are a wide number of different LSDs many of them share common cellular phenotypes (Cox and Cachón-González 2012; Platt et al. 2012) with some examples outlined in Table 4.1. Identifying therapies that may benefit a wide range of common cellular pathologies in LSDs, a robust cell model of a well characterised LSD should be used.

Furthermore, cells and cellular models have been extensively used in drug screening (Silverman et al. 1998; Huang et al. 2012; Xu et al. 2014). Most drug compounds are identified in cells highlighting the importance of having a robust cellular model (Geng et al. 2011; Chandrachud et al. 2015; Jang et al. 2016). Nonetheless, many drug screen approaches for LSDs have not gone to clinic. Therefore, developing a more robust and appropriate drug screen that may lead to the identification of compounds beneficial to several LSDs is needed, and thus is explored in this Chapter.

### **4.1.1 NPC1 disease**

Niemann-Pick disease type C1 (NPC1) is a childhood neurodegenerative LSD caused by mutation in the NPC1 protein (Lloyd-Evans et al. 2008). NPC1 disease is characterised by lysosomal accumulation of cholesterol, sphingosine, sphingomyelin, ganglioside GM1, lyso-(bis)-phosphatidic acid (LBPA) and other materials. Lysosomal  $Ca^{2+}$  signalling and endo-lysosomal trafficking defects are also an important part of NPC1 disease pathogenesis (te Vrugte et al. 2004; Lloyd-Evans and Waller-Evans 2019).

NPC1 disease is caused by the loss-of-function mutation in the *NPC1* gene which encodes for a lysosomal transmembrane protein (Vanier 2010). The NPC1 protein is believed to transport sphingosine, cholesterol and potentially other substrates across lysosomal membranes (Malathi et al. 2004; Ioannou 2005; Lloyd-Evans et al. 2008). Like with other LSDs, NPC1 patients exhibit neurodegeneration, motor dysfunction, progressive dementia and seizures (Vanier 2010; Salsano et al. 2012). Cellular phenotypes include lysosomal expansion, lipid storage, endo-lysosomal defects and lysosomal Ca<sup>2+</sup> homeostasis defects which are common across several LSDs (Table 4.1).

**Table 4.1: Examples of common cellular phenotypes in LSDs.** Outlined examples of altered cellular mechanisms across LSDs (Lloyd-Evans and Platt 2011; Haslett 2015; Lloyd-Evans and Haslett 2016; Lloyd-Evans and Waller-Evans 2019).

Phenotype	Description	Examples of LSDs with these phenotypes	References
Expanded lysosomal system	Lysosomal volume and number are increased in LSDs	NPC1, CLN2, CLN3, CLN5, NPA, Fabry...	(Lachmann et al. 2004; Xu et al. 2014; Mukherjee et al. 2019)
Lipid accumulation (cholesterol, gangliosides, sphingolipids and others)	Lipids accumulate and are mislocalised in LSDs.	NPC1, Gaucher, CLN2, CLN5, CLN8, Pompe...	(te Vruchte et al. 2004; Hermansson et al. 2005; Aerts et al. 2008; Schulze and Sandhoff 2011; Platt et al. 2012; Kim and kim 2014)
Ca <sup>2+</sup> stress	Ca <sup>2+</sup> levels in organelles such as ER, lysosome and mitochondria are altered in LSDs.	NPC1, CLN5, Sandhoff, Gaucher, CLN8, CLN3...	(Korkotian et al. 1999; Pelled et al. 2003; Lloyd-Evans et al. 2008; Kolikova et al. 2011; Lloyd-Evans and Platt 2011; Chandrachud et al. 2015)
Autophagy defects	Many LSDs have defects in the autophagic system and autophagic vacuole accumulation.	NPC1, NPC2, CLN3, CLN5, CLN6, CLN8...	(Xu et al. 2010; Thelen et al. 2012; Passantino et al. 2013; Chandrachud et al. 2015; Shipley 2019)
ER stress	ER stress has been reported in LSDs, particularly in one with ganglioside GM1 storage	NPC1, GM1 gangliosidosis, CLN1, CLN3, CLN8	(Kim et al. 2006a; Sano et al. 2009; Galizzi et al. 2011; Klein et al. 2011; Wu et al. 2014)
Endocytosis	Defects in endocytosis and endo-lysosomal trafficking has been reported in many LSDs	NPC1, Pompe, NPA, CLN2, CLN3	(Lachmann et al. 2004; Fukuda et al. 2006; Ballabio and Gieselmann 2009; Mukherjee et al. 2019)
Mitochondrial dysfunction	Defects in mitochondrial function and mitochondrial due to lysosomal dysfunction	NPC1, Gaucher, ML IV, Cystinosis, CLN3, CLN8	(Jolly et al. 2002; Jennings Jr et al. 2006; Luiro et al. 2006; Sansanwal et al. 2010; de la Mata et al. 2016; Wos et al. 2016)

NPC1 dysfunction has been reported in several LSDs and even other neurodegenerative diseases such as Huntington's disease (Schweitzer et al. 2009). Additionally, the cellular aspects of NPC1 disease has already been widely characterised, meaning that cellular phenotypes are well known and broadly understood (Millard et al. 2000; Ioannou 2005; Tamura et al. 2007; Lloyd-Evans et al. 2008; Kwon et al. 2009; Lloyd-Evans and Platt 2011; Maue et al. 2012; Sztolsztener et al. 2012; Gong et al. 2016; Zhao et al. 2016). Furthermore, one factor that makes NPC1 an attractive option for drug screening is that the cascade of disease events is known, with sphingosine first being affected followed by  $Ca^{2+}$ , then endo-lysosomal trafficking defects and so on (Lloyd-Evans and Platt 2011). Therefore, NPC1 is a suitable choice for large drug screening to identify small molecules that may be of benefit to NPC1 disease and other LSDs.

Additionally, drugs that have been identified as beneficial for NPC1 have subsequently been reported to also be of benefit to other lysosomal storage diseases such as miglustat for Gaucher and Sandhoff disease (Cox et al. 2000; Tallaksen and Berg 2009) and arimoclomol for Fabry disease and Sandhoff disease (Kirkegaard et al. 2010; Kirkegaard et al. 2016). Characterising a fast-growing cell line such as *Npc1*<sup>-/-</sup> knockout cells, to determine if it has robust NPC1 phenotypes (Table 4.2) would provide a model that can then be used for drug screening of a large number of small molecules.

A fast growing *Npc1*<sup>-/-</sup> glia model was partly characterised and previously used in NPC1 disease publication (Lloyd-Evans et al. 2008). The presence of some NPC1 phenotypes in these *Npc1*<sup>-/-</sup> glia had already been confirmed before this study including sphingomyelin accumulation, sphingosine trafficking, lysosomal  $Ca^{2+}$  defects and oxidative stress. Therefore, this study further confirms the presence of NPC1 phenotypes in these *Npc1*<sup>-/-</sup> glia to characterise a possible fast-growing cell model that can be used for drug screening for LSDs. Furthermore, glia cells have been previously used as a powerful tool for disease modelling and drug screening (Griffin et al. 2020).

**Table 4.2: Outline of the cell lines used in Chapter 4.**

Cell line	Description	Mutation
<i>Npc1</i> <sup>+/+</sup> glia	<i>Apparently healthy control glia cell line</i>	N/A
<i>Npc1</i> <sup>-/-</sup> glia	<i>Npc1 knockout glia cell line</i>	<i>Npc1</i> <sup>-/-</sup>
Control 1 HF	<i>Apparently healthy control 1 (GM05399) cell line</i>	N/A
NPC1 HF	<i>NPC1 patient (GM03123) cell line</i>	I1061T/P23S

### 4.1.2 Cellular drug screening

Cellular phenotypes provide an unbiased set-up for drug discovery through identification of new targets and pathways that may be therapeutically important (Chandrachud et al. 2015; Szabo et al. 2017). Additionally, using multiple phenotypes in the drug discovery process increases the possibility of identification and translation of clinical therapies. Understanding and using cellular phenotypes for drug screening for LSDs permits tailor-made identification of drugs by specifically targeting cellular dysfunction in LSDs, allowing therapies to be found for this unmet medical need (Szabo et al. 2017). Nonetheless, if the screen is not designed appropriately, compounds that may be of benefit to a disease could be missed; for example, in NPC1 drug screens that focused on cholesterol as the phenotype being screened which led to miglustat, the only approved therapy for NPC1, not coming up as a drug hit (Yu et al. 2014). This further highlights the importance of carefully selecting the type of drug screen that is most robust for the disease being explored.

### 4.1.3 Chapter aims

This chapter aimed to characterise the cellular phenotypes of a NPC1 disease glia cell line (Table 4.1) that may be used for drug screening and further confirmation studies. Additionally, in this chapter the assays that could be used for LSDs drug screening are outlined. These were ascertained by confirming the presence of NPC1 cellular phenotypes in *Npc1*<sup>-/-</sup> glia, such as organelle expansion and morphological changes (Figure 4.1 – 4.4) and demonstrating the appropriate assays that may be used once the cell line was confirmed as an NPC1 model.

## **4.2 Summary of Methods**

To confirm NPC1 cellular phenotypes in the *Npc1*<sup>-/-</sup> glia, lysosomal area was determined using LysoTracker (Section 2.3.2), Ganglioside GM1 levels were explored using cholera toxin B subunit with a FITC tag (CtxB-FITC), autophagic vacuoles were examined using CytolD green (Sections 2.3.4) and ER stress was investigated using ER-Tracker green (Section 2.3.5).

The effects of miglustat treatment on cholesterol storage and lysosomal volume was done by incubating glia cells with 50 µM miglustat for 24 hours or 7 days (Section 2.1.3). Treated cells were then stained with the auto-fluorescent antibiotic filipin (Section 2.2.3) which in this case was done using a plate assay by seeding 60,000 cells per wells before fixation and staining with filipin. Similarly, lysosomal volume in treated cells was carried out using a LysoTracker plate assay (Section 2.3.3).

Different methods of standardising the lysosomal plate assay (Section 2.3.3) were examined by looking at either dividing the LysoTracker reading by the nuclear stain Hoechst 33342 (Section 2.2.5) or seeding equal cells numbers in at least 4 wells per cell line per N (Section 2.3.3).

To examine the effects of different concentration of arimoclomol on lysosomal storage cells treated with arimoclomol (Section 2.1.3) were examined using LysoTracker signalling with the LysoTracker plate assay (Sections 2.3.3.). Similarly, the screen for arimoclomol-like compounds was carried out by treating cells with the compounds (Sections 2.1.3) before carrying out the LysoTracker plate assay on the treated cells (Sections 2.3.3) with arimoclomol treated cells included as a control. The arimoclomol treated cell was an important internal control as these screens were not all done at once but across many weeks due to the number of compounds being screened.

The effects of arimoclomol treatment on the cholesterol defects in the *Npc1*<sup>-/-</sup> glia cells and the NPC1 HF cells were done by using filipin (Section 2.2.3) on fixed cells having been treated with 200 µM arimoclomol for three days (Section 2.1.4). Patient cells were used as they have a critical mutation that may potentially mean that greater arimoclomol effect may be observed due to the fact that arimoclomol is proposed to act as a NPC1 chaperone for the I1061T mutation (Table 4.2). To confirm the effects

of arimoclomol on heat shock protein 70 (HSP70) localisation and levels, cells were treated with 200  $\mu$ M arimoclomol for three days (Section 2.1.4), fixed, and stained with HSP70 antibody (Section 2.2.4)

The staining performed in Section 4.3.1 – 4.3.4, 4.3.6 & 4.3.9 – 4.3.11 were imaged using the inverted Colibri widefield fluorescence microscope (Section 2.4.1) and analysed using Image J (Section 2.4.2).

## **4.3 Results**

### **4.3.1 Lysosomal expansion in *Npc1*<sup>-/-</sup> glia**

The first phenotype validated in *Npc1*<sup>-/-</sup> glia was an increase in lysosomal volume and accumulation which indicated storage of materials in the lysosome. *Npc1*<sup>-/-</sup> glia have a significantly greater area of lysosomal staining compared to the *Npc1*<sup>+/+</sup> glia, indicative of an expanded lysosomal system (Figure 4.1 A & B). The significant increase in lysosomal staining in *Npc1*<sup>-/-</sup> glia was also observed by LysoTracker plate assay (Figure 4.1 C). The LysoTracker plate assay facilitates a possible high-throughput method for drug screening of compounds against this cellular phenotype. These findings all ratify an increase in lysosomal accumulation and expansion in *Npc1*<sup>-/-</sup> glia (Figure 4.1) as has been shown before (Lachmann et al. 2004).

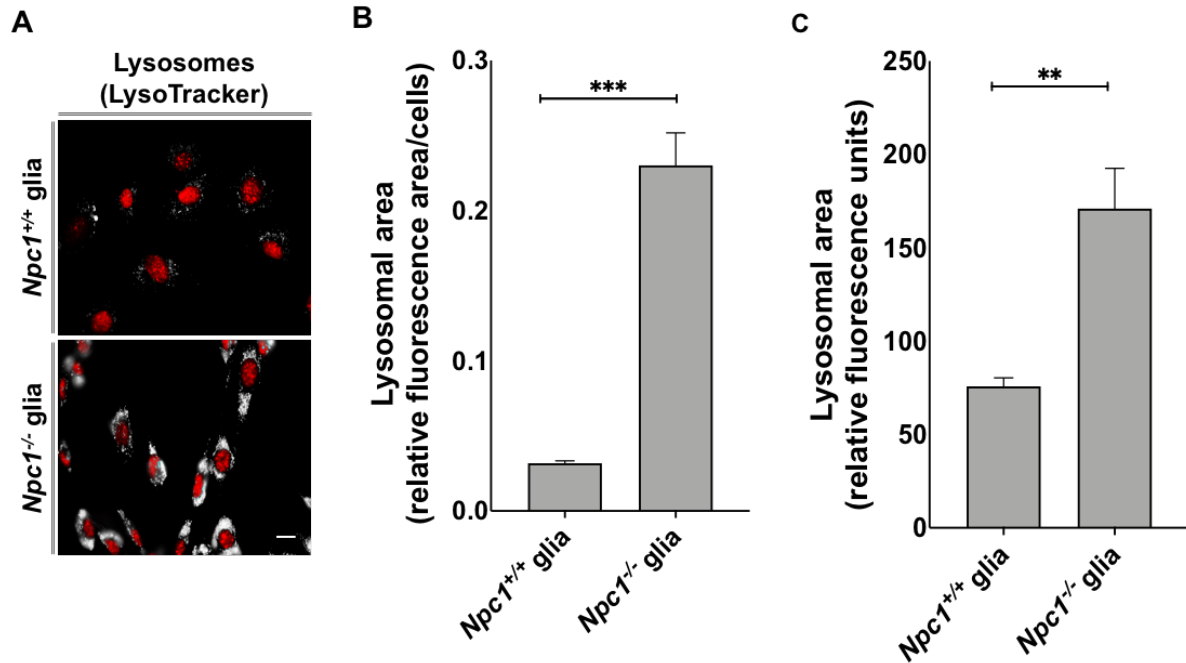


**Figure 4.1: Lysosomal area is increased in *Npc1*<sup>-/-</sup> glia.** **A:** Representative images of lysosomal staining (LysoTracker) quantified in **B** with Hoescht 33342 nuclear counter stain pseudo coloured red. Scale bar = 10  $\mu$ m. **B:** Quantitative analysis of lysosomal area in *Npc1*<sup>+/+</sup> and *Npc1*<sup>-/-</sup> glia from **A**. The graphs are from N = 1 and the error bars indicate SEM. **C:** Quantitative plate reader data of *Npc1*<sup>+/+</sup> glia and *Npc1*<sup>-/-</sup> glia stained with LysoTracker. The graph was made from N = 5. The error bars indicating SEM. \*\*p  $\leq$  0.01, \*\*\*p  $\leq$  0.001, two tailed t-test.

#### 4.3.2 Ganglioside GM1 accumulation in *Npc1*<sup>-/-</sup> glia

A standard cellular phenotype of NPC1 disease is the mis-trafficking and lysosomal accumulation of lipids, such as ganglioside GM1 (Sugimoto et al. 2001; Trushina et al. 2006; Blank et al. 2007). Use of the ganglioside GM1-specific stain CtxB-FITC fixed showed a significant increase in ganglioside GM1 in the *Npc1*<sup>-/-</sup> glia (Figure 4.2). This is indicative of accumulation of ganglioside GM1 in the *Npc1*<sup>-/-</sup> glia which suggests endo-lysosomal trafficking defects or altered enzyme activity that causes ganglioside GM1 to accumulate in lysosomes (Lachmann et al. 2004).

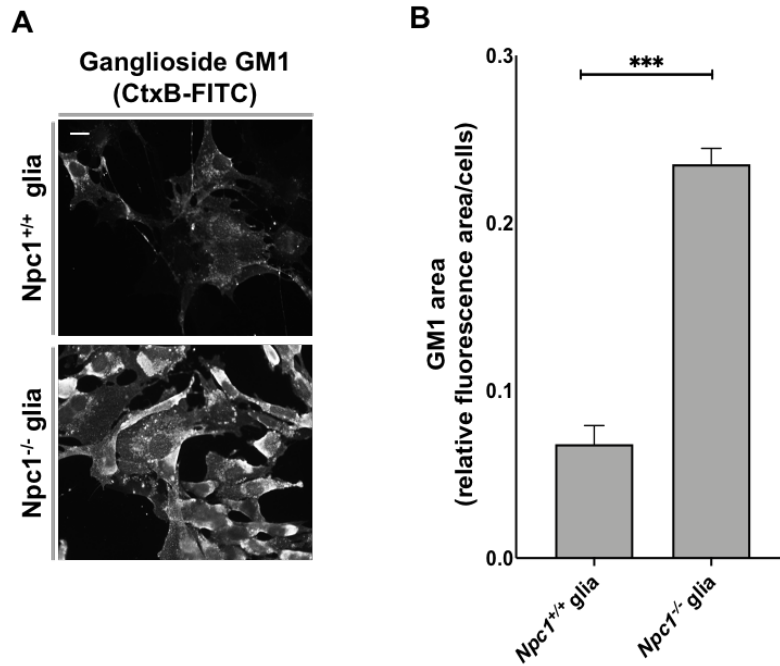


**Figure 4.2: Ganglioside GM1 is increased in *Npc1*<sup>-/-</sup> glia.** **A:** Representative images of ganglioside GM1 (CtxB-FITC) quantified in **B**. Scale bar = 10  $\mu$ m. **B:** Quantitative analysis of GM1 ganglioside staining area in *Npc1*<sup>+/+</sup> glia and *Npc1*<sup>-/-</sup> glia. The graph represents data from N = 3. The error bars indicate SEM. \*\*\*p  $\leq$  0.001, two tailed t-test.

#### 4.3.3 Autophagic vesicle accumulation in *Npc1*<sup>-/-</sup> glia

Autophagic vacuole accumulation is not only an NPC1 disease phenotype but has been seen in other LSDs such as CLN8 534 HF as shown in Chapter 3 and reported in the literature (Martinez-Vicente et al. 2010; Jing and Lim 2012; Passantino et al. 2013; Boland et al. 2018). Therefore, to confirm the presence of autophagic vacuole accumulation in *Npc1*<sup>-/-</sup> glia, Cyto-ID green was used to visualise autophagic compartments. A significant increase in Cyto-ID staining was observed in *Npc1*<sup>-/-</sup> glia compared to the *Npc1*<sup>+/+</sup> glia, indicative of increased levels of autophagy caused by either increased production or reduced clearance (Figure 4.2).

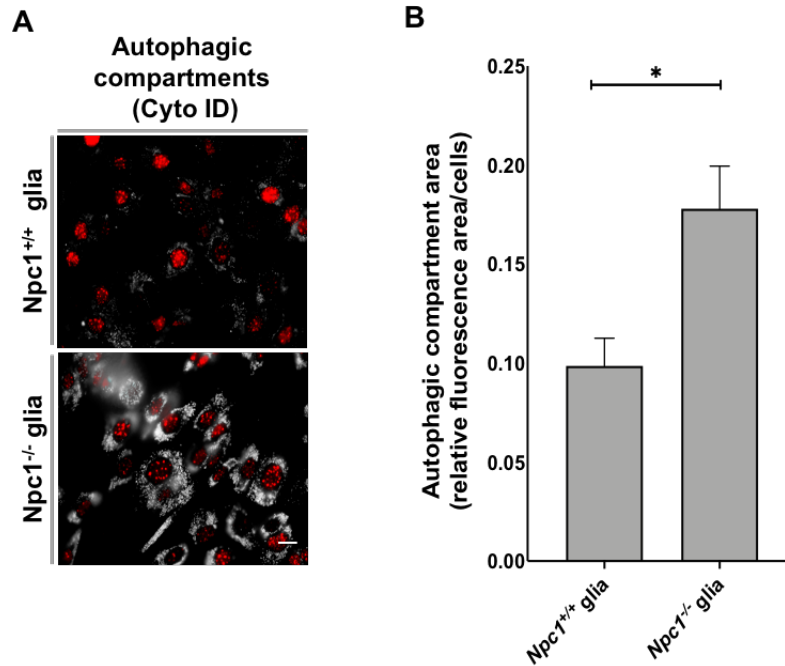


**Figure 4.3: Autophagic compartments are increased in *Npc1*<sup>-/-</sup> glia.** **A:** Representative images of autophagic compartments (Cyto-ID) quantified in **B** with a Hoescht 33342 nuclear counter stain pseudo coloured red. Scale bar = 10  $\mu$ m. **B:** Quantitative analysis of autophagic compartment area in *Npc1*<sup>+/+</sup> glia and *Npc1*<sup>-/-</sup> glia. The graphs represent data from N = 3. The error bars indicate SEM. \* $p \leq 0.05$ , two tailed t-test.

#### 4.3.4 ER stress in *Npc1*<sup>-/-</sup> glia

The last phenotype to be confirmed in *Npc1*<sup>-/-</sup> glia was the presence of ER stress since the elevation of ER stress has been previously reported in NPC1 disease (Klein et al. 2011). Using ER-Tracker, a significant increase in ER staining area was observed (Figure 4.4) indicating a denser ER structure which may be a result of increased ER stress and providing another phenotype for drug screening.

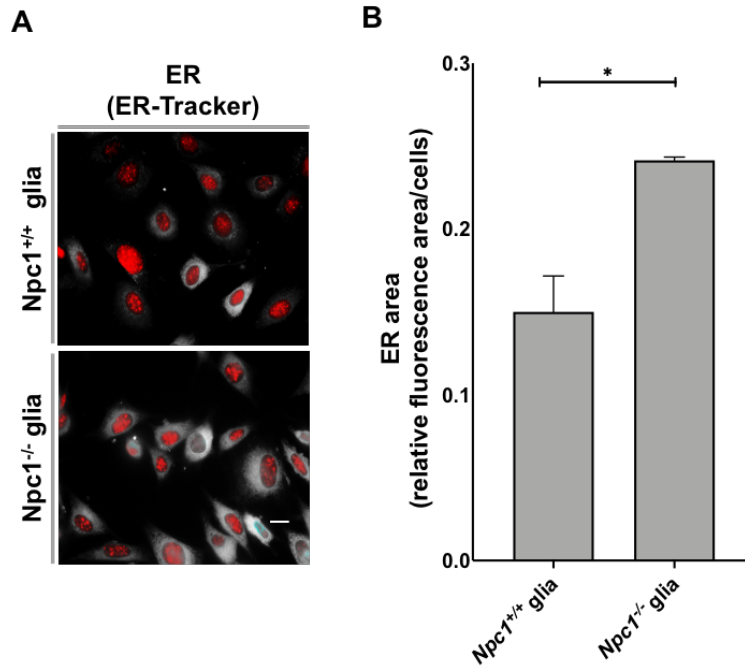


**Figure 4.4: Endoplasmic reticulum area is increased in *Npc1*<sup>-/-</sup> glia.** **A:** Representative images of ER staining (ER-Tracker) quantified in **B** with a Hoescht33342 nuclear counter stain pseudo coloured red. Scale bar = 10  $\mu$ m. **B:** Quantitative analysis of ER area in *Npc1*<sup>+/+</sup> glia and *Npc1*<sup>-/-</sup> glia. The graphs represent data from N = 3. The error bars indicate SEM. \* $p \leq 0.05$ , two tailed t-test.

#### 4.3.5 Choosing the most appropriate phenotype for a successful drug screen

When designing a drug screening assay, the selection of a rapid assay and robust phenotype is paramount. *Npc1*<sup>-/-</sup> glia have a clear and robust lysosomal expansion phenotype that can be measured using LysoTracker plate assays (Figure 4.1). Miglustat is currently the only approved therapy for NPC1 disease and is known to decrease lysosomal storage and reduce lysotracker fluorescence in NPC1 patient peripheral blood B cells (Lachmann et al. 2004). Previous studies have reported lipid storage was found to decrease in NPC1 cells after 5 days treatment with miglustat (te Vruchte et al. 2004). In this Chapter, however, the LysoTracker plate assay showed decreased lysosomal accumulation in *Npc1*<sup>-/-</sup> glia following 50  $\mu$ M miglustat treatment for 3 days (Figure 4.5). On the other hand, the Filipin plate assay which measures cholesterol levels does not highlight any alteration in cholesterol accumulation in NPC1 following treatment with miglustat (Figure 4.5). These results confirm previous reports that miglustat treatment does not reduce cholesterol levels biochemically further indicating that this may not be the most appropriate phenotype for drug screening (te Vruchte et al. 2004; Yu et al. 2014).

Overall lysosomal volume provides a great overview of lysosomal storage and lysosomal dysfunction, as such drug screening against lysosomal volume was chosen as it can identify compounds that may be of benefit to lysosomal storage and potentially benefit not only cellular function but also disease progression and severity as seen with miglustat in NPC1 (Lachmann et al. 2004; Patterson et al. 2007; Ficioglu 2008; Stein et al. 2012).

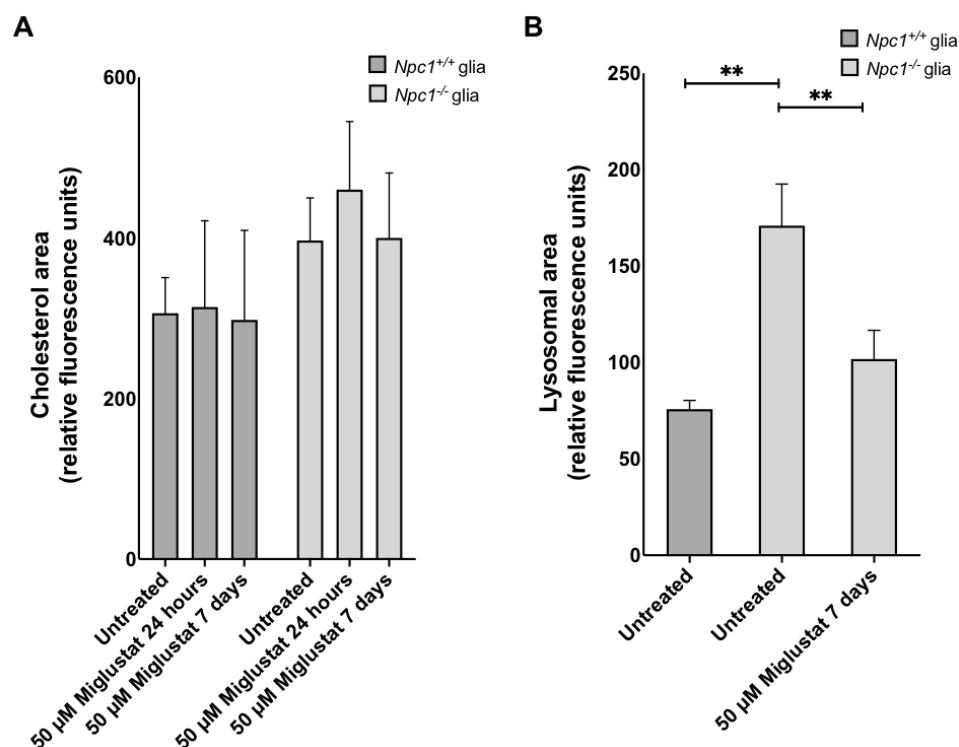


**Figure 4.5: Miglustat treatment has no effect on cholesterol storage but does affect lysosomal volume. A:** Cholesterol plate assay (Filipin) in *Npc1<sup>+/+</sup>* and *Npc1<sup>-/-</sup>* glia treated with 50  $\mu$ M Miglustat for 24 hours or 7 days. The graph represents data from 4 technical repeats and error bars indicate SEM. **B:** Lysosomal plate assay (LysoTracker) in *Npc1<sup>+/+</sup>* and *Npc1<sup>-/-</sup>* glia treated with 50  $\mu$ M Miglustat for 7 days. The graph represents data from N = 5. The error bars represent SEM.

#### 4.3.6 Choosing an appropriate standardisation method

Alongside selecting the robust and appropriate phenotypes to carry out a drug screen, the correct design of assays is critical including the standardisation of that method. For example, many genetic experiments often use housekeeping genes as a standard; however, the expression of these may be affected in LSDs (Vallim et al. 2019; Brokowska et al. 2020) making them an inappropriate standard.

When using the LysoTracker plate assay in order to make sure the assay is robust different methods for standardising between different samples in the assay were tested. Here nuclear staining as a standardisation method was tested. Nuclear staining across LSDs, using the DNA binding stain Hoechst, was observed to be variable (Figure 4.6 A). This inconsistency in nuclear staining was also observed in glia cells (Figure 4.6 B). When standardising against nuclear staining in the plate, however, the results showed no increase in lysosomal volume in NPC1 (Fig. 4.6C) compared to the control. This result observed, demonstrates that the use of the nuclear stain as a standardisation method in the LysoTracker plate assay is not appropriate as the increase in nuclear staining in NPC1 leads to the lysosomal phenotype being missed.

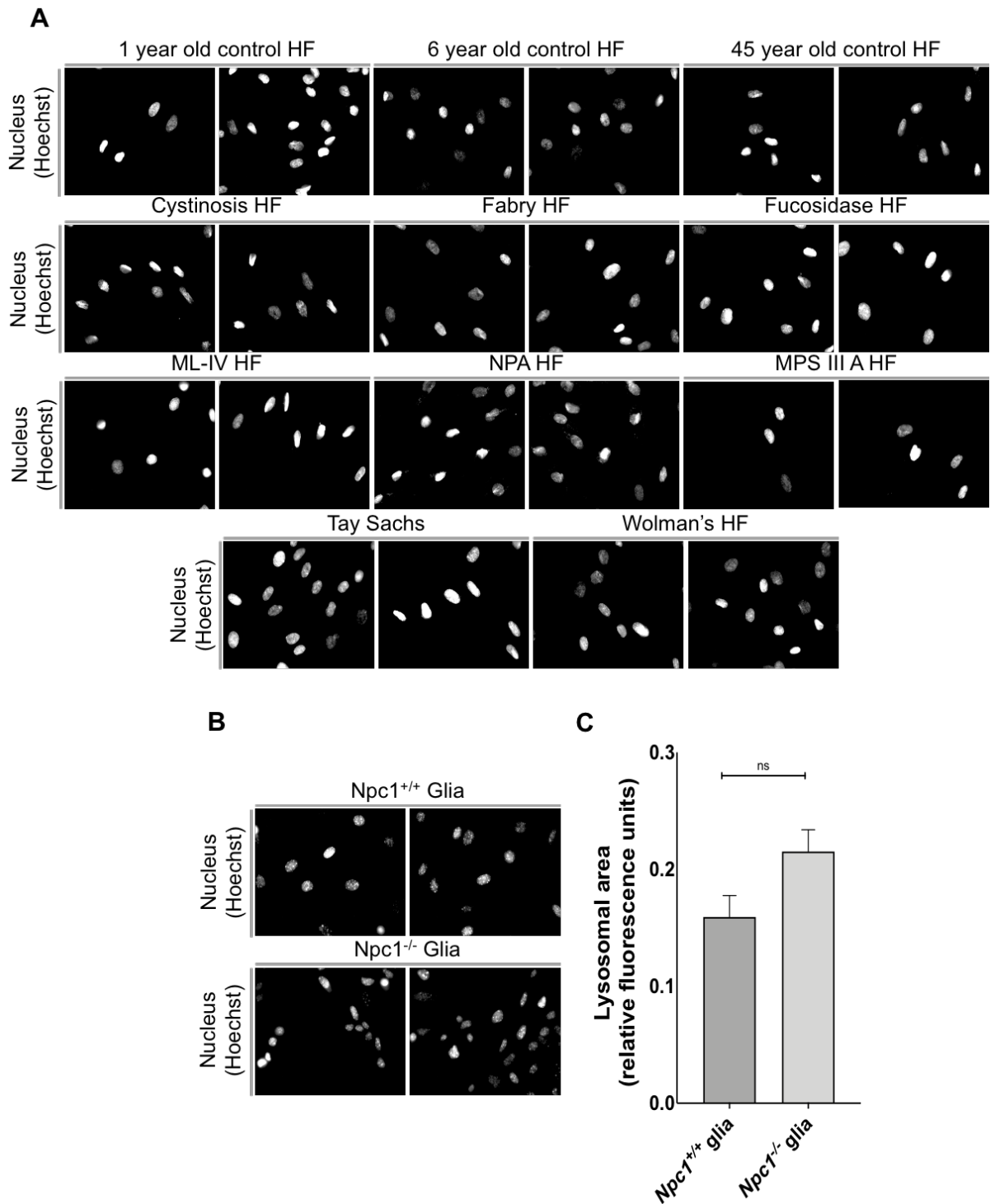


**Figure 4.6: Nuclear staining is variable across LSDs.** **A:** Nuclear staining (Hoechst33342) across *Npc1*<sup>+/+</sup> and LSDs patient HF cell lines. **B:** Nuclear staining (Hoechst staining) in *Npc1*<sup>+/+</sup> and *Npc1*<sup>-/-</sup> Glia cell lines. **C:** Lysosomal plate assay (LysoTracker) in *Npc1*<sup>+/+</sup> and *Npc1*<sup>-/-</sup> glia standardised to nuclear staining. The graph was made from data from N = 5. The error bars indicate SEM.

It was clear that nuclear staining could not be used to standardise lysosomal staining in drug screens. Consequently, cell number was tested as a standardisation method in LysoTracker plate assays (Figure 4.7.). Different cell numbers were plated on the LysoTracker plate assay to determine which would be most appropriate for drug screening. As cell number increases, so does the level of fluorescence seen in the LysoTracker plate assay (Figure 4.7). In order to avoid oversaturation of cells along with the fact that the greatest statistical difference between *Npc1*<sup>-/-</sup> and *Npc1*<sup>+/+</sup> was first seen at 60,000 cells meant that 60,000 cells were chosen as the optimal cell number to use when standardising against cell number.

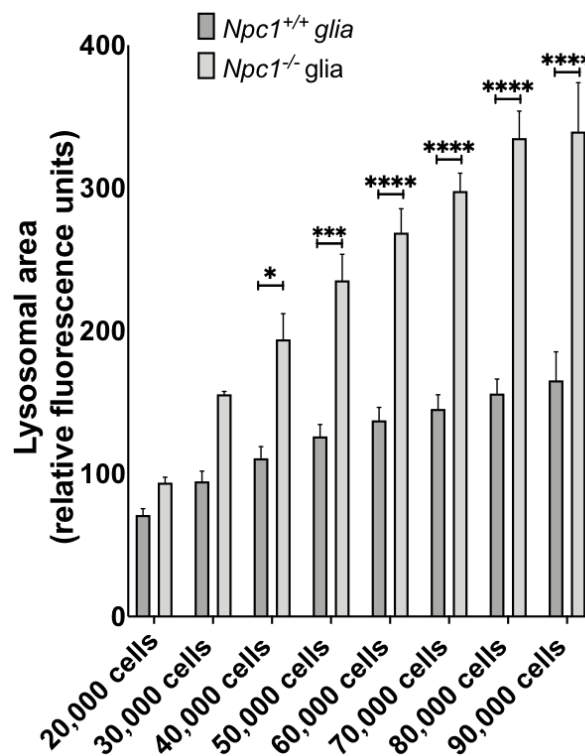


**Figure 4.7: Lysosomal 96-well plate assay comparing different cell seeding densities in *Npc1*<sup>+/+</sup> and *Npc1*<sup>-/-</sup>.** Lysosomal plate assay (LysoTracker) in *Npc1*<sup>+/+</sup> and *Npc1*<sup>-/-</sup> glia. The graph represents data from N = 5. The error bars indicate SEM. \*p ≤ 0.05, \*\*p ≤ 0.01, \*\*\*p ≤ 0.001, \*\*\*\*p ≤ 0.0001, two-way ANOVA with post-hoc Tukey.

#### 4.3.7 Determining the working concentration of arimocloamol for NPC1

It is also important to understand the working concentration of the drugs being screened. Arimocloamol is a drug that has been previously reported to be beneficial for LSDs such as NPC1, Gaucher disease and other neurodegenerative diseases

(Ingemann and Kirkegaard 2014; Kirkegaard et al. 2016; Fog et al. 2018; Penke et al. 2018; Shukla and Tekwani 2020). Therefore, the LysoTracker plate assay was optimised for a screen of arimoclomol-like compounds.

When determining the correct concentration of arimoclomol and arimoclomol-like compounds to use in a cellular screen, a range of concentrations of arimoclomol and its effects on lysotracker fluorescence in *Npc1<sup>-/-</sup>* glia was first tested. A tri-phasic response was seen where only 200  $\mu$ M arimoclomol significantly reduced lysosomal volume (Figure 4.8). The reduction in lysosomal volume was not observed at lower (50  $\mu$ M & 100  $\mu$ M) or higher (400  $\mu$ M & 800  $\mu$ M) concentrations of arimoclomol (Figure 4.8). These results indicate that 200  $\mu$ M arimoclomol is the most appropriate concentration for use in screening of arimoclomol-like compounds.

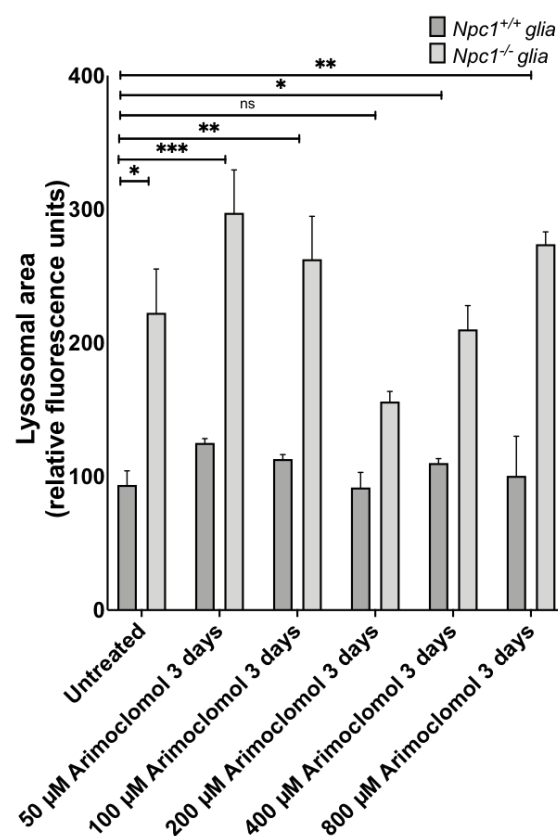


**Figure 4.8: Arimoclomol treatment decreases lysosomal volume at one concentration but not others in *Npc1<sup>-/-</sup>* and *Npc1<sup>+/+</sup>* glia cells.** Lysosomal plate assay (LysoTracker) in *Npc1<sup>+/+</sup>* and *Npc1<sup>-/-</sup>* glia treated with different concentrations of arimoclomol. The graph represents data from N = 3. \*p  $\leq$  0.05, \*\*p  $\leq$  0.01, \*\*\*p  $\leq$  0.001, two-way ANOVA with post-hoc Tukey.

#### 4.3.8 Cholesterol levels following arimoclomol treatment in *Npc1*<sup>-/-</sup> glia

To explore the effect of arimoclomol on cholesterol accumulation in NPC1, the main storage component in NPC1 disease, the levels of cholesterol were examined with the autofluorescent antibiotic filipin in cells treated with 200  $\mu$ M arimoclomol for 3 days. In untreated *Npc1*<sup>-/-</sup> glia there is typically a presence of punctate filipin positive endosomes and lysosomes which indicates cholesterol storage with a ~3-fold increase when measured by plate reader (Figure 4.9 B). Arimoclomol treatment has had no impact on the levels or localisation of the cholesterol storage in *Npc1*<sup>-/-</sup> glia (Figure 4.10).

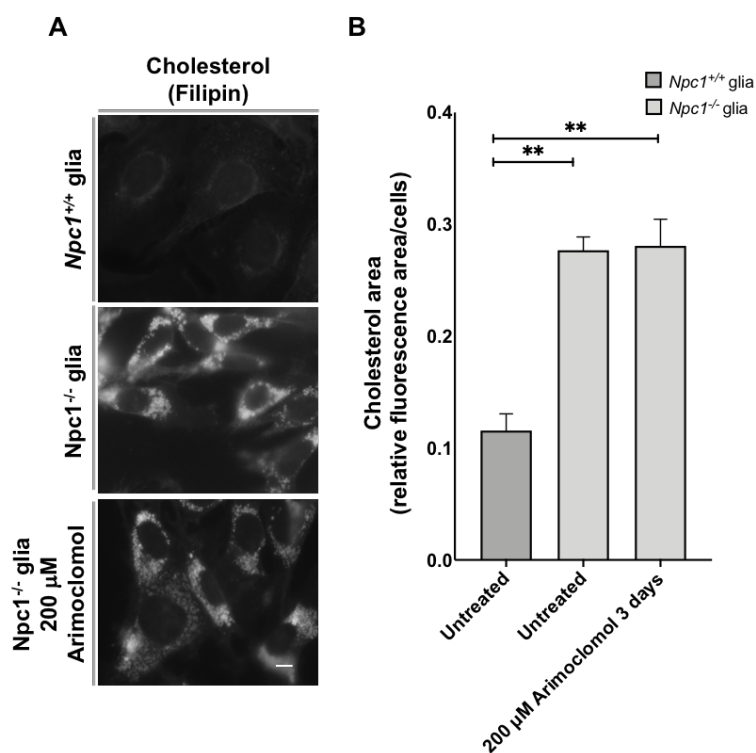


**Figure 4.9: Cholesterol levels *Npc1*<sup>-/-</sup> glia treated with arimoclomol.** **A:** Representative images of cholesterol (Filipin) quantified in **B**. Scale bar = 10  $\mu$ m. **B:** Quantitative analysis of cholesterol staining area in *Npc1*<sup>+/+</sup> glia and *Npc1*<sup>-/-</sup> glia. The graph represents data from N = 3. The error bars indicate SEM. \*\*p  $\leq$  0.01, two-way ANOVA with post-hoc Tukey.

#### 4.3.9 Cholesterol levels following arimoclomol treatment in NPC patient HF

The effect of arimoclomol on patient cells was explored following the lack of effect on cholesterol storage in *Npc1*<sup>-/-</sup> glia (Figure 4.10). This was done to explore whether arimoclomol proposed chaperone effect on the I1061T NPC1 mutation, which traps

NPC1 in the ER (Gelstrophe et al. 2008), meant that arimoclomol treatment had a different effect in the I1061T NPC1 patient cells than on the knockout *Npc1*<sup>-/-</sup> glia. NPC1 patient HFs were treated with 200 μM arimoclomol and the levels of cholesterol were examined using filipin. These results showed that arimoclomol treatment reduces cholesterol accumulation in the NPC1 patient HF (Figure 4.10).

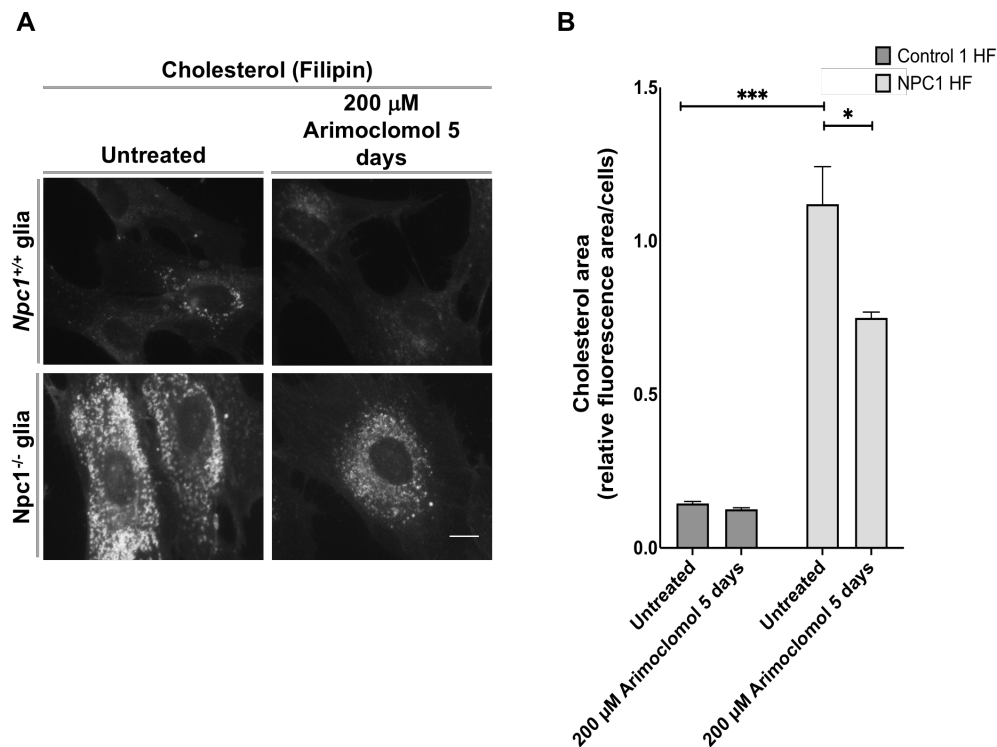


**Figure 4.10: Cholesterol storage levels in NPC1 patient cells treated with arimoclomol.** **A:** Representative images of cholesterol (filipin) quantified in **B**. Scale bar = 10 μm. **B:** Quantitative analysis of cholesterol staining area in *Npc1*<sup>+/+</sup> and *Npc1*<sup>-/-</sup> glia. The graph represents data from N = 3. The error bars indicate SEM. \*p ≤ 0.05, \*\*\*p ≤ 0.001, two-way ANOVA with post-hoc Tukey.

#### 4.3.10 HSP70 levels following arimoclomol treatment in *Npc1*<sup>-/-</sup> glia

Arimoclomol has been reported, as its mechanism of action, to increase heat shock protein 70 (HSP70) expression (Hesselink 2017) which we have now confirmed by treating NPC1 cells with arimoclomol and staining for HSP70 with a HSP70 antibody (Chapter 2 Section 2.2.4). These data (Figure 4.11) show that arimoclomol can increase the expression of HSP70 in *Npc1*<sup>-/-</sup> glia following 200 μM arimoclomol treatment.

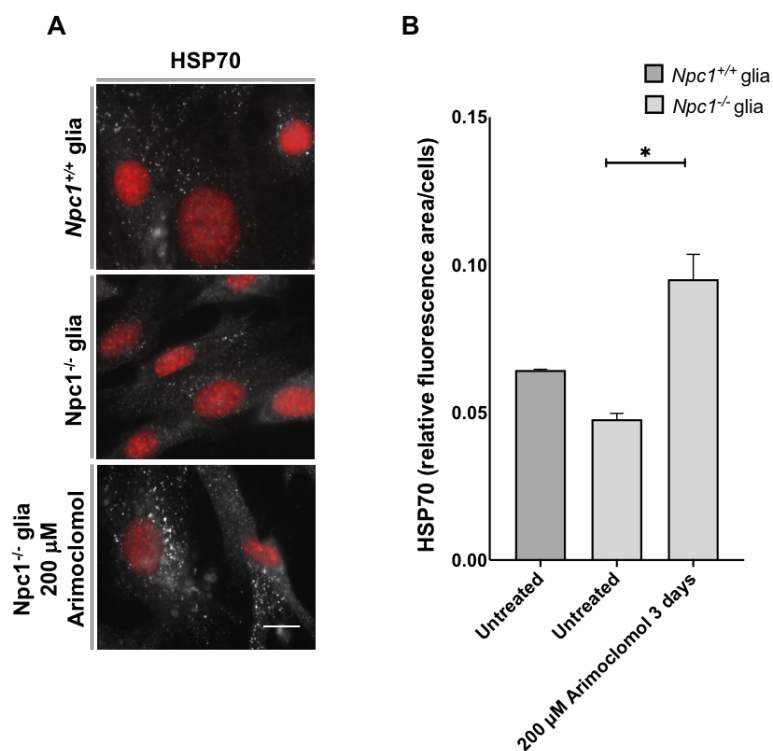


**Figure 4.11: HSP70 levels in *Npc1*<sup>-/-</sup> glia treated with arimoclochol.** **A:** Representative images of HSP70 (anti-HSP70) quantified in **B** with a Hoescht 33342 nuclear counter stain pseudo coloured red. Scale bar = 10 μm. **B:** Quantitative analysis of HSP70 staining area in *Npc1*<sup>+/+</sup> glia and *Npc1*<sup>-/-</sup> glia. The graph represents data from N = 3. The error bars indicate SEM. \*\*p ≤ 0.01, two tailed t-test.

#### 4.3.11 Arimoclochol-like compound drug screen using *Npc1*<sup>-/-</sup> glia

Having confirmed the presence of NPC1 phenotypes in the *Npc1*<sup>-/-</sup> glia, these cells were used for a drug screening project to investigate the possible beneficial effects of arimoclochol-like compounds provided by a pharmaceutical company. These compounds were identified by a pharmaceutical company to have similar properties and/or structure to miglustat or arimoclochol. The primary screen of the arimoclochol-like compounds in the *Npc1*<sup>-/-</sup> glia comprised of 46 compounds tested at 50, 100 and 200 μM (Figure 4.12) to determine if these had an effect at the same or lower concentration than arimoclochol. Compounds that act at lower concentrations are more likely to be beneficial to patients as these lower concentrations are easier to be achieved in physiological conditions (Lipinski et al. 2001; Hughes et al. 2011).

Of the compounds tested, 23 were toxic and caused extensive cell death at all concentrations, thus were taken further (Figure 4.12). Of the other 23 compounds,

some were toxic at higher concentrations (> 100  $\mu$ M). Only four of the compounds (drugs 7, 32, 36 & 40; Figure 4.12) that had no effect on cell numbers and viability showed decreases in lysosomal area, as detected by LysoTracker plate assay standardised to cell number. Of these 4, only drug 7 and drug 40 exhibit a greater reduction in lysosomal area than the arimoclomol internal control (Figure 4.12). These results highlight the benefit of robust models for primary drug screens which has identified four compounds that were then taken forward for further secondary screens against other cellular phenotypes for NPC1 disease and may be tested for other LSDs. Although, drug 05, drug 10, drug 24, drug 30 and drug 42 appear to also reduce lysosomal volume in Figure 4.12 these compounds were observed to be cytotoxic which was confirmed by using a cytotoxicity assay (data not shown).

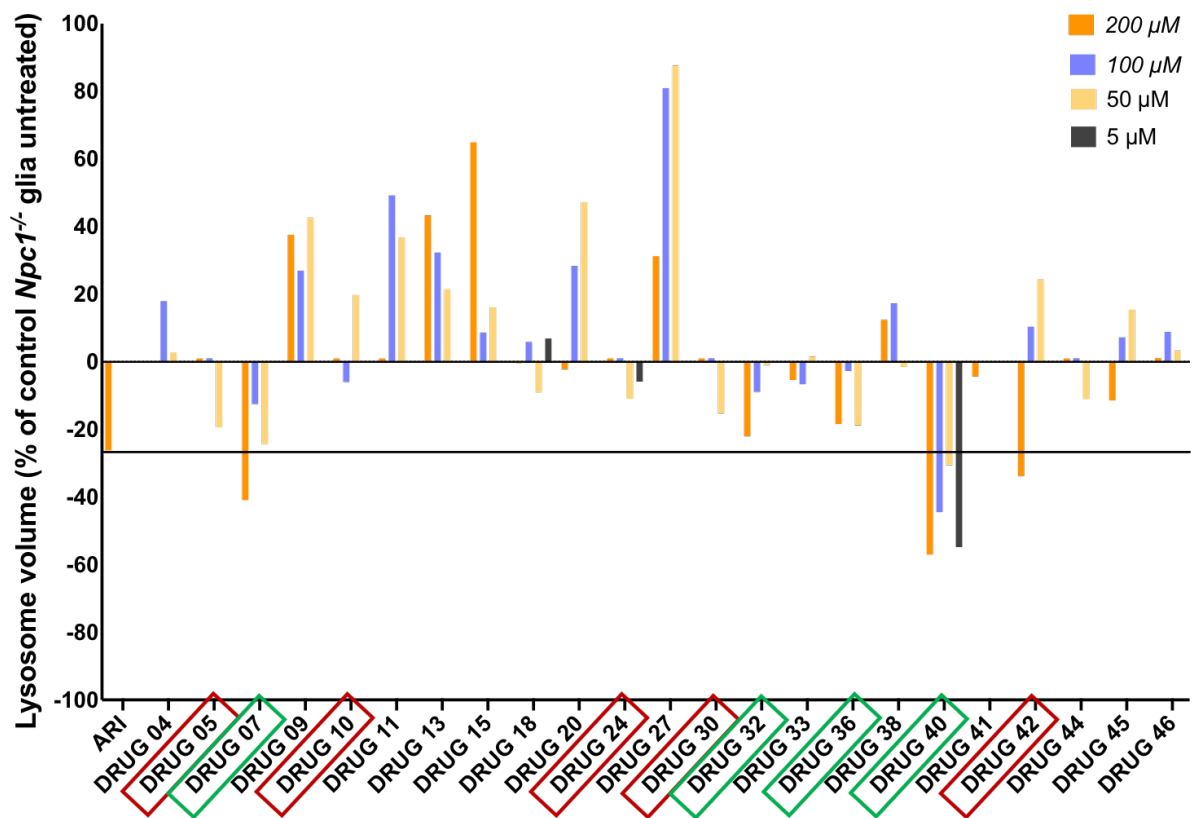


**Figure 4.12: Arimoclomol-like compound screen in *Npc1*<sup>-/-</sup> glia.** Lysosomal plate assay (LysoTracker) of *Npc1*<sup>-/-</sup> glia treated with different arimoclomol-like compounds. The data is shown as a percentage of the untreated *Npc1*<sup>-/-</sup> glia calculated from the relative fluorescence units. Arimoclomol-treated *Npc1*<sup>-/-</sup> glia represented by the orange bar on the far left (ARI) were included as internal controls. The red boxes represent the compounds that were found to be cytotoxic. The data represent a primary drug screen carried out by Dr Bernardo Barrios Crispi under the supervision of Rafael A. Badell-Grau. Drugs outlined by red boxes were cytotoxic and drugs that outlined by green boxes were selected for further screening. N = 2.

## **4.4 Discussion**

This chapter aimed to first confirm the presence of NPC1 cellular phenotypes in the *Npc1*<sup>-/-</sup> glia model and then examine the optimal phenotype that should be used for drug screening. The *Npc1*<sup>-/-</sup> glia model characterisation was completed by confirming increased lysosomal volume, increased and mis-localised ganglioside GM1, increased autophagic compartments and have ER stress (Figure 4.1 – 4.4). Once the presence of NPC1 phenotypes were confirmed, this Chapter demonstrated that lysosomal volume made a more appropriate phenotype for drug screening than cholesterol. The dangers of choosing the incorrect method of standardisation was also shown which could lead to drug hits being missed.

Additionally, this Chapter determined the optimal working concentration of arimoclomol as well as confirmed that arimoclomol treatment not only increases HSP70 expression but also has a different effect on the I1061T NPC1 mutation as proposed previously. The optimised method was then used to screen compounds with similar properties to arimoclomol which successfully identified 4 compounds that have been taken forward for further screening demonstrating how proper drug screening design can lead to the identification of compounds that may be of benefit to LSDs.

### **4.4.1 Confirmation of NPC1 disease phenotypes in *Npc1*<sup>-/-</sup> glia**

Lysosomal staining was clearly increased in *Npc1*<sup>-/-</sup> glia, as has been previously reported in NPC1 disease due to lysosomal storage (Lloyd-Evans 2006). Furthermore, ganglioside GM1 storage, which is characteristic of NPC1 disease (Lachmann et al. 2004), is indicative of endo-lysosomal trafficking dysfunction (Sugimoto et al. 2001) and was also confirmed in our *Npc1*<sup>-/-</sup> glia cell model (Figure 4.2). Defects in autophagy have been reported in NPC1 disease (Xu et al. 2010; Wheeler and Sillence 2019), which were confirmed in the *Npc1*<sup>-/-</sup> glia (Figure 4.3). Similarly, reports of ER stress in NPC1 disease pathogenesis were also confirmed (Figure 4.4) in the *Npc1*<sup>-/-</sup> glia.

Confirming the presence of these phenotypes in the *Npc1*<sup>-/-</sup> glia suggests that this cell line can be used as robust quantifiable phenotypes for drug screening. Additionally, glia cells are fast growing brain derived cells which makes them a great model for high-throughput drug screening of LSDs. The presence of robust

phenotypes in the cell model also allows for multiple phenotypes to be used for further drug confirmations. Having multiple cellular phenotypes for screening allows prospective drugs to be screened against a variety of cellular dysfunctions, leading to the identification of better hits since drugs that are of benefit to multiple cellular phenotypes are more likely to be clinically translated (Chandrachud et al. 2015; Jang et al. 2016; Szabo et al. 2017).

These cellular phenotypes confirmed in the *Npc1*<sup>-/-</sup> glia are not only important and useful for drug screening to find compounds that may be of benefit to NPC1 disease (Sano et al. 2009; Annunziata et al. 2018) and other lysosomal storage diseases exhibiting these phenotypes. For example, lysosomal storage, measured using LysoTracker, is a consistent and reproducible phenotype seen across most LSDs independent of the type of accumulated material (Xu et al. 2014; Alshehri 2019). Similarly, autophagy defects (Thelen et al. 2012; Chandrachud et al. 2015), lipid storage (Hermansson et al. 2005; Lloyd-Evans and Platt 2010; Platt et al. 2012) and ER-stress (Tessitore et al. 2004) are present in the pathology of many LSDs.

Although there have been many drug screens in for LSDs (Chen et al. 1999; Zheng et al. 2007; Motabar et al. 2010; Geng et al. 2011; Ribbens et al. 2013; Xu et al. 2014; Jang et al. 2016; Pugach et al. 2018) few have gone through to clinic which highlights not only the difficulty of drug screening in LSDs but the importance of designing robust drug screen that may be more likely to find drugs that could make it to patients. Therefore, once cellular phenotypes have been determined it is important that the drug screening conditions such as the phenotypes used, standardising method and length of treatment need to be properly determined in order to identify more appropriate potential therapies.

#### **4.4.2 Selecting appropriate phenotypes for drug screening**

Having confirmed the presence of NPC1 cellular phenotypes in the *Npc1*<sup>-/-</sup> glia, it was important to then select the correct phenotypes for screening and implement appropriate standardisation. In selecting the correct phenotype for drug screening, an understanding of the cellular mechanisms involved in the pathogenesis of disease is critical.

In this case, given that the drugs would be screened across LSDs, it is important to understand and select appropriate phenotypes that could be screened for, such as those outlined in Table 4.2. In NPC disease, for example, cholesterol storage and mislocalisation in lysosomes is well-known and extensively characterised (Karten et al. 2002; te Vrugte et al. 2004; Ioannou 2005; Vanier 2010). Although cholesterol storage has been reported to be by far the most prominent lipid store in peripheral tissues it does not seem to respond to the only currently EMA approved therapy for NPC1 disease which is miglustat (te Vrugte et al. 2004; Stein et al. 2012; Yu et al. 2014).

On the other hand, LysoTracker does respond to miglustat treatment as it provides a better overview of storage in LSDs such as NPC1 disease (Xu et al. 2014). Glycosphingolipids are a smaller component of the lipid storage seen in NPC1 disease when compared to cholesterol; however, glycosphingolipids reduction following miglustat treatment can be measured by the use of LysoTracker (te Vrugte et al. 2004) indicating that there is a good signal to noise and is a good phenotype to use for drug screening.

Also, as can be seen in this chapter miglustat takes 3-5 days to have an effect, some cellular drug screens currently are carried out in 24 hours which would also lead to potential drug that may be of benefit to a disease being missed (Yu et al. 2014). It is important not only to select the appropriate phenotype to use in a drug screen but also to use the appropriate length of treatment in order to make sure that compounds that may be of benefit to a disease such as miglustat or better than miglustat are identified.

Nevertheless, even though LysoTracker seems to provide a great overview of lysosomal storage and a potential drug screening method there are some cases where LysoTracker may not be appropriate. This is because LysoTracker is a pH sensitive probe which means that in LSDs where there is a defect in lysosomal pH, LysoTracker signal may appear to be lower than the control which may be confused with less lysosomal volume when in fact in these diseases there is lysosomal accumulation (Coen et al. 2012; Guha et al. 2014). In most LSDs, however, this is not an issue and LysoTracker remains among the best phenotypic assay that can be used in drug screening (Xu et al. 2014).

Furthermore, LysoTracker has been reported to not alter cellular function and is not cytotoxic with a relatively well understood mechanism (Duvvuri et al. 2004; Pierzyńska-Mach et al. 2014). LysoTracker has been used as a clinical monitoring tool due to the fact that it has a single wavelength emission meaning increases in fluorescence are due to changes in lysosomal number and size (Rahman et al. 2016). Moreover, LysoTracker has been used in clinical monitoring of NPC1 patient following miglustat treatment which revealed that miglustat reduced lysosomal storage to near normal levels in peripheral blood C lymphocyte from NPC1 patients confirmed by a reduction in ganglioside GM1 measure by CtxB (Lachmann et al. 2004; te Vrugte et al. 2004). Therefore, the results in this Chapter along with the literature led this study to select LysoTracker as a robust tool for drug screening in LSDs.

After selecting an appropriate cellular phenotype for the initial drug screen, it is important to select a suitable method for standardising screening (Figure 4.6). The most robust and common phenotype across the LSDs is lysosomal area increase and can be used in plate assay (Xu et al. 2014). Although a clear increase in lysosomal staining was seen by lysosomal staining via microscopy, this was not seen when standardising LysoTracker plate assay to nuclear staining. Nuclear staining was variable across several of the LSDs (Figure 4.6), making this method of standardisation inappropriate for LSD drug screening. This may be due to the fact that there are alterations in gene expression profiles in LSDs (Mazzoccoli et al. 2013; Richardson et al. 2016; Vallim et al. 2019; Brokowska et al. 2020) that might cause the nuclear structure to be altered. Variable nuclear staining meant that its use for standardisation would preclude detection of differences such as that observe in lysosomal area in the *Npc1<sup>-/-</sup>* glia. Therefore, if the assay does not detect the well-known lysosomal storage in NPC1 also seen in this study (Figure 4.1), then that assay would not be appropriate to detect compounds that may be of benefit to this cellular dysfunction.

Similarly, other standardisation methods, such as protein assay preclude detection of differences in lysosomal volume due to the reported changes in gene expression in LSDs such as Hunter syndrome, Mucopolysaccharidosis, Fabry and Sandhoff (Mazzoccoli et al. 2013; Richardson et al. 2016; Vallim et al. 2019; Brokowska et al. 2020). Using protein concentration produces similar results because NPC1 cells may have increased ER stress (Klein et al. 2011), leading to changes in protein expression

when compared to a control. This potential ER stress was also confirmed in this Chapter (Figure 4.4), further indicating that protein expression is not a viable standardisation method for the LysoTracker plate assay. Furthermore, some drug compounds being screened may increase protein expression such as arimoclomol (Kirkegaard et al. 2010; Kirkegaard et al. 2016) which may affect the results of a drug screen using protein expression as standardisation method leading to potential beneficial compounds being missed.

During this study, it was also determined that cell number could be used as a standardisation method for the LysoTracker plate assay. It was found that the optimal cell number was 60,000 as it was the point at which the greatest statistical significance began as well as being the point before saturation and before the cell begin to grow on top of each other which could lead to issues with the signal.

The LysoTracker plate assay with *Npc1*<sup>-/-</sup> glia and cell number standardisation as outlined in this Chapter were, used by another project alongside this study for drug screening of novel arimoclomol-like compounds for NPC1 disease in order to identify novel compounds that may be better than arimoclomol for NPC1 disease and potentially other LSDs. As mentioned above, these compounds were identified by a pharmaceutical company to be compounds that had similar structure and similar properties to miglustat or arimoclomol. Therefore, these compounds may also have similar beneficial effects to LSDs, and some may even work at lower concentrations. Compounds that act at lower concentrations tend to be more likely to be beneficial to patients as they are more likely to reach these lower concentrations *in vivo* (Hughes et al. 2011).

#### **4.4.3 Arimoclomol in NPC1 disease**

Once the cellular phenotypes in the *Npc1*<sup>-/-</sup> glia were confirmed and the appropriate screen method was determined, this study explored the effects of arimoclomol, a drug previously reported to be beneficial for NPC1 disease (Ingemann and Kirkegaard 2014), and more recently, Gaucher disease (Fog et al. 2018), and other neurodegenerative diseases (Penke et al. 2018; Shukla and Tekwani 2020). In fact, an official regulatory submission has recently been made to the US Food and Drug Administration for arimoclomol in NPC1 disease (Orphazyme 2020).

The exact mechanisms of action of arimoclomol in NPC1 disease are not fully understood. Arimoclomol has been previously reported to increase HSP70 levels in cells (Hesselink 2017) and this study ratifies these findings (Figure 4.11). *Npc1*<sup>-/-</sup> glia were shown to have higher levels of HSP70 following arimoclomol treatment. It has been suggested that arimoclomol may act as a chaperone for misfolded proteins (Hesselink 2017; Fog et al. 2018) such as some mutant NPC1 protein in certain patient mutations.

This study found that arimoclomol potentially has a beneficial effect on lysosomal storage in *Npc1*<sup>-/-</sup> glia (Figure 4.8). An interesting tri-phasic response was observed in cells treated with arimoclomol, showing that arimoclomol had a beneficial effect on lysosomal volume at a concentration of 200  $\mu$ M and not any lower or higher. The tri-phasic effect observed following arimoclomol treatment (Figure 4.8) could, however, be specific to the NPC null glia model used and further studies should investigate whether this effect is seen in patient cells with mutant protein that may have enhanced expression due to the HDAC inhibition properties of arimoclomol. The fact that arimoclomol only works at one concentration has been previously reported by another group at a conference but has not yet been published; however, the reason behind this is not understood and may complicate its use in patients as the working concentration needs to be exact. Nonetheless, the reduction in lysosomal area seen in *Npc1*<sup>-/-</sup> glia was robust which indicates that there is a clear beneficial lysosomal reduction following arimoclomol treatment *in vitro* (Figure 4.8).

There was no change in cholesterol accumulation in *Npc1*<sup>-/-</sup> glia (Figure 4.9); however, a decrease in cholesterol accumulation was seen in NPC1 patient HF (Figure 4.10). This suggests that arimoclomol may only have a beneficial effect on cholesterol storage through the increase of mutant NPC1 protein expression in cells or via chaperoning of misfolded NPC1 protein that is known to result from the I1061T patient mutation (Schultz et al. 2016). The decrease in cholesterol in response to arimoclomol is therefore not seen in the glia model as there is no NPC1 for arimoclomol to chaperone or increase the expression of. These data are the first to demonstrate that arimoclomol therefore has two beneficial effects, first as a chaperone and second as a stabilizer of lysosomal function via increased expression of HSP70 as was originally suggested (Kirkegaard et al. 2010; Kirkegaard et al. 2016).

Nevertheless, there was a beneficial effect on lysosomal accumulation following arimoclomol treatment in *Npc1*<sup>-/-</sup> glia, suggesting a benefit beyond NPC1 chaperoning of arimoclomol in LSDs. The increase in HSP70 is thought to stabilise the interaction between acid sphingomyelinase (ASM), which has reduced activity in NPC1 disease, and other proteins which may be beneficial to diseases with secondary defects such as NPC1 (Penke et al. 2018). Arimoclomol therefore acts not only by trafficking NPC1, but also by stabilising protein interaction in lysosomes, thus the knockout *Npc1*<sup>-/-</sup> glia will only exhibit the benefit of HSP70 and not the chaperoning of misfolded proteins.

The use of patient cells for drug screening seems more appropriate given the better representation of the disease being screened. Nonetheless, there are difficulties associated with patient fibroblast growth, such as the time and labour required to accumulate cultures with enough cells to perform the primary drug screen. For example, to carry out the LysoTracker plate assay for CLN8 in Chapter 3 using HFs, could take over 2 weeks to grow enough cells to do one N; whereas, using the glia cells could take as little as 3 days. This further shows how the *Npc1*<sup>-/-</sup> glia, which is a fast-growing cell line, can be used for primary screens to detect potential therapies for further screening and confirmation in patient cells.

#### **4.4.4 Future work**

There are no clear antibodies that can be used to detect CLN8 protein in CLN8 disease, despite four being tested in this study. It would be of interest to examine whether arimoclomol may have beneficial effects in CLN8 disease either via increasing protein expression changes, by chaperoning misfolded proteins or by increasing HSP70 which may lead to an increase in the ASM activity defect seen in Chapter 3 (Figure 3.11). This complicates testing of the effects of arimoclomol on CLN8. Additionally, the variability observed in CLN8 phenotypes in Chapter 3 also meant that it is more complicated to screen drugs in CLN8 disease. Nonetheless, this study had planned to carry out arimoclomol drug screens in CLN8 disease and possibly other NCLs but this was not possible as obtaining a CLN8 knockout cell line was beyond the budget of this project. Furthermore, it was not possible to do the arimoclomol screening with few phenotypes identified in CLN8 534 HF as the project

was ended early due to the pandemic which meant there was no time for this to be done (further outlined in Chapter 6).

#### **4.5 Conclusion**

This Chapter confirmed the presence of NPC1 cellular phenotypes in the fast-growing *Npc1*<sup>-/-</sup> glia, allowing these to be used as a cellular model for drug screening for the identification of drugs of benefit to these cellular phenotypes. These phenotypes may further facilitate the identification of compounds beneficial to many other LSDs and other diseases that exhibit lysosomal dysfunctions.

Arimoclomol has a beneficial effect on lysosomal storage in NPC1 disease, not only by affecting the mutant NPC1 protein in patient cells but also via another mechanisms. This may provide a potential therapy for lysosomal storage, thus the effects of arimoclomol on other lysosomal storage diseases should be explored further.

# **Chapter 5 Drug repurposing for lysosomal storage diseases**

## **5.1 Introduction**

Once therapeutic targets are identified in lysosomal diseases, such as those outlined in Chapter 3 and Chapter 4, high-throughput drug screening can be undertaken to ascertain potential therapeutic interventions. To date, with the exception of CLN2 and NPC1, the LSDs investigated in this thesis lack any approved or effective treatments, and the enzyme replacement therapy (ERT) identified for CLN2 is deemed too expensive for clinical use in some countries as was initially the case in the United Kingdom where it is currently costed at over £500,000 per patient per year (Smith 2019). Given the immense detriment posed to patients by LSDs the identification of novel therapies would satisfy an urgent unmet medical need.

### **5.1.1 Drug repurposing**

Drug development of novel therapies is an extremely arduous, slow and expensive process, and as such repurposing of known drugs for a new application, or to treat another disease, has recently become more and more common (Pushpakom et al. 2019). The repurposing of known compounds for new diseases also offers a pathway to drug discovery with potentially lower development costs and faster development timelines (Pushpakom et al. 2019). Furthermore, repurposing drugs that have already been tested in patients means that there is safety information already available for these drugs increasing the likelihood of them reaching patients and reducing the development costs (Pushpakom et al. 2019). An example of successful drug repurposing for LSDs is miglustat, a drug originally developed for HIV, to treat NPC1 disease and Gaucher disease (Cox et al. 2000; Patterson et al. 2007).

### **5.1.2 Enzyme assay high-throughput drug screening**

High-throughput drug (HTS) screening enables testing of a large number of compounds to act as inhibitors, activators and stabilising chaperones of target proteins. One of the main advantages of HTS is that it provides a method that generally leads to the identification of potential therapies faster than conventional methods (Pereira and Williams 2007). HTS is a process that can be utilised to identify small molecule drugs that may be of benefit to a disease from large compound drug libraries using miniaturised assays that allow for large number of compounds to be screened thus decreasing the costs of drug screening (Pereira and Williams 2007). Previous studies have successfully identified potential pharmacological compounds for several LSDs such as Gaucher, CLN3, Fabry disease and others (Maegawa et al. 2009; Marugan et al. 2010; Motabar et al. 2010; Goldin et al. 2012; Ribbens et al. 2013; Chandrachud et al. 2015; Jang et al. 2016). To date, however, no compounds identified this way have been approved as a therapy for patients. Nonetheless, the glucosylceramidase chaperone ambroxol, identified by HTS (Maegawa et al. 2009), is being tested in clinical trials for Gaucher disease (NCT01463215, NTC03950050 & NTC04388969).

Previous studies have found that levels of lipids such as galactosylceramide (GalCer) the primary component of myelin, are altered in CLN8 patient post-mortem brains (Hermansson et al. 2005). GalCer is catabolised by the enzyme galactosylceramidase (GALC) and mutation in GALC are known to give rise to the LSDs Globoid cell leukodystrophy also known as Krabbe disease (Ribbens et al. 2013; Berardi et al. 2014; Sprately et al. 2016). Therefore, screening compounds that increase or stabilise GALC activity may be of benefit to Krabbe disease as well as CLN8 disease. A GALC enzyme assay can be used for HTS to screen large drug libraries to detect compounds that can act as activators, inhibitors or chaperones to de-stabilised enzymes.

### **5.1.3 Miglustat repurposing**

As outlined in Chapter 1 (Section 1.3.5) miglustat (*N*-butyl-1-deoxnojirimycin) is an imino sugar analogue of D-glucose and a small molecule therapy that is orally available. It is a blood brain barrier permeant drug that reduces glycolipid biosynthesis

leading to lipid storage reduction (Lachmann et al. 2004). Miglustat is currently the only FDA approved therapy for the LSD Gaucher disease and is the only EMA approved therapy for the treatment of NPC1 and Gaucher disease. Additionally, miglustat has been shown to improve lysosomal dysfunction both *in vitro* and *in vivo* (Lachmann et al. 2004; Patterson et al. 2007; Pollock et al. 2008; Stein et al. 2012). Therefore, miglustat is already an approved therapy for two LSDs and is a prime example of drug repurposing (Cox et al. 2000; Lachmann et al. 2004; Badell-Grau 2016).

Miglustat acts by inhibiting the enzyme glucosylceramide synthase (Figure 5.1) resulting in the biosynthesis of glycosphingolipids being partially inhibited and ultimately causing a reduction in lysosomal lipid storage that alleviates cellular dysfunction (Platt et al. 1994; Lachmann et al. 2004; Badell-Grau 2016). Miglustat has been reported to not only reduce storage but also lead to improvements in trafficking defects, such as trafficking in ganglioside GM1, and increase Purkinje neuron function and survival in NPC1 disease (Lachmann et al. 2004; Patterson et al. 2007; Elliot-Smith et al. 2008; Stein et al. 2012).

Miglustat treatment has been reported to be beneficial to diseases that have glycosphingolipid storage which is a common storage molecule across the LSDs (Sugimoto et al. 2001; Lachmann et al. 2004). Glycosphingolipid storage has been identified in several NCLs including CLN8 disease, as such it may be of interest to examine the potential effects of miglustat treatment on some NCLs (Hermansson et al. 2005; Kollman et al. 2013). Furthermore, miglustat was reported to have beneficial effects in CLN5 disease cell models leading to it being given to two CLN5 patients in the UK under compassionate use (Shipley 2019).

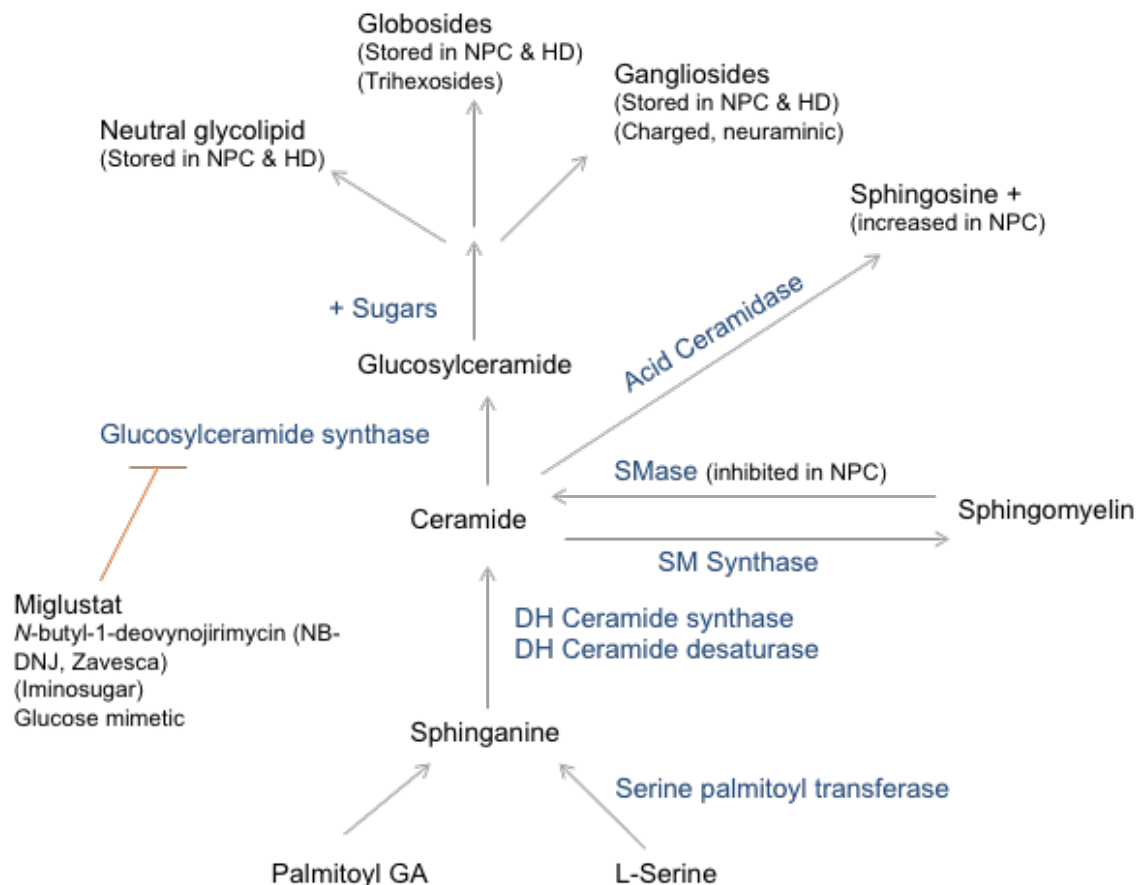


**Figure 5.1: Sphingolipid biosynthesis pathway and miglustat mechanism of action.** Outline of the sphingolipid synthesis pathway with the enzymes involved. The red line indicates the point in the pathway at which miglustat acts. Miglustat partially inhibits the glucosylceramide synthase and thus reduces the productions of the lipids after this point in the pathway.

#### 5.1.4 Curcumin nutraceuticals

As outlined in Chapter 1, nutraceuticals such as curcumin have been reported to be beneficial for LSDs like NPC1 (Lloyd-Evans et al. 2008). Curcumin has been reported to have beneficial effects in a wide range of diseases across thousands of publications and is thought to be of benefit for NPC1 disease due to its ability to modulate  $\text{Ca}^{2+}$  levels (Lloyd-Evans et al. 2008; Monroy et al. 2013; Shanmugam et al. 2015). Some lysosomal storage diseases such as NPC1 are known to have reduced lysosomal  $\text{Ca}^{2+}$  content which contributes to disease pathogenesis (Lloyd-Evans et al. 2008). Curcumin has been shown to be a weak SERCA inhibitor (Bilmen et al. 2001) which leads to ER  $\text{Ca}^{2+}$  leak which increases cytosolic  $\text{Ca}^{2+}$  and consequently rescues

endo-lysosomal trafficking and fusion defects in LSDs like NPC1 (Lloyd-Evans et al. 2008).

The beneficial effects of curcumin on NPC1 disease were first reported in a study by Lloyd-Evans *et al.* (2008) in which they treated *Npc1*<sup>-/-</sup> knockout mouse glial cells with 30  $\mu$ M curcumin and found that treatment restored sphingolipid trafficking due to the ability of curcumin to increase cytosolic Ca<sup>2+</sup>. Lloyd-Evans *et al.* (2008) also reported that curcumin treatment (150 mg/kg per day from the first day post-weaning) in the *Npc1*<sup>-/-</sup> mouse led to improved mouse coat condition, increased weight, reduced tremor and increased activity compared to the untreated illustrating a beneficial effect of curcumin treatment in the *Npc1*<sup>-/-</sup> mouse. Similarly, Borbon *et al.* (2012) reported that the *Npc1*<sup>-/-</sup> mouse treated with curcumin had ~16% increase in lifespan compared to the untreated mouse. Following these reports other studies have further confirmed the beneficial effects of curcumin in both *in vivo* and *in vitro* NPC1 (Efthymiou et al. 2014; Williams et al. 2014).

Curcumin is an easily available compound that is the colouring in the common food flavouring turmeric and is known to cross the blood brain barrier (Tsai et al. 2011) which makes this an attractive possible compound to treat LSDs. Following the reports that curcumin may be of benefit to NPC1 disease many NPC1 patients started taking different curcumin nutraceuticals (Vockley 2009). Curcumin nanoformulations have been developed as nutraceutical due to the reported beneficial effect of curcumin. This is because curcumin needs to be combined in a lipid vehicle nanoformulations in order to allow for curcumin to better cross the blood gut barrier but the impact of these nanoformulations is often ignored (Bi et al. 2017). Some reports have shown that some lipidated nanoformulations of curcumin do not provide benefit to NPC1 disease (Borbon et al. 2012). The effects of two nanoformulations on LSDs were explored in several LSDs.

### **5.1.5 Chapter aims**

The overall aim of this chapter was to identify potential drugs that may be repurposed for other LSDs. This was done by performing HTS enzymatic drug screens to identify potential modulators of GALC, which may be of benefit to diseases with defects in GALC activity such as Krabbe disease or CLN8 as mentioned above.

Furthermore, in this Chapter the potential of miglustat to ameliorate cellular dysfunction in the NCLs CLN2, CLN7 and CLN8 was tested. Finally, the chapter also explores the mechanisms by which curcumin may be of benefit to several LSDs, namely, NPC1, CLN7, CLN8 and CLN10.

**Table 5.1: Outline of the patient cell lines used in Chapter 5.**

Cell line	Description	Mutation
Control 1 HF	Apparently healthy control 1 (GM05399) cell line	N/A
Control 2 HF	Apparently healthy control 2 (GM05400) cell line	N/A
CLN8 462 HF	CLN8 patient cell line	c.543 + 1G>A homozygous
CLN8 533 HF	CLN8 patient cell line	Q194R/c.66delG
CLN8 534 HF	CLN8 patient cell line	A30P homozygous
CLN8 535 HF	CLN8 patient cell line	Y158C/c.66delG
CLN7 474 HF	CLN7 patient cell line	c.1393C>T,p.Arg465Trp homozygous
CLN2 HF	CLN2 patient (GM16486) cell line	R127Q & IVS5-1G>C
NPC1 HF	NPC1 patient (GM03123) cell line	I1061T/P23S
NPA HF	NPA patient (GM00112) cell line	L302P/L302P
<i>Npc1</i> <sup>+/+</sup> glia	Apparently healthy control glia cell line	N/A
<i>Npc1</i> <sup>-/-</sup> glia	<i>Npc1</i> knockout glia cell line	<i>Npc1</i> <sup>-/-</sup>

## **5.2 Summary of Methods**

The cells used in this chapter are outlined in Table 5.1 and were cultured as outlined in Section 2.1. The GALC enzyme assay optimisation, as well as the screens, were carried out as outlined in Chapter 2 Section 2.7.

For the exploration of the effects of miglustat treatment on CLN2 HF, CLN7 HF and CLN8 HF, cells were treated with miglustat as outlined in Section 2.1.3. The effects of miglustat treatment on cellular phenotypes were explored by looking at lysosomal area using LysoTracker (Section 2.3.2), autophagic vacuole area using CytolD (Section 2.3.4), ganglioside GM1 levels were examined using Cholera toxin B subunit with a FITC tag (CtxB-FITC; Section 2.2.4) and mitochondrial Ca<sup>2+</sup> levels as well as ER Ca<sup>2+</sup> levels were examined using Fura 2,AM with CCCP and ryanodine respectively to

release  $\text{Ca}^{2+}$  as outlined in Section 2.3.7. The effects of miglustat on lysosomal area on CLN8 patient cells treated miglustat as outlined in Section 2.1.3 was explored using LysoTracker as a microplate assay as stated in Section 2.3.3.

The  $\text{Ca}^{2+}$  levels in the ER in control 1, NPC1, Niemann-Pick Type A (NPA), CLN3, CLN7 474, CLN8 534 and CLN10 HFs (Table 5.1) were explored in Section 5.2.9 below using Fura 2,AM with 2  $\mu\text{M}$  ionomycin and 1  $\mu\text{M}$  thapsigargin to release  $\text{Ca}^{2+}$ , as outlined in Section 2.3.7. Similarly, the relative amount of  $\text{Ca}^{2+}$  in the lysosome in Control 1, NPC1, NPA, CLN3, CLN7 474, CLN8 534 and CLN10 HFs (Table 5.1) was explored with Fura 2,AM using 500  $\mu\text{M}$  GPN, after emptying other  $\text{Ca}^{2+}$  stores with 2  $\mu\text{M}$  ionomycin, to release lysosomal  $\text{Ca}^{2+}$  as explained in Section 2.3.7. For Control 1 HF and NPC1 HF (Table 5.1) treated with different curcumin nanoformulations as outlined in Sections 2.1.5 the levels of mitochondrial  $\text{Ca}^{2+}$  were examined using 5  $\mu\text{M}$  antimycin / 5  $\mu\text{M}$  oligomycin as explained in Section 2.3.8. The levels of  $\text{Ca}^{2+}$  inside the mitochondria was further visualised in *Npc1<sup>+/+</sup>* and *Npc1<sup>-/-</sup>* glia treated with curcumin nanoformulations, as delineated in Section 2.1.5, by using the  $\text{Ca}^{2+}$  probe Rhod-2,AM which loads into and is then retained by mitochondria as outlined in Section 2.3.9.

To explore the effects of the curcumin nanoformulations on lysosomal and cholesterol area LysoTracker (Section 2.3.2) and filipin (Section 2.2.3) respectively were used in Control 1, NPC1, NPA, CLN3, CLN7 474, CLN8 534 and CLN10 HFs (Table 5.1) previously treated with the curcumin nanoformulations as outlined in Section 2.1.5.

The staining mentioned above were all imaged using the inverted Colibri widefield fluorescence microscope (Section 2.4.1) and analysed using Image J (Section 2.4.2). All the statistical analysis were carried out in Prism 8 as mentioned in Chapter 2 Sections 2.8.

## **5.3 Results**

### **5.3.1 Galactosylceramidase (GALC) enzyme assay optimisation**

As mentioned above, alterations in levels of GalCer in CLN8 patients have been previously reported (Hermansson et al. 2005) and as such a GALC enzyme assay may be used to find compounds that may be of benefit to CLN8 and other LSDs with GALC activity defects such as Krabbe disease (Jang et al. 2016). The fluorescent substrate 4-methylumbelliferone (4MU)  $\beta$ -galactoside was used and is considered as being a specific substrate for GALC when used in conjunction with 11 mM  $\text{AgNO}_3$  which abolishes  $\beta$ -galactosidase activity (Martino et al. 2009). Adding 0.5 mg/ml sodium taurocholate (TCNa; Figure 5.2A) also further increased the activity of GALC (Wiederschain et al. 1992; Kiyokawa et al. 2004; Ribbens et al. 2013). Although previous separate studies have reported the use of  $\text{AgNO}_3$  to generate a specific GALC assay and the use of TCNa to enhance GALC activity, these have not been tested together before. A clear increase of ~75% in GALC enzyme activity was observed when TCNa was added (Figure 5.2A). The length of the assay was then examined and was found that fluorescence from the 4MU substrate increased linearly over the incubation period (Figure 5.2B).

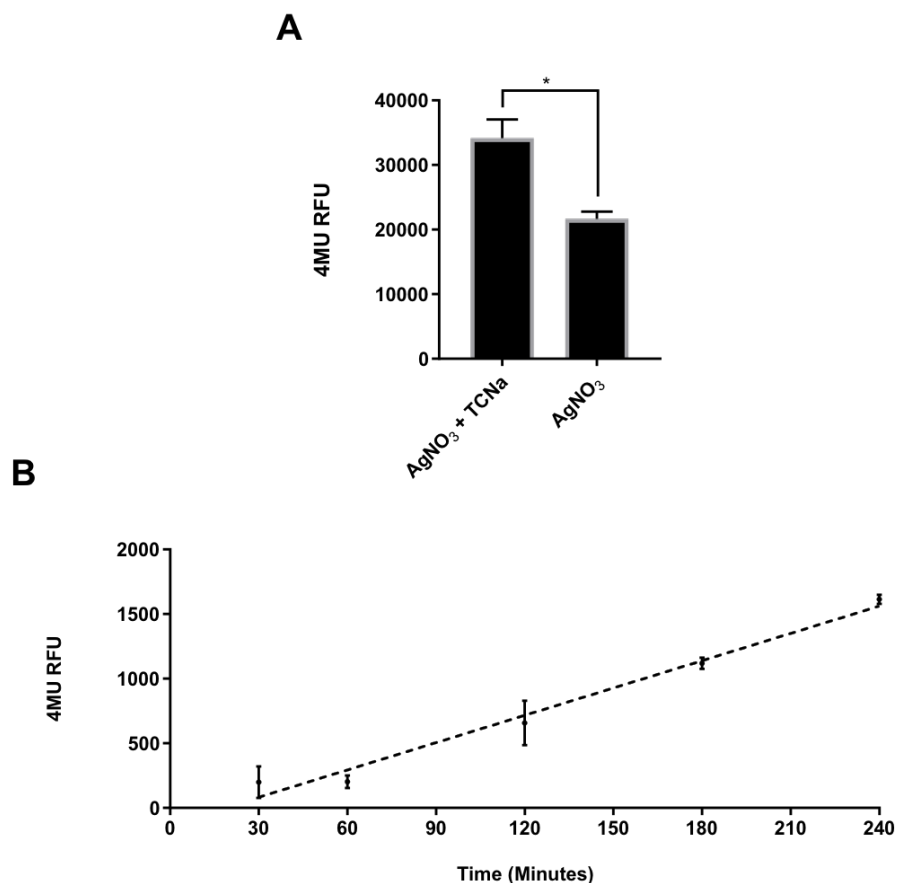


**Figure 5.2: GALC enzyme assay optimisation. A:** GALC 4-methylumbelliferone (4MU) fluorescent plate assay optimisation using control 1 HF homogenate. The graph represents data from N = 3. Error bars represent SEM. \*p ≤ 0.05, two-tailed t-test **B:** Emergence of 4MU fluorescence overtime in GALC assay in control 1 HF. Baseline fluorescence of heat-inactivate samples was subtracted at easy time point. Graph represents data from data from N = 5 and error bars indicate SEM.

### 5.3.2 GALC enzyme based high throughput drug screen

The GALC assay was used to carry out a drug screen of 635 small molecules from a stratified National Institute of Health FDA approved library. The primary screen was carried out at a concentration of 1 μM using homogenates of the control 1 HFs. Prior to carrying out the primary screen the autofluorescence of the compounds was established within the plate in order to subtract any background. The primary screen of the 635 small molecules found that 549 of these compounds decreased, to varying extent, GALC activity; whereas, 86 of the small molecule compounds increased enzyme activity. These data have been represented as heat maps (Figure 5.3) which also indicate that there is no bias with regard to the positioning of the hits on the plates.

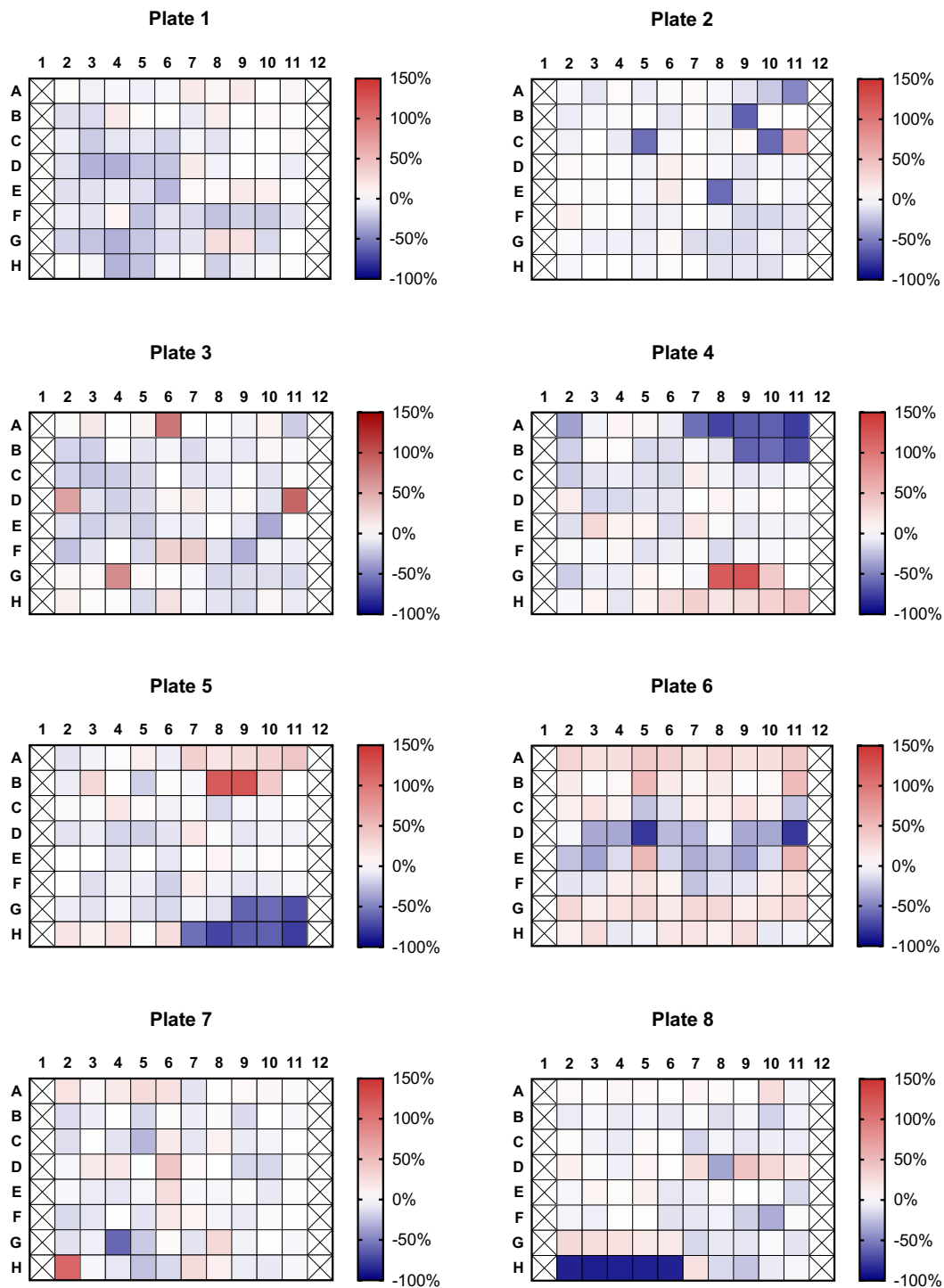


**Figure 5.3: Heatmaps of GALC primary drug screen.** Heatmaps illustrates effect of 1  $\mu$ M small molecule compounds on GALC activity normalised relative to intraplate DMSO vehicle only control. Activators, displaying an increase in enzyme activity, are indicated in red; whereas, inhibitors, displaying a decrease in enzyme activity, are indicated in blue. No change in GALC activity is depicted in white. All vehicle only DMSO control wells are denoted with an 'X'.

Following the primary screen, it was important to check whether the screen carried out was statistically robust by calculating the Z-factor which was done as outlined by Zhang *et al.* (1999). The Z-factor was calculated from the standard deviation of the sample and the negative (DMSO only) control readings. The primary screen was found to be statistically robust with  $Z > 0.0$  for all drug plates and even with most  $Z > 0.5$  (Figure 5.4). Hits from plates 8 and 10 which had particularly low Z-values of around  $Z = 0.1$  and  $Z = 0.2$  respectively, were eliminated.

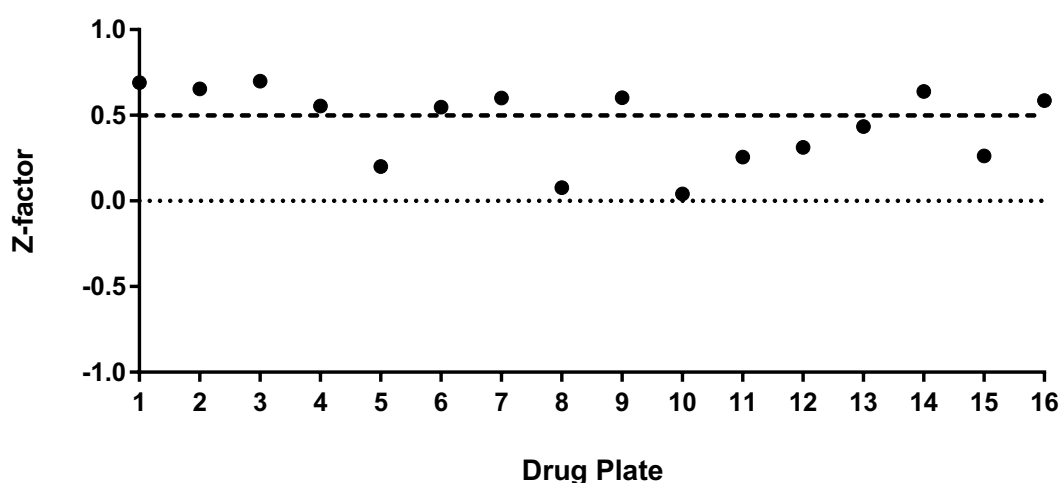


**Figure 5.4: Statistical quality control of the GALC primary drug screen.** Z-factor scores were calculated for the 96-well plates from the vehicle-only DMSO controls (Zhang *et al.* 1999). The dotted line indicates Z-factor of 0.0 to clearly see  $Z > 0$  to easily identify z-factors that were statistically robust. The dashed line indicates a Z-factor of 0.5 to which helps see the most robust plates that had a  $Z > 0.5$ .

In order to properly select the compounds that would be taken forward for further screening, a threshold was set of -42% and +50% inhibition and activation respectively (Figure 5.5). This threshold led to 44 compounds being selected for further screening (Figure 5.5). As well as the compounds that passed the set threshold, ambroxol, mycophenolate mofetil and valproic acid were also taken forward for further screening (Figure 5.5), as these drugs have been identified in other studies as potential therapies for LSDs (Maegawa *et al.* 2009; Seehafer *et al.* 2011; Ambrosi *et al.* 2015; Magalhaes *et al.* 2018; Augustine *et al.* 2019). Ambroxol was chosen as it was previously identified as a chaperone for misfolded GALC (Narita *et al.* 2016) via pH-dependent inhibitory stabilisation of residues near the active site (Maegawa *et al.* 2009). Mycophenolate

mofetil was taken forwards as it was being investigated in clinical trial for inborn error of metabolism (NCT00383448) and a clinical trial for inherited metabolic disorders (NCT01043640). Valproic acid was taken further as it has been reported to have neuroprotective and antioxidant effects as well as possible beneficial effects for the LSD Gaucher disease (Terbach and Williams 2009; Fourcade et al. 2010; Hayashi et al. 2014). As a result of both the thresholding and the literature 47 compounds were taken forward for further screening.

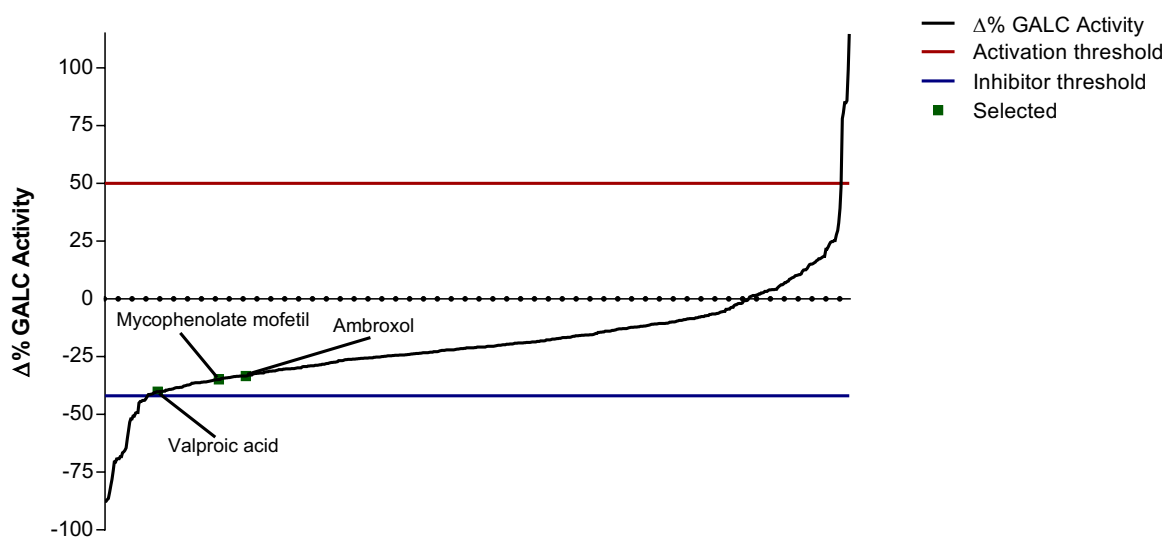


**Figure 5.5: Determination of thresholding for the selection of activating and inhibiting compounds of GALC.** Small molecules compounds ranked by % effect on GALC activity relative to the vehicle-only DMSO controls. The red denotes the upper threshold of an increase of +50% GALC activity used to choose hit compounds (those that fall above the line) that would be explored further. The blue line denotes the lower threshold set of -42% GALC activity that that was used to choose compounds (those below the line) that that was used to choose compounds (those below the line) that would be taken further. Ambroxol, mycophenolate mofetil and valproic acid are outlined in the graph as there were selected for further investigation even though they did not reach the threshold due to previous reports of other beneficial characteristics.

### 5.3.2 Secondary GALC enzyme screen to confirm the hits

The next step in the enzymatic drug screen was to carry out a secondary screen to confirm the hits and also identify which of the compounds had any effect on GALC at a lower concentration of 0.1  $\mu\text{M}$ . This would potentially allow for better and more potent drugs being identified that have an effect on enzyme activity at a lower concentration (Figure 5.6). The second screen was also important to check the reproducibility of the

primary screen and found that of the 47 small molecules taken forward 7 displayed consistent changes in enzyme activity at both 1  $\mu\text{M}$  and 0.1  $\mu\text{M}$  (Figure 5.6) which were ambroxol, rantidine HCL, neostigmine Br, ouabain, quinpirole HCL, ibudilast and mycophenolate mofetil.

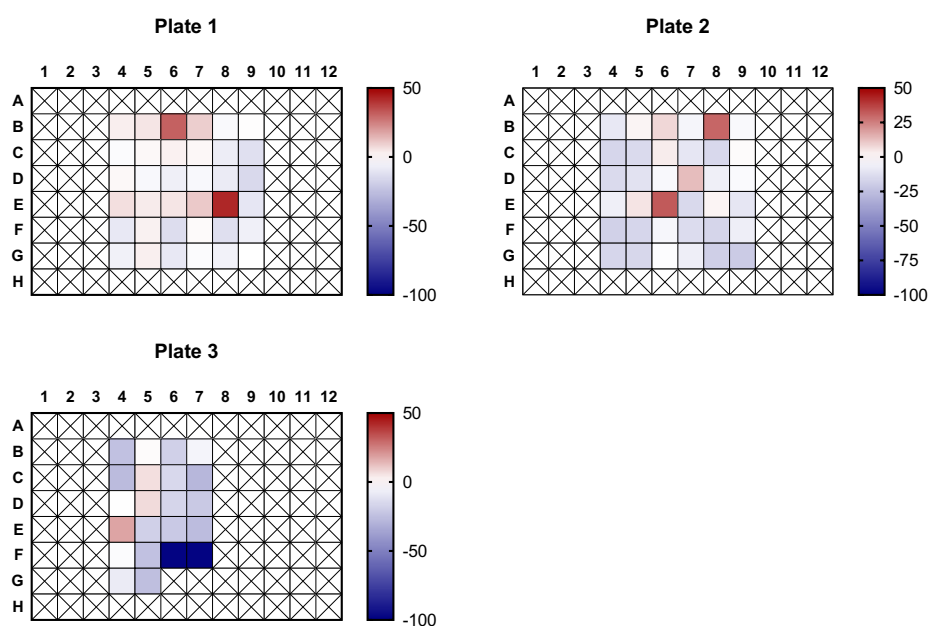


**Figure 5.6: Heatmaps of GALC secondary drug screen.** Heatmaps illustrate effect of 10  $\mu\text{M}$  and 0.1  $\mu\text{M}$  small molecules compounds on GALC activity normalised relative to intraplate DMSO vehicle only control. Activators, displaying an increase in enzyme activity, are indicated in red; whereas, inhibitors, displaying a decrease in enzyme activity, are indicated in blue. No change in GALC activity is depicted in white. All vehicle only DMSO control wells are denoted with an 'X'. The secondary screen had robust statistical parameters with a mean Z-factor of 0.62. SEM of  $\pm 0.11$ .

As part of the secondary screen, the 47 compounds selected were also screened at 0.1  $\mu\text{M}$  for their effects against temperature destabilised GALC. The GALC enzyme was destabilised by freeze/thaw cycles which destabilises protein structure and decreases enzyme activity (Bhatnagar et al. 2007). Screening against destabilised enzyme may identify compounds, normally those identified as inhibitors, which can also act as molecular chaperones that stabilise enzyme conformation, such as ambroxol, ibudilast and mycophenolate mofetil, which in the act of stabilising the enzyme structure now appear as activators (Figure 5.7).

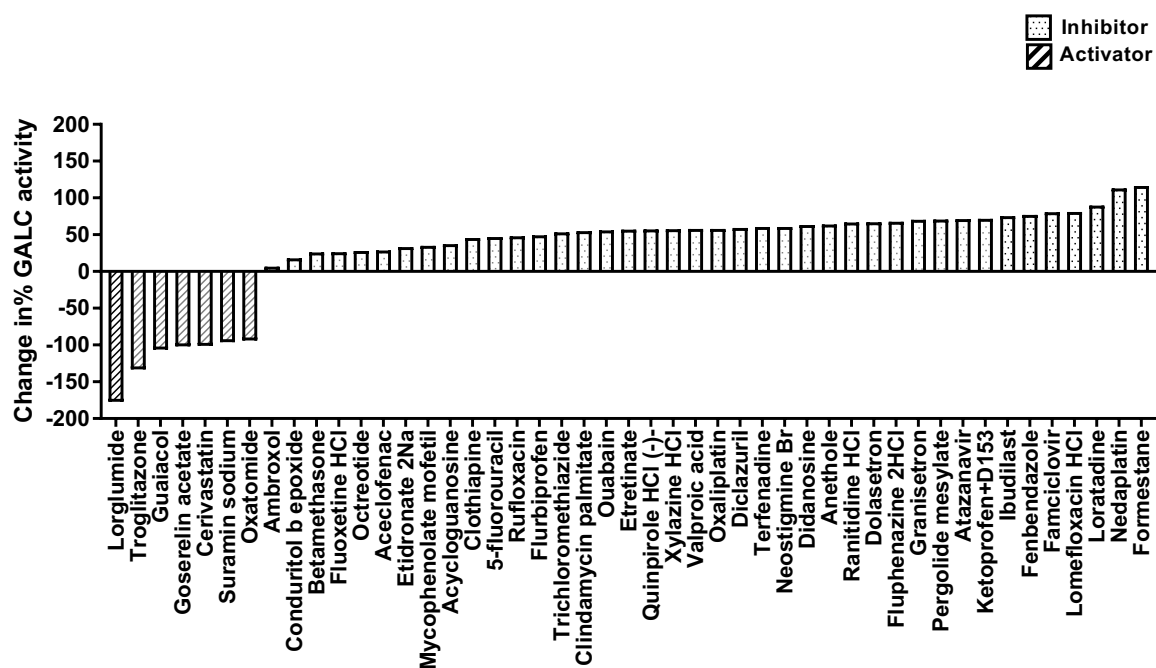


**Figure 5.7: Secondary screen on destabilised GALC.** Change in GALC activity as a percentage of untreated homogenate following freeze/thaw cycles for destabilisation of GALC.

### 5.3.3 Selecting modulators of GALC for cell-based screening

The secondary screens against destabilised GALC allowed for around 40 small molecule chaperones to be identified. Of these potential small molecule chaperones, 7 small molecules that had an effect at lower concentrations (Figure 5.6) were identified. Based on a combination of the results of the primary screen, the secondary screen and their favourable physiochemistry outlined in Table 5.2 (Lipinski et al. 2001), 3 compounds were selected for progressing to testing in cells. These 3 hit compounds were further explored in Krabbe disease patient cells in a final year project and will be further explore in other LSD patient cells by the ELE lab.

**Table 5.2: Physical and chemical properties of compounds that activated destabilised GALC and were chosen for subsequent cell-based screening.** Compounds in bold denote the compounds that were selected for further screening. Underlined text indicates the characteristic that led these compounds to be excluded from further screening.

Compounds	Molecular Mass	H acceptor	H donor	xLogP3:	Target
<b>Ambroxol</b>	378.108	3	3	2.6	Secolytic agent
<b>Ibudilast</b>	230.311	2	0	3.36	Phosphodiesterase inhibitor
<b>Mycophenolate mofetil</b>	433.501	8	1	3.2	IMPDH inhibitor
Rantidine HCL	350.865	<u>7</u>	<u>3</u>	<u>0.2</u>	<u>H2 receptor antagonist</u>
Neostigime Br	303.2	3	0	<u>-1.6</u>	<u>Acetylcholinesterase inhibitor</u>
Quabain	<u>584.659</u>	<u>12</u>	<u>8</u>	<u>-1.7</u>	<u>Na<sup>+</sup>/K<sup>+</sup> ATPase inhibitor</u>
Quiniprole HCL	255.659	12	<u>2</u>	2-7	Dopamine receptor agonist

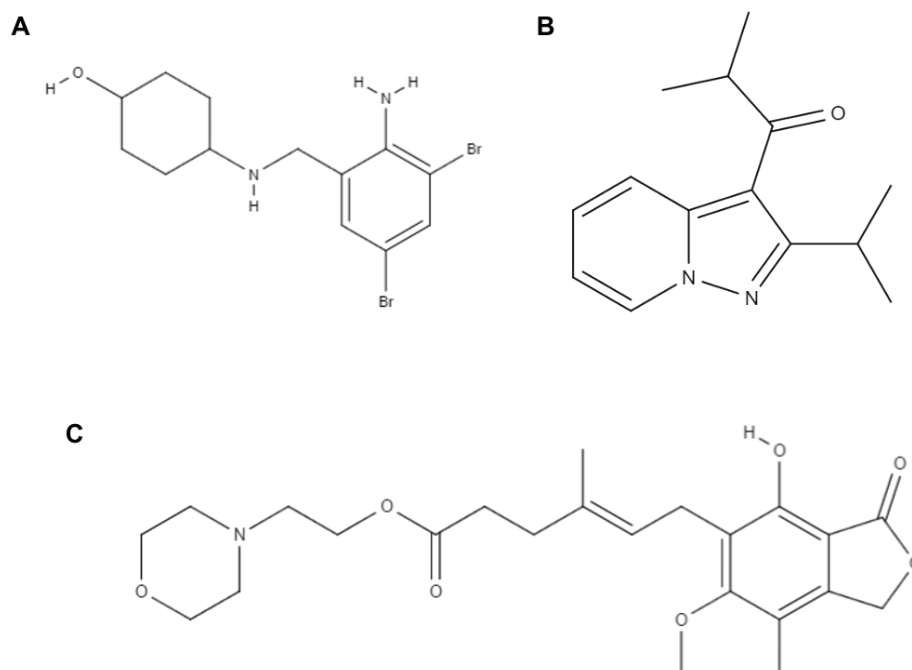


**Figure 5.8: Structure of compounds taken further for cell-based screening.** Chemical structures of the selected small molecules (A) ambroxol (CID:2132), (B) ibudilast (CID:3671) and (C) mycophenolate mofetil (CID:5281078). Structures were adapted from PubChem (PubChem CID 2132 ; PubChem CID 3671 ; PubChem CID 5281078).

#### **5.3.4 Repurposing miglustat for CLN2, CLN7 and CLN8**

Miglustat, an approved therapy for the LSD Gaucher disease and NPC1 (Bennett and Mohan 2013), has been suggested to be of benefit to other LSDs such as Fabry disease and CLN5 disease (Heare et al. 2007). As a result of this, the effects of miglustat on CLN2, CLN7 and CLN8 patient cells was explored starting with its effects on lysosomal area (measured in live cells using LysoTracker green as outlined in Section 5.2). All three, NCLs explored in this section display a significant increase in lysosomal staining area when compared to the control with a more than 3-fold increase in CLN2 HF, more than 2-fold increase in CLN7 474 HF and a 3-fold increase in CLN8 534 HF (Figure 5.9). Of the three diseases, CLN2 HF was the only one that showed a significant 1.5-fold decrease in lysosomal area between the untreated and the miglustat treated cells (Figure 5.9 B). The treated CLN7 474 HF and CLN8 354 HF were no longer significantly higher than the untreated controls indicating that a reduction in lysosomal volume (of 1.3-fold and 1.6-fold respectively) was seen following treatment.

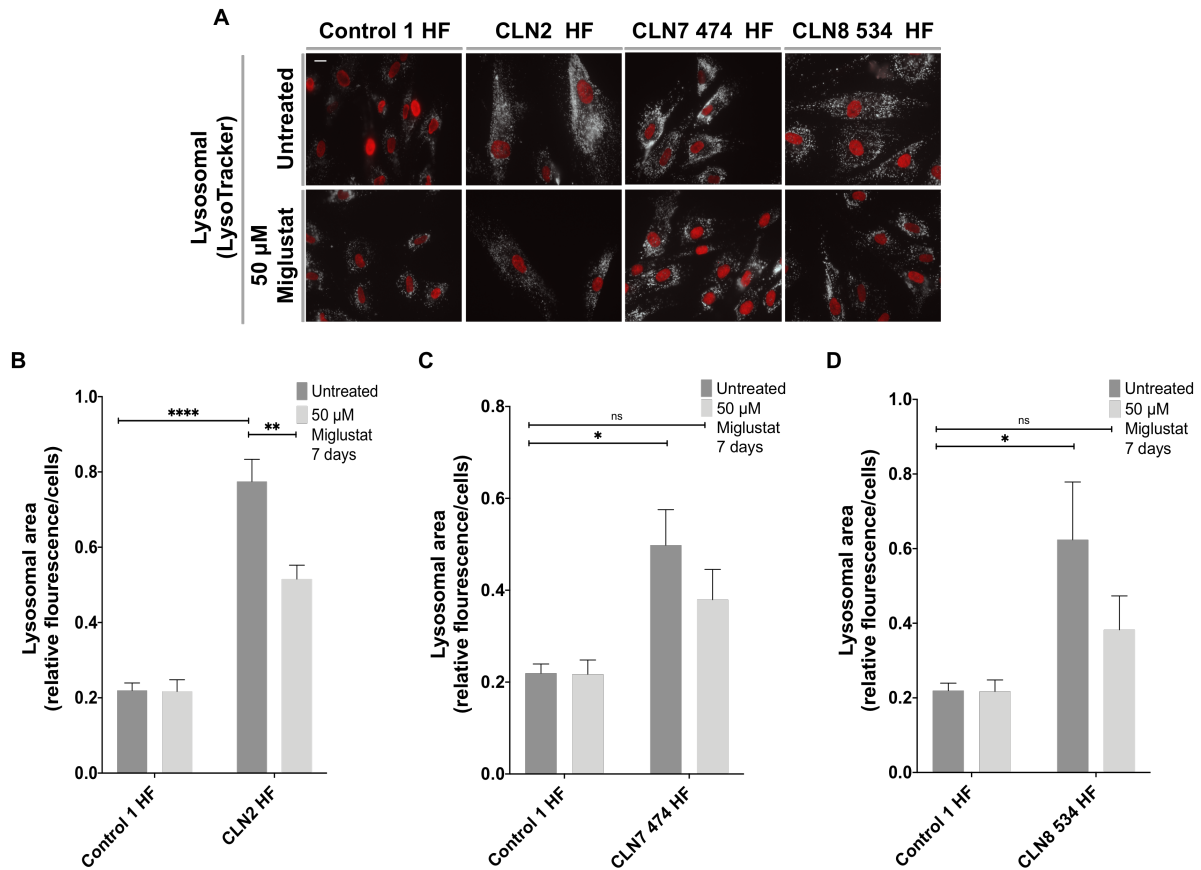


**Figure 5.9: Effect of miglustat on lysosomal area in CLN2, CLN7 and CLN8 patient cells. A:** Representative images of lysosomal staining (LysoTracker, greyscale) quantified in **B-D** with a Hoescht33342 nuclear counter stain pseudo coloured red. Scale bar = 10 µm. Quantitative analysis of lysosomal area in control, CLN2 (**B**), CLN7 (**C**) and CLN8 (**D**) patient fibroblasts. The graph represents data N = 4. Error bars indicate SEM. \* $p \leq 0.05$ , \*\* $p \leq 0.01$ , \*\*\*\* $p \leq 0.0001$ , two-way ANOVA with post-hoc Tukey.

### 5.3.5 Effect of miglustat on autophagy in CLN2, CLN7 and CLN8

As a decrease in the lysosomal area was seen in CLN2 HF, CLN7 474 HF and CLN8 534 HF the effects of miglustat treatment on further cellular phenotypes was examined. The next cellular phenotype that was examined was autophagic vacuole accumulation (Figure 5.10). As seen in Figure 5.10, untreated CLN7 474 HF had significantly more autophagic vacuole staining, using CytolD, compared to the untreated control; whereas, the miglustat treated CLN7 474 HF was no longer significantly higher than the untreated control (Figure 5.10 B). Miglustat has no effect on the area of autophagic vacuole staining in CLN2 HF as both the treated and untreated were significantly higher than the control 1 HF (Figure 5.10 B). There was a

large amount of variability seen in CLN8 534 HF (as seen in Chapter 3) which means that there was no significant difference seen in either the untreated or the treated CLN8 534 HF (Figure 5.10 D).

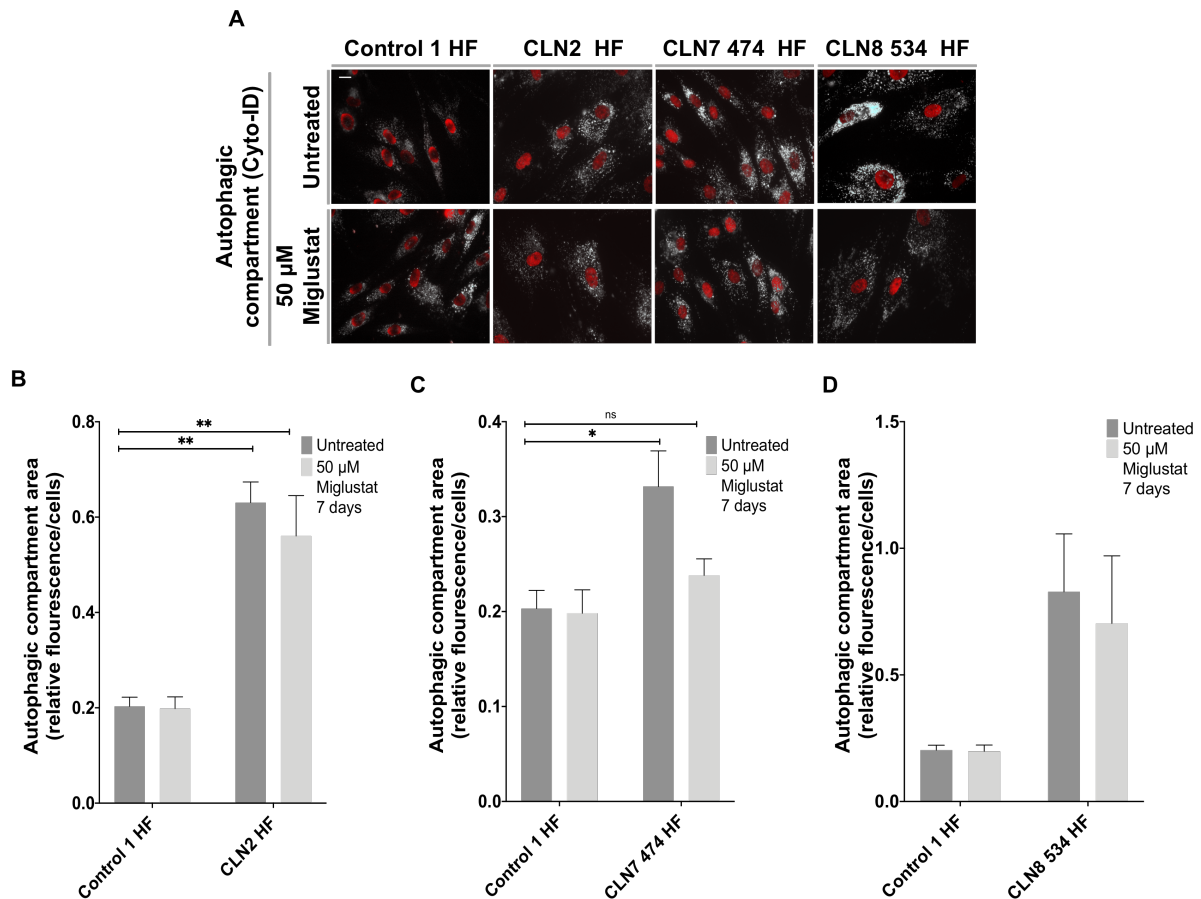


**Figure 5.10: Autophagic compartment area in CLN2, CLN7 and CLN8 patient cells following miglustat treatment. A:** Representative images of autophagic compartment staining (Cyto-ID, greyscale) quantified in **B**, with a Hoescht33342 nuclear counter stain pseudo coloured red. Scale bar = 10 µm. **B:** Quantitative analysis of autophagic compartment area in control, CLN2, CLN7 and CLN8 patient fibroblasts. The graph represents data from N = 3. The error bars indicate SEM. \* $p \leq 0.05$ , \*\* $p \leq 0.01$ , two-way ANOVA with post-hoc Tukey.

### 5.3.6 Effect of miglustat on ganglioside GM1 in CLN2, CLN7 and CLN8

Another classical phenotype seen in many LSDs is endo-lysosomal (Lachmann et al. 2004) trafficking and accumulation of ganglioside GM1 and thus the localisation of ganglioside GM1 was measured using CtxB-FITC. An increase in miss localised ganglioside GM1 in puncta is indicative of endo-lysosomal defect and of accumulation

of the ganglioside GM1 lipid (Sugimoto et al. 2001). Miglustat has previously been shown beneficial to the endo-lysosomal trafficking and storage of ganglioside GM1 which led this study to test this in the NCLs CLN2, CLN7 and CLN8 (Figure 5.11). All CLN2 HF, CLN7 474 HF and CLN8 534 HF showed a significant increase in punctate distribution of ganglioside GM1 (Figure 5.11). Following miglustat treatment the localisation of punctate ganglioside GM1 is significantly reduced in CLN2 HF compared to the untreated indicating that miglustat may be of benefit to this cellular phenotype in CLN2 disease (Figure 5.11 A & B). CLN7 474 HF and CLN8 534 HF do not show a significant decrease in punctate ganglioside GM1 following miglustat treatment; however, the treated CLN7 474 HF and CLN8 534 HF no longer have significantly higher percentage of cells with punctate ganglioside GM1 (Figure 5.11 A, C & D) potentially suggesting an improvement in the localisation of ganglioside GM1.

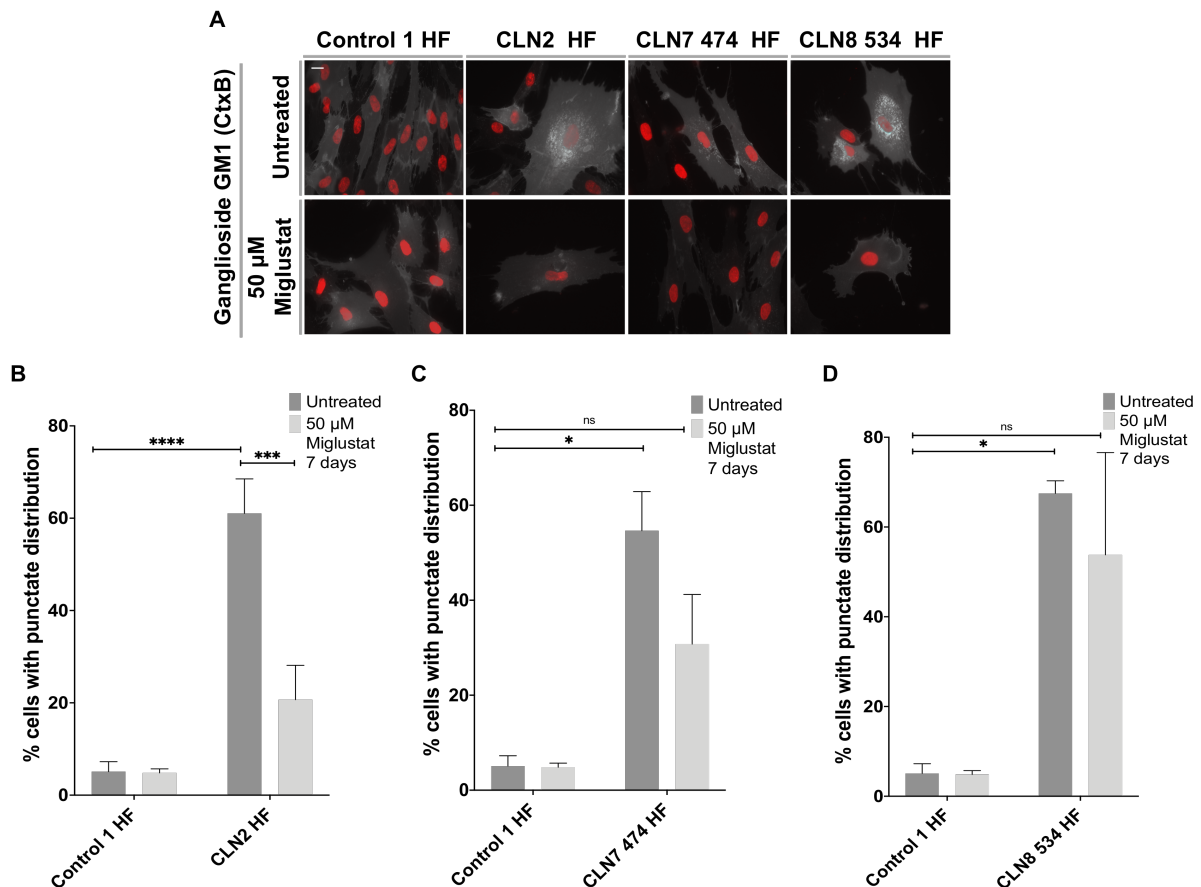


**Figure 5.11: Effect of miglustat on ganglioside GM1 punctate distribution in CLN2, CLN7 and CLN8 patient fibroblasts.** **A:** Representative images of ganglioside GM1 (CtxB-FITC, greyscale) quantified in **B-D**, with a Hoescht33342 nuclear counter stain pseudo coloured red. Scale bar = 10  $\mu\text{m}$ . Count analysis of percentage cells with ganglioside GM1 puncta present in control, CLN2 (**B**), CLN7 (**C**) and CLN8 (**D**) patient fibroblast. The graph represents data from N = 4. The error bars indicate SEM. \* $p \leq 0.05$ , \*\*\* $p \leq 0.001$ , \*\*\*\* $p \leq 0.0001$ , two-way ANOVA with post-hoc Tukey.

### 5.3.7 Effect of miglustat on $\text{Ca}^{2+}$ stores in CLN2, CLN7 and CLN8

Lysosomal storage of glycosphingolipids has previously been shown to impact upon lysosomal, ER and mitochondrial  $\text{Ca}^{2+}$  stores and homeostasis (Lloyd-Evans et al. 2008). The effect of miglustat treatment on  $\text{Ca}^{2+}$  stores was explored starting with CCCP which induced mitochondrial  $\text{Ca}^{2+}$  release as outlined in Chapter 2. This showed that although CLN2 HF, CLN7 474 HF and CLN8 534 HF have slightly lower overall CCCP mediated  $\text{Ca}^{2+}$  release values there was no significant difference seen between these and the control (Figure 5.12). There was also no significant effect of miglustat treatment on the levels of CCCP mediated  $\text{Ca}^{2+}$  release (Figure 5.12).

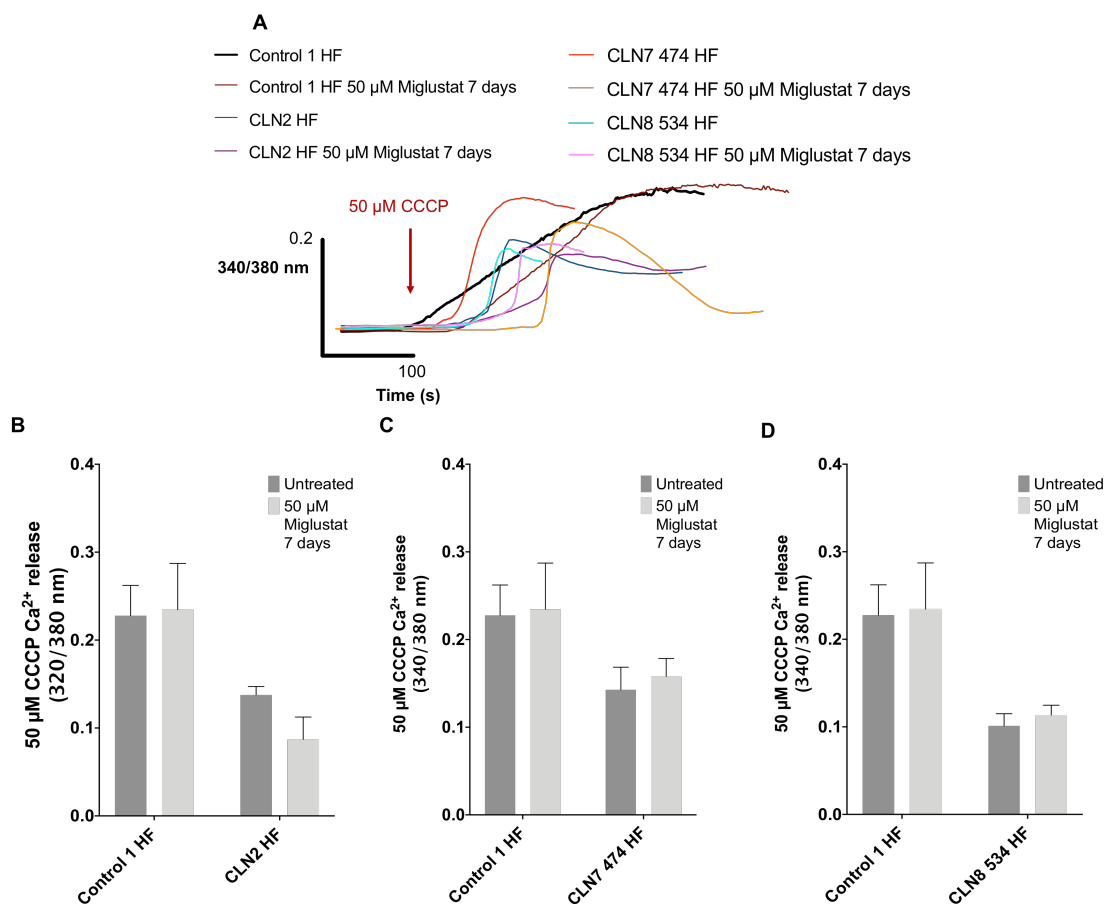


**Figure 5.12: CCCP mediated mitochondrial  $\text{Ca}^{2+}$  release in CLN2, CLN7 and CLN8 patient fibroblast following miglustat treatment.** **A:** Representative traces of the average data for CCCP (indicated by the red arrow) mediated mitochondrial  $\text{Ca}^{2+}$  quantified in **(B-D)**. Quantified change in intracellular  $\text{Ca}^{2+}$  release following CCCP **(A)** in control 1 HF, CLN2 HF **(B)**, CLN7 474 HF **(C)** & CLN8 534 HF **(D)** with whole cells selected as the region of interest in  $N = 3-5$ . Error bars indicate SEM.

Ryanodine mediated  $\text{Ca}^{2+}$  release from the ER ryanodine receptor and basal resting  $\text{Ca}^{2+}$  levels also showed no clear difference between the control 1 HF and CLN2 HF, CLN7 474 HF and CLN8 534 HF (Figure 5.13). Additionally, there was no significant effect of miglustat treatment on basal  $\text{Ca}^{2+}$  or ryanodine mediated ER  $\text{Ca}^{2+}$  release (Figure 5.13).

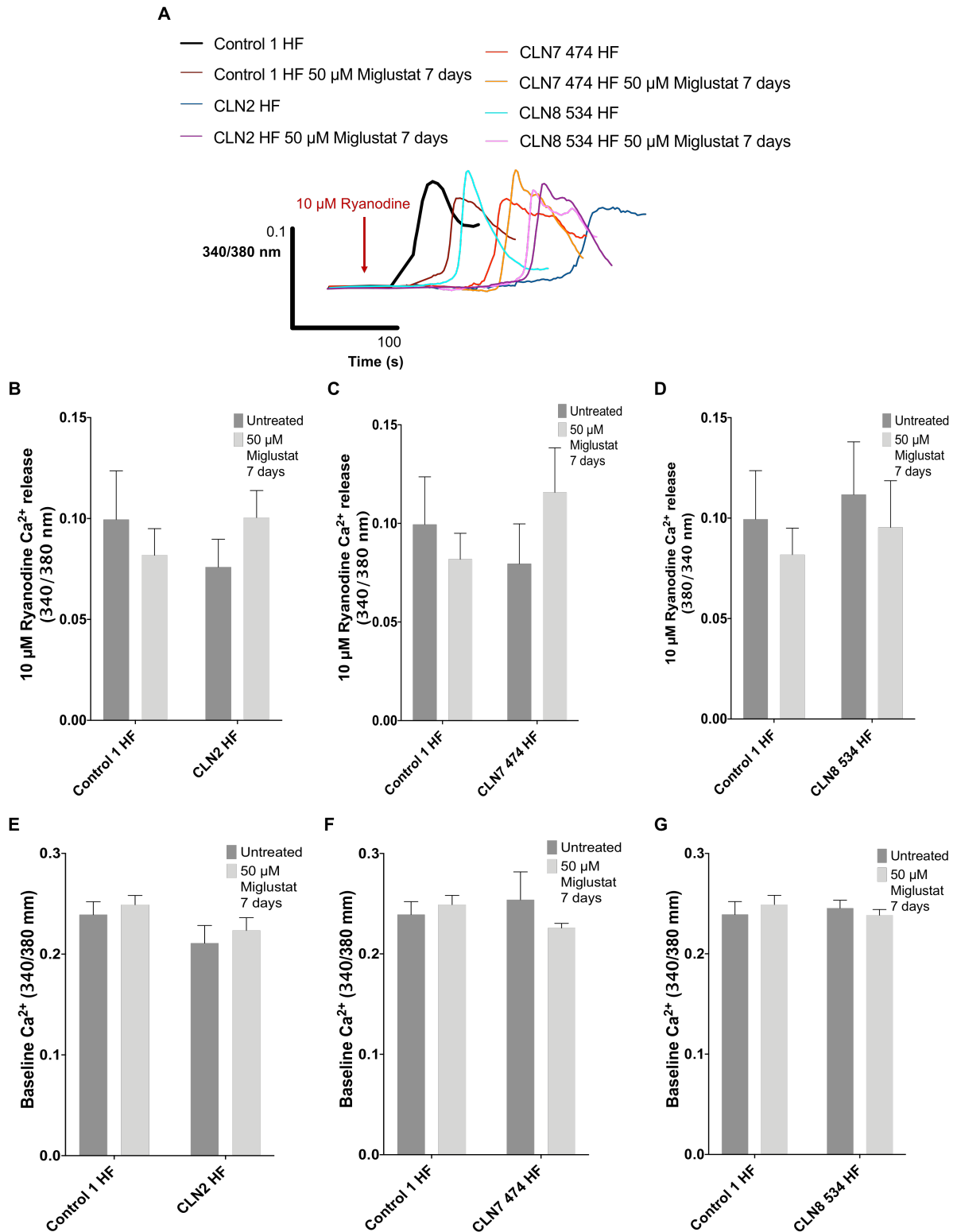


**Figure 5.13: Ryanodine mediated  $\text{Ca}^{2+}$  release in CLN2, CLN7 and CLN8 patient fibroblast following miglustat treatment. A:** Representative traces of the average data for ryanodine (indicated by the red arrow) mediated ER  $\text{Ca}^{2+}$  quantified in (B-D). Quantified change in intracellular  $\text{Ca}^{2+}$  release following ryanodine (A) in control 1 HF, CLN2 HF (B), CLN7 474 HF (C) & CLN8 534 HF (D). (E-G) Intracellular  $\text{Ca}^{2+}$  release in control 1 HF, CLN2 HF (E), CLN7 474 HF (F) & CLN8 534 HF (G) with whole cells selected as the region of interest in N = 4-5. Error bars indicate SEM.

### 5.3.8 Lysosomal volume following miglustat in CLN8

The potential beneficial effect of miglustat in CLN8 534 HF seen above led this project to explore the effect of miglustat on lysosomal volume in all CLN8 patient cell lines using a lysotracker plate assay (Figure 5.14). As seen in Chapter 3, Figure 3.1, the only one of the CLN8 patient cells lines that had a significant increase in lysosomal volume, when measured by plate assay using LysoTracker green, was CLN8 534 HF. The LysoTracker following treatment with miglustat was no longer significant in the CLN8 534 HF compared to the untreated control 1 HF (Figure 5.14). Miglustat treatment has no effect on lysosomal volume on any of the other CLN8 patient cell lines (Figure 5.14).

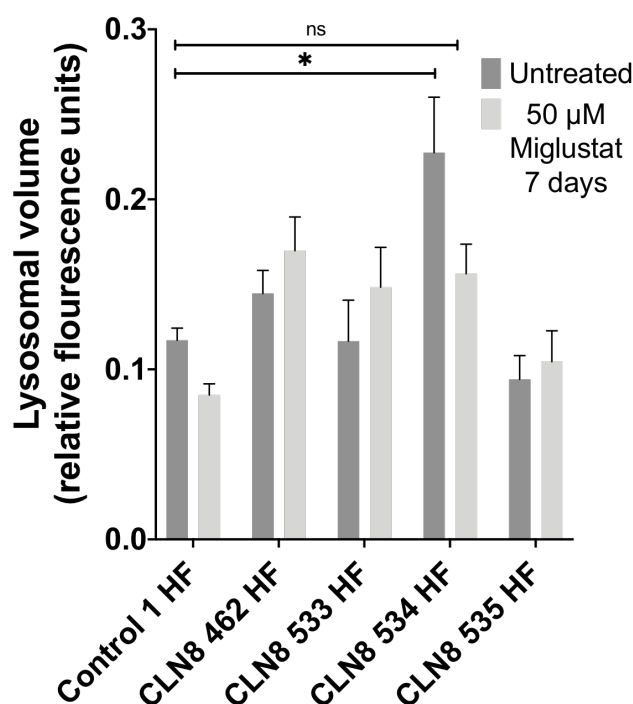


**Figure 5.14: Lysotracker plate assay in CLN8 patient cells following miglustat treatment.** Quantitative plate reader data of control 1 HF and CLN8 HF cells stained with LysoTracker following 7-day treatment with 50  $\mu$ M miglustat. Graphs represent data from N = 2. The error bars indicate SEM. In each N comprised of 5 well of cells per cell line. \* $p \leq 0.05$ , Two-way ANOVA with post-hoc Tukey.

### **5.3.9 Curcumin nutraceuticals for NPC1, NPA, CLN3, CLN7, CLN8 and CLN10**

As mentioned above, in Section 5.1.4 and in Chapter 1, curcumin has been proposed to have beneficial effects for NPC1 disease through its ability to modulate  $\text{Ca}^{2+}$  (Lloyd-Evans et al. 2008). Therefore, organelle  $\text{Ca}^{2+}$  defects in several lysosomal storage diseases were explored to identify LSDs that may benefited from curcumin nutraceuticals. This was done by starting with analysis of lysosomal  $\text{Ca}^{2+}$  by inducing lysosomal  $\text{Ca}^{2+}$  release into the cytoplasm of Fura 2,AM loaded cells using 500  $\mu\text{M}$  GPN after clamping, and therefore removing, of all other  $\text{Ca}^{2+}$  stores with 2  $\mu\text{M}$  ionomycin (Figure 5.15). NPC1 patient cells are used here as a control NPC1 disease is known to have reduced lysosomal  $\text{Ca}^{2+}$  (Lloyd-Evans et al. 2008).

The reduction in lysosomal  $\text{Ca}^{2+}$  seen in CLN8 534 HF (Figure 3.16) was further confirmed in Figure 5.15. Similarly, GPN induced  $\text{Ca}^{2+}$  release was significantly lower in NPA, CLN7 474 HF, CLN8 534 HF, CLN10 HF and as expected in NPC1. On the other hand, CLN3 HF displayed significantly increased lysosomal  $\text{Ca}^{2+}$  (Figure 5.15) as has also been reported previously (Chandrachud et al. 2015).

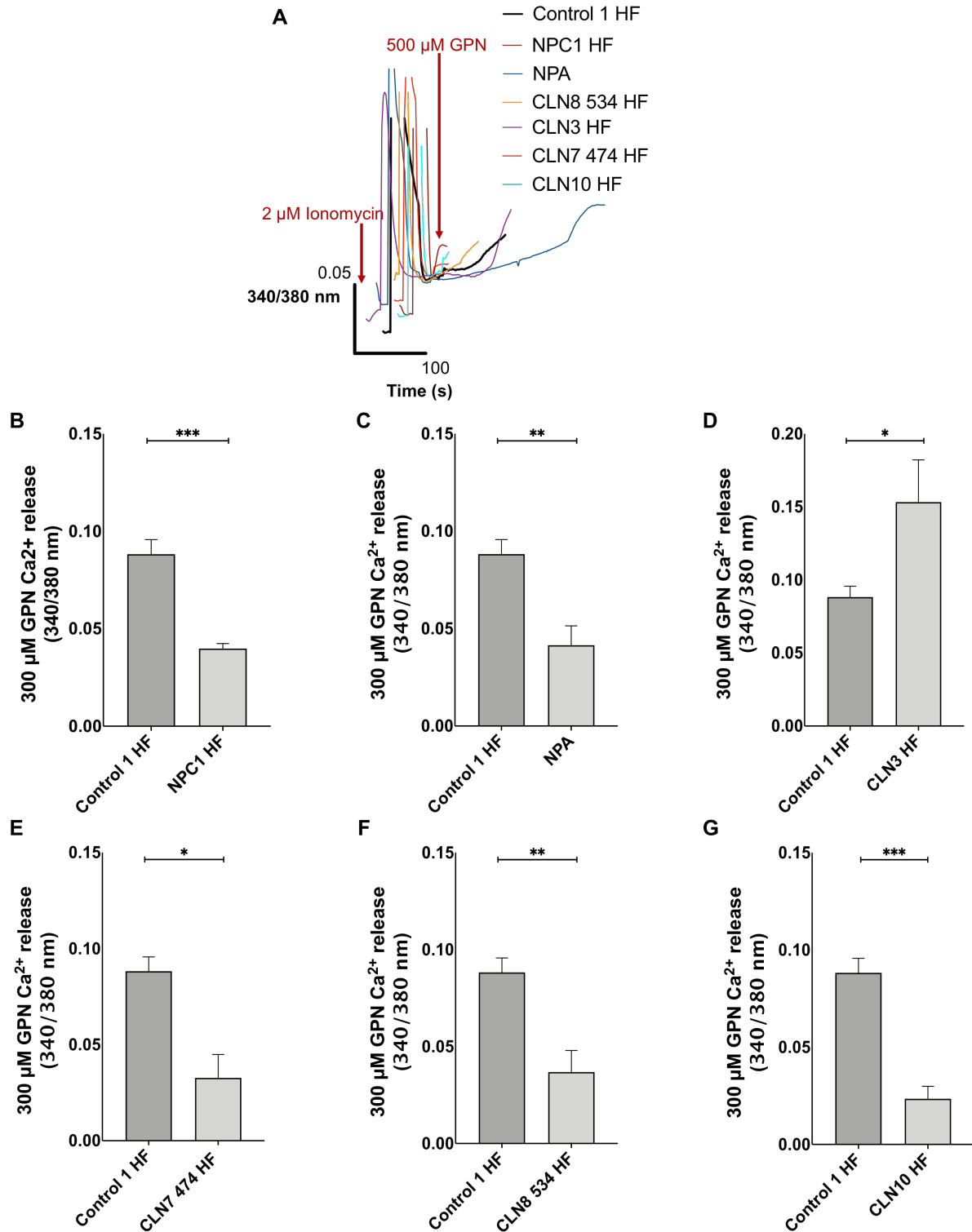


**Figure 5.15: GPN-mediated lysosomal  $\text{Ca}^{2+}$  is decreased in NPC1, CLN7 474, CLN8 and CLN10 but increased in NPA and CLN3.** **A:** Representative traces of the average data for GPN (indicated by the red arrow) mediated lysosomal  $\text{Ca}^{2+}$  release quantified in **(B-G)**. Quantified changes in intracellular  $\text{Ca}^{2+}$  release following GPN **(A)** in NPC1 HF **(B)**, NPA HF **(C)**, CLN3 HF **(D)**, CLN7 474 HF **(E)**, CLN8 534 HF **(F)** HF, CLN10 HF **(G)** and control 1 HF with whole cells selected as the region of interest.  $N = 3-5$ . The error bars indicate SEM. \* $p \leq 0.05$ , \*\* $p \leq 0.01$ , \*\*\* $p \leq 0.001$ , \*\*\*\* $p \leq 0.0001$ , two tailed t-test.

Following the defects in lysosomal  $\text{Ca}^{2+}$  seen in Figure 5.15 the levels of ER  $\text{Ca}^{2+}$  were examined before treatment with curcumin nanoformulations. Thapsigargin, which as outlined in Chapter 2 Section 2.3.8, is a competitive inhibitor of SERCA that results in ER  $\text{Ca}^{2+}$  release via the ER  $\text{Ca}^{2+}$  leak channels that subsequently activates  $\text{Ca}^{2+}$  induced  $\text{Ca}^{2+}$  release from the ER RyR and IP<sub>3</sub> receptors allowing for ER  $\text{Ca}^{2+}$  content to be measured (Figure 5.16).

Thapsigargin at a concentration of 1  $\mu\text{M}$  induced ER  $\text{Ca}^{2+}$  release, in NPC1 HF and CLN3 HF ER  $\text{Ca}^{2+}$  was the same as the control 1 HF (Figure 5.16), as previously reported (Lloyd-Evans et al. 2008; Chandrachud et al. 2015), suggesting no defect in ER  $\text{Ca}^{2+}$  content. NPA HF displayed a significant decrease in thapsigargin mediated  $\text{Ca}^{2+}$  release (Figure 5.16) suggesting a decrease in ER  $\text{Ca}^{2+}$  content, which is in keeping with previous data (Ginzburg and Futerman 2005). Conversely, CLN7 474 HF, CLN8 534 HF and CLN10 HF displayed significantly higher ER  $\text{Ca}^{2+}$  content following thapsigargin mediated  $\text{Ca}^{2+}$  release (Figure 5.16).

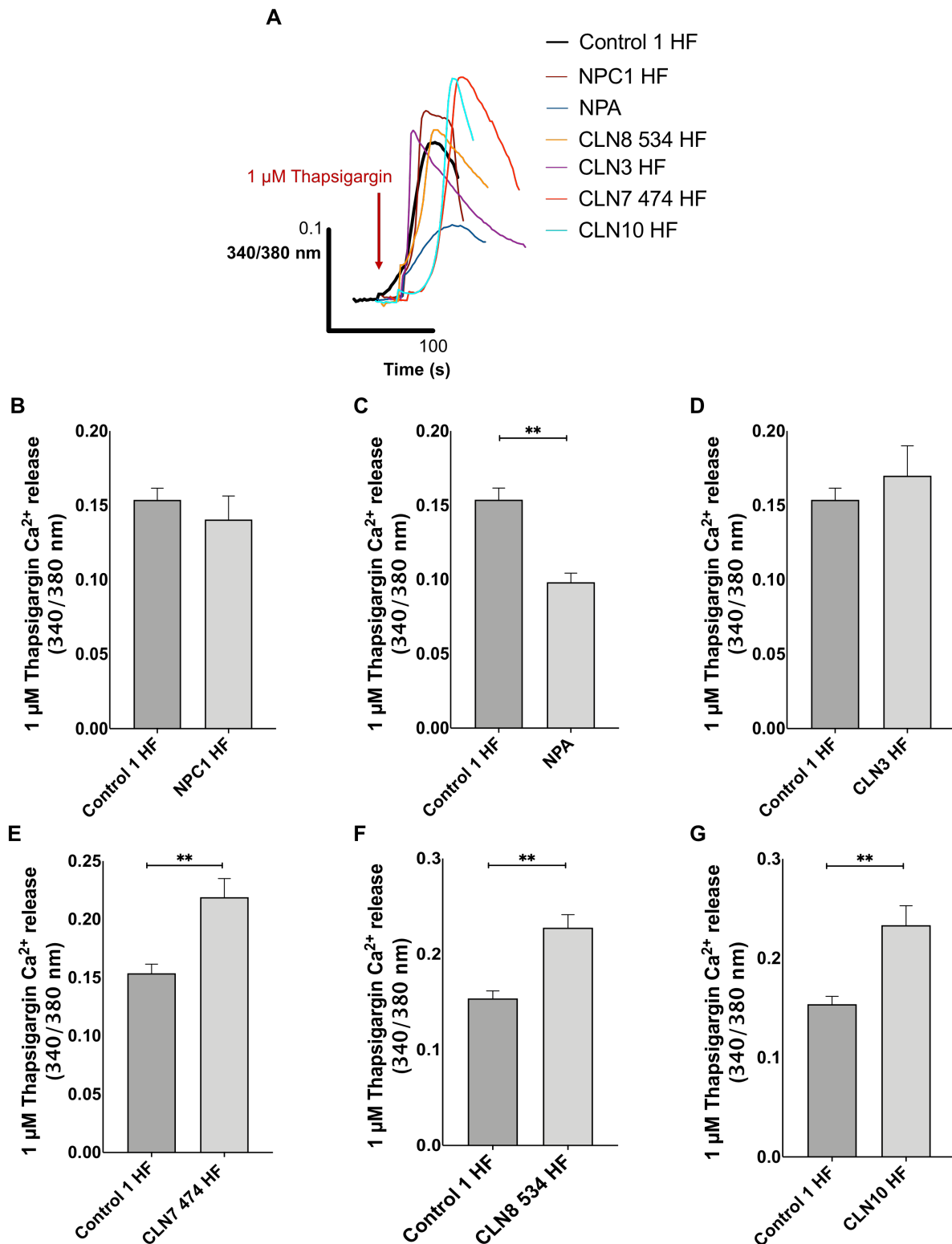


**Figure 5.16: Thapsigargin mediated  $\text{Ca}^{2+}$  is increased in CLN7, CLN8 and CLN10 but decreased in NPC.**  
**A:** Representative traces of the average data for thapsigargin (indicated by the red arrow) mediated ER  $\text{Ca}^{2+}$  release quantified in (B-G). Quantified changes in intracellular  $\text{Ca}^{2+}$  release following thapsigargin (A) in NPC1 HF (B), NPA HF (C), CLN3 HF (D), CLN7 474 HF (E), CLN8 534 HF (F), CLN10 HF (G), and control 1 HF with whole cells selected as the region of interest. N = 4-6. The error bars indicate SEM.  $**p \leq 0.01$ , two tailed t-test.

The levels of ER  $\text{Ca}^{2+}$  were also examined using ionomycin as it releases  $\text{Ca}^{2+}$  from all stores except from acidic organelles as outlined in Chapter 2 Section 2.3.8. As the ER is by far the biggest  $\text{Ca}^{2+}$  store, with mitochondrial  $\text{Ca}^{2+}$  and resting cytosolic  $\text{Ca}^{2+}$  levels being negligible in healthy cells as well as lysosomal  $\text{Ca}^{2+}$  being impermeant to ionomycin, a high concentration of ionomycin in the absence of extracellular  $\text{Ca}^{2+}$  mediates  $\text{Ca}^{2+}$  release predominantly from the ER (Figure 5.17).

There was no difference seen in ionomycin mediated  $\text{Ca}^{2+}$  release in NPC1 HF, NPA HF, CLN3 HF, CLN7 474 and CLN8 534 HF (Figure 5.16). This suggests that ER  $\text{Ca}^{2+}$  content is similar in these cell lines compared to the control 1 HF. On the other hand, CLN10 HF had significantly increased ionomycin mediated  $\text{Ca}^{2+}$  release (Figure 5.16).

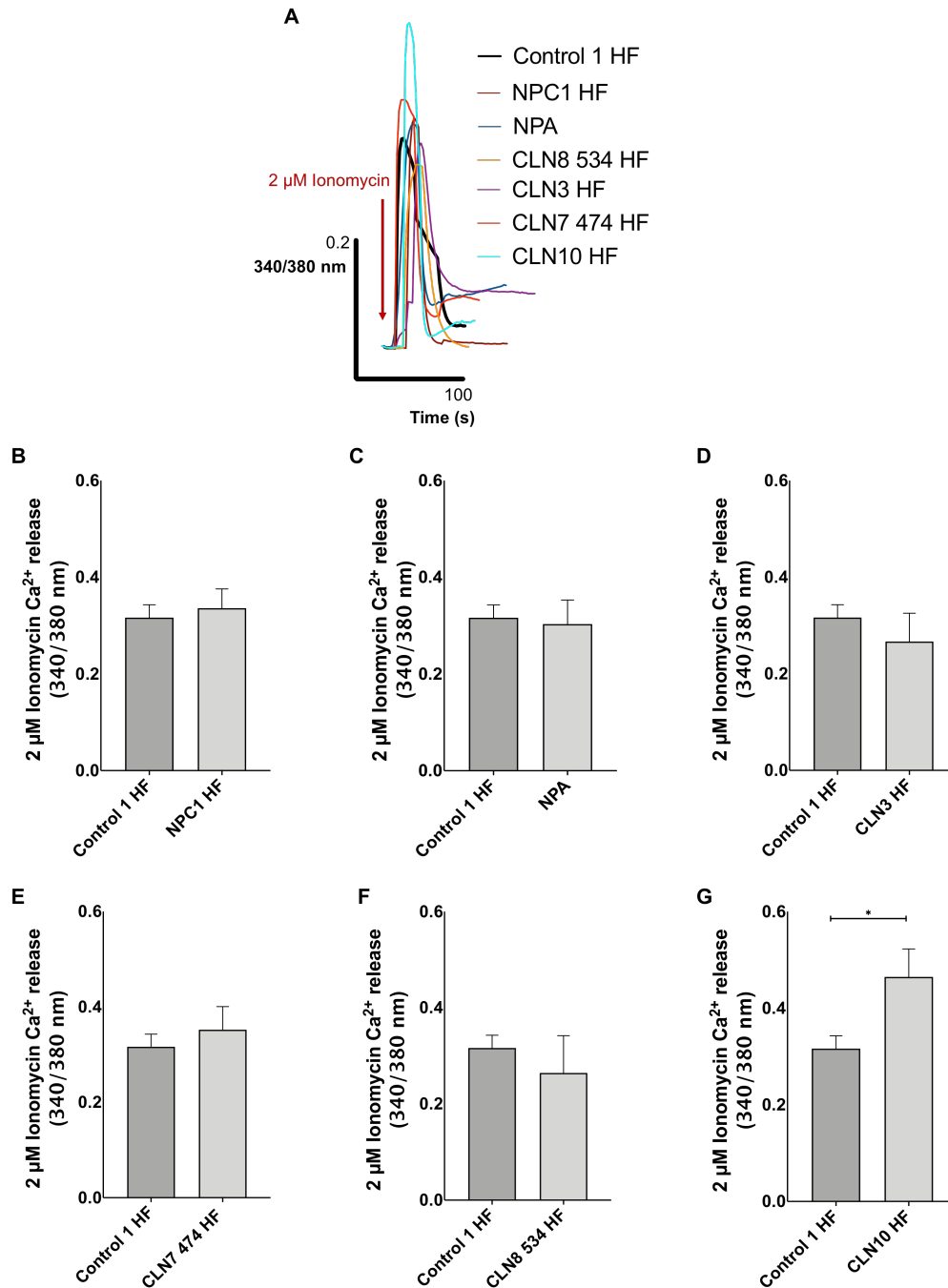


**Figure 5.17: Ionomycin mediated  $\text{Ca}^{2+}$  is significantly increased in CLN10 but not altered in NPC1, NPA, CLN3, CLN7 and CLN8.** **A:** Representative traces of the average data for ionomycin (indicated by the red arrow) mediated ER  $\text{Ca}^{2+}$  released quantified in **(B-G)**. Quantified changes in intracellular  $\text{Ca}^{2+}$  release following ionomycin **(A)** in NPC1 HF **(B)**, NPA HF **(C)**, CLN3 HF **(D)**, CLN7 474 HF **(E)**, CLN8 534 **(F)** HF, CLN10 HF **(G)** and control 1 HF with whole cells selected as the region of interest in N = 8-12. The error bars indicate SEM. \*\* $p \leq 0.01$ , two tailed t-test.

Curcumin has been proposed to increase cytosolic  $\text{Ca}^{2+}$ , and as prolonged elevation in cytosolic  $\text{Ca}^{2+}$  can be excitotoxic (Lloyd-Evans et al. 2008; D'Orsi et al. 2015), levels of basal  $\text{Ca}^{2+}$  were examined which was done by simply measuring baseline Fura-2,AM fluorescence levels (Figure 5.18). As can be seen in Figure 5.18 there was no difference in basal  $\text{Ca}^{2+}$  levels in NPC1 HF, NPA HF, CLN3 HF, CLN7 474 HF, CLN8 534 HF and CLN10 HF compared to the control.

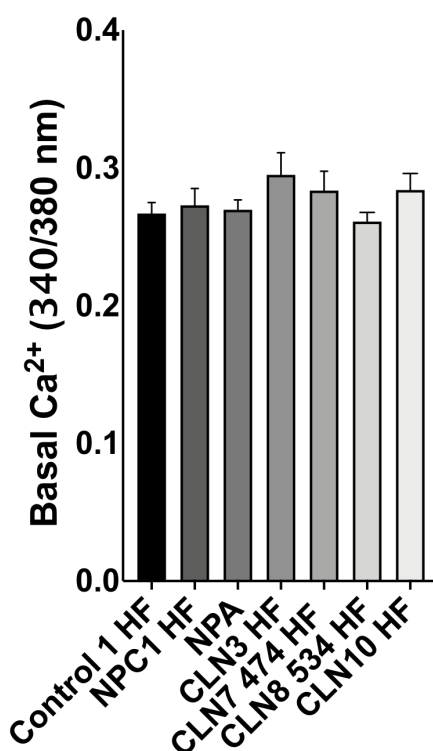


**Figure 5.18: Basal  $\text{Ca}^{2+}$  is unchanged in NPC1, NPA, CLN7 CLN8 and CLN10.** Quantified intracellular  $\text{Ca}^{2+}$  levels in NPC1 HF, NPA HF, CLN3 HF, CLN7 474 HF, CLN8 534 HF, CLN10 HF and control 1 HF with whole cells selected as the region of interest in  $N = 4-5$ . The error bars indicate SEM. No statistical significance was seen by one-way ANOVA with post hoc Tukey.

As curcumin has been reported to be beneficial to NPC1 potentially due to the decrease in lysosomal  $\text{Ca}^{2+}$  content (Lloyd-Evans et al. 2008) along with the decrease in lysosomal  $\text{Ca}^{2+}$  seen in NPA, CLN7 474 HF, CLN8 534 HF and CLN10 HF (Figure 5.15) the ability of two curcumin nanoformulations (Table 5.3) at  $30 \mu\text{M}$  for 4 and 24 hours to reduce lysosomal storage in these diseases was explored. As mentioned in the introduction, curcumin is formulated into lipid vehicle nanoformulations in order to increase its ability to cross the blood brain barrier, as such when testing the effect of

curcumin in patient cells. It is important to test the nanoformulations and not just curcumin on its own as this would be representative of what patients would take (this was explored and is outlined in the publication Badell-Grau *et al.* in prep).

**Table 5.3: Properties of the curcumin nanoformulations screened.**

Name in this study	Formulation	Producer	Reported lipid content	% Curcuminoid
BCM95s	BCM-95	Life Extension	Turmeric essential oil, lecithin, triglycerides, beeswax, sunflower oil	93%
SLN <sub>L</sub>	Solid lipid curcumin particle (Longvida)	Nutrivene	Soy lecithin, palmitate, stearic acid	23%

BCM95s curcumin treatment at 30  $\mu$ M for 24-hours led to significantly decreased lysosomal volume in CLN7 474 HF and CLN8 534 HF both of which, before treatment, have significantly higher lysosomal volume compared to the control (Figure 5.19 Ai, D & E). This suggests that BCM95s may ameliorate lysosomal dysfunction in CLN7 and CLN8 disease. In contrast, CLN3 HF and NPA HF which also have significantly higher lysosomal volume compared to the control 1 HF did not display a reduction in lysosomal volume following treatment with BCM95s (Figure 5.19 Ai, B & C). As such, BCM95s does not seem to have any beneficial effect on NPA and CLN3.

When patient cells were treated with SLN<sub>L</sub> curcumin (Figure 5.19 Aii) the cells appeared to shrivel, and cytotoxicity was observed with floating cells in some of the experimental repeats making it not possible to quantify the lysosomal area following treatment. The cytotoxic and possible increase in lysosomal volume seen suggests that SLN<sub>L</sub> curcumin may be detrimental to LSDs patients and even the control 1 HF.

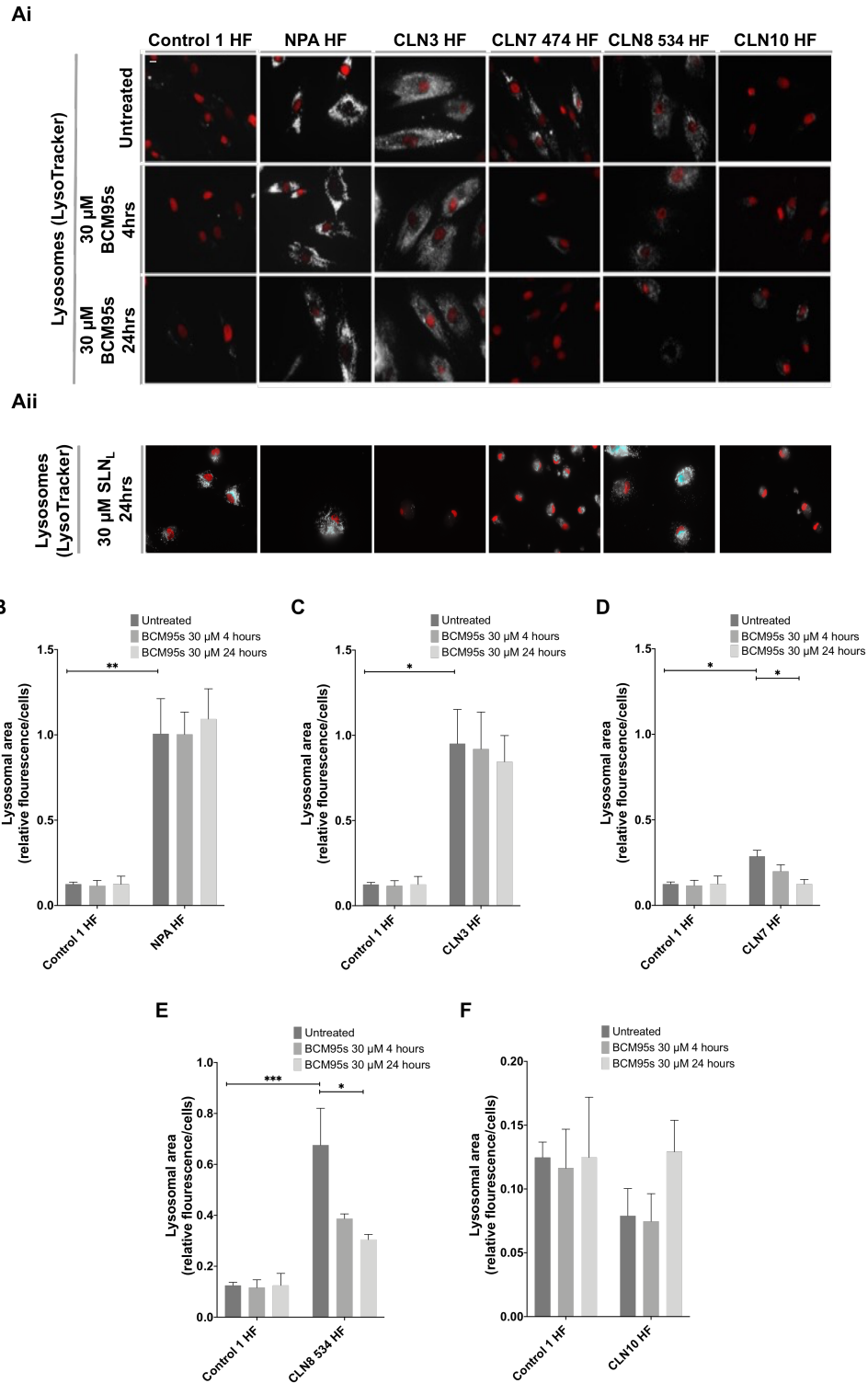


**Figure 5.19: Lysosomal area in NPA, CLN3, CLN7, CLN8 and CLN10 patient cells following curcumin BCM95s.** **Ai:** Representative images of lysosomal straining (LysoTracker, greyscale) of untreated and BCM95s curcumin treated cells quantified in **B-F**, with a Hoescht33342 nuclear counter stain pseudo coloured red. **Aii:** Representative images of lysosomal straining (LysoTracker) of cells treated with SLN curcumin. Scale bar = 10  $\mu$ m. Quantitative analysis of lysosomal area in NPA (**B**), CLN3 (**C**), CLN7 474 (**D**), CLN8 534(**E**) and CLN10 (**F**) patient fibroblasts. The graph represents data from N = 3-4. The error bars indicate SEM. \* $p \leq 0.05$ , \*\* $p \leq 0.01$ , two-way ANOVA with post-hoc Tukey.

Following the potential benefits seen on lysosomal area, the effects of BCM95s curcumin on cholesterol puncta area (Figure 5.20) were investigated, as cholesterol is a common secondary storage molecule across many LSDs (Platt et al. 2012; Vanier and Latour 2015). All the cell lines explored, NPA HF, CLN3 HF, CLN7 474 HF, CLN8 534 HF, CLN10 HF appeared to have increased cholesterol puncta; however, only NPA HF, CLN3 HF and CLN10 HF had significantly increased cholesterol puncta compared to the control 1 HF (Figure 5.21 A, B, C & F). There was no effect on the levels of cholesterol puncta area following BCM95s treatment (Figure 5.20).

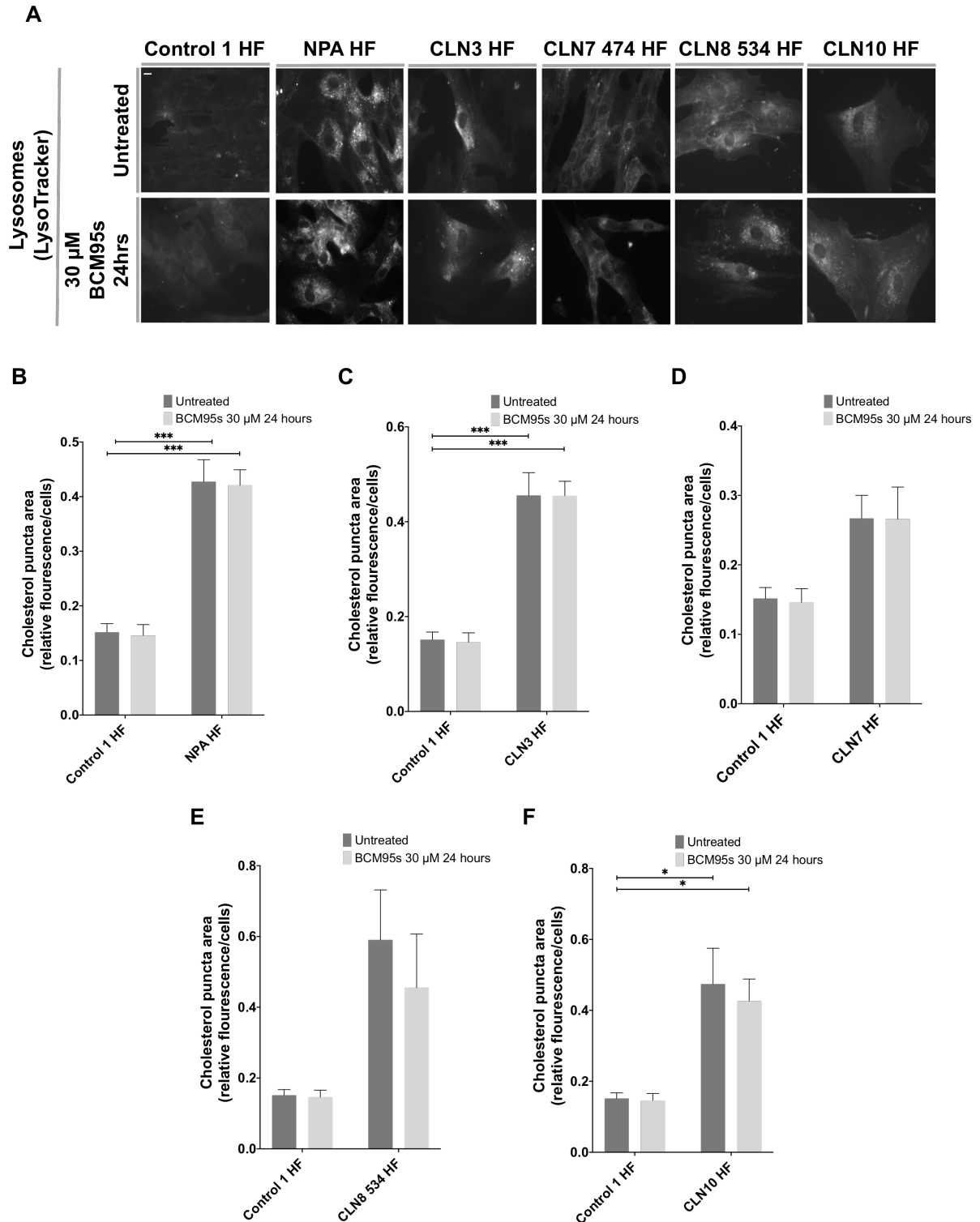


**Figure 5.20: Elevated cholesterol area in NPA, CLN3, CLN7 and CLN8 and CLN10 is not affected by BCM95s treatment. A:** Representative images of cholesterol staining (filipin) quantified in **B-F** of untreated and BCM95s curcumin treated cells. Scale bar = 10  $\mu$ m. Quantitative analysis of lysosomal area in NPA (**B**), CLN3 (**C**), CLN7 474 (**D**), CLN8 534 (**E**) and CLN10 (**F**) patient fibroblasts. The graph represents data from N = 3-4. The error bars indicate SEM. \* $p \leq 0.05$ , \*\* $p \leq 0.01$ , two-way ANOVA with post-hoc Tukey.

During this project, and in other projects carried out in the Lloyd-Evans lab (Badell-Grau *et al.* in prep), *in vitro* cytotoxicity was seen with some of the nanoformulations of curcumin, including those being taken by NPC patients. Of 7 nanoparticles tested, 3 were found to be toxic and this could not be attributed to either the nanoparticle alone as it did not induce toxicity in the absence of curcumin or its ability to release ER  $\text{Ca}^{2+}$  as all were equally efficient and elevated basal  $\text{Ca}^{2+}$  to the same extent after 24 hours (Badell-Grau *et al.* in prep).

To determine how the combination was inducing toxicity, changes in mitochondrial  $\text{Ca}^{2+}$  levels in NPC1 patient HF were explored. This was done by treating the cells with two different curcumin nanoformulations, a fatty acid enriched  $\text{SLN}_L$  that incurs toxicity, as mentioned above in Figure 5.19, and a non-fatty acid containing BCM95s, at a concentration of  $30\mu\text{M}$  for 24 hours, loaded the cells with Fura 2,AM and stimulated mitochondrial  $\text{Ca}^{2+}$  release using  $5\mu\text{M}$  antimycin /  $5\mu\text{M}$  oligomycin (Figure 5.21) as explained in Chapter 2. Following treatment with both nanoformulations in NPC1 patient and control HFs no significant reductions in mitochondrial  $\text{Ca}^{2+}$  release was observed apart from the control HF treated with  $\text{SLN}_L$  which had a significant 3.5-fold lower mitochondrial  $\text{Ca}^{2+}$  (Figure 5.21) compared to the untreated control.

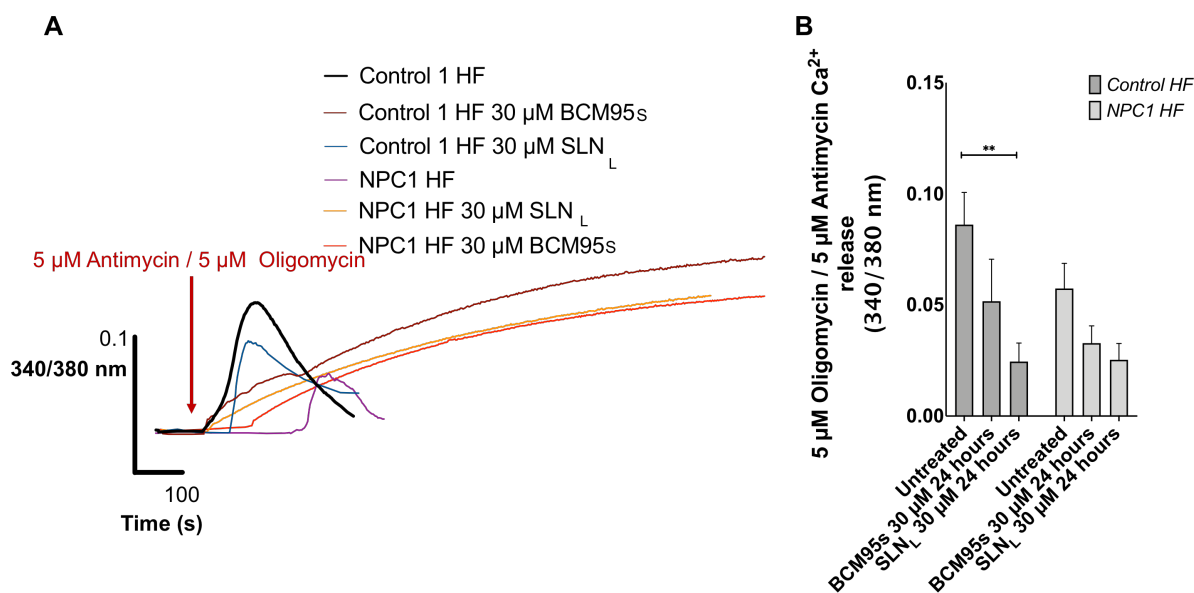


**Figure 5.21: Treatment with curcumin nanoformulations decreases Antimycin / Oligomycin mediated mitochondria Ca<sup>2+</sup> release in control HF.** **A:** Representative traces of the average data for antimycin / oligomycin (indicated by the red arrow) mediated mitochondrial Ca<sup>2+</sup> released quantified in **(B)**. **B:** Quantified changes in intracellular Ca<sup>2+</sup> release following antimycin / oligomycin NPC1 HF and control 1 HF with whole cells selected as the region of interest. N = 4-5. The error bars indicate SEM. \*\*p  $\leq$  0.01, two-way ANOVA with post-hoc Tukey.

Having observed reduced mitochondrial Ca<sup>2+</sup> in control cells following 24 hour treatment with BCM95s and SLN<sub>L</sub> curcumin nanoformulations the levels of Ca<sup>2+</sup> in the mitochondria were explored using another methods of measuring Ca<sup>2+</sup> with Rhod-2,AM as outlined in Chapter 2. The use of Rhod-2,AM (Figure 5.22) was loaded into both cytoplasm and mitochondria and then following a pulse chase, it was removed from the cytoplasm by the multi drug efflux pumps but the Rhod-2,AM was retained in the mitochondria as the rhodamine dye is trapped in the mitochondria. This further confirmed the reduction in mitochondrial Ca<sup>2+</sup> seen in *Npc1*<sup>-/-</sup> glia compared to the *Npc1*<sup>+/+</sup> control as well as a further reduction in mitochondrial Ca<sup>2+</sup> in both cell lines following 24-hour treatment with the curcumin nanoformulations BCM95s and SLN<sub>L</sub>. The fine puncta seen when staining with Rhod-2,AM corresponds to mitochondrial Ca<sup>2+</sup> stores which in the untreated cells are dispersed throughout the cytosol with the presence of more Ca<sup>2+</sup> inside the wild-type mitochondria (higher peaks in the associated graphs).

After treatment with SLN<sub>L</sub> for 24 hours, however, the puncta appears to cluster in the perinuclear region in the control *Npc1*<sup>+/+</sup> glia whilst swelling of mitochondria is observed in the *Npc1*<sup>-/-</sup> cells treated with SLN<sub>L</sub> which indicates, in both cases, the presence of mitochondrial stress, albeit to a greater extent in *Npc1*<sup>-/-</sup>. BCM95s, which does not cause any toxicity, also reduces the peak height of Ca<sup>2+</sup> within mitochondria in both *Npc1*<sup>+/+</sup> and *Npc1*<sup>-/-</sup>. Nonetheless, it also increases cytosolic Ca<sup>2+</sup> via inhibition of ER SERCA and as such a combination of elevated cytosolic Ca<sup>2+</sup> and reduced mitochondrial Ca<sup>2+</sup> can be seen. No damage to the mitochondrial network was observed following BCM95s as was observed with SLN<sub>L</sub>.

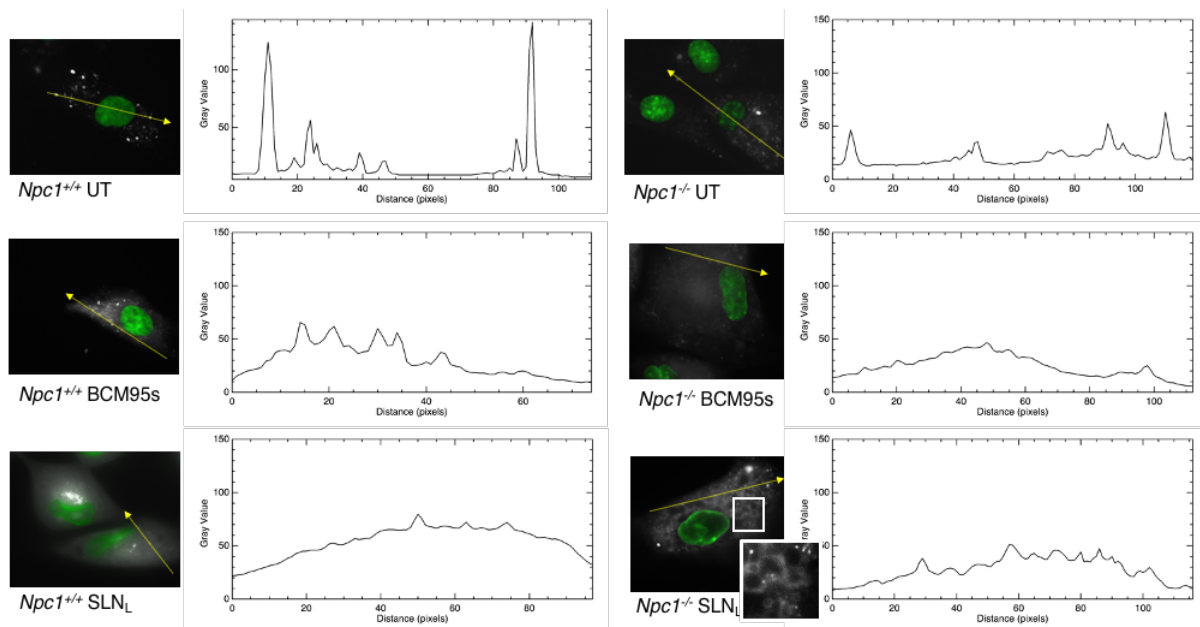


**Figure 5.22: Mitochondrial Ca<sup>2+</sup> staining in *Npc1*<sup>-/-</sup> and control glia following 24-hour treatment with 30 μM curcumin nanoformulations.** Representative images with graph displaying the signal intensity of mitochondrial Ca<sup>2+</sup> content with a Hoescht33342 nuclear counter stain pseudocoloured green. The representative images were selected from N = 3.

## **5.4 Discussion**

In this Chapter the aim was to identify potential drugs or nutraceuticals that could be repurposed as beneficial therapies for other LSDs including the CLN8 disease. Through HTS using an enzyme drug screen, this project has uncovered 3 small molecule compounds that may be of benefit to treat LSDs with deficiencies in GALC. This Chapter also identified that there may be other LSDs in which miglustat may have beneficial effects on lysosomal storage and ganglioside GM1 localisation including CLN2, CLN7 and CLN8. Finally, this Chapter identified the mechanism by which certain curcumin nanoformulations incur toxicity and that the nanoformulation BCM95s may be beneficial in decreasing storage in LSDs that have decreased lysosomal  $\text{Ca}^{2+}$ .

### **5.4.1 GALC enzyme drug screen**

It seems reasonable that recombinant protein should be used for HTS enzymatic drug screening; however, using recombinant protein is very expensive and has been previously reported to be less accurate than cellular homogenate for HTS due to the lack of native cofactors (Golding et al. 2012). The approach in the project was to use control cell homogenate rather than the mutant enzyme. Whilst initially perhaps counter-intuitive, this provides a method to detect compounds that can modulate enzyme activity in different ways. The control enzyme does not have any mutations which means that hits that are activators, inhibitors and chaperones may be identified which in turn may be effective against a wider variety of enzyme mutations in patients (Kollman et al. 2013). To date very few enzyme chaperones have been tested in the clinic (e.g. ambroxol) despite a considerable HTS approach to identify such molecules (Motabar et al. 2010; Geng et al. 2011; Goldin et al. 2012; Golding et al. 2012; Ribbens et al. 2013; Jang et al. 2016). These HTS approaches exclusively use mutant enzyme, as such this project utilised a different approach for the HTS screen in the project.

Chaperones often interact directly with the target protein acting as competitive inhibitors which in incorrectly folded protein stabilise the enzyme structure (Berardi et al. 2014). This further highlights the benefit of using control cell homogenate as it ensures that changes in correctly folded enzyme activity are due to direct interaction with the target enzymes rather than modulation of other processes that may be altered

in the disease cells (Geng et al. 2011). Additionally, it has been pointed out in the literature that using control protein for HTS screening increases the assay signal and sensitivity (Inglese et al. 2007) as patient protein only has partial function (Deane et al. 2011) and may only allow for the identification of mutation specific chaperones (Berardi et al. 2014; Suzuki 2014).

To date more than 147 mutations in GALC have been identified (Sprately et al. 2016) some of which have been identified to lead to misfolded protein that is retained in the ER and then degraded by ER quality control machinery (Berardi et al. 2014). As such proteostasis inhibitors and HDAC modulators have been suggested to be potential treatments for LSDs. Nonetheless, clinical evidence so far suggests that long term upregulation of the genome is not viable as over time cells find ways to prevent or compensate for changes in expression and thus the benefit from these types of treatment may be minimal (Xu et al. 2007). On the other hand, small molecule compounds that act as chaperones that stabilise misfolded proteins which prevents it from being degraded in the ER and allows it to be transported to the lysosome are likely to work for longer.

Restoring as much as 10% GALC activity in Krabbe disease has been reported, in principle, to be sufficient to prevent galactosylsphingosine accumulation and downstream oligodendrocyte cell loss (Parenti 2009). Also, for Gaucher disease, it has been reported that 10% activity of GBA1, the enzyme affected in this disease, is sufficient for restoring normal function, as such the threshold that needs to be achieved is low. Nonetheless, one of the main issues is whether the drug can cross the blood brain barrier (BBB) which is the problem with ambroxol (discussed below) a GBA1 chaperone that was extremely promising up to clinical trials and worked in peripheral tissues but does not appear to cross the BBB at clinically relevant plasma concentrations (Weiser 2008).

In order to carry out a specific drug screen against GALC enzyme activity it was first important to set up a GALC enzyme assay; this assay used the fluorescent substrate 4MU  $\beta$ -galactoside assay, which was made specific for GALC using AgNO<sub>3</sub>. Using AgNO<sub>3</sub> has been reported to abolish  $\beta$ -galactosidase activity (Martino et al. 2009). A literature search indicated that the use of AgNO<sub>3</sub> makes this enzyme assay specific to GALC and that the addition of sodium taurocholate would further increase

the activity of GALC (Wiederschain et al. 1992; Kiyokawa et al. 2004; Ribbens et al. 2013) which was confirmed (Figure 5.2).

Nonetheless, toward the end of this project a colleague in the lab determined that AgNO<sub>3</sub> does not fully reduce  $\beta$ -galactosidase activity in HF homogenate (Alshehri 2019). Therefore, the results from the enzymatic drug screen outlined in this Section 5.3 of this Chapter and those discussed below cannot be attributed with full confidence to GALC alone. The hits found during the enzymatic drug screen may in fact be modulating  $\beta$ -galactosidase, GALC or both. In the primary screen, however,  $\alpha$ -lobeline was found to act as a weak inhibitor of the assay which has previously been reported as an inhibitor and chaperone of GALC (Lee et al. 2010b; Berardi et al. 2014). This implies that whilst the assay is not entirely specific, it does allow for some measurement of GALC activity; however, as some  $\beta$ -galactosidase activity remains it must be viewed as an assay of both enzymes. As such, the hits identified must in future be tested in fibroblasts from both GM1 gangliosidosis and Krabbe disease patients.

Ambroxol was another one of the hits from the HTS that was found to act as a chaperone of GALC. Nonetheless, as mentioned above, it is not possible to be fully sure whether the small molecule hits are interacting with GALC or  $\beta$ -galactosidase. The only way to confirm whether the hit may be of benefit to diseases where GALC is affected would be to carry out further tests in those diseases. A final year student that was supervised during this project tested the hits in control 1 HF cells and Krabbe HF patient cells and found that ambroxol and Ibudilast had a potential beneficial effect on lysosomal pH in Krabbe HF cells; whereas, mycophenolate mofetil was cytotoxic (Brimer 2017).

The results from this enzyme are still extremely interesting; particularly, ambroxol as it has previously been reported to be a chaperone for glucocerebrosidase (GBA1) the enzyme that is defective in Gaucher disease (Maegawa et al. 2009). Maegawa *et al.* (2009) found that ambroxol acts as a perfect chaperone as it binds to miss folded GBA1 in the ER which stabilises the enzyme so that it is transported to the lysosome and ambroxol then falls off in the lysosome due to the pH. Taken together, the findings in this report provide preliminary data that ambroxol may help restore lysosomal pH and may be beneficial to defects in GALC,  $\beta$ -galactosidase and GBA1. As defects in

GALC have been reported in CLN8 disease previously (Hermansson et al. 2005) the effects of ambroxol treatment should be explored in CLN8. This was going to be carried out during this project but due to unforeseen time constraints it was not possible to complete these experiments.

The fact that the literature has already reported the potential beneficial effects of ambroxol in LSDs, such as being a GBA1 chaperone, along with the fact that in this study it was seen to be a potential chaperone of the destabilised enzyme made this compound the lead hit. Nonetheless, it is important to first confirm whether the drug hits identified in this project target GALC. This may be done by using purified GALC enzyme; however, this was beyond the budget of this project as sufficient purified enzyme for thermal denaturation or circular dichroism studies is expensive. It was part of the plan of this project to confirm potential beneficial effects of the drug hits in Krabbe HF cells and other LSDs that have defects in GALC, but there was not enough time to complete this. Future work should confirm the effect of ambroxol, ibudilast and mycophenolate mofetil on cellular dysfunction of LSD patient cells with known defects in GALC or  $\beta$ -galactosidase such as Krabbe disease patient cells and GM1 gangliosides patient cells.

It is not difficult, however, to see how ambroxol might target all three enzymes as there is evidence from imino sugar compounds for galactose and glucose that are able to bind the same enzymes (Giugliani et al. 2013). Miglustat (*N*-butyl-1-deoxynojirimycin), an imino sugar analogue of D-glucose, targets glucosylceramide synthase (Figure 5.1); however, sometimes miglustat and migalastat, the galactose equivalent, as well as glucose target the same enzyme. Therefore, it is possible that ambroxol may target both GALC and  $\beta$ -galactosidase as such making a pro-drug version via medicinal chemistry that crosses the blood brain barrier may present an effective treatment for CLN8, Krabbe or LSDs with  $\beta$ -galactosidase deficiencies such as GM1 gangliosidosis (Alshehri 2019).

Interestingly, mycophenolate mofetil has been trial in CLN3 but the results did not show much improvement (NCT01399047). It was trailed in CLN3 due to its anti-inflammatory properties (Sokolowski et al. 1995; Seehafer et al. 2011; Augustine et al. 2019) as inflammation has been observed in CLN3 mouse models (Grubman et al. 2014); however, inflammation is often a downstream phenotype in other LSDs with

glycosphingolipid storage. This highlights the importance of understanding disease events from cells to animal models and biochemical analysis of tissues. If disease phenotypes are well characterised, then pathogenic cascade of events can be determined, as has been done for NPC1 disease (Lloyd-Evans and Platt 2010), which increases the chances of finding a therapy that is beneficial to patients.

#### **5.4.2 Miglustat for NCLs**

Miglustat is currently being used to treat 2 different LSDs as outlined in Section 5.1 above. It is also currently in trials to treat other lysosomal storage diseases such as GM2 gangliosidosis (NTC0382201). Miglustat also went through trials for MPS but was found to not have significant beneficial effect (Ortolano 2016). As mentioned above, miglustat may be beneficial in disease that have glycosphingolipid storage which has been reported in the NCLs (Hermansson et al. 2005; Kollman et al. 2013).

##### **5.4.2.1 Lysosomal area following miglustat treatment**

In this report CLN2 HF, CLN7 474 HF and CLN8 534 HF were all found to have significantly elevated lysosomal area which indicates lysosomal expansion and storage (Figure 5.9). Following 50  $\mu$ M miglustat treatment for 7 days, CLN2 HF had significantly lower lysosomal area compared to the untreated CLN2 HF (Figure 5.9 A & B) which would indicate a decrease in lysosomal accumulation and possibly ameliorating lysosomal function as has been reported for NPC1 disease following miglustat treatment (Lachmann et al. 2004; te Vruchte et al. 2004; Patterson et al. 2007). Similarly, CLN7 474 HF and CLN8 534 HF displayed a decrease in lysosomal area which was not significantly lower to the untreated but was also no longer significantly higher than the control 1 HF. This indicates that miglustat may also have a slight positive effect on lysosomal accumulation in CLN7 and CLN8, a longer incubation time may be necessary as glycosphingolipid turnover is slow (Skotland et al. 2016).

#### 5.4.2.2 Autophagic compartment area following miglustat treatment

Similar to lysosomal volume, CLN2 HF and CLN7 474 HF have significantly more autophagic compartment area (Figure 5.10) which indicates either accumulation of or a failing to clear autophagosomes. Despite a potential improvement in lysosomal function, there was no significant effect following miglustat treatment on autophagic vacuole area in any of the cell lines examined; however, CLN7 474 HF treated with miglustat no longer had significantly increased autophagic compartment volume compared to untreated control 1 HF. This may indicate that the treatment is starting to have an effect on the autophagic dysfunction in CLN7 cells and suggests that a longer treatment might ameliorate this downstream phenotype.

Autophagic staining in CLN8 534 HF appears to be higher than the control 1 HF but was extremely variable as seen in Chapter 3 (Figure 3.4). The high degree of variability may explain the lack of significance between the CLN8 534 HF and control 1 HF in autophagic compartment area staining. Longer miglustat treatment may allow more time for the autophagic system to clear the backlog and clear defective mitochondria. As such future experiments with longer miglustat treatment should be carried out in CLN2, CLN7 and CLN8 patient cells.

#### 5.4.2.3 Ganglioside GM1 area following miglustat treatment

Accumulation of ganglioside GM1 in lysosomes may indicate defects in the transport of lipids out of the lysosome, in their degradation or in endo-lysosomal trafficking (Lachmann et al. 2004). Endo-lysosomal trafficking defects have also been shown to improve following miglustat treatment in another disease with lysosomal dysfunction (Lachmann et al. 2004). There are several lysosomal enzymes that are involved in the breakdown of glycosphingolipids such as  $\beta$ -galactosidase which is affected in CLN8 534 (Chapter 3 Figure 3.11). Furthermore, the CLN8 protein has been suggested to be required for the transport of many lysosomal proteins to the lysosome (di Ronza et al. 2018). This highlights another reason why miglustat may be of benefit to certain CLN8 disease mutations that cause glycolipid storage.

Therefore, the localisation of ganglioside GM1 was examined (Figure 5.11) which showed similar results to those seen in lysosomal volumes (Figure 5.9). All three cell lines examined, CLN2 HF, CLN 7 474 HF and CLN8 534 HF had a significant increase

in the percentage of cells with punctate ganglioside GM1 staining. Normally, ganglioside GM1 staining is more diffuse indicating predominantly plasma membrane distribution; however, when it is being accumulated in lysosomes or there is a lipid trafficking defect leading to lysosomal and cellular dysfunction ganglioside GM1 staining displays clear punctate distribution (Lachmann et al. 2004; Acosta et al. 2016).

Miglustat treatment led to a significant decrease in punctate distribution of ganglioside GM1 in CLN2 HF which indicates decrease in lipid storage in lysosomes which may be due to increase in enzyme activity or that the localisation was normalised due to improved lipid-trafficking as has been reported in NPC1 disease following miglustat treatment (Lachmann et al. 2004). Regardless, reduction in lipid storage is beneficial for lysosomal function and has previously been reported to lead to improved cellular function and increased cell survival in LSDs such as NPC1 (Lachmann et al. 2004; Stein et al. 2012).

#### 5.4.2.4 Organelle $\text{Ca}^{2+}$ following miglustat treatment

Defects in  $\text{Ca}^{2+}$  levels in different cellular compartments and the effect of miglustat treatment on these were explored in CLN2 HF, CLN7 474 HF and CLN8 534 HF. Ryanodine mediated ER  $\text{Ca}^{2+}$  release showed no significant alteration in ER  $\text{Ca}^{2+}$  in any of these three cell lines (Figure 5.13). CCCP mediates  $\text{Ca}^{2+}$  release from the mitochondria, however, was seen to be lower in all three cell lines. Nonetheless, miglustat treatment had no effect on CCCP mediated  $\text{Ca}^{2+}$  release.

The CCCP mediated  $\text{Ca}^{2+}$  release appears to be faster in the CLN2 HF, CLN7 474 HF and CLN8 534 HFs than the control regardless of treatment which may be due to the membranes in the patient cells being depolarised leading to a faster  $\text{Ca}^{2+}$  response. In fact, mitochondrial membrane depolarisation has been reported previously in LSDs such as Pompe disease and Gaucher disease (Raben et al. 2012; Cleeter et al. 2013). Additionally, previous work has also found mitochondria  $\text{Ca}^{2+}$  defects in the CLN8<sup>mnd</sup> mouse (Kolikova et al. 2011). Mitochondrial membrane depolarisation can be measured using the cationic fluorescent probes (Facompré et al. 2000) which could be used in future studies to investigate mitochondrial membrane depolarisation in CLN2, CLN7 and CLN8.

In this study, lysosomal  $\text{Ca}^{2+}$  was found to be lower in CLN7 474 HF and CLN8 534 HF (Figure 5.15 A, E & F). It may be of interest to examine the effects of miglustat treatment on lysosomal  $\text{Ca}^{2+}$  in CLN2, CLN7 and CLN8 as previous studies have shown that miglustat treatment improves the lysosomal  $\text{Ca}^{2+}$  defects in NPC1 (Fineran et al. 2016). Additionally, miglustat has been shown to correct the SERCA  $\text{Ca}^{2+}$  uptake defect in the Sandhoff disease *Hexb*<sup>-/-</sup> mouse model (Pelled et al. 2003).

Therefore, the potential improvements that were seen on ganglioside GM1 distribution following miglustat treatment along with the literature suggests that it may be the case that miglustat rescues the lysosomal  $\text{Ca}^{2+}$  defect in CLN7 474 HF and CLN8 534 HF and as such this should be explored. Nonetheless, the effects of miglustat treatment on lysosomal  $\text{Ca}^{2+}$  and lysosomal  $\text{Ca}^{2+}$  levels in CLN2 HF were not explored due to the pandemic (Chapter 6 Table 6.1). Future experiments should be carried out to first determine whether there is a lysosomal  $\text{Ca}^{2+}$  defect in CLN2 HF and whether miglustat is able to rescue this defect in CLN7 474 HF, CLN8 534 HF and, if present, in CLN2 HF.

#### 5.4.2.5 Effect of miglustat on lysosomal area in other CLN8 patient cells

Following the potential decrease in lysosomal area seen in CLN8 534 HF after miglustat treatment the effects of miglustat on lysosome area measured via fluorescence plate assay was examined across the other CLN8 patient cell lines (Figure 5.14). As seen in Chapter 3 (Figure 3.1), only CLN8 534 HF had significantly higher lysosome staining which was no longer significant following miglustat treatment. There was not much change seen in the other CLN8 patient cell lines after miglustat treatment which may be due to the variability in cellular phenotypes observed in CLN8 patient cells in Chapter 3.

It is important to note that CLN8 disease is an extremely variable disease within and between patients as described and discussed in Chapter 3. This means that any improvement seen in CLN8 534 HF needs to be rigorously validated due to variability in disease phenotype. Additionally, any possible compounds that show benefit in CLN8 should be explored in many different patient mutations in order to ascertain whether they may be of benefit to all CLN8 patient mutations or if they are only beneficial to certain mutations.

#### 5.4.2.6 Miglustat treatment overview

Miglustat, which is the available disease modifying treatment for NPC1, has been shown to not decrease cholesterol accumulation in *Npc1*<sup>-/-</sup> mouse model (te Vrugte et al. 2004). Miglustat treatment in NPC1 has not only been shown to reduce lysosomal storage but also has been found to ameliorate endo-lysosomal trafficking defects and rescue Purkinje neurons functions and survival (Lachmann et al. 2004; Patterson et al. 2007; Stein et al. 2012). This indicates that although a small molecule therapy does not ameliorate all cellular dysfunction it may still be a disease modifying therapy.

Overall, the more phenotypes a drug therapy is able to improve, the better the drug is and the more likely it is to be clinically applicable (Kolter and Sandhoff 2005; Szabo et al. 2017). Nonetheless, this is not always the case for example, cyclodextrin reduces all storage in NPC1 disease but clinical trials found it caused hearing loss (Crumling et al. 2017) leading to the trial being halted in Europe. Therefore, even if a drug appears to ameliorate more phenotypes in a drug screen several factors need to be weighed up when selecting which drug to take forward, such as, effectiveness, toxicity and the ability to cross blood brain barrier (Kolter and Sandhoff 2005).

It is important, however, that the results be taken with relative caution as the effect of miglustat treatment, although potentially beneficial, still needs to be further validated and explored in animal models. Future work into the potential benefit of miglustat for certain NCLs would allow to uncover whether miglustat may lead to beneficial effects in patients.

That being said, the fact that it showed some potential benefit, particularly in CLN2, after further validation, may provide a possible therapy that could improve patient quality of life and disease. Furthermore, miglustat has extensive safety background, as it underwent clinical trial studies for HIV (Pollock et al. 2008), NPC1 disease (Lachmann et al. 2004), Gaucher Disease (Bennett and Mohan 2013) and as a potential male contraceptive (van der Spoel et al. 2002). The metabolism of miglustat is well understood and is known to be removed from the body in the urine with minimal and manageable side effects. Therefore, miglustat represents a drug that could be repurposed with relative ease.

### 5.4.3 Curcumin for LSD with Ca<sup>2+</sup> defects

Previous reports of the beneficial effects of unformulated curcumin in LSDs such as NPC1 (Lloyd-Evans et al. 2008; Efthymiou et al. 2014; Williams et al. 2014) as well as work in the Lloyd-Evans lab have shown that the beneficial effects following curcumin treatment results from the ability of curcumin to modulate Ca<sup>2+</sup> levels, rather than antioxidant effects (Badell-Grau *et al.* in prep). This study thus explored the possible benefits of two different curcumin nanoformulations in several LSDs that have ER and lysosomal Ca<sup>2+</sup> defects (Figure 5.15, 5.16, 5.17 & 5.19).

Curcumin is commonly formulated into lipid vectors as this improves delivery of curcumin across the blood gut barrier, leading to higher concentrations of curcumin reaching the blood as well as decreased renal clearance (Bi et al. 2017). These curcumin nanoformulations will therefore facilitate therapeutic concentrations of curcumin in the blood; however, evidence from other LSDs such as NPC disease indicates that the use of curcumin nanoformulations may be dangerous given the aforementioned toxicity (Badell-Grau *et al.* in prep). It is therefore important, that the toxicity as well as the beneficial effects of these curcumin nanoformulations is properly explored in other LSDs to mitigate that issues, such as those seen in NPC, do not occur in other LSDs.

Of the two curcumin nanoformulations tested, only BCM95s led to a decrease in lysosomal area in LSDs with decreased GPN-mediated lysosomal Ca<sup>2+</sup> release (Figure 5.16 & 5.19). BCM95s did not have any beneficial effect on lysosomal area (Figure 5.19) on NPA, which has low ER Ca<sup>2+</sup> (Figure 5.16 & 5.17), presumably due to a lack of ER Ca<sup>2+</sup> for release to increase cytosolic Ca<sup>2+</sup>. Additionally, lowering ER Ca<sup>2+</sup> further in LSDs with low ER Ca<sup>2+</sup>, such as NPA, may be detrimental.

That NPA showed significantly decreased ER Ca<sup>2+</sup> (Figure 5.16) when measured using thapsigargin and not ionomycin is noteworthy. Changes in ER Ca<sup>2+</sup> incurred by thapsigargin are due to alterations in ER channels, leading to ER Ca<sup>2+</sup> release as described by (Ginzburg and Futerman 2005). Ionomycin conversely releases Ca<sup>2+</sup> from all non-acidic Ca<sup>2+</sup> stores and is thus not fully specific to ER Ca<sup>2+</sup>.

Of the cell lines with decreased lysosomal Ca<sup>2+</sup>, CLN10 exhibited the least change following BCM95s treatment. In fact, BCM95s treatment might lead to a slight increase in lysosomal volume, but not significantly so. That CLN10 has decreased lysosomal

area when using the LysoTracker probe (Figure 5.19) is currently poorly understood but may be due to a defect in lysosomal pH in CLN10 (Kirkham 2020), as LysoTracker is a pH-dependant probe (Xu et al. 2014).

An increase in cytosolic  $\text{Ca}^{2+}$  facilitates fusion of lysosomes with the plasma membrane for exocytosis, and fusion with other endo-lysosomal vesicles. Therefore, the capacity of curcumin to increase cytosolic  $\text{Ca}^{2+}$  increases lysosomal fusion events, further reducing lysosomal storage as vesicle machinery fusion is  $\text{Ca}^{2+}$  dependant (Lloyd-Evans et al. 2008). This is particularly true in LSDs with decreased lysosomal  $\text{Ca}^{2+}$  as the curcumin-mediated increase in  $\text{Ca}^{2+}$  compensates for this reduced lysosomal  $\text{Ca}^{2+}$  (Lloyd-Evans et al. 2008).

The reduced lysosomal  $\text{Ca}^{2+}$  in these LSDs can be produced by many factors. It is possible that the contact points between the ER and the lysosome are affected in the NCLs, leading to higher ER  $\text{Ca}^{2+}$  and lower lysosomal  $\text{Ca}^{2+}$  (Garrity et al. 2016; Atakpa et al. 2018). Possible defects in ER-lysosomal contact points have been reported previously in CLN8 disease as CLN8 may interact with proteins such as VAPA which are involved in ER-lysosomal contact points (Passantino et al. 2013). This is clearly not the case in CLN3 which has elevated lysosomal  $\text{Ca}^{2+}$  and no change in ER  $\text{Ca}^{2+}$ . CLN3 does not have decreased lysosomal  $\text{Ca}^{2+}$  and is thus not benefited by curcumin-mediated increased cytosolic  $\text{Ca}^{2+}$ .

SLN<sub>L</sub> curcumin was seen to not be beneficial to any of the LSDs tested in the Chapter (Figure 5.19). Furthermore, other work in the ELE lab showed that SLN<sub>L</sub> curcumin could detriment to NPC1 disease. This was particularly true in NPC1 *in vivo* fish models which were negatively affected by SLN<sub>L</sub> curcumin treatment (Badell-Grau *et al.* in prep). It was not possible to fully quantify the effects of SLN<sub>L</sub> treatment in the LSDs tested as it was cytotoxic in many cases. As Borbon *et al.* (2012) reported, curcumin formulated into lipidated vectors such as SLN<sub>L</sub> have little to no benefit in NPC1. It is feasible that the SLN<sub>L</sub> lipid content may also lead to increased lysosomal storage which is detrimental to LSDs that already have lysosomal storage.

SLN<sub>L</sub> detracts lysosomal storage phenotypes through toxicity from a combination of the nanoparticle fatty acid lipid mix in conjunction with curcumin, and its effect on the mitochondria (Figure 5.21 & Figure 5.22; Badell-Grau *et al.* in prep). Previous publications have suggested that some approved formulations may actually modulate

physiologically relevant targets (Pottel et al. 2020) which may be the case with the fatty acid mixed with curcumin in nutraceuticals such as SLN<sub>L</sub>. As outlined in Chapter 1, the mitochondria act as a Ca<sup>2+</sup> buffer, maintaining low cytosolic Ca<sup>2+</sup>. Mitochondrial defects that affect its ability to buffer Ca<sup>2+</sup> have been linked to neurodegeneration in LSDs like CLN8 (Kolikova et al. 2011). SLN<sub>L</sub> may therefore be producing cytotoxicity by affecting mitochondrial Ca<sup>2+</sup>, leading to further cell stress in LSD patient cells.

Although BCM95s reduced lysosomal storage in CLN7 474 HF and CLN8 534 HF, and potentially rescued the CLN10 pH defect (Figure 5.19), no benefit was observed to lysosomal cholesterol mis-localisation and storage following BCM95s treatment. Curcumin treatment has been previously reported to decrease cholesterol storage in NPC1 (Lloyd-Evans et al. 2008); this is not the case in the NCLs which may be due to the activity of enzymes involved in the processing of cholesterol, such as acid lipase (Dudland and Francis 2015) being affected in the NCLs and not in NPC1. While no changes in acid lipase activity were observed in CLN8 in this study (Chapter 3 Figure 3.11), other enzymes involved in cholesterol processing may be defective or the variability in CLN8 may have obscured defects in acid lipase. Therefore, BCM95s may be of benefit to lysosomal storage in CLN7 474 HF, CLN8 534 HF and lysosomal pH defects in CLN10 but does not ameliorate cholesterol storage in these diseases. The effects of BCM95s on further cellular phenotypes in these diseases and other NCLs and LSDs should be explored in future.

Badell-Grau *et al.* (in prep) and this report identified and elucidated the detrimental effects of certain curcumin nanoformulations to LSDs. A comprehensive understanding of compounds under consideration for therapeutic benefit to any disease, and how their formulations affect diseases such as LSDs is therefore critical. The consideration of nutraceuticals for novel therapies is an important frontier in medical science, but these findings illustrate that unforeseen negative effects may mitigate any benefits and that it is imperative to clinically test formulations of these drugs prior to condoning their use by the public.

## **5.5 Conclusion**

The HTS identified 3 compounds ambroxol, mycophenolate mofetil and ibudilast as possible chaperones for GALC or  $\beta$ -galactosidase. These results present 3 compounds with the potential benefit for diseases such as Krabbe disease, GM1 gangliosidosis and CLN8 disease. Further research should confirm the potential benefits of these compounds as they represent a possible way to repurpose FDA approved drugs for these LSDs that currently have no therapy.

In this Chapter, miglustat was also identified to have potential beneficial effects in CLN2, CLN7 and CLN8 which presents a possible drug that may be quickly developed as it is already approved for other diseases with extensive safety data. Nonetheless, further work is required in order to confirm the benefits to these diseases such as exploring the effects of miglustat on other cellular phenotypes like lysosomal  $\text{Ca}^{2+}$ , mitochondrial depolarisation using MitoTracker CMXRos and endo-lysosomal trafficking using a live pulse-chase CtxB-FITC assay.

As most LSDs are lipid storage diseases, the use of lipidated vehicles for treatment may not be the most appropriate approach as the lipids in the treatment may increase the load on an already strained lysosomal network. It is also extremely important to take care when formulating or considering the use of compounds that may have benefit to LSDs with other compounds that may lead to unforeseen toxic effects which may cause the end formulation to in fact be detrimental instead of beneficial to the disease.

# **Chapter 6 Overall Discussion & Conclusions**

## **6.1 Summary of findings**

There is a dearth of knowledge in the cellular mechanisms behind CLN8 disease. This thesis aimed to investigate the cellular phenotypes in CLN8 disease and use these phenotypes for drug screening and drug repurposing for LSDs.

The results in Chapter 3 showed a high amount of phenotypic variability in the cellular phenotypes in CLN8 disease patient fibroblasts making most of them unsuitable for drug screening. These results revealed that the variability in cellular phenotypes in CLN8 disease was not only between patient cell lines but also within the patient cell lines. Nonetheless, certain phenotypes, such as Ca<sup>2+</sup> dyshomeostasis and lysosomal enzyme activity deficiencies, were robust enough that they may be used for drug screening, particularly in the CLN8 patient cell line CLN8 534 HF.

Chapter 4 confirmed the presence of classical NPC1 phenotypes in a fast-growing glia cell model that are robust and can be used for drug screening for compounds that may be beneficial to LSD common phenotypes. In this Chapter the use of this LSDs glia model in a drug screen was confirmed by screening arimoclomol-like compounds that may have beneficial effects on the cellular dysfunction in several LSDs with mutation that may have partial protein function, including CLN8 disease. Furthermore, in Chapter 4 arimoclomol was found to be beneficial in reducing lysosomal storage in NPC1 disease by two mechanisms, one is by directly affecting mutant NPC1 protein in patient cells and a second undetermined mechanism, likely by stabilisation of lysosomal function by HSP70 (Kirkegaard et al. 2010), that also reduces lysosomal storage in the absence of NPC1 protein.

Arimoclomol may be beneficial to CLN8, especially the cell lines with variable phenotypes, as residual functional protein may be increased. Additionally, the stabilisation of lysosomal function, especially lysosomal enzymes, by arimoclomol induced elevation of lysosomal enzyme activity may also prove beneficial for CLN8 considering the changes in enzyme activity observed in this project and reported in the literature (di Ronza et al. 2018; Bajaj et al. 2020). Unfortunately, due to the closure

of the lab during the pandemic it was not possible to carry out the test of arimoclomol in CLN8 cells as was planned.

Chapter 5 focused on drug repurposing for LSDs, which, through high-throughput drug screening against the activity of GALC, found 3 compounds that may be of benefit to GALC or  $\beta$ -galactosidase or both. The next step is to test their impact on Krabbe, GM1 gangliosidosis and CLN8 cells, this was planned but was also impacted by the pandemic (Table 6.1). In Chapter 5 the effects of miglustat on several cellular phenotypes of CLN2, CLN7 and CLN8 patients' cells, such as lysosomal accumulation and ganglioside GM1 storage, suggest that miglustat may be beneficial for these diseases. Finally, work in this chapter found that some curcumin nanoformulations may be beneficial to LSDs with decreased lysosomal  $\text{Ca}^{2+}$  or elevated ER  $\text{Ca}^{2+}$  content; whilst, some curcumin nanoformulations may in fact be detrimental to LSDs owing to the lipid content of their formulation. This work highlights the care that needs to be taken by patients and families when considering the use of neutraceuticals and that clearly more work is required here to understand the potential impact of non-standard drug formulation materials upon lysosomal storage disorder cellular and tissue phenotypes.

## **6.2 Discussion**

### **6.2.1 CLN8 phenotypic variability**

It is important to note that rare diseases by their nature make it more difficult to obtain samples which makes it harder to overcome obstacles such as the high degree of variability seen in CLN8 patient cell lines during this project. Rare disease research often lacks statistical power due to the low number of patient samples. In fact, there have been calls for a decrease in the dependence on statistical significance when it comes to rare disease research due to the difficulty to obtain statistical power (Mitani and Haneuse 2020). Additionally, the variability in CLN8 patient cells makes it more difficult to achieve statistical significance requiring a vast number of Ns which makes HTS unfeasible. It is important to note that the phenotypic variability seen in CLN8 is specific to CLN8 and does not arise from any of the methods used as can be seen by the far lower degree of variability observed in CLN2, CLN7 (Chapter 5 Figure 5.9 &

5.10), *Npc<sup>-/-</sup>* glia (Chapter 4 Figure 4.1 – 4.4) and in other LSDs (Lloyd-Evans et al. 2008; Chandrachud et al. 2015; Vanier and Latour 2015) including the NPC1 HF as shown by Alshehri and Lloyd-Evans (data not shown).

Due to the variability observed in CLN8 throughout this project meant that CLN8 patient cells were not the most suitable for drug screening. The variability means that higher repeat numbers are needed to obtain significance making drug screens of large number of compounds harder and more expensive. Alternative models for CLN8 disease such as knockout cell lines were explored but the cost and time to obtain these were not within the remit of this project. Furthermore, there is a mouse model of CLN8 disease (Kuronen et al. 2012) but it was not available during this project making its use impossible. Nonetheless, the phenotypes observed in CLN8 patient HFs merit further investigation and different approaches to increase our understanding of the underlining disease mechanism.

The absence of a full knockout cell line or mouse material meant it was not possible to determine a baseline of these phenotypes. A knockout would elucidate whether the phenotypes are truly due to the production of residual mutant CLN8 protein as if the knockout has different phenotypes than the CLN8 patient HF this would demonstrate that mutant protein is functioning in some way. Nonetheless a knockout may show that even without the presence of CLN8 the variability is present which could indicate that there may be modifying proteins that impact CLN8 pathways. During the project the use of siRNA was also considered; however, the lack of a CLN8 antibody and the fact that the half-life of the CLN8 protein is not known means that testing for silencing was not possible. After having worked on the cellular phenotypes of CLN8 for two years trying to understand the variability it became apparent that no more time could be lost which led this study to explore alternatives for HTS.

### **6.2.2 LSD drug screening model**

Having spent over half of the length of this project attempting to record and understand the cellular phenotypes and the variability of these in CLN8 disease patient cells it became clear that these may not be appropriate for HTS. Consequently, it was decided to report and document why robust cellular screening phenotypes are critical. In order for this, NPC1 disease was used mainly due to the fact that the cells have

robust phenotypes (Lloyd-Evans et al. 2008), there are existing approved treatments (Lachmann et al. 2004; Patterson et al. 2007; Stein et al. 2012) allowing for the screens to be validated and there has been some HTS screening carried out previously although none that have had great success.

Chapter 4 demonstrates that LysoTracker, one of the phenotypes that could be used for CLN8 534 HF, was a robust HTS screening tool for NPC1 disease allowing the identification of miglustat and arimoclomol. Previous studies that focused on cholesterol as a screening tool alongside short incubation times typical of HTS meant that approved drugs like miglustat were being missed (Yu et al. 2014).

The *Npc1*<sup>-/-</sup> glia cell line not only had robust phenotypes but also was a fast-growing cell line which facilitates drug screening of large number of compounds increasing the likelihood of finding compounds that may be of benefit to a disease (Sofroniew and Vinter 2010). It is important to choose the correct system for drug screening with robust phenotypes which increases the likelihood of finding compounds that actually ameliorate the cellular dysfunction which in turn increases the likelihood of identifying compounds that may be of benefit to the disease (Zheng et al. 2015; Cooper et al. 2018).

The use of this cell model during this project enabled the identification of multiple arimoclomol like compounds which were of benefit to phenotypes in the glia cells. This showed that the use of knockout models with correct choice of phenotypes that have a dynamic range can accurately identify drugs that may be of benefit to LSDs. Nonetheless, knockout models may not always be the best model as sometimes it may be beneficial to screen against the mutant protein as shown in Chapter 4 with the effect of arimoclomol on mutant NPC1 observed. Ultimately, LSD patients are not knockout, so the best cell type to use is mutant patient cells but with a robust phenotype such as LysoTracker. Thus, for CLN8 this was a problem as the phenotypes are not robust and are variable within experiments as discussed above.

Overall, the development of the *Npc1*<sup>-/-</sup> glia screening model provided a platform for other projects to perform drug screens to further identify other compounds that may be of benefit to NPC1 disease and other LSDs. Therefore, a robust model as the one shown in Chapter 4 provides a strong first step for the identification of compounds that should be tested further in the search for LSD therapies.

### 6.2.3 LSD drug screening

It is important to note that this project focused on drug repurposing instead of screening completely novel compounds. As mentioned in Chapter 5 drug development of novel compounds is a long, expensive and complicated process with an extremely high failure rate (Szabo et al. 2017; Pushpakom et al. 2019). Therefore, drug repurposing has become more and more popular as known compounds have been found to have new application in treating other diseases (Pushpakom et al. 2019) as repurposing offer pathways to drug developing using drugs that have already been studied and are known to be safe, decreasing development costs and increase development timelines. Additionally, the use of cellular phenotype-based drug screening is widely used in drug discovery (Silverman et al. 1998; Chandrachud et al. 2015; Huang et al. 2020).

The absence of many robust phenotypes in the CLN8 patient cell lines led this study to choose drug HTS via the use of enzyme assay as was shown in Chapter 5. As mentioned previously, CLN8 has been reported to act as a chaperone of certain lysosomal enzymes (di Ronza et al. 2018; Bajaj et al. 2020) which may explain the defects in lysosomal enzyme activities observed during this study (Chapter 3 Figure 3.11). Therefore, compounds that stabilise lysosomal enzymes and act as chaperones may be of benefit in CLN8 disease as it may help overcome the deficiency in CLN8 function. Alternatively, a compound like arimoclomol that stabilises lysosomes, acts as a chaperone and is a genome upregulator may also be beneficial to CLN8 patients. Although, there may be less lysosome enzymes reaching the lysosome the residual enzyme activity in lysosomes might be boosted by stabilisation effect of increased HSP70 on lysosomal LBPA (Kirkegaard et al. 2010). Additionally, the upregulation of their biosynthesis might result in more production and perhaps some might make their way out of the ER in absence of functional CLN8. Nonetheless, this report managed to create a drug screen that found compounds independent of the variable CLN8 cells that may have a potential to treat CLN8 through repurposing.

Furthermore, some drugs were tested such as miglustat and curcumin nanoformulations using the CLN8 cellular phenotypes, but the variability ultimately meant that screening large numbers of compounds was not possible. The variability also meant that the number of phenotypes that were examined was limited and as

mentioned in Chapter 4 the more cellular phenotypes used in drug screening the higher the likelihood of successful candidates being identified (Szabo et al. 2017).

Drug repurposing has been previously successful in LSDs with the development of miglustat a drug initially believed to act as an anti-retroviral and anti-HIV drug which failed, as it does not enter the ER at a high enough concentration to have a significant effect in HIV patients in clinical trial (Dedera et al. 1990; Tierney et al. 1995; Ficicioglu 2008). Therefore, by the time the drug was explored as a treatment for storage diseases such as Gaucher disease and NPC1 disease, due to the fact that it inhibits glycosphingolipid biosynthesis, there was already some safety data in patients making it more likely to be approved and less likely to fail due to safety concerns. This highlights not only the advantages of repurposing drugs but more importantly the success of doing so in LSDs.

Therefore, drug repurposing offers a proven route to drug development for LSDs as such this project focused on screen drugs that may be repurposed for LSDs such as those outlined in Chapter 5. For example, the drugs identified in the HTS in Chapter 5 such as ambroxol show potential to treat LSDs such as CLN8 with deficiencies in GALC and/or  $\beta$ -galactosidase as well as already having known safety data from trials in Gaucher disease, Parkinson disease and acute cough (NCT01463215, NCT02941822 & NCT03415269). Unfortunately, ambroxol was reported to not be able to cross the blood brain barrier (Weiser 2008); however, the potential beneficial result of ambroxol in Chapter 5 warrant drugs with similar structure and properties to be explored in order to identify candidates that may be beneficial to LSDs in a similar or better manner with the ability to cross the BBB as was carried out for arimoclomol-like compounds during this study (Chapter 4 Figure 4.12).

Another example of drug repurposing carried out during this project was the screen of compounds with similar structure and similar properties to arimoclomol in Chapter 4 when confirming the NPC1 cellular model as a robust model for drug screening for LSDs. This showed some compounds that have potential to reduce storage in LSDs, particularly, NPC1 but potential others and further experiments are currently being carried out in the Lloyd-Evans lab to further explore the potential of these compounds as LSD therapies.

A further example is the potential use of miglustat to treat CLN2, CLN7 and CLN8 as NCLs have been reported to store glycosphingolipids (Jabs et al. 2008; Kang et al. 2014). The results seen during this project offer at the least preliminary data that suggest that miglustat may be of benefit to these diseases and, if further confirmed, offers a pathway for a therapy for these diseases that would be faster than developing novel drugs, ultimately helping patients of these diseases with an unmet medical need.

Neutraceutical compounds that may be of benefit to certain LSDs were identified and explored in Chapter 5 with one curcumin nanoformulation being identified to be beneficial to LSDs with decreased lysosome  $\text{Ca}^{2+}$ . Nonetheless, there is a potential danger with the use of neutraceuticals due to the toxicity observed from the lipid delivery vehicle added to the curcumin formulation. This danger associated with the inactive ingredients has recently been reported with some being shown to potentially directly modulate physiologically relevant targets (Pottel et al. 2020). Therefore, although curcumin may be of benefit to LSDs with lysosomal  $\text{Ca}^{2+}$  defects, care must be taken with these off the counter treatments.

### **6.3 Future direction**

As mentioned above throughout this project several compounds were identified to have potential therapeutic benefits to LSDs and as such additional cellular based and potentially animal based experiments should explore the potential of these to be used as therapies in LSDs. It is important to explore the effect of the compounds like miglustat, ambroxol and the compounds identified in Chapter 4 in more cellular phenotypes and possibly LSD animal models in order to confirm whether these may in fact be beneficial to these diseases.

An example of this is exploring the effects of the compounds identified in Chapter 4 on ganglioside levels and localisation as well as the ability of these drugs to increase the levels of NPC1 transport to the lysosome. These experiments were in fact planned and started during this project but were not completed due to unforeseen time constraints (Table 3.1).

**Table 6.1 Experiments impacted due to lab closure.** This table outlines experiment that were set up or planned but were not carried out due to the closure of the lab during the pandemic and how these may be mitigated for publications.

Experiments impacted	What was going to be done	How to mitigate
Dexamethasone impact on CLN8 expression, to confirm impact of altered CLN8 levels as cause of variability	In absence of antibody test for CLN8 expression in cells treated with dexamethasone using qPCR	Based on the preliminary result in Chapter 3 showing an increase in CLN8 in control cells this experiment will be repeated by a post doc in the ELE lab
Arimoclomol-like screen hits further validation	The effects of the Arimoclomol-like screen hits on ganglioside GM1 using CtxB and NPC1 transport to the lysosome using NPC1 antibody	Glycolipid shown to be reduced in the knockout (data not shown). The cholesterol data that shows changes in the NPC1 mutant but not knockout (Chapter 4) indicates that this must be due to residual NPC1 function. Furthermore, as HSP70 levels are increased in knockout and there is no impact cholesterol it is not that changes in HSP70 responsible for this leaving mutant NPC1
Arimoclomol screening in CLN8 HF's	The effects of 200 $\mu$ M arimoclomol treatment for 3 days on CLN8 534 HF phenotypes (e.g. LysoTracker) were going to be explored	Dexamethasone data in Chapter 3 provides evidence gene expression modulators may be of benefit to CLN8 disease
Ambroxol screening in CLN8 HF's	The effects of ambroxol treatments on CLN8 534 HF phenotypes (e.g. LysoTracker) were going to be explored	There is preliminary data of improved function in Krabbe cells (final year project of Brimer supervised by me). Additionally, post doc in the ELE lab will continue this project through to patenting and publication
Miglustat further screening in CLN2, CLN7 and CLN8 HF's	The effects of 50 $\mu$ M miglustat treatment for 5 days on CLN2, CLN7 and CLN8 HF's in further phenotypes such as lysosomal $Ca^{2+}$ were going to be carried out	ELE lab is currently developing an improved alternative to miglustat which a post doc funded on that project will test across the NCLs

The effects of miglustat treatment on CLN2, CLN7 and CLN8 on further cellular phenotypes such as lysosomal  $Ca^{2+}$  should be explored as miglustat has been reported to ameliorate lysosomal  $Ca^{2+}$  defect in NPC1 (Fineran et al. 2016). Therefore, the effect of miglustat treatment on lysosomal  $Ca^{2+}$  in CLN2, CLN7 and CLN8 should be carried out to determine whether miglustat corrects lysosomal  $Ca^{2+}$  defects in these

diseases. Similarly, the effects of miglustat on other cellular phenotypes such as cellular excitotoxicity should be carried out in future.

The effects of arimoclomol treatment on CLN8 phenotypes and CLN8 protein expression should also be explored further. Future experiments with CLN8 patient cells treated with arimoclomol should explore, if possible, the protein levels of CLN8 by western blotting. Moreover, as there have been reports linking the CLN8 expression levels and Gaucher disease severity, if drugs that alter CLN8 expression are identified their effects on Gaucher disease should be explored and potentially other LSDs which may be benefited by increased CLN8 expression. CLN8 has been shown to be involved in the transport of lysosomal enzyme (di Ronza et al. 2018; Bajaj et al. 2020) thus increasing its expression may lead to increased transport of lysosomal enzyme to the lysosome potentially alleviating lysosomal storage in LSDs.

Ultimately, it is important that drugs that may be of benefit to diseases are developed through to patients as such future direction should determine which drugs of the hits outlined above are taken further. Miglustat is a good option for repurposing and has been successful in the past in LSDs due to the safety data available; however, it is now a generic compound which unfortunately means that it may be difficult to find finance for the trials.

On the other hand, novel compounds such as arimoclomol would need to be tested further in not only mutant cells but then in animal models followed by testing in patients to determine the drug properties such as pharmacokinetics and pharmacodynamics. In the case of arimoclomol some of the data has already been acquired by Orphazyme in their trials of arimoclomol treatment for NPC1 (Orphazyme 2020) but has not been disclosed. Although the drugs outlined in this report have shown some preliminary promise for the treatment of some LSDs it is important that they are not only taken further in the lab but also that they are taken forward by companies that can provide funding and help take these molecules from benchside to patient to improve their quality of life.

## **6.4 Conclusions**

Through the synthesis of these Chapters the understanding and knowledge of the cellular phenotypes behind CLN8 disease began to be uncovered. Although due to the extremely variable nature seen, which in itself is a phenotype of the disease, further work is required to fully understand the mechanisms of cellular pathogenesis underlying this devastating neurodegenerative disease. This, however, adds to the current understanding of CLN8 disease and suggests a path for further interrogation of the molecular reasons underlying the variability and the disease (as discussed in Chapter 3).

In the absence of a robust CLN8 cellular model, this report validated and used two NPC1 cellular models, a knockout and a patient mutation model, as a classical example of a well characterised LSDs. These cells were used to generate and demonstrate the most appropriate method to screen for compounds that may be of benefit to LSDs. Using this platform, the greater effect of arimoclomol in NPC1 I1061T patient cells compared to knockout glia was identified. This suggests a mutation specific chaperone effect for arimoclomol. A new HTS approach by screening compounds that mimic arimoclomol identified more potent approved molecules for repurposing. These compounds, and arimoclomol, may be of use to CLN8 disease where the variability may be explained by residual protein function.

Furthermore, an enzymatic screen in control cells identified potential chaperones that could overcome defect in lysosomal enzymatic activity that has been reported as a result of direct loss of function in CLN8. Ultimately, this thesis has shown that an absence of appropriate phenotypes is not necessarily a restriction to HTS as alternative approaches can be utilised and that perhaps the most important point when designing any screen is to understand the underlying cell biology of the disease. In the case of this project, the variability is a component of the disease, which presumably occurs via the different CLN8 mutant proteins which may most likely be treated by chaperones. Understanding the variability and identifying chaperones that may be of benefit to mutant CLN8 should be the focus of future drug discovery for CLN8 disease.

## References

Acosta, W. et al. 2016. High-throughput imaging method for direct assessment of GM1 ganglioside levels in mammalian cells. *Data in Brief* 6, pp. 1016-1022.

Ademowo, O. S. et al. 2017. Lipids (per) oxidation in mitochondria: an emerging target in ageing process? *Biogerontology* 18, pp. 859-879.

Adobe. 2012. Photoshop CS6. San Jose, California, United States of America: Adobe.

Aerts, J. M. et al. 2008. Biomarkers for lysosomal storage disorders: identification and application as exemplified by chitotriosidase in Gaucher disease. *Acta Paediatrica* 97, pp. 7-14.

Alshehri, A. 2019. *Identifying and characterizing lysosomal storage disease phenotypes for utilization in novel screening and monitoring assays*. Cardiff University.

Ambrosi, G. et al. 2015. Ambroxol-induced rescue of defective glucocerebrosidase is associated with increased LIMP-2 and saposin C levels in GBA1 mutant Parkinson's disease cells. *Neurobiology of Disease* 82, pp. 235-242.

Anderson, G. W. et al. 2013. Human pathology in NCL. *Biochimica et Biophysica Acta* 1832(11), pp. 1807-1826.

Annunziata, I. et al. 2018. Mitochondria-associated ER membranes (MAMs) and lysosomal storage diseases. *Cell Death & Disease* 9(3), p. 328.

Ashe, K. M. et al. 2011. Iminosugar-based inhibitors of glucosylceramide synthase increase brain glycosphingolipids and survival in a mouse model of Sandhoff disease. *PLoS One* 6, p. e21758.

Atakpa, P. et al. 2018. IP<sub>3</sub> receptor preferentially associate with ER-lysosome contact sites and selectively deliver Ca<sup>2+</sup> to lysosomes. *Cell Reports* 25(11),

Auburger, G. et al. 2012. Primary skin fibroblasts as a model of Parkinson's disease. *Molecular Neurobiology* 46(1), pp. 20-27.

Augustine, E. F. et al. 2019. Short-term administration of mycophenolate is tolerated in CLN3 disease (Juvenile Neuronal Ceroid Lipofuscinosis). *Journal of Inherited Metabolic Disease Reports* 43, pp. 117-124.

Badell-Grau, R. A. 2016. *The role of the lysosome in Huntington's disease pathogenesis: development of a new clinical therapy*. Cardiff University.

Bagur, R. and Hajnóczky, G. 2017. Intracellular Ca<sup>2+</sup> sensing: a role in calcium homeostasis and signaling. *Molecular Cell* 66(6), pp. 780-788.

- Bajaj, L. et al. 2020. A CLN6-CLN8 complex recruits lysosomal enzymes at the ER for Golgi transfer. *Journal of Clinical Investigation* 29, p. 130955.
- Ballabio, A. 2016. The awesome lysosome. *EMBO Molecular Medicine* 8, pp. 73-76.
- Ballabio, A. and Gieselmann, V. 2009. Lysosomal disorders: From storage to cellular damage. *Biochimica et Biophysica Acta - Molecular Cell Research* 1793(4), pp. 684-696.
- Balsalobre, A. et al. 2000. Resetting of circadian time in peripheral tissues by glucocorticoid signaling. *Science* 289(5488), pp. 2344-2347.
- Banugaria, S. G. et al. 2011. The impact of antibodies on clinical outcomes in diseases treated with therapeutic protein: lessons learned from infantile Pompe disease. *Genetics in Medicine* 13(8), pp. 729-736.
- Batten, F. E. 1903. Cerebral degeneration with symmetrical changes in the maculae in two members of a family. *Transactions of the Ophthalmological Societies of the United Kingdom*, pp. 386-390.
- Batten, F. E. 1914. Family cerebral degeneration with macular change (so-called juvenile form of family amaurotic idiocy). *The Quarterly Journal of Medicine* 7, pp. 444-454.
- Bayleran, J. et al. 1987. Tay-Sach disease with hexosaminidase A: characterization of defective enzyme in two patients. *American Journal of Human Genetics* 41(4), pp. 532-548.
- Beck, M. 2017. Treatment strategies for lysosomal storage disorders. *Developmental Medicine & Child Neurology* 60(1), pp. 13-18.
- Beckenkamp, A. et al. 2015. Differential expression and enzymatic activity of DPPIC/CD26 affects migration ability of cervical carcinoma cells. *PLOS One* 10(7), p. e0134305.
- Beel, S. et al. 2017. Progranulin functions as a Cathepsin D chaperone to stimulate axonal outgrowth in vivo. *Human Molecular Genetics* 26(15), pp. 2850-2863.
- Beesley, C. et al. 2017. CLN8 disease caused by large genomic deletions. *Molecular Genetics & Genomic Medicine* 5(1), pp. 82-91.
- Bennett, L. L. and Mohan, D. 2013. Gaucher disease and its treatment options. *Annals of Pharmacotherapy* 47, pp. 1182-1193.
- Berardi, A. S. et al. 2014. Pharmacological chaperones increase  $\beta$ -galactocerebrosidase activity in fibroblasts from Krabbe patients. *Molecular Genetics and Metabolism* 112(4), pp. 294-301.

Berg, T. O. et al. 1994. Use of glycy-L-phenylalanine 2-naphthylamide, a lysosome-disrupting cathepsin C substrate, to distinguish between lysosome and prelysosomal endocytic vacuoles. *Biochemical Journal* 300, pp. 229-236.

Berman, M. C. 2000. Characterisation of thapsigargin-releasable  $\text{Ca}^{2+}$  from the  $\text{Ca}^{2+}$  ATPase of sarcoplasmic reticulum at limiting  $[\text{Ca}^{2+}]$ . *Biochimica et Biophysica Acta (BBA) - Biomembranes* 1509(1-2), pp. 42-54.

Berridge, M. J. et al. 2000. The versatility and universality of calcium signalling. *Nature Reviews Molecular Cell Biology* 1, pp. 11-21.

Bertamini, M. et al. 2002. Mitochondrial oxidative metabolism in motor neuron degeneration (mnd) central nervous system. *European Journal of Neuroscience* 16, pp. 2291-2296.

Bhatnagar, B. S. et al. 2007. Protein stability during freezing: separation of stresses and mechanisms of protein stabilization. *Pharmaceutical Development and Technology* 12, pp. 505-523.

Bi, C. et al. 2017. Particle size effect of curcumin nanosuspensions on cytotoxicity, cellular internalization, in vivo pharmacokinetics and biodistribution. *Nanomedicine* 13(3), pp. 943-953.

Bilmen, J. G. et al. 2001. Inhibition of the SERCA  $\text{Ca}^{2+}$  pump by curcumin. Curcumin putatively stabilizes the interaction between the nucleotide-binding and phosphorylation domains in the absence of ATP. *European Journal of Biochemistry* 268(23), pp. 6318-6327.

Black, R. L. et al. 1960. Dexamethasone: antirheumatic properties, hormonal effects and adverse reactions (a 16 month study). *Arthritis & Rheumatology* 3, pp. 112-128.

Blank, N. M. et al. 2007. Cholera toxin binds to lipid rafts but has limited specific for ganglioside GM1. *Immunology & Cell Biology* 85(5), pp. 378-382.

Boland, B. et al. 2018. Promoting the clearance of neurotoxic proteins in neurodegenerative disorders of ageing. *Nature Review Drug Discovery* 17(9), pp. 660-688.

Boles, D. J. and Proia, R. L. 1995. The molecular basis of HEXA mRNA deficiency caused by the most common Tay-Sachs disease mutation. *American Journal of Human Genetics* 56(716-724),

Borbon, I. A. et al. 2012. Lack of efficacy of curcumin on neurodegeneration in the mouse model of Neimann-Pick C1. *Pharmacology Biochemistry and Behavior* 101(1), pp. 125-131.

Bosch, M. E. and Kielian, T. 2019. Astrocytes in juvenile neuronal ceroid lipofuscinosis (CLN3) display metabolic and calcium signaling abnormalities. *Journal of Neurochemistry* 148(5), pp. 612-624.

- Bosnall, D. R. and Lall, G. S. 2013. Protein kinase C differentially regulates entrainment of the mammalian circadian clock. *Chronobiology International* 30(4), pp. 460-469.
- Braakman, I. and Hebert, D. N. 2013. Protein folding in the endoplasmic reticulum. *Cold Spring Harbor Perspectives in Biology* 5(5), p. a013201.
- Bramwell, K. K. C. et al. 2014. Lysosomal  $\beta$ -Glucuronidase regulates lyme and rheumatoid arthritis severity. *Journal of Clinical Investigation* 124(1), pp. 311-320.
- Brandl, C. J. et al. 1986. Two Ca<sup>2+</sup> ATPase genes: homologies and mechanistic implications of deduced amino acid sequences. *Cell* 44(4), pp. 597-607.
- Brimer, A. 2017. *Developing small molecule drugs for neurodegenerative diseases*. Cardiff University.
- Brini, M. and Carafoli, E. 2009. Calcium pumps in health and disease. *Physiological Reviews* 89(4), pp. 1341-1378.
- Broadhead, D. M. and Butterworth, J. 1977. The diagnosis of Gaucher's disease in liver using 4-methylumbelliferyl-beta-D-glucopyranoside. *Clinica Chimica Acta* 75(1), pp. 155-161.
- Broadhead, D. M. and Butterworth, J. 1978. Pompe's disease: diagnosis in kidney and leucocytes using 4-methylumbelliferyl-alpha-D-glucopyranoside. *Clinical Genetics* 13(6), pp. 504-510.
- Brokowska, J. et al. 2020. Expression of gene involved in apoptosis is dysregulated in mucopolysaccharidoses as revealed by pilot transcriptomic analyses. *Cell Biology International* 3, p. doi: 10.1002/cbin.11332.
- Brooks, D. A. et al. 2016. Stop - codon read - through for patients affected by a lysosomal storage disorder . . *Trends in Molecular Medicine* 12, pp. 367-373.
- Brunkhorst, R. et al. 2014. Fingolimod for the treatment of neurological diseases-state of plya and future perspectives. *Frontiers in Cellular Neuroscience* 12, p. 283.
- Bultynck, G. et al. 2014. Bax inhibitor-1 is likely a pH-sensitive calcium leak channel, not a H<sup>+</sup>/ca<sup>2+</sup> exchanger. *Science Signaling* 7(343), p. pe22.
- Burstein, S. et al. 1984. Stimulation of sphingomyelin hydrolysis by cannabidiol in fibroblasts from Niemann-Pick patients. *Biochemical and Biophysical Research Communications* 121(1), pp. 168-173.
- Calcraft, P. J. et al. 2009. NAADP mobilizes calcium from acidic organelles through two-pore channels. *Nature* 459, pp. 596-600.

- Camp, L. A. and Hofman, S. L. 1993. Purification and properties of a palmitoyl-protein thioesterase that cleaves palmitate from H-Ras. *Journal of Biological Chemistry* 268(30), pp. 22566-22574.
- Cannelli, N. et al. 2006. Novel mutations in *cln8* in Italian variant late infantile neuronal ceroid lipofuscinosis: another genetic hit in the Mediterranean. *Neurogenetics* 7, pp. 111-117.
- Cao, Y. et al. 2006. Autophagy is disrupted in a knock-in mouse model of juvenile neuronal ceroid lipofuscinosis. *Journal of Biological Chemistry* 281(29), pp. 20483-20493.
- Cao, Y. et al. 2011. Distinct early molecular responses to mutations causing vLINCL and JNCL presage ATP synthase subunit C accumulation in cerebellar cells. *PLoS ONE* 17(6), p. 2.
- Carafoli, E. 1974. Mitochondrial uptake of calcium ions and the regulation of cell function. *Biochemical Society Symposia* (39), pp. 89-109.
- Carafoli, E. and Krebs, J. 2016. Why Calcium? How calcium became the best communicator. *Journal of Biological Chemistry* 291, pp. 20849-20857.
- Cardone, M. 2007. Prospects for gene therapy in inherited neurodegenerative diseases. *Current Opinion in Neurology* 20, pp. 15–18.
- Castedo, M. et al. 2002. Mammalian target of rapamycin (mTOR): pro- and anti-apoptotic. *Cell Death & Differentiation* 9, pp. 99-100.
- Caudron, E. et al. 2015. Enzymatic diagnosis of Fabry disease using a fluorometric assay on dried blood spots: and alternative methodology. *European Journal of Medical Genetics* 58(12), pp. 681-684.
- Celsi, F. et al. Mitochondria, calcium and cell death: a deadly triad in neurodegeneration. *Biochimica et Biophysica Acta* 1787(6), pp. 335-344.
- Celsi, F. et al. 2009. Mitochondria, calcium and cell death: a deadly triad in neurodegeneration. *Biochimica et Biophysica Acta* 1787(6), pp. 335-344.
- Chandrachud, U. et al. 2015. Unbiased Cell-based Screening in a Neuronal Cell Model of Batten Disease Highlights an Interaction between Ca<sup>2+</sup> Homeostasis, Autophagy, and CLN3 Protein Function. *Journal of Biological Chemistry* 290(23), pp. 14361-14380.
- Chang, T. Y. et al. 2006. Cholesterol sensing, trafficking, and esterification. *Annual Review of Cell and Developmental Biology* 22, pp. 129-157.
- Chen, C. S. et al. 1999. Broad screening test for sphingolipid-storage diseases. *Lancet* 354, pp. 901-905.

Christensen, K. A. et al. 2002. pH-dependent regulation of lysosomal calcium in macrophages. *Journal of Cell Science* 115, pp. 599-607.

Clapham, D. E. 2007. Calcium signaling. *Cell* 131, pp. 1047-1158.

Cleeter, M. W. J. et al. 2013. Glucocerebrosidase inhibition causes mitochondrial dysfunction and free radical damage. *Neurochemistry International* 62(1), pp. 1-7.

Coen, K. et al. 2012. Lysosomal calcium homeostasis defects, not proton pump defects, cause endo-lysosomal dysfunction in PSEN-deficient cells. *Journal of Cell Biology* 198(1), pp. 25-35.

Cohen, P. A. 2014. Hazard of hindsight -- monitoring the safety of nutritional supplements. *The New England Journal of Medicine* 370(14), pp. 1277-11280.

Connolly, G. P. 1998. Fibroblast models of neurological disorders: Fluorescence Measurements studies. *Trends in Pharmacology Sciences* 19(5), pp. 171-177.

Cook, S. R. et al. 2020. Detrimental effects of zwitterionic buffers on lysosomal homeostasis in cell lines and iPSC-derived neurons. *AMRC Open Research* 2, p. 21.

Cooper, D. J. et al. 2018. Phenotypic screening with primary neurons to identify drug targets for regeneration and degeneration. *Molecular and Cellular Neuroscience* 80, pp. 161-169.

Cortes, C. J. and La Spada, A. R. 2014. The many faces of autophagy dysfunction in Huntington's disease: from mechanistic pathway to therapeutic opportunities. *Drug Discovery Today* 19, pp. 963-971.

Cox, T. et al. 2000. Novel oral treatment of Gaucher's disease with N-butyldeoxynojirimycin (OGT 918) to decrease substrate biosynthesis. *Lancet* 355(9214), pp. 1481-1485.

Cox, T. M. and Cachón-González, M. B. 2012. The cellular pathology of lysosomal disease. *The Journal of Pathology* 226, pp. 241-254.

Creasy, B. M. et al. 2007. New assay using fluorogenic substrates and immunofluorescence staining to measure cysteine Cathepsin activity in live cell subpopulations. *Cytometry Part A* 71(2), pp. 114-123.

Crumling, M. A. et al. 2017. Cyclodextrins and iatrogenic hearing loss: new drugs with significant risk. *Frontiers in cellular neuroscience* 11, p. 355.

D'Orsi, B. et al. 2015. Bax regulates neuronal Ca<sup>2+</sup> homeostasis. *The Journal of Neuroscience* 35(4), pp. 1706-1722.

Das, A. K. et al. 2001. Biochemical analysis of mutations in palmitoyl-protein thioesterase causing infantile and late-onset forms of neuronal ceroid lipofuscinosis. *Human Molecular Genetics* 10(13), pp. 1431-1439.

- de Duve, C. 2005. The lysosome turns fifty. *Nature Cell Biology* 7, pp. 847-849.
- de Duve, C. et al. 1955. Tissue fractionation studies. 6. Intracellular distribution patterns of enzyme in rat-liver tissue. *Biochemical Journal* 60, pp. 604-617.
- de la Mata, M. et al. 2016. Mitochondrial dysfunction in lysosomal storage disorders. *Diseases* 4(4), p. 31.
- De Luisi, A. and Hofer, A. M. 2003. Evidence that Ca(2+) cycling by the plasma membrane Ca(2+)-ATPase increases the 'excitability' of the extracellular Ca(2+)-sensing receptor. *Journal of Cell Science* 116(Pt 8), pp. 1527-1538.
- de Mezer, M. et al. 2011. Mutant CAG repeats of Huntingtin transcript fold into hairpins, form nuclear foci and are targets for RNA interference. *Nucleic Acids Research* 39, pp. 3852-3863.
- Deane, J. E. et al. 2011. Insights into Krabbe disease from structure of galactocerebrosidase. *Proceeding of the National Academy of Sciences of the United States of America* 108(37), pp. 15169-15173.
- Dedera, D. et al. 1990. Attenuation of HIV-1 infectivity by an inhibitor of oligosaccharide processing. *AIDS Research and Human Retroviruses* 6(6), pp. 785-794.
- Dhami, R. et al. 2006. Identification of novel biomarkers for niemann-pick disease using gene expression analysis of acid sphingomyelinase knockout mice. *Molecular Therapy* 13(3), pp. 556-564.
- Di Paola, S. et al. 2018. TRPML1: The Ca<sup>(2+)</sup> retaker of lysosome. *Cell Calcium* 69, pp. 112-121.
- di Ronza, A. et al. 2018. CLN8 is an endoplasmic reticulum cargo receptor that regulates lysosome biogenesis. *Nature Cell Biology* 20, pp. 1370-1377.
- Dong, X. et al. 2009. Activating mutations of the TRPML1 channel revealed by proline-scanning mutagenesis. *Journal of Biological Chemistry* 284(46), pp. 32040-32052.
- Dong, X. P. et al. 2008. The type IV mucopolipidosis-associated protein TRPML1 is an endolysosomal iron release channel. *Nature* 455(992-996),
- Dong, X. P. et al. 2010. PI(3,5)P2 controls membrane traffic by direct activation of mucolipin Ca<sup>2+</sup> release channels in the endolysosome. *Nature Communications* 1(4), p. 38.
- Douillard-Guilloux, G. et al. 2010. Restoration of muscle functionality by genetic suppression of glycogen synthesis in a murine model of Pompe disease. *Human Molecular Genetics* 19, pp. 684-696.
- Du, X. and Yang, H. 2013. Endosomal cholesterol trafficking: protein factors at a glance. *Acta Biochimica et Biophysica Sinica* 45, pp. 11-17.

Duchen, M. R. 2000. Mitochondria and calcium: from cell signalling to cell death. *The Journal of Physiology* 529(Pt 1), pp. 57-68.

Dudland, J. A. and Francis, G. A. 2015. Lysosomal acid lipase: at the crossroads of normal and atherogenic cholesterol metabolism. *Frontiers in Cell and Developmental Biology* 3(3), p. doi:10.3389/fcell.2015.00003.

Duvvuri, M. et al. 2004. Weak base permeability characteristics influence the intracellular sequestration site in the multidrug-resistant human leukemic cell line HL-60. *The Journal of Biological Chemistry* 279(31), pp. 32367-32367.

Efthymiou, A. G. et al. 2014. Rescue of an in vitro neuron phenotypes identified in Niemann-Pick disease, Type C1 induced pluripotent stem cell-derived neurons by modulating the WNT pathway and calcium signaling. *Stem Cells Translational Medicine* 4(3), pp. 230-238.

Elleder, A. et al. 1997. Follow-up study of subunit c of mitochondrial ATP synthase (SCMAS) in Batten disease and in unrelated lysosomal disorders. *Acta Neuropathologica* 93, pp. 379-390.

Elleder, M. et al. 1995. Tissue culture loading test with storage granules from animal models of neuronal ceroid-lipofuscinosis (Batten disease): testing their lysosomal degradability by normal and Batten cells. *American Journal of Medical Genetics* 5(57), pp. 212-221

Elliot-Smith, E. et al. 2008. Beneficial effects of substrate reduction therapy in a mouse model of GM1 gangliosidosis. *Molecular Genetics and Metabolism* 94(2), pp. 204-211.

Elliott, S. et al. 2016. Pilot study of newborn screening for six lysosomal storage diseases using tandem mass spectrometry. *Molecular Genetics and Metabolism* 118(4), pp. 304-309.

Erie, C. et al. 2015. Altered lysosomal positioning affects lysosomal functions in a cellular model of Huntington's disease. *European Journal Neuroscience* 42, pp. 1941-1951.

European Medicine Agency. 2017. *Brineura*. Available at: <https://www.ema.europa.eu/en/medicines/human/EPAR/brineura> [Accessed: 06/06/2020].

European Medicines Agency. 2016. *First oral treatment for Fabry disease recommended for approval in the EU*. Available at: [https://www.ema.europa.eu/en/news/first-oral-treatment-fabry-disease-recommended-approval-eu#:~:text=The%20European%20Medicines%20Agency%20\(EMA,enzyme%20called%20alpha%2Dgalactosidase%20A](https://www.ema.europa.eu/en/news/first-oral-treatment-fabry-disease-recommended-approval-eu#:~:text=The%20European%20Medicines%20Agency%20(EMA,enzyme%20called%20alpha%2Dgalactosidase%20A). [Accessed: 06/06/2020].

Ezaki, J. et al. 1999. A lysosomal proteinase, the late infantile neuronal ceroid lipofuscinosis gene ( CLN2 ) product, is essential for degradation of a hydrophobic

protein, the subunit c of ATP synthase. *Journal of Neurochemistry* 72(6), pp. 2573-2582.

Facompré, M. et al. 2000. Relationship between cell cycle changes and variations of the mitochondrial membrane potential induced by etoposide. *Molecular Cell Biology Research Communications* 4(1), pp. 37-42.

Fan, G. et al. 2015. Gating machinery of InsP3R channels revealed by electron cryomicroscopy. *Nature* 527(7578), pp. 336-341.

Ficicioglu, C. 2008. Review of miglustat for clinical management in Guacher disease type 1. *Therapeutics and Clinical Management* 4(2), pp. 425-431.

Fill, M. and Copello, J. A. 2002. Ryanodine receptor calcium release channels. *Physiological Reviews* 82(4), pp. 893-922.

Fineran, P. et al. 2016. Pathogenic mycobacteria achieve cellular persistence by inhibiting the Niemann-Pick Type C disease cellular pathway. *Wellcome Open Research* 1, p. 18.

Flanagan, J. J. et al. 2009. The pharmacological chaperone 1-deoxyojirimycin increases the activity and lysosomal trafficking of multiple mutant forms of acid alpha-glucosidase. *Human Mutation* 30, pp. 1683–1692.

Fog, C. K. et al. 2018. The heat shock protein amplifier arimoclomol improves refolding, maturation and lysosomal activity of glucocerebrosidase. *EBioMedicine* 38, pp. 142-153.

Fourcade, S. et al. 2010. Valproic acid induces antioxidant effects in X-linked adrenoleukodystrophy. *Human Molecular Genetics* 19(10), pp. 2005-2014.

Fukuda, T. et al. 2006. Dysfunction of endocytic and autophagic pathways in a lysosomal storage disease. *Annals of Neurology* 59(4), pp. 700-708.

Fyrst, H. and Saba, J. D. 2010. An update on sphingosine-1-phosphate and other sphingolipid mediators. *Nature Chemical Biology* 6(7), p. 489.

Gadoth, N. and Oksenberg, A. 2014. Sleep and sleep disorders in rare hereditary diseases: A reminder for the paediatrician, paediatric and adult neurologist, general practitioner, and sleep specialist. *Frontier in Neurology* 5, p. 133.

Galione, A. 2011. NAADP Receptors. *Cold Spring Harbor Perspectives in Biology* 3(1), p. a004036.

Galione, A. and Churchill, G. C. 2002. Interactions between calcium release pathways: multiple messengers and multiple stores. *Cell Calcium* 32(5-6), pp. 343-354.

Galizzi, G. et al. 2011. Different early ER-stress responses in the CLN8(mnd) mouse model of neuronal ceroid lipofuscinosis. *Neuroscience Letters* 488, pp. 258-262.

Garrity, A. G. et al. 2016. The endoplasmic reticulum, not the pH gradient, drives calcium refilling of lysosomes. *eLife* 5, p. e15887.

Gault, C. R. et al. 2010. An overview of sphingolipid metabolism: from synthesis to breakdown. *Advances in Experimental Medicine and Biology* 688, pp. 1-23.

Gelstrophe, M. E. et al. 2008. Niemann-Pick type C1 I1061T mutant encodes a functional protein that is selected for endoplasmic reticulum-associated degradation due to protein misfolding. *Journal of Biological Chemistry* 283(13), pp. 8229-8236.

Geng, H. et al. 2011. Novel patient cell-based HTS assay for identification of small molecules for a lysosomal storage disease. *PLOS One* 6(12), p. e29504.

Ginzburg, L. and Futerman, A. H. 2005. Defective calcium homeostasis in the cerebellum in a mouse model of Niemann-Pick A disease. *Journal of Neurochemistry* 95, pp. 1619-1628.

Giugliani, R. et al. 2013. A phase 2 study of migalastat hydrochloride in females with Fabry disease: selection of population, safety and pharmacodynamics effects. *Molecular Genetics and Metabolism* 109(1), pp. 86-92.

Glick, D. et al. 2010. Autophagy: cellular and molecular mechanisms. *The Journal of Pathology* 221, pp. 3-12.

Goldin, E. et al. 2012. High throughput screening for small molecule therapy for Gaucher disease using patient tissue as a source of mutant glucocerebrosidase. *PLoS One* 7(1), p. e29861.

Golding, E. et al. 2012. High throughput screening for small molecule therapy for Gaucher disease using patient tissue as the source of mutant glucocerebrosidase. *PLOS One* 7(1), p. e29861.

Gong, X. et al. 2016. Structural insights into the Niemann-Pick C1 (NPC1)-mediated cholesterol transfer and ebola infection. *Cell* 165, pp. 1467-1478.

Goodman, A. O. G. et al. 2011. Asymptomatic sleep abnormalities are a common early feature in patient with Huntington's disease. *Current Neurology and Neuroscience Reports* 11(2), pp. 211-217.

Gotoda, Y. et al. 1998. Missense and nonsense mutations in the lysosomal alpha-mannosidase gene (MANB) in severe and mild forms of alpha-mannosidosis. *American Journal of Human Genetics* 63(4), pp. 1015-1024.

GraphPad. 2018. One-way ANOVA followed by Dunnett's multiple comparisons test was performed using GraphPad Prism version 7.00 for Mac. La Jolla, California, USA.

Green, K. N. et al. 2008. SERCA pump activity is physiologically regulated by presenilin and regulates amyloid beta production. *The Journal of General Physiology* 132(2), p. i1. doi: 10.1085/JGP1322OIA1081.

- Griffin, K. et al. 2020. Human Stem Cell-derived Aggregates of Forebrain Astroglia Respond to Amyloid Beta Oligomers. *Tissue Engineering Part A* 26(9-10), pp. 527-542.
- Groh, J. et al. 2017. Fingolimod and Teriflunomide Attenuate Neurodegeneration in Mouse Models of Neuronal Ceroid Lipofuscinosis. *Molecular Therapy* 25(8), pp. 1889-1899.
- Grubman, A. et al. 2014. Deregulation of biometal hoemostasis: the missing link for neuronal ceroid lipofuscinoses? *Metallomics* 6(4), pp. 932-943.
- Grynkiewicz, G. et al. 1985. A new generation of  $Ca^{2+}$  indicators with greatly improved fluorescence properties. *The Journal of Biological Chemistry* 260(6), pp. 3440-3450.
- Guarneri, R. et al. 2004. Retinal oxidation, apoptosis and age- and sex-differences in the mnd mutant mouse, a model of neuronal ceroid lipofuscinosis. *Brain Research* 1014, pp. 209-220.
- Guerrera, M. and Ladisch, S. 2003. N-Butyldeoxynojirimycin inhibits murine melanoma cell ganglioside metabolism and delays tumor onset. *Cancer Letter* 201(1), pp. 31-40.
- Guerrero-Hernandez, A. et al. 2010. An intelligent sarco-endoplasmic reticulum  $Ca^{2+}$  store: release and leak channels have differential access to a concealed  $Ca^{2+}$  pool. *Cell Calcium* 48(2-3), pp. 143-149.
- Guha, S. et al. 2014. Approaches for detecting lysosomal alkalinization and impaired degradation in fresh and cultured RPE cells: evidence for a role in retinal degenerations. *Experimental Eye Research* 126, pp. 68-76.
- Gunn, G. et al. 2014. Long - term nonsense suppression therapy moderates MPS I - H disease progression. *Molecular Genetics and Metabolism* 111, pp. 374-381.
- Gunter, T. E. and Pfeiffer, D. R. 1990. Mechanisms by which mitochondria transport calcium. *American Journal of Physiology* 258(5 Pt 1), pp. C755-786.
- Gómez, N. M. et al. 2018. TRPML: Transporters of metals in lysosomes essential for cell survival? *The Journal of the Federation of American Societies for Experimental Biology* 32(2), pp. 782-794.
- Haddad, S. E. et al. 2012. CLN5 and CLN8 protein association with ceramide synthase: biochemical and proteomic approaches. *Electrophoresis* 33, pp. 3798-3809.
- Hannun, Y. A. and Bell, R. M. 1989. Regulation of protein kinase C by sphingosine and lysosphingolipids. *Clinica Chimica Acta* 185(3), pp. 333-345.

Haslett, L. J. 2015. *Lysosomal storage disorders and neurodegenerative disease; related mechanisms of pathogenesis and identification of novel therapeutic targets*. Cardiff University.

Hasting, M. H. et al. 2003. A clockwork web: circadian timing in brain and periphery, in health and disease. *Nature Reviews Neuroscience* 4(8), pp. 649-661.

Hayashi, A. et al. 2014. Pathological fracture and pyogenic osteomyelitis in a patient with type 2 Gaucher disease. *Brain & Development* 36(9), pp. 830-833.

Headlam, H. A. et al. 2006. Inhibition of Cathepsins and related proteases by amino acid, peptide, and protein hydroperoxides. *Free Radical Biology and Medicine* 40(9), pp. 1539-1548.

Heare, T. et al. 2007. Severe endothelial dysfunction in the aorta of mouse model of Fabry disease; partial prevention by N-butyldeoxynojirimycin treatment. *Journal of Inherited Metabolic Disease* 30(1), pp. 79-87.

Heintz, N. 1993. Cell death and the cell cycle: a relationship between transformation and neurodegeneration? *Trends in Biochemical Sciences* 18(5), pp. 157-159.

Hennermann, J. B. et al. 2016. Treatment with pentosan polysulphate in patients with MPS I: results from an open label, randomized, monocentric phase II study . *Journal of Inherited Metabolic Disease* 39(6), pp. 831–837.

Hermansson, M. et al. 2005. Mass spectrometric analysis reveals changes in phospholipid, neutral sphingolipid and sulfatide molecular species in progressive epilepsy with mental retardation, EPMR, brain: a case study. *Journal of Neurochemistry* 95(3), pp. 609-617.

Hesselink, K. 2017. Biomoclolmol and Arimoclolmol: HSP-co-Inducers for the treatment of protein misfolding disorders, neuropathy and neuropathic pain. *Journal of Pain & Relief* 6(1), pp. DOI: 10.4172/2167-0846.1000279.

Hocquemiller, M. et al. 2016. Adeno - associated virus - based gene therapy for CNS diseases. *Human Gene Therapy* 27, pp. 478-496.

Holpainen, J. M. et al. 2001. Elevated lysosomal pH in neuronal ceroid lipofuscinoses (NCLs). *European Journal of Biochemistry* 268(22), pp. 5851-5856.

Hood, S. and Amir, S. 2017. Neurodegeneration and the circadian clock. *Frontiers in Aging Neuroscience* 9, p. 170.

Hopwood, J. J. et al. 1979. A fluorometric assay using 4-methylumbelliferyl alpha-L-iduronide for the estimation of alpha-L-iduronidase activity and the detection of Hurler and Scheie Syndromes. *Clinical Chimica Acta* 92(2), pp. 257-265.

Huang, H. P. et al. 2012. Induced pluripotent stem cell technology for disease modeling and drug screening with emphasis on lysosomal storage diseases. *Stem Cell Research & Therapy* 3, p. 34.

Huang, S. et al. 2020. Recent advances in modulators of circadian rhythms: an update and perspective. *Journal of Enzyme Inhibition and Medicinal Chemistry* 35(1), pp. 1267-1286.

Hughes, J. P. et al. 2011. Principle of early drug discovery. *British Journal of Pharmacology* 162(6), pp. 1239-1249.

Hughes, M. E. et al. 2010. *CIRCA: Circadian gene expression profiles*. Available at: [Accessed: May 2017].

Ingemann, L. and Kirkegaard, T. 2014. Lysosomal storage disease and the heat shock response: convergence and therapeutic opportunities. *Journal of Lipid Research* 55(11), pp. 2198-2210.

Inglese, J. et al. 2007. Reporting data from high-throughput screening of small-molecule libraries. *Nature Chemical Biology* 3(8), pp. 438-441.

Ioannou, Y. A. 2005. Guilty until proven innocent: the case of NPC1 and cholesterol. *Trends in Biochemical Sciences* 30, pp. 498-505.

Ismael, F. O. et al. 2016. Role of myeloperoxidase oxidants in the modulation of cellular lysosomal enzyme function: a contributing factor to macrophage dysfunction in Atherosclerosis? *PLOS One* 11(12), p. e0168844.

Jabs, S. et al. 2008. Accumulation of bis(monoacylglycero) phosphate and gangliosides in mouse models of neuronal ceroid lipofuscinosis. *Journal of Neurochemistry* 106, pp. 1415-1425.

Jack, R. M. et al. 2006. The use of acarbose inhibition in the measurement of acid alpha-glucosidase activity in blood lymphocytes for the diagnosis of pompe disease. *Genetics in Medicine* 8(5), pp. 307-312.

Jalanko, A. and Braulke, T. 2009. Neuronal ceroid lipofuscinoses. *Biochimica et Biophysica Acta* 1793, pp. 697-709.

Jang, D. S. et al. 2016. Cell-based high-throughput screening identifies galactocerebrosidase enhancers as potential small-molecule therapies for Krabbe's disease. *Journal of Neuroscience Research* 94, pp. 1231-1245.

Jennings Jr, J. J. et al. 2006. Mitochondrial aberrations in mucopolidosis type IV. *The Journal of Biological Chemistry* 281(51), pp. 39041-39050.

Jing, K. and Lim, K. 2012. Why is autophagy important in human diseases? *Experimental & Molecular Medicine* 44(2), pp. 69-72.

- Johansson, M. et al. 2007. Activation of endosomal dynein motors by stepwise assembly of Rab7-RILP-P150 glued, ORP1L, and the receptor betaLII sepctrin. *Journal of Cell Biology* 176(4), pp. 459-471.
- Jolly, R. D. et al. 2002. Mitochondrial dysfunction in the neuronal ceroid-lipofuscinoses (Batten disease). *Neurochemistry International* 40(6), pp. 565-571.
- Junaid, M. A. and Pullarket, R. K. 1999. Increased brain lysosomal pepstatin-insensitive proteinase activity in patients with neurodegenerative diseases. *Neuroscience Letters* 264, pp. 157-160.
- Kabbara, A. A. and Allen, D. G. 2001. The use of the indicator fluo-5N to measure sarcoplasmic reticulum calcium in single muscle fibres of the cane toad. *The Journal of Physiology* 534(Pt 1), pp. 87-97.
- Kang, S. et al. 2014. Altered levels of  $\alpha$ -synuclein and sphingolipids in Batten disease lymphoblast cells. *Gene* 539(2), pp. 181-185.
- Karten, B. et al. 2002. Cholesterol accumulates in cell bodies, but is decreased in distal axons, of Niemann-Pick C1- deficient neurons. *Journal of Neurochemistry*, pp. 1154-1163.
- Keeling, K. M. 2016. Nonsense suppression as an approach to treat lysosomal storage diseases. *Diseases* 4, p. 32.
- Keeling, K. M. et al. 2001. Gentamicin - mediated suppression of Hurler syndrome stop mutations restores a low level of  $\alpha$  - I - iduronidase activity and reduces lysosomal glycosaminoglycan accumulation . *Human Molecular Genetics* 10, pp. 291-299.
- Kenninen, K. M. et al. 2013. Altered biometal homeostasis is associated with CLN6 mRNA loss in mouse neuronal ceroid lipofuscinosis. *Biology Open* 2(6), pp. 635-646.
- Kim, S. and kim, K. T. 2014. Therapeutic approaches for inhibition protein aggregation in Huntington's disease. *Experimental Neurobiology* 23, pp. 36-44.
- Kim, S. J. et al. 2006a. Endoplasmic reticulum stress-induces caspase-4 activation mediates apoptosis and neurodegeneration in INCL. *Human Molecular Genetics* 15(11), pp. 1826-1834.
- Kim, S. J. et al. 2006b. Palmitoyl-protein thioesterase-1 deficiency leads to the activation of caspase-9 and contributes to a rapid neurodegeneration in INCL. *Human Molecular Genetics* 15(10), pp. 1580-1586.
- Kingma, S. D. K. et al. 2013. An algorithm to predict phenotypic severity in mucopolysaccharidosis type I the first month of life. *Orphanet Journal of Rare Diseases* 8, p. 99.
- Kirichok, Y. et al. 2004. The mitochondrial calcium uniporter is highly selective ion channel. *Nature* 427(6972), pp. 360-364.

Kirkegaard, T. et al. 2016. Heat shock protein-based therapy as a potential candidate for treating the sphingolipidoses. *Science Translational Medicine* 8(355), p. 355ra118.

Kirkegaard, T. et al. 2010. Hsp70 stabilizes lysosomes and reverts Niemann-Pick disease-associated lysosomal pathology. *Nature* 463, pp. 549-553.

Kirkham, E. D. 2020. *The role of lysosomal ion homeostasis and lysosomal proteases in healthy ageing and neurodegeneration*. Cardiff University.

Kishnani, P. et al. 2017. Duvoglustat HCl Increases Systemic and Tissue Exposure of Active Acid  $\alpha$ -Glucosidase in Pompe Patients Co-administered with Alglucosidase  $\alpha$ . *Molecular Therapy* 25(5), pp. 1199-1208.

Kiyokawa, E. et al. 2004. Recognition of sphingomyelin by lysenin and lysenin-related proteins. *Biochemistry* 43, pp. 9766-9773.

Klein, A. et al. 2011. Lack of activation of the unfolded protein response in mouse and cellular models of Niemann-Pick Type C disease. *Neurodegenerative Diseases* 8(3), pp. 124-128.

Klionsky, D. J. 2014. Citing recent declines in the discovery of new ATG genes, some scientists now suggest that the end of autophagy research may be within sight. *Autophagy* 10(5), pp. 715-716.

Koga, H. et al. 2011. Constitutive upregulation of chaperone-mediated autophagy in Huntington's disease. *The Journal Neuroscience* 31, pp. 18492-18505.

Kohlschütter, A. and Schulz, A. 2016. CLN2 Disease (Classic Late Infantile Neuronal Ceroid Lipofuscinosis). *Pediatric Endocrinology Reviews* 13(1), pp. 682-688.

Kolikova, J. et al. 2011. Deficient mitochondrial Ca<sup>2+</sup> buffering in the CLN8(mnd) mouse model of neuronal ceroid lipofuscinosis. *Cell Calcium* 50, pp. 491-501.

Kollman, K. et al. 2013. Cell biology and function of neuronal ceroid lipofuscinosis-related protein. *Biochimica et Biophysica Acta* 1832(11), pp. 1866-1881.

Kolter, T. and Sandhoff, K. 2005. Principles of lysosomal membrane digestion: stimulation of sphingolipid degradation by sphingolipid activator proteins and anionic lysosomal lipids. *The Annual Review of Cell and Developmental Biology* 21, pp. 81-103.

Korkotian, E. et al. 1999. Elevation of intracellular glucosylceramide levels results in an increase in endoplasmic reticulum density and in functional calcium stores in cultured neurons. *Journal of Biological Chemistry* 274(31), pp. 21673-21678.

Kousi, M. et al. 2012. Update of the mutation spectrum and clinical correlations of over 360 mutations in eight genes that underlie the neuronal ceroid lipofuscinoses. *Human Mutation* 33, pp. 42-63.

- Koussounadis, A. et al. 2015. Relationship between differentially expressed mRNA and mRNA-protein correlations in a xenograft model system. *Scientific Reports* 5(10775), p. doi: 10.1038/srep10775.
- Kunkel, G. T. et al. 2013. Targeting the sphingosine-1-phosphate axis in cancer, inflammation and beyond. *Nature Review Drug Discovery* 12, pp. 688-702.
- Kuronen, M. et al. 2012. Galactolipid deficiency in the early pathogenesis of neuronal ceroid lipofuscinosis model *Cln8mnd*: Implications to delayed myelination and oligodendrocyte maturation. *Neuropathology and Applied Neurobiology* 38, pp. 471-486.
- Kwon, H. J. et al. 2009. Structure of N-terminal domain of NPC1 reveals distinct subdomains for binding and transfer of cholesterol. *Cell* 137, pp. 1213-1224.
- Lachmann, R. H. et al. 2004. Treatment with miglustat reverses the lip-trafficking defect in Niemann-Pick disease type C. *Neurobiology of Disease* 16, pp. 654-658.
- Leake, D. S. et al. 1982. Properties and subcellular localization of acid phosphatase activity in cultured arterial smooth muscle cells. *European Journal of Biochemistry* 15(2-3), pp. 557-563.
- Lee, J. H. et al. 2015. Presenilin 1 Maintains Lysosomal Ca(2+) Homeostasis via TRPML1 by Regulating vATPase-Mediated Lysosome Acidification. *Cell Reports* 12(9), pp. 1430-1444.
- Lee, J. H. et al. 2010a. Lysosomal proteolysis and autophagy require presenilin 1 and are disrupted by Alzheimer-related PS1 mutations. *Cell* 141(7), pp. 1146-1158.
- Lee, W. C. et al. 2010b. Molecular characterization of mutations that cause globoid cell leukodystrophy and pharmacological rescue using small molecule chemical chaperones. *The Journal of Neuroscience* 30(16), pp. 5489-5497.
- Lim, D. et al. 2008. Calcium homeostasis and mitochondrial dysfunction in striatal neurons of Huntington disease. *The Journal of Biological Chemistry* 283, pp. 5780-5789.
- Lim, S. M. et al. 2016. Patient fibroblasts-derived induced neurons demonstrate autonomous neuronal defects in adult-onset Krabbe disease. *Oncotarget* 7(46), pp. 74496-74509.
- Lipinski, C. A. et al. 2001. Experimental and computational approaches to estimate solubility and permeability in drug discovery and development settings. *Advanced Drug Delivery Reviews* 46, pp. 3-26.
- Liu, C. and Hermann, T. E. 1978. Characterization of ionomycin as calcium ionophore. *The Journal of Biological Chemistry* 253, pp. 5892-5894.

- Liu, E. A. and Lieberman, A. P. 2019. The intersection of lysosomal and endoplasmic reticulum calcium with autophagy defects in lysosomal disease. *Neuroscience letters* 697, pp. 10-16.
- Lloyd-Evans, E. 2006. *Cell biology of Niemann-Pick type C disease*. D Phil, University of Oxford.
- Lloyd-Evans, E. and Haslett, L. 2016. The lysosomal storage disease continuum with ageing-related neurodegenerative disease. *Ageing Research Reviews* 8, p. doi: 10.1016/j.arr.2016.1007.1005.
- Lloyd-Evans, E. et al. 2008. Niemann-Pick disease type C1 is a sphingosine storage disease that causes deregulation of lysosomal calcium. *Nature Medicine* 14, pp. 1247-1255.
- Lloyd-Evans, E. et al. 2003. Lyso-glycosphingolipids mobilize calcium from brain microsomes via multiple mechanisms. *Biochemical Journal* 375(Pt 3), pp. 561-565.
- Lloyd-Evans, E. and Platt, F. M. 2010. Lipids on trial: the search for the offending metabolite in Niemann-Pick type C disease. *Traffic* 11(4), pp. 419-428.
- Lloyd-Evans, E. and Platt, F. M. 2011. Lysosomal Ca<sup>2+</sup> homeostasis: role in pathogenesis of lysosomal storage disease. *Cell Calcium* 50, pp. 200-205.
- Lloyd-Evans, E. and Waller-Evans, H. 2019. Lysosomal Ca<sup>2+</sup> homeostasis and signaling in health and disease. *Cold Spring Harbor Perspectives in Biology*, p. a035311 DOI: 035310.031101/cshperspect.a035311.
- Lonka, L. et al. 2000. The neuronal ceroid lipofuscinosis CLN8 membrane protein is a resident of the endoplasmic reticulum. *Human Molecular Genetics* 9, pp. 1691-1697.
- Luiro, K. et al. 2006. Batten disease (JNCL) is linked to disturbances in mitochondrial, cytoskeletal, and synaptic compartments. *Journal of Neuroscience Research* 84(5), pp. 1124-1138.
- Luzio, J. P. et al. 2007. Lysosomes: fusion and function. *Nature Reviews Molecular Cell Biology* 8, pp. 622 – 632.
- Lyly, A. et al. 2009. Novel Interactions of CLN5 support molecular networking between neuronal ceroid lipofuscinosis proteins. *BMC Cell Biology* 10, p. 83.
- Maceyka, M. et al. 2014. The potential of histone deacetylase inhibitors in Niemann-Pick Type C disease. *The FEBS Journal* 280(24), p. doi:10.1111/febs.12505.
- MacLennan, D. H. et al. 1985. Amino-acid sequence of a Ca<sup>2+</sup> + Mg<sup>2+</sup>-dependent ATPase from rabbit muscle sarcoplasmic reticulum, deduced from its complementary DNA sequence. *Nature* 316(6030), pp. 696-700.

- MacPhee, I. J. and Barker, P. A. 1997. Brain-derived neurotrophic factor binding to the p75 neurotrophin receptor reduces TrkA signaling while increasing serine phosphorylation in the TrkA intracellular domain. *The Journal of Biological Chemistry* 272, pp. 23547-23551.
- Maegawa, G. H. B. et al. 2009. Identification and characterization of ambroxol as enzyme enhancement agent for Gaucher disease. *Journal of Biological Chemistry* 284, pp. 23502-23516.
- Magalhaes, J. et al. 2018. Effects of ambroxol on the autophagy-lysosome pathway and mitochondria in primary cortical neurons. *Scientific Reports* 8, p. 1385.
- Magnusson, G. 1994. Synthesis of glycosphingolipids and corresponding neoglycolipids. *Advanced drug delivery reviews* 13(3), pp. 267-284.
- Makkar, R. et al. 2020. Nutraceuticals in neurological disorders. *International Journal of Molecular Sciences* 21(12), p. E4424.
- Malathi, K. et al. 2004. Mutagenesis of the putative sterol-sensing domain of yeast Niemann Pick C-related protein reveals a primordial role in subcellular sphingolipid distribution. *The Journal of Cell Biology* 164, pp. 547-556.
- Malik, B. R. et al. 2019. Autophagic and endo-lysosomal dysfunction in neurodegenerative disease. *Molecular Brain* 12(1), p. 100.
- Malo, N. et al. 2006. Statistical practise in high-throughput screening data analysis. *Nature Biotechnology* 24, pp. 167-175.
- Marotta, D. et al. 2017. NCLs and ER: A stressful relationship. *Biochimica et Biophysica Acta* 1863, pp. 1273-1281.
- Marshall, J. et al. 2010. Substrate reduction augments the efficacy of enzyme therapy in a mouse model of Fabry disease. *PLoS One* 5, p. e15033.
- Martina, J. A. et al. 2012. MTORC1 functions as a transcriptional regulator of autophagy by preventing nuclear transport of TFEB. *Autophagy* 8(6), pp. 903-914.
- Martina, J. A. et al. 2014. The nutrient-responsive transcription factor TFE3 promotes autophagy, lysosomal biogenesis, and clearance of cellular debris. *Science Signaling* 7(309), p. ra9.
- Martinez-Vicente, M. et al. 2010. Cargo recognition failure responsible for inefficient autophagy in Huntington's disease. *Nature Neuroscience* 13, pp. 567-576.
- Martino, S. et al. 2009. Specific determination of beta-galactocerebrosidase activity via competitive inhibition of beta-galactosidase. *Clinical Chemistry* 55(3), pp. 541-548.
- Marugan, J. J. et al. 2010. Evaluation of 2-Thioxo-2,3,5,6,7,8-hexahydropyrimidol[4,5-d]pyrimidin-4(1H)-one analogues as GAA activators. *European Journal of Medicinal Chemistry* 45(5), pp. 1880-1897.

Maue, R. A. et al. 2012. A novel mouse model of Niemann-Pick Type C disease carrying a D1005g-NPC1 mutation comparable to commonly observed human mutation. *Human Molecular Genetics* 21(4), pp. 730-750.

Mauri, V. et al. 2013. A rapid and sensitive method for measuring N-acetylglucosaminidase activity in cultured cells. *PLOS One* 8(6), p. e68060.

Maxfield, F. R. and Wüstner, D. 2012. Analysis of cholesterol trafficking with fluorescent probes. *Methods in Cell Biology* 108, pp. 367-393.

Mayes, J. S. et al. 1981. Differential assay for lysosomal alpha-galactosidases in human tissue and its application to Fabry's disease. *Clinical Chimica Acta* 112(2), pp. 247-251.

Mazzoccoli, G. 2011. The timing clock of life. *Journal of Biological Regulators and Homeostatic Agents* 25(1), pp. 137-143.

Mazzoccoli, G. et al. 2013. Circadian transcriptome analysis in human fibroblasts from Hunter syndrome and impact of iduronate-2-sulfatase treatment. *BMC Medical Genomics* 6, p. 37.

Medina, D. L. et al. 2015. Lysosomal calcium signalling regulates autophagy through calcineurin and TFEB. *Nature Cell Biology* 17(3), pp. 288-299.

Medina, D. L. et al. 2011. Transcriptional activation of lysosomal exocytosis promotes cellular clearance. *Developmental Cell* 21(3), pp. 421-430.

Megias-Vericat, J. E. et al. 2017. Early experience with compassionate use of 2 hydroxypropyl - beta - cyclodextrin for Niemann - Pick type C disease: review of initial published cases . *Neurological Sciences* 38(5), pp. 727-743.

Meikle, P. J. and Hopwood, J. J. 2003. Lysosomal storage disorders: emerging therapeutic options require early diagnosis. *European Journal of Paediatrics* 162, pp. S34-S37.

Meikle, P. J. et al. 1999. Prevalence of lysosomal storage disorders. *JAMA* 281(3), pp. 249-254.

Melchionda, M. et al. 2016. Ca<sup>2+</sup>/H<sup>+</sup> exchange by acidic organelles regulates cell migration in vivo. *Journal of Cell Biology* 212(7), pp. 803-813.

Millard, E. E. et al. 2000. Niemann-Pick Type C1 (NPC1) Overexpression Alters Cellular Cholesterol Homeostasis. *Journal of Biological Chemistry* 275, pp. 38445-38451.

Minckley, T. F. et al. 2019. Sub-nanomolar sensitive GznP3 reveals TRPML1-mediated neuronal Zn<sup>2+</sup> signals. *Nature Communications* 10(1), p. 4806.

Mishra, P. et al. 2019. Descriptive Statistics and Normality Tests for Statistical Data. *Annals of Cardiac Anaesthesia* 22(1), pp. 67-72.

Mitani, A. A. and Haneuse, S. 2020. Small data challenges of studying rare diseases. *JAMA Network Open* 3(3), p. e201965.

Miyayama, T. et al. 2018. Silver nanoparticles induce lysosomal-autophagic defects and decreased expression of transcription factor EB in A549 human lung adenocarcinoma cells. *Toxicology in Vitro* 46, pp. 148-154.

Mizushima, N. et al. 1998. A protein conjugation system essential for autophagy. *Nature* 395, pp. 395-398.

Moheimani, F. et al. 2012. Inhibition of lysosomal function in the macrophages incubated with elevated glucose concentrations: a potential contributory factor in diabetes-associated atherosclerosis. *Atherosclerosis* 223(1), pp. 144-151.

Mole, S. E. et al. 2011. *The Neuronal Ceroid Lipofuscinoses (Batten Disease)*. Oxford, United Kingdom: Oxford University Press.

Monroy, A. et al. 2013. Curcumin and neurodegenerative disease. *Biofactors* 39(1), pp. 122-132.

Montero, M. et al. 2001. Mitochondrial  $Ca^{2+}$ -induced  $Ca^{2+}$  release mediated by the  $Ca^{2+}$  uniporter. *The American Society for Cell Biology* 12(1), pp. 63-71.

Morimoto, M. et al. 2018. Bi-allelic CCDC47 Variants Cause a Disorder Characterized by Woolly Hair, Liver Dysfunction, Dysmorphic Features, and Global Developmental Delay. *American Journal of Human Genetics* 103(5), pp. 794-807.

Motabar, O. et al. 2010. High throughput screening for inhibitors of Alpha-Galactosidase. *Current Chemical Genomics* 4, pp. 67-73.

Mu, T. W. et al. 2009. Proteostasis Regulators and Pharmacologic Chaperones Synergize to Correct Protein Misfolding Diseases. *Cell* 134(5), pp. 769-781.

Mukherjee, A. B. et al. 2019. Emerging new roles of the lysosome and neuronal ceroid lipofuscinoses. *Molecular Neurodegeneration* 14(1), p. 4.

Musiek, E. S. et al. 2015. Sleep, circadian rhythms, and the pathogenesis of Alzheimer disease. *Experimental & Molecular Medicine* 47(3), p. e148.

Nagoshi, E. et al. 2004. Circadian gene expression in individual fibroblast: cell-autonomous and self-sustained oscillators pass time to daughter cells. *Cell* 119(5), pp. 693-705.

Narita, A. et al. 2016. Amboxol chaperone therapy for neuronopathic gaucher disease: A pilot study. *Annals of Clinical and Translational Neurology* 3(3), pp. 200-215.

Nasri, H. et al. 2014. New concepts in nutraceuticals as alternative for pharmaceuticals. *International Journal of Preventive Medicine* 5(12), pp. 1487-1499.

Neueder, A. and Bates, G. P. 2014. A common gene expression signature in Huntington's disease patient brain regions. *BMC Medical Genomics* 7,

Nixon, R. A. 2013. The role of autophagy in neurodegenerative diseases. *Nature Medicine* 19(8), pp. 983-997.

Nixon, R. A. 2020. The aging lysosome: an essential catalyst for late-onset neurodegenerative diseases. *The FASEB Journal* 1868(9),

Nowakowski, R. W. et al. 1988. Diagnosis of feline GM1 gangliosidosis by enzyme assay of cultured conjunctival cells. *Investigative Ophthalmology & Visual Science* 29(3), pp. 487-490.

Nowroozi, N. et al. 2001. High beta-galactosidase and ganglioside GM1 levels in the human parotid gland. *Archives of Otolaryngology - Head & Neck Surgery* 127(11), pp. 1381-1384.

Odaumpatta, R. and Mohanapriya, A. 2020. Next generation sequencing exome data analysis aids in the discovery of SNP and INDEL patterns in Parkinson's disease. *Genomics* S0888-7543(20), pp. 30103-30108.

Olivova, P. et al. 2009. Effects of sample collection on alpha-galactosidase a enzyme activity measurements in dried blood spots on filter paper. *Clinica Chimica Acta* 2009(1-2), pp. 159-162.

Onyenwoke, R. U. and Brenman, J. E. 2015. Lysosomal storage disease - regulation neurodegeneration. *Journal of Experimental Neuroscience* 9, pp. 81-91.

Orphazyme. 2020. Orphazyme initiates rolling submission of new drug application for arimoclomol with US FDA in Niemann-Pick disease type C. Copenhagen, Denmark.

Ortolano, S. 2016. Small molecules: substrate inhibitors, chaperones, stop-codon read through, and beyond. *Journal of Inborn Errors of Metabolism & Screening* 4, pp. 1-11.

Pal, A. et al. 2006. Huntingtin-HAP40 complex is a novel Rab5 effector that regulates early endosome motility and is up-regulated in Huntington's disease. *The Journal of Cell Biology* 172, pp. 605-618.

Palmer, D. N. et al. 2013. NCL disease mechanisms. *Biochimica et Biophysica Acta (BBA) - Molecular Basis of Disease* 1832(11),

Palmieri, M. et al. 2011. Characterization of the CLEAR network reveals an integrate control of cellular clearance pathways. *Human Molecular Genetics* 20, pp. 3852-3866.

Pantazopoulos, H. et al. 2018. Circadian rhythms in regulation of brain processes and role in psychiatric disorders. *Neural Plasticity* 2018, p. 2892657.

Parenti, G. 2009. Treating lysosomal storage disease with pharmacological chaperones: from concept to clinics. *EMBO Molecular Medicine* 1(5), pp. 268-279.

Parenti, G. et al. 2012. New strategies for the treatment of lysosomal storage diseases. *International Journal of Molecular Medicine* 31(1), pp. 11-20.

Passantino, R. et al. 2013. Identifying protein partners of CLN8, an ER-resident protein involved in neuronal ceroid lipofuscinosis. *Biochimica et Biophysica Acta* 1833(3), pp. 529-540.

Patel, S. and Cai, X. 2014. Evolution of acidic Ca<sup>2+</sup> stores and their resident Ca<sup>2+</sup> - permeable channels. *Cell Calcium* 57(3), pp. 222-230.

Patterson, M. C. et al. 2007. Miglustat for treatment of Niemann-Pick C disease: a randomised controlled study. *The Lancet Neurology* 6, pp. 765-772.

Pelled, D. et al. 2003. Inhibition of calcium uptake via the sarco/endoplasmic reticulum Ca<sup>2+</sup>-ATPase in a mouse model of Sandhoff disease and prevention by treatment with N-butyldeoxynojirimycin. *Journal of Biological Chemistry* 278(32), pp. 29496-29501.

Penke, B. et al. 2018. Heat shock proteins and autophagy pathways in neuroprotection: from molecular bases to pharmacological interventions. *International Journal of Molecular Sciences* 19(1), p. 325.

Pereira, D. A. and Williams, J. A. 2007. Origin and evolution of high throughput screening. *British Journal of Pharmacology* 152, pp. 53-61.

Perera, R. M. and Zoncu, R. 2016. The lysosome as a regulatory hub. *Annual Review of Cell and Developmental Biology* 32, pp. 223-253.

Persaud-Sawin, D. A. et al. 2007. Neuronal ceroid lipofuscinosis: a common pathway? *Pediatric Research* 61, pp. 146-152.

Petcherski, A. et al. 2019. An autophagy modifier screen identifies small molecules capable of reducing autophagosome accumulation in a model of CLN3-mediated neurodegeneration. *Cells* 8(12), p. 1531.

Pierzyńska-Mach, A. et al. 2014. Evaluation of acridine orange, LysoTracker Red, and quinacrine as fluorescent probes for long-term tracking of acidic vesicles. *Cytometry A* 85, pp. 729-737.

Pitt, S. J. et al. 2010. TPC2 is a novel NAADP-sensitive Ca<sup>2+</sup> release channel, operating as a dual sensor of luminal pH and Ca<sup>2+</sup>. *Journal of Biological Chemistry* 285(45), pp. 35039-35046.

Pittman, J. K. 2011. Vacuolar Ca(2+) uptake. *Cell Calcium* 50(2), pp. 139-146.

Platt, F. M. et al. 2012. The cell biology of disease: lysosomal storage disorders: the cellular impact of the lysosomal dysfunction. *The Journal of Cell Biology* 199, pp. 723-734.

Platt, F. M. and Jeyakumar, M. 2008. Substrate reduction therapy. *Acta Paediatrica* 97, pp. 88–93.

Platt, F. M. et al. 1994. N-butyldeoxygalactonojirimycin inhibits glycolipid biosynthesis but does not affect N-linked oligosaccharide processing. *The Journal of Biological Chemistry* 269, pp. 27108-27114.

Pollock, S. et al. 2008. N-Butyldeoxynojirimycin is a broadly effective anti-HIV therapy significantly enhanced by targeted liposome delivery. *AIDS* 22, pp. 1961-1969.

Porto, C. et al. 2012. Pharmacological enhancement of alpha-glucosidase by the allosteric chaperone N-acetylcysteine. *Molecular Therapy* 20(12), pp. 2201-2211.

Pottel, J. et al. 2020. The activities of drug inactive ingredients on biological targets. *Science* 369(6502), pp. 403-413.

Prenc, E. M. and Natowicz, M. R. 1992. Diagnosis of alpha-mannosidosis by measuring alpha-mannosidase in plasma. *Clinical Chemistry* 38(4), pp. 501-503.

PubChem **CID 2132**. Identifier **CID 2132**.

PubChem **CID 3671**. Identifier **CID 3671**.

PubChem **CID 5281078**. Identifier **CID 5281078**.

Pugach, E. K. et al. 2018. High-content screen for modifiers of Niemann-Pick type C disease in patient cells. *Human Molecular Genetics* 27, pp. 2101-2112.

Puri, V. et al. 2003. Sphingolipid storage induces accumulation of intracellular cholesterol by stimulating SREBP-1 cleavage. *The Journal of Biological Chemistry* 278, pp. 20961-20970.

Pushpakom, S. et al. 2019. Drug repurposing: progress, challenges and recommendations. *Nature Reviews Drug Discovery* 18, pp. 41-58.

Raben, N. et al. 2012. Autophagy and mitochondria in Pompe disease: nothing is so new as what has long been forgotten. *American Journal of Medical Genetics* 160C(1), pp. 13-21.

Rahman, N. et al. 2016. Soluble adenyl cyclase is essential for proper lysosomal acidification. *Journal of General Physiology* 148(4), pp. 325-339.

Ranta, S. et al. 2001. Studies of homogenous population: CLN5 and CLN8. *Advances in Genetics* 45, pp. 123-140.

Ranta, S. et al. 1999. The neuronal ceroid lipofuscinoses in human EPMR and *mnd* mutant mice are associated with mutations in CLN8. *Nature Genetics* 23, pp. 233-236.

- Reinhardt, K. et al. 2010. Novel CLN8 mutations confirm the clinical and ethnic diversity of late infantile neuronal ceroid lipofuscinosis. *Clinical Genetics* 77(1), pp. 79-85.
- Ribbens, J. et al. 2013. A high-throughput screening assay using Krabbe disease patient cells. *Analytical Biochemistry* 434(1), pp. 15-25.
- Richardson, K. et al. 2016. Circadian profiling in two mouse models of lysosomal storage disorders; Niemann Pick type-C and Sandhoff disease. *Behavioural Brain Research* 297, pp. 213-223.
- Riikonen, R. et al. 2000. CSF insulin-like growth factor-1 in infantile neuronal ceroid lipofuscinosis. *Neurology* 54(9), pp. 1828-1832.
- Rocha, N. et al. 2009. Cholesterol sensor ORP1L contacts the ER protein VAP to control RAB7-RILP-P150 glued and late endosome positioning. *Journal of Cell Biology* 185(7), pp. 1209-1225.
- Rodríguez, A. et al. 1997. Lysosomes behave as Ca<sup>2+</sup> regulated exocytic vesicles in fibroblasts and epithelial cells. *Journal of Cell Biology* 137(1), pp. 93-104.
- Rosato, A. S. et al. 2019. TRPML1 links lysosomal calcium to autophagosome biogenesis through the activation of CaMKK  $\beta$ /VP34 pathway. *Nature Communications* 10(1), p. 5630.
- Rosenbloom, B. et al. 2011. The incidence of Parkinsonism in patients with type 1 Gaucher disease : data from the ICGG Gaucher Registry . *Blood Cells , Molecules & Diseases* 46(1), pp. 95-102.
- Ruas, M. et al. 2010. Purified TPC isoforms form NAADP receptors with distinct roles for Ca<sup>2+</sup> signaling and endolysosomal trafficking. *Current Biology* 20, pp. 8-6.
- Rusimini, P. et al. 2019. Trehalose induces autophagy via lysosomal-mediated TFEB activation in models of motoneuron degeneration. *Autophagy* 15(4), pp. 631-651.
- Rusyn, E. et al. 2008. CLN3p impacts galatocylceramide transport, raft morphology, and lipid content. *Pediatric Research* 63, pp. 625-631.
- Saftig, P. et al. 2010. Lysosomal membrane proteins: life between acid and neutral conditions. *Biochemical Society Transactions* 38(6), pp. 1420 – 1423.
- Salsano, E. et al. 2012. Vertical supranuclear gaze palsy in Niemann-Pick type c disease. *Neurological Sciences* 33, pp. 1225-1232.
- Sano, R. et al. 2009. GM1-ganglioside accumulation at the mitochondria-associated ER membranes links ER stress to Ca(2+)-dependent mitochondrial apoptosis. *Molecular Cell* 36(3), pp. 500-511.

Sansanwal, P. et al. 2010. Mitochondrial autophagy promotes cellular injury in nephropathic cystinosis. *Journal of the American Society of Nephrology* 21(2), pp. 272-283.

Sardiello, M. et al. 2009. A gene network regulating lysosomal biogenesis and function. *Science* 325, pp. 473-477.

Schibler, U. and Sassone-Corse, P. 2002. A web of circadian pacemakers. *Cell* 111(7), pp. 919-922.

Schiffmann, R. 2010. Therapeutic approaches for neuronopathic lysosomal storage disorders. *Journal of Inherited Metabolic Disease* 33, pp. 373–379.

Schneider, C. A. et al. 2012. NIH Image to ImageJ: 25 years of image analysis. *Nature Methods* 9, pp. 671-675.

Schultz, M. L. et al. 2016. Lysosome and endoplasmic reticulum quality control pathways in Niemann-Pick type C disease. *Brain Research* 1649(Pt B), pp. 181-188.

Schulze, h. and Sandhoff, K. 2011. Lysosomal lipid storage diseases. *Cold Spring Harbor Perspectives in Biology* 3, p. doi: 10.1101/cshperspect.a004804.

Schulze, H. and Sandhoff, K. 2014. Sphingolipids and lysosomal pathologies. *Biochimica et Biophysica Acta* 1841(5), pp. 799-810.

Schweitzer, J. K. et al. 2009. Neurodegeneration in Niemann-Pick type c disease and Huntingtons disease: impact of defects in membrane trafficking. *Current Drug Targets* 10, pp. 653-665.

Schöder, B. A. et al. 2010. The proteome of lysosomes. *Proteomics* 10(22), pp. 4053-4076.

Seehafer, S. S. et al. 2011. Immunosuppression alters disease severity in juvenile Batten disease mice. *Journal of Neuroimmunology* 230(1-2), pp. 169-172.

Settembre, C. et al. 2013. Signals from the lysosome: a control centre for cellular clearance and energy metabolism . *Nature Reviews Molecular Cell Biology* 14, pp. 283–296.

Settembre, C. et al. 2011. TFEB links autophagy to lysosomal biogenesis. *Science* 332(6036), pp. 1429-1433.

Settembre, C. and Medina, D. L. 2015. Chapter 3 - TFEB and the CLEAR network. *Methods in cell biology* 126, pp. 45-62.

Shacka, J. J. 2012. Mouse models of neuronal ceroid lipofuscinoses: Useful pre-clinical tools to delineate disease pathophysiology and validate therapeutics. *Brain Research Bulletin* 88, pp. 43-57.

Shang, Y. Y. et al. 2017. Alisertib promotes apoptosis and autophagy in melanoma through p38 MAPK-mediated aurora a sinagling. *Oncotarget* 8(63), pp. 107076-107088.

Shanmugam, M. K. et al. 2015. The multifaceted role of curcumin in cancer prevention and treatment. *Molecules* 20(2), pp. 2728-2769.

Shim, H. S. et al. 2007. Rapid activation of CLOCK by Ca<sup>2+</sup>-dependent protein kinase C mediates resting of the mammalian circadian clock. *EMBO Reports* 8(4), pp. 366-371.

Shipley, K. S. 2019. *Identifying and treating the mechanisms leading to cellular dysfunction in a rare form childhood epilepsy (late infantile neuronal ceroid lipofuncinosis, CLN5 disease)*. Cardiff University.

Shukla, S. and Tekwani, B. L. 2020. Histone deacetylases inhibitors in neurodegenerative diseases, neuroprotection and neuronal differentiation. *Frontiers in Pharmacology* 11, p. 537.

Sidransky, E. et al. 2009. Multicenter analysis of glucocerebrosidase mutations in Parkinson's disease. *The New England Journal of Medicine* 361(17), pp. 1651-1661.

Silverman, L. et al. 1998. New assay technologies for high-throughput screening. *Current Opinion in Chemical Biology* 2(3), pp. 397-403.

Simons, K. and Ikonen, E. 1997. Functional rafts in cell membranes. *Nature* 387, pp. 567-575.

Simpson, M. A. et al. 2004. Infantile-onset symptomatic epilepsy syndrome casue by homozygous loss-of-function mutation of Gm3 synthase. *Nature Genetics* 36, pp. 1225-1229.

Skotland, T. et al. 2016. Determining the turnover of glycosphingolipid species by stable-isotope tracer lipidomics. *Journal of Molecular Biology* 428(24), pp. 4856-4856.

Smith, A. 2019. *Brineura hit with NICE rejection*. PharmaTimes online. Available at: [http://www.pharmatimes.com/news/brineura\\_hit\\_with\\_nice\\_rejection\\_1279019](http://www.pharmatimes.com/news/brineura_hit_with_nice_rejection_1279019) [Accessed: 02/06/2020].

Smith, P. K. et al. 1985. Measurement of protein using Bicinchoninic acid. *Analytical Biochemistry* 150(1), pp. 76-85.

Sofroniew, M. V. and Vinter, H. V. 2010. Astrocytes: biology and pahtology. *Acta Neuropathologica* 119(1), pp. 7-35.

Sokolowski, A. R. et al. 1995. Mycophenolate mofetil (MMF, RS-61443) inhibits inflammation and smooth muscle cell proliferation in rat aortic allografts. *Transplant Immunology* 3(4), pp. 342-351.

Son, J. H. et al. 2012. Neuronal autophagy and neurodegenerative disease. *Experimental & Molecular Medicine* 44(2), pp. 89-98.

Specchio, N. et al. 2020. Changing times for CLN2 disease: the era of enzyme replacement therapy. *Therapeutics and Clinical Risk Management* 16, pp. 213-222.

Sprately, S. J. et al. 2016. Molecular mechanisms of disease pathogenesis differ in Krabbe disease variants. *Traffic* 17(8), pp. 908-922.

Stein, V. M. et al. 2012. Miglustat improves Purkinje cell survival and alters microglial phenotypes in feline Niemann-Pick disease type C. *Journal of Neuropathology & Experimental Neurology* 71, pp. 434-448.

Striano, P. et al. 2007. Clinical and electrophysiological features of epilepsy in Italian patients with CLN8 mutations. *Epilepsy & Behavior* 10, pp. 187-191.

Stutzmann, G. E. et al. 2004. Dysregulated IP3 signalling in cortical neurons of knock-in mice expressing an Alzheimer's-linked mutation in presenilin1 results in exaggerated Ca<sup>2+</sup> signals and altered membrane excitability. *The Journal of Neuroscience* 24(2), pp. 508-513.

Sugimoto, Y. et al. 2001. Accumulation of cholera toxin and GM1 ganglioside in the early endosome of Niemann-Pick C1-deficient cells. *Proceedings of the National Academy of Sciences of the United States of America* 98, pp. 12391-12396.

Sutrina, S. L. and Chen, W. W. 1984. Lysosomal involvement in cellular turnover of plasma membrane sphingomyelin. *Biochimica et Biophysica Acta* 793(2), pp. 169-179.

Suzuki, Y. 2014. Emerging novel concept of chaperones therapies for protein misfolding diseases. *Proceeding of the Japan Academy, Series B Physical and Biological Sciences* 90(5), pp. 145-162.

Szabo, M. et al. 2017. Cell and small animal models for phenotypic drug discovery. *Drug Design, Development and Therapy* 11, pp. 1957-1967.

Sztolsztener, M. E. et al. 2012. Impaired dynamics of the late endosome/lysosome compartment in human Niemann-Pick type C skin fibroblasts carrying mutations in NPC1 gene. *Molecular BioSystems* 8, pp. 1197-1205.

Takeshima, H. et al. 2015. New and notable ion-channels in the sarcoplasmic/endoplasmic reticulum: do they support the process of intracellular Ca<sup>2+</sup> release? *The Journal of Physiology* 593(15), pp. 3241-3251.

Tallaksen, C. M. E. and Berg, J. E. 2009. Miglustat therapy in juvenile Sandhoff disease. *Journal of Inherited Metabolic Disease* 32(S1), pp. 289-293.

Tamura, H. et al. 2007. Niemann-Pick type C disease: Novel NPC1 mutations and characterization of the concomitant acid sphingomyelinase deficiency. *Molecular Genetics and Metabolism* 87, pp. 113-121.

te Vruchte, D. et al. 2004. Accumulation of glycosphingolipids in Niemann-Pick C disease disrupts endosomal transport. *The Journal of Biological Chemistry* 279(25), pp. 26167-26175.

Terbach, N. and Williams, R. S. B. 2009. Structure-functions studies for the panacea, Valproic acid. *Biochemical Society Transactions* 37, pp. 1126-1132.

Tessitore, A. et al. 2004. GM1-ganglioside-mediated activation of the unfolded protein response causes neuronal death in a neurodegenerative gangliosidosis. *Molecular Cell* 15(5),

Thelen, M. et al. 2012. Disruption of the autophagy-lysosome pathway is involved in neuropathology of the nclf mouse model of neuronal ceroid lipofuscinosis. *PLoS ONE* 7(4), p. e35493.

Tierney, M. et al. 1995. The tolerability and pharmacokinetics of N-butyl-deoxynojirimycin in patients with advanced HIV disease (ACTG 100). The AIDS Clinical Trials Group (ACTG) of the National Institute of Allergy and Infectious Diseases. *Journal of Acquired Immune Deficiency Syndromes and Human Retrovirology* 10(15), pp. 549-553.

Tiscione, S. A. et al. 2019. Disease-associated mutations in Niemann-Pick type C1 alter ER calcium signaling and neuronal plasticity. *Journal of Cell Biology* 218(12), pp. 4141-4156.

Trushina, E. et al. 2006. Mutant huntingtin inhibits clathrin-independent endocytosis and causes accumulation of cholesterol in vitro and in vivo. *Human Molecular Genetics* 15, pp. 3578-3591.

Tsai, Y. et al. 2011. Curcumin and its nano-formulation: the kinetics of tissue distribution and blood-brain barrier penetration. *International Journal of Pharmaceutics* 416(1), pp. 331-338.

US Food & Drug Administration. 2017. *FDA approves first treatment for a form of Batten disease.* Available at: [https://www.fda.gov/news-events/press-announcements/fda-approves-first-treatment-form-batten-disease#:~:text=Brineura%20is%20the%20first%20FDA,%2D1%20\(TPP1\)%20deficiency](https://www.fda.gov/news-events/press-announcements/fda-approves-first-treatment-form-batten-disease#:~:text=Brineura%20is%20the%20first%20FDA,%2D1%20(TPP1)%20deficiency). [Accessed].

US Food & Drug Administration. 2018. *FDA approves new treatment for a rare genetic disorder, Fabry disease.* Available at: <https://www.fda.gov/news-events/press-announcements/fda-approves-new-treatment-rare-genetic-disorder-fabry-disease#:~:text=FDA%20approves%20new%20treatment%20for%20a%20rare%20genetic%20disorder%2C%20Fabry%20disease,-Share&text=The%20U.S.%20Food%20and%20Drug,of%20adults%20with%20Fabry%20disease.&text=Fabry%20disease%20is%20rare%20and%20affects%20both%20males%20and%20females>. [Accessed: 06/06/2020].

- Vallim, J. R. S. et al. 2019. Rhythmic changes in Fabry disease: inversion and non-oscillatory pattern in 6-sulfatoxymelatonin daily profile. *Chronobiology International* 36(4), pp. 470-480.
- van der Spoel, A. C. et al. 2002. Reversible infertility in male mice after oral administration of alkylated imino sugars: a nonhormonal approach to male contraception. *Proceedings of the National Academy of Science of the United States of America* 99, pp. 17173-17178.
- van der Veen, S. J. et al. 2020. Developments in the treatment of Fabry disease. *Journal of Inherited Metabolic Disease* 21, p. doi: 10.1002/jimd.12228.
- van Diggelen, O. P. et al. 1999. A rapid fluorogenic palmitoyl-protein thioesterase assay: pre- and postnatal diagnosis of INCL. *Molecular Genetics and Metabolism* 66(4), pp. 240-244.
- van Diggelen, O. P. et al. 2005. A new fluorimetric enzyme assay for the diagnosis of Niemann-Pick A/B, with specificity of natural sphingomyelinase substrate. *Journal of Inherited Metabolic Disease* 28(5), pp. 733-741.
- Vance, J. E. et al. 1997. Abnormalities in mitochondria-associated membrane and phospholipid biosynthetic enzymes in the mnd/mnd mouse model of neuronal ceroid lipofuscinosis. *Biochimica et Biophysica Acta* 1344, pp. 286-299.
- Vanier, M. T. 2010. Niemann-Pick disease type C. *Orphanet Journal of Rare Disease* 5, p. 16.
- Vanier, M. T. and Latour, P. 2015. Laboratory diagnosis of Niemann-Pick disease type C: the filipin staining test. *Methods in Cell Biology* 126, pp. 357-375.
- Vanier, M. T. and Millat, G. 2003. Niemann-Pick disease type C. *Clinical Genetics* 64, pp. 269-281.
- Vantaggiato, C. et al. 2009. A novel CLN8 mutation in late-infantile-onset neuronal ceroid lipofuscinosis (LINCL) reveals aspects of CLN8 neurobiological function. *Human Mutation* 30, pp. 1104-1116.
- Vidal-Donet, J. M. et al. 2013. Alterations in ROS activity and lysosomal pH account for distinct patterns of macroautophagy in LINCL and JNCL fibroblasts. *PLOS One* 8(2), p. e55526.
- Virk, S. S. et al. 1985. Ca<sup>2+</sup> transport and Ca<sup>2+</sup> dependant ATP hydrolysis by Golgi vesicle from lactating rat mammary glands. *Biochemical Journal* 226(3), pp. 741-748.
- Viswanathan, K. et al. 2012. Nonpeptidic lysosomal modulators derived from Z-phe-ala-diazomethylketone for treating protein accumulation diseases. *ACS Medicinal Chemistry Letters* 3(11), pp. 920-924.

Vockley, C. W. 2009. *What is curcumin?* National Niemann-Pick Disease Foundation, INC. Available at: <https://nnpdf.org/issues-regarding-curcumin-therapy-for-npc/> [Accessed: 09/06/2020].

Waller-Evans, H. and Lloyd-Evans, E. 2015. Regulation of TRPML1 function. *Biochemical Society Transactions* 43(3), pp. 442-446.

Wang, D. et al. 2012a. The designer aminoglycoside NB84 significantly reduces glycosaminoglycan accumulation associated with MPS I-H in the *Idua-W392X* mouse. *Molecular Genetics and Metabolism* 105(1), pp. 116-125.

Wang, X. et al. 2012b. TPC proteins are phosphoinositide-activated sodium-selective ion channels in endosomes and lysosomes. *Cell* 151(2), pp. 372-383.

Wassall, S. R. et al. 2004. Order from disorder, corralling cholesterol with chaotic lipids. The role of polyunsaturated lipids in membrane raft formation. *Chemistry and Physics of Lipids* 132, pp. 79-88.

Wassif, C. A. et al. 2016. High incidence of unrecognized visceral/neurological late-onset Niemann-Pick disease, type C1, predicted by analysis of massively parallel sequencing data sets. *Genetics in Medicine* 18, pp. 41-48.

Wassif, C. A. et al. 2002. Cholesterol storage defect in RSH/Smith-Lemli-Opitz syndrom fibroblasts. *Molecular Genetics and Metabolism* 75, pp. 325-334.

Wei, Y. et al. 2018. Origin of the autophagosome membrane in mammals. *BioMed Research International* 2018, p. 1012789.

Weidberg, H. et al. 2010. LC3 and GATE-16/GABARAP subfamilies are both essential yet act differently in autophagosome biogenesis. *The EMBO Journal* 29(11), pp. 1792-1802.

Weimer, J. M. et al. 2002. The neuronal ceroid lipofuscinoses: mutations in different proteins result in similar disease. *Neuromolecular Medicine* 1(2), pp. 111-124.

Weiser, T. 2008. Ambroxol: A CNS drug? *CNS Neuroscience & Therapeutics* 14(1), pp. 17-24.

Wheeler, S. and Sillence, D. J. 2019. Niemann-Pick type C disease: cellular pathology and pharmacotherapy. *Journal of Neurochemistry*, p. <https://doi.org/10.1111/jnc.14895>.

Wiederschain, G. et al. 1992. Characterization of 6-hexadecanoylamino-4-methylumbelliferyl-beta-D-galactopyranoside as fluoregenic substrate of galactocerebrosidase for the diagnosis of Krabbe disease. *Clinical Chimica Acta* 205,

Wilkinson, P. et al. 2010. EMMA--mouse mutant resources for the international scientific community. *Nucleic Acid Research* 38, pp. D570-576.

Williams, I. M. et al. 2014. Improved neuroprotection using miglustat, curcumin and ibuprofen as a triple combination therapy in Niemann-Pick disease type C1 mice. *Neurobiology of Disease* 67, pp. 9-17.

Williams, R. J. P. 2006. The evolution of calcium biochemistry. *Biochimica et Biophysica Acta* 1763(11), pp. 1139-1146.

Winchester, B. et al. 1990. Inhibition of alpha-L-fucosidase by derivatives of deoxyfuconojirimycin and deoxymannojirimycin. *Biochemical Journal* 265(1), pp. 277-282.

Winter, E. and Ponting, C. P. 2002. TRAM, LAG1 and CLN8: members of a novel family of lipid-sensing domains? *Trends in Biochemical Sciences* 27, pp. 381-383.

Wos, M. et al. 2016. Mitochondrial dysfunction in fibroblasts derived from patients with Niemann-Pick type C disease. *Archives of Biochemistry and Biophysics* 593, pp. 50-59.

Wu, D. et al. 2014. The Batten disease gene *CLN3* confers resistance to endoplasmic reticulum stress induced by tunicamycin. *Biochemical and Biophysical Research Communications* 447(1), pp. 115-120.

Wulff, K. et al. 2010. Sleep and circadian rhythm disruption in psychiatric and neurodegenerative diseases. *Nature Reviews Neuroscience* 11(8), pp. 589-599.

Xu, J. et al. 2010. Cholesterol trafficking is required for mTOR activation in endothelial cells. *PNAS* 107(10), pp. 4764-4769.

Xu, M. et al. 2014. A phenotypic compound screening assay for lysosomal storage diseases. *Journal of Biomolecular Screening* 19(1), pp. 168-175.

Xu, W. S. et al. 2007. Histone deacetylase inhibitors: molecular mechanisms of action. *Oncogene* 26(37), pp. 5541-5552.

YaV, V. et al. 1993. Applications of a new fluorimetric enzyme assay for the diagnosis of aspartylglucosaminuria. *Journal of Inherited Metabolic Disease* 16(6), pp. 929-934.

Yu, D. et al. 2014. Niemann-Pick Disease Type C: Induced Pluripotent Stem Cell-Derived Neuronal Cells for Modeling Neural Disease and Evaluating Drug Efficacy. *Journal of Biomolecular Screening* 19(8), pp. 1164-1173.

Zeiss. 2008. Axiovision version 4.7.1 software. Oberkochen, Germany: Zeiss.

Zelnik, N. et al. 2007. A novel mutation of the *CLN8* gene : is there a Mediterranean phenotype ? *Pediatric Neurology* 36(6), pp. 411-413.

Zeman, W. and Dyken, P. 1969. Neuronal ceroid-lipofuscinosis (Batten's disease): relationship to amaurotic family idiocy? *Pediatrics* 44, pp. 570-583.

Zhang, C. K. et al. 2012. Genome-wide association study of N370S homozygous Gaucher disease reveals the candidacy of CLN8 gene as a genetic modifier contributing to extreme phenotypic variation. *American Journal of Hematology* 87(4), pp. 377-383.

Zhang, J. H. et al. 1999. A simple statistical parameter for use in evaluation and validations of high throughput screening assays. *Journal of Biomolecular Screening* 4, pp. 67-73.

Zhang, Z. et al. 2006. Palmitoyl-protein thioesterase-1 deficiency mediates the activation of the unfolded protein response and neuronal apoptosis in INCL. *Human Molecular Genetics* 15(2), pp. 337-346.

Zhao, Y. et al. 2016. Structure of glycosylated NPC1 luminal domain C reveals insights into NPC2 and Ebola virus interactions. *FEBS Letters* 590, pp. 605-612.

Zheng, W. et al. 2007. Three classes of glucocerebrosidase inhibitors identified by quantitative high-throughput screening are chaperone leads for Gaucher disease. *Proceedings of the National Academy of Sciences of the United States of America* 104, pp. 13192-13197.

Zheng, W. et al. 2015. Phenotypic screens as a renewed approach for drug discovery. *Drug Discovery Today* 18(0), pp. 1067-1073.

Zisapel, N. 2018. New perspectives on the role of melatonin in human sleep, circadian rhythms and their regulation. *British Journal of Pharmacology* 175(16), pp. 3190-3199.

# Appendix

## A3.1 Lysosomal enzyme assays in CLN8 patient fibroblasts

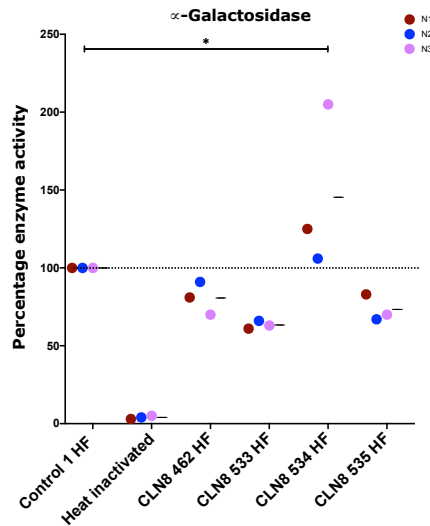


**Figure A3.1: α-Galactosidase enzyme activity in CLN8 patient cells.** Enzyme activity of the lysosomal enzyme α-galactosidase as a % of control 1 HF where control 1 HF enzyme activity was 100%. The black dotted line indicates the mean activity of control 1 HF. Each point indicates a different technical repeat and the black line indicate the mean. \*  $p \leq 0.05$ , One-way ANOVA.

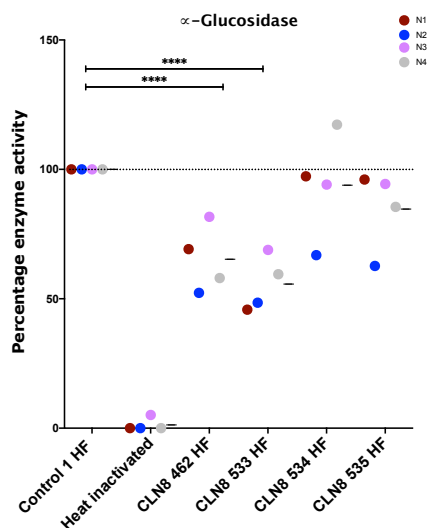


**Figure A3.2: α-Glucosidase enzyme activity in CLN8 patient cells.** Enzyme activity of the lysosomal enzyme α-glucosidase as a % of control 1 HF where control 1 HF enzyme activity was 100%. The black

dotted line indicates the mean activity of control 1 HF. Each point indicates a different technical repeat and the black line indicate the mean. \*\*\*\* $p < 0.001$ , One-way ANOVA.

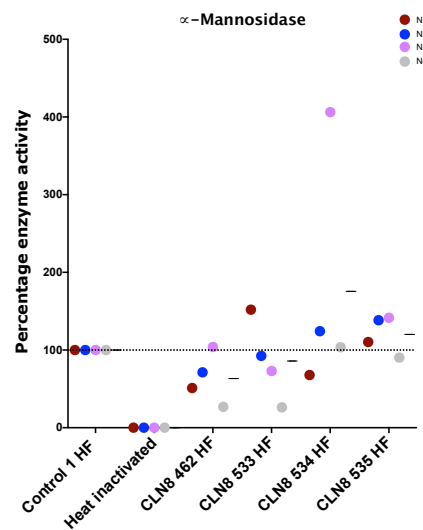


**Figure A3.3: α-Mannosidase enzyme activity in CLN8 patient cells.** Enzyme activity of the lysosomal enzyme α-mannosidase as a % of control 1 HF where control 1 HF enzyme activity was 100%. The black dotted line indicates the mean activity of control 1 HF. Each point indicates a different technical repeat and the black line indicate the mean.

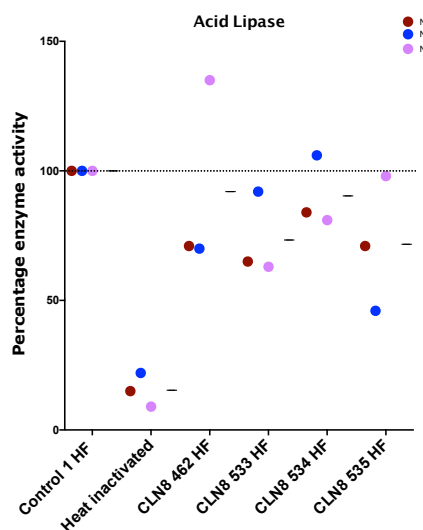


**Figure A3.4: Acid lipase enzyme activity in CLN8 patient cells.** Enzyme activity of the lysosomal enzyme acid lipase as a % of control 1 HF where control 1 HF enzyme activity was 100%. The black dotted line indicates the mean activity of control 1 HF. Each point indicates a different technical repeat and the black line indicate the mean.

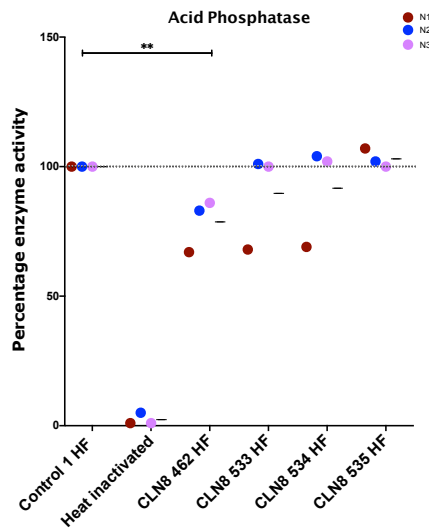


**Figure A3.5: Acid phosphatase enzyme activity in CLN8 patient cells.** Enzyme activity of the lysosomal enzyme acid phosphatase as a % of control 1 HF where control 1 HF enzyme activity was 100%. The black dotted line indicates the mean activity of control 1 HF. Each point indicates a different technical repeat and the black line indicate the mean. \*\*p < 0.01, One-way ANOVA.

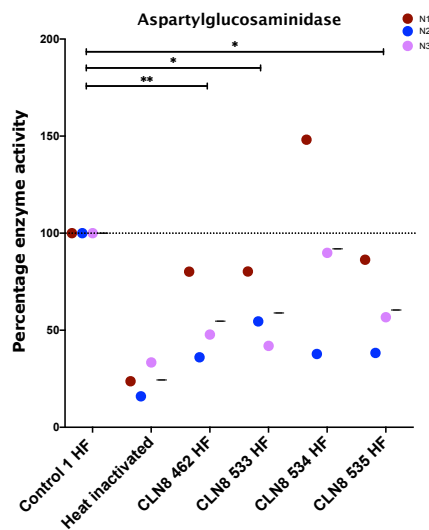


**Figure A3.6: Aspartylglucosaminidase enzyme activity in CLN8 patient cells.** Enzyme activity of the lysosomal enzyme Aspartylglucosaminidase as a % of control 1 HF where control 1 HF enzyme activity was 100%. The black dotted line indicates the mean activity of control 1 HF. Each point indicates a different technical repeat and the black line indicate the mean. \*p ≤ 0.05, \*\*p < 0.01, One-way ANOVA.

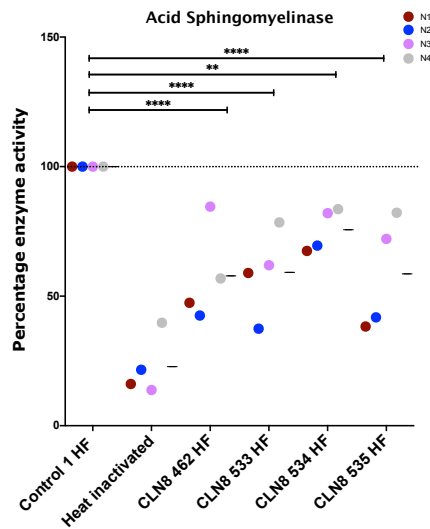


**Figure A3.7: Acid sphingomyelinase enzyme activity in CLN8 patient cells.** Enzyme activity of the lysosomal enzyme acid sphingomyelinase as a % of control 1 HF where control 1 HF enzyme activity was 100%. The black dotted line indicates the mean activity of control 1 HF. Each point indicates a different technical repeat and the black line indicate the mean. \*\* $p < 0.01$ , \*\*\*\* $p < 0.001$ , One-way ANOVA.

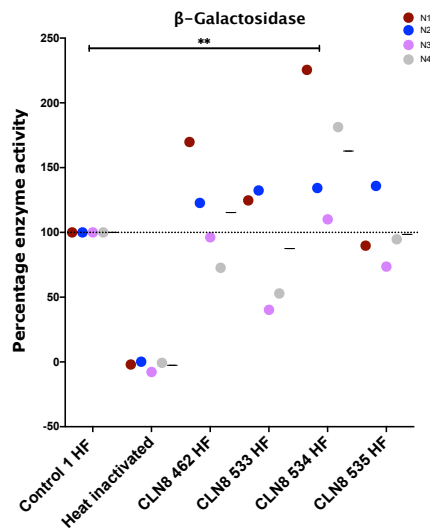


**Figure A3.8: β-Galactosidase enzyme activity in CLN8 patient cells.** Enzyme activity of the lysosomal enzyme β-galactosidase as a % of control 1 HF where control 1 HF enzyme activity was 100%. The black dotted line indicates the mean activity of control 1 HF. Each point indicates a different technical repeat and the black line indicate the mean. \*\* $p < 0.01$ , One-way ANOVA.

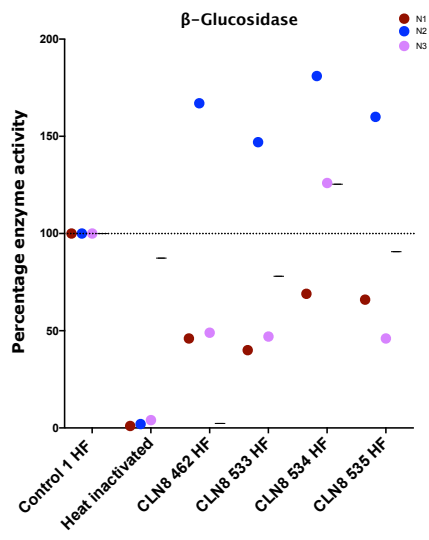


**Figure A3.9:  $\beta$ -Glucosidase enzyme activity in CLN8 patient cells.** Enzyme activity of the lysosomal enzyme  $\beta$ -glucosidase as a % of control 1 HF where control 1 HF enzyme activity was 100%. The black dotted line indicates the mean activity of control 1 HF. Each point indicates a different technical repeat and the black line indicate the mean.

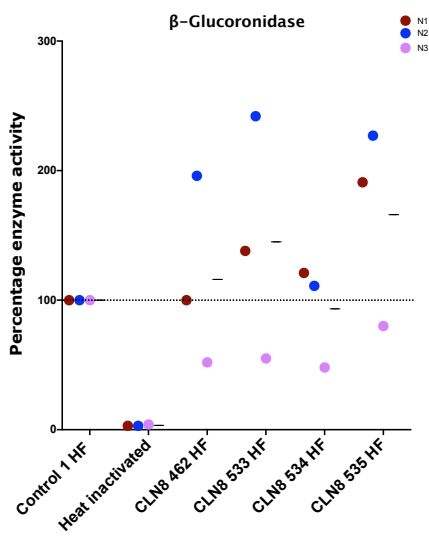


**Figure A3.10:  $\beta$ -Glucuronidase enzyme activity in CLN8 patient cells.** Enzyme activity of the lysosomal enzyme  $\beta$ -glucuronidase as a % of control 1 HF where control 1 HF enzyme activity was 100%. The black dotted line indicates the mean activity of control 1 HF. Each point indicates a different technical repeat and the black line indicate the mean. \* $p \leq 0.05$ , \*\* $p < 0.01$ , One-way ANOVA.

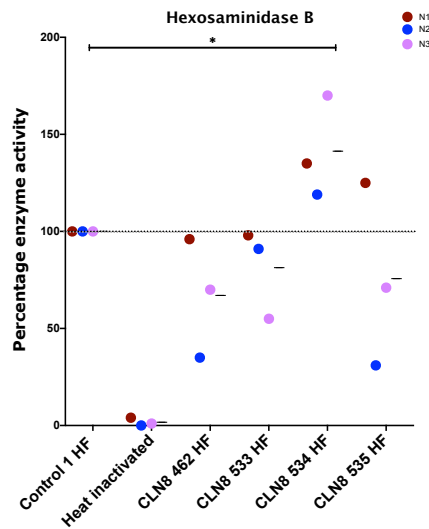


**Figure A3.11: Hexosaminidase B enzyme activity in CLN8 patient cells.** Enzyme activity of the lysosomal enzyme  $\beta$ -hexosaminidase as a % of control 1 HF where control 1 HF enzyme activity was 100%. The black dotted line indicates the mean activity of control 1 HF. Each point indicates a different technical repeat and the black line indicate the mean. \* $p \leq 0.05$ , One-way ANOVA.

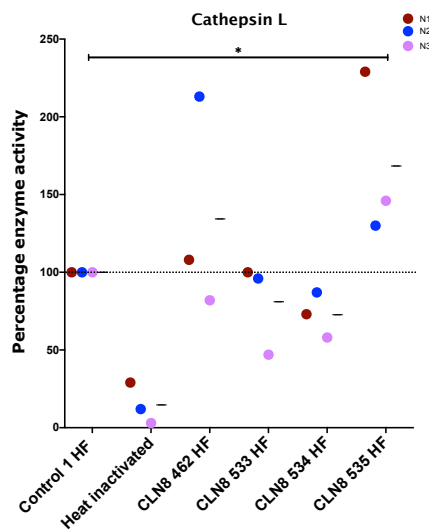


**Figure A3.12: Cathepsin L enzyme activity in CLN8 patient cells.** Enzyme activity of the lysosomal enzyme Cathepsin L as a % of control 1 HF where control 1 HF enzyme activity was 100%. The black dotted line indicates the mean activity of control 1 HF. Each point indicates a different technical repeat and the black line indicate the mean. \* $p \leq 0.05$ , One-way ANOVA.

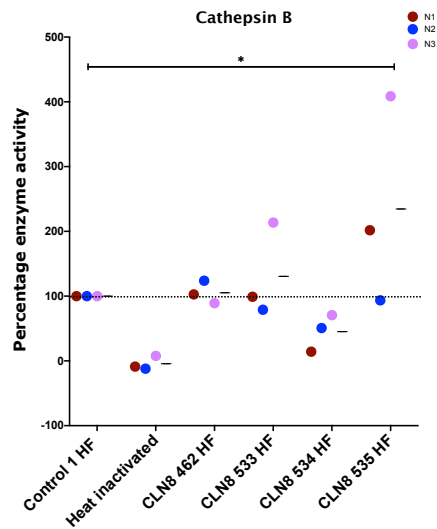


**Figure A3.13: Cathepsin B enzyme activity in CLN8 patient cells.** Enzyme activity of the lysosomal enzyme Cathepsin B as a % of control 1 HF where control 1 HF enzyme activity was 100%. The black dotted line indicates the mean activity of control 1 HF. Each point indicates a different technical repeat and the black line indicate the mean. \* $p \leq 0.05$ , One-way ANOVA.

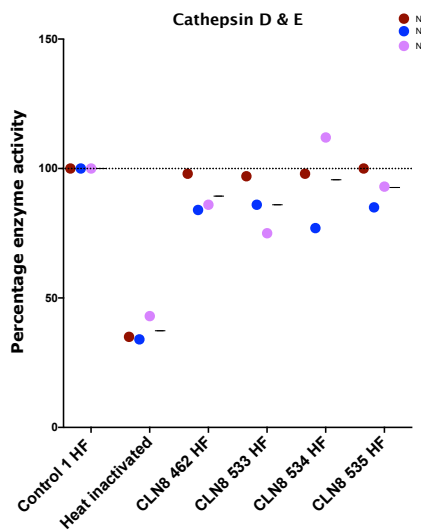


**Figure A3.14: Cathepsin D & E enzyme activity in CLN8 patient cells.** Enzyme activity of the lysosomal enzyme  $\beta$ -glucuronidase as a % of control 1 HF where control 1 HF enzyme activity was 100%. The black dotted line indicates the mean activity of control 1 HF. Each point indicates a different technical repeat and the black line indicate the mean.

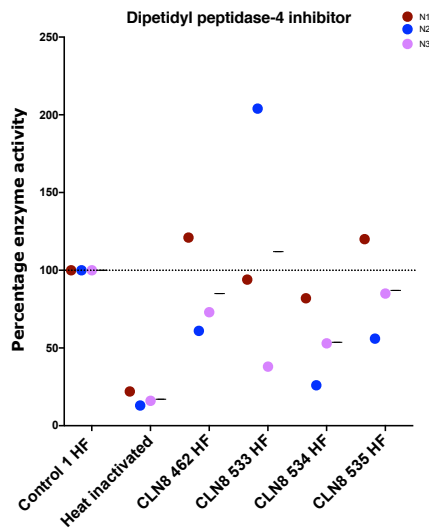


**Figure A3.15: Dipeptidyl peptidase-4 inhibitor enzyme activity in CLN8 patient cells.** Enzyme activity of the lysosomal enzyme dipeptidyl peptidase-4 inhibitor as a % of control 1 HF where control 1 HF enzyme activity was 100%. The black dotted line indicates the mean activity of control 1 HF. Each point indicates a different technical repeat and the black line indicate the mean.

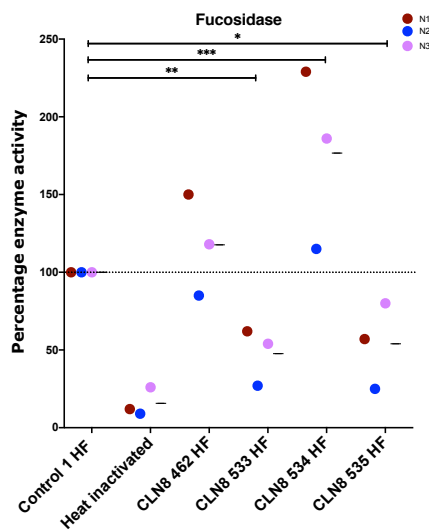


**Figure A3.16: Fucosidase enzyme activity in CLN8 patient cells.** Enzyme activity of the lysosomal enzyme fucosidase as a % of control 1 HF where control 1 HF enzyme activity was 100%. The black dotted line indicates the mean activity of control 1 HF. Each point indicates a different technical repeat and the black line indicate the mean. \* $p \leq 0.05$ , \*\* $p < 0.01$ , \*\*\* $p < 0.001$ , One-way ANOVA.

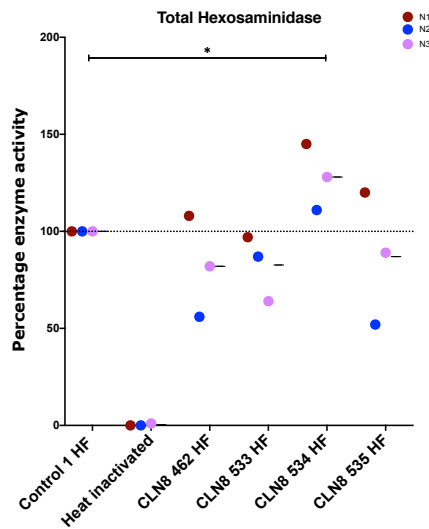


**Figure A3.17: Total Hexosaminidase enzyme activity in CLN8 patient cells.** Enzyme activity of the lysosomal enzyme hexosaminidase as a % of control 1 HF where control 1 HF enzyme activity was 100%. The black dotted line indicates the mean activity of control 1 HF. Each point indicates a different technical repeat and the black line indicate the mean. \* $p \leq 0.05$ , One-way ANOVA.

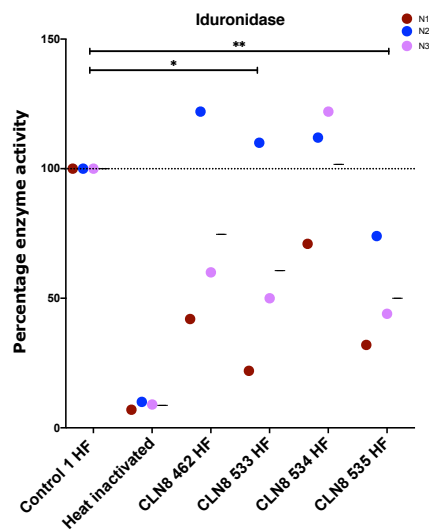


**Figure A3.18: Iduronidase enzyme activity in CLN8 patient cells.** Enzyme activity of the lysosomal enzyme iduronidase as a % of control 1 HF where control 1 HF enzyme activity was 100%. The black dotted line indicates the mean activity of control 1 HF. Each point indicates a different technical repeat and the black line indicate the mean. \* $p \leq 0.05$ , \*\* $p < 0.01$ , One-way ANOVA.

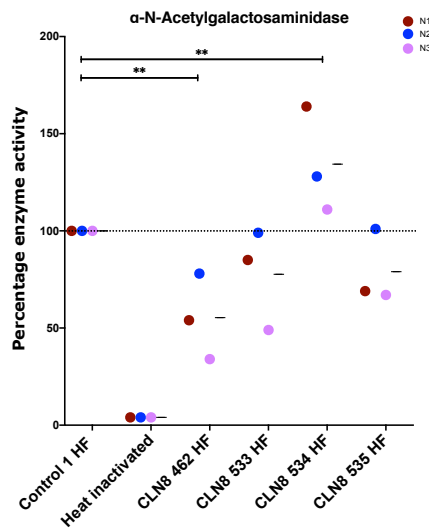


**Figure A3.19: α-N-Acetylgalactosaminidase enzyme activity in CLN8 patient cells.** Enzyme activity of the lysosomal enzyme α-N-Acetylgalactosaminidase as a % of control 1 HF where control 1 HF enzyme activity was 100%. The black dotted line indicates the mean activity of control 1 HF. Each point indicates a different technical repeat and the black line indicate the mean. \*\*p < 0.01, One-way ANOVA.

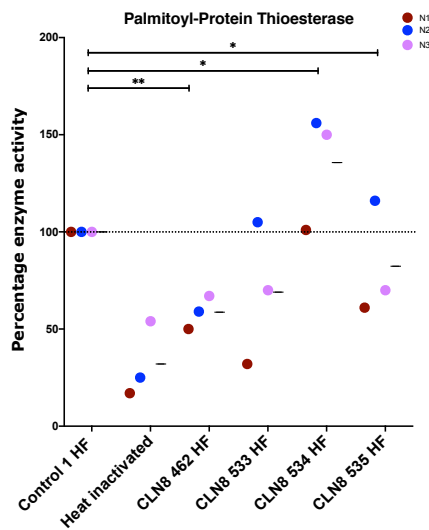


**Figure A3.20: Palmitoyl-Protein Thioesterase 1 enzyme activity in CLN8 patient cells.** Enzyme activity of the lysosomal enzyme Palmitoyl-Protein Thioesterase 1 as a % of control 1 HF where control 1 HF enzyme activity was 100%. The black dotted line indicates the mean activity of control 1 HF. Each point indicates a different technical repeat and the black line indicate the mean. \*\*p < 0.01, \*\*\*p < 0.001, One-way ANOVA.

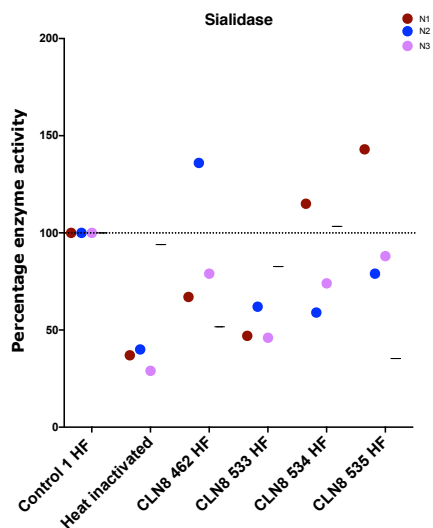


**Figure A3.21: Sialidase enzyme activity in CLN8 patient cells.** Enzyme activity of the lysosomal enzyme sialidase as a % of control 1 HF where control 1 HF enzyme activity was 100%. The black dotted line indicates the mean activity of control 1 HF. Each point indicates a different technical repeat and the black line indicate the mean.

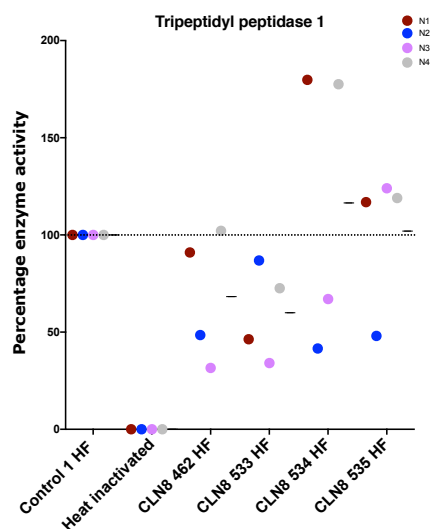


**Figure A3.22: Tripeptidyl peptidase 1 enzyme activity in CLN8 patient cells.** Enzyme activity of the lysosomal enzyme tripeptidyl peptidase 1 as a % of control 1 HF where control 1 HF enzyme activity was 100%. The black dotted line indicates the mean activity of control 1 HF. Each point indicates a different technical repeat and the black line indicate the mean.

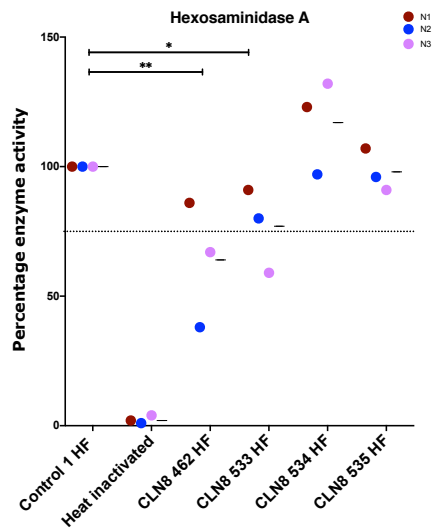


**Figure A3.22: Hexosaminidase A enzyme activity in CLN8 patient cells.** Enzyme activity of the lysosomal enzyme tripeptidyl peptidase 1 as a % of control 1 HF where control 1 HF enzyme activity was 100%. The black dotted line indicates the mean activity of control 1 HF. Each point indicates a different technical repeat and the black line indicate the mean.